Nanotechnology Applied in the Design of the Next Generation of Canadian Concrete Pavement Surfaces

by

Marcelo Andres Gonzalez Hormazabal

A thesis
presented to the University of Waterloo
in fulfillment of the
thesis requirement for the degree of
Doctor of Philosophy
in
Civil Engineering

Waterloo, Ontario, Canada, 2014

AUTHOR'S DECLARATION

I hereby declare that I am the sole author of this thesis. This is a true copy of the thesis, including any required final revisions, as accepted by my examiners.

I understand that my thesis may be made electronically available to the public.

Abstract

High friction response in pavement improves road safety, while reduced noise production from the tire-pavement interface benefits public health and the economy of a country. According to Transport Canada, highway crashes cost Canadians approximately $67 billion annually. The economic impact of noise is difficult to quantify; however, billions of dollars have been invested in noise barriers as noise mitigation alternatives.

Roadway safety is related to many factors including the friction characteristics or skid resistance of pavements. Lack of sufficient friction at the tire-pavement interface is a significant contributing factor to vehicle crashes. Skid resistance of pavement is affected by both: the microtexture of the pavement as related to the fine and coarse aggregate properties in the mortar phase of the concrete mixture; and by the macrotexture, which is defined as the measurable grooves formed in the plastic concrete during the finishing operation, or created in the hardened pavement with cutting heads consisting of uniformly spaced circular diamond saw blades.

Traffic noise is also a growing concern for public health and the country's economy. Tire-pavement noise predominates over the other sources of roadway noise in many circumstances. Under accelerating conditions, the tire-pavement noise is dominant at speeds greater than 35 to 45 km/h for cars, and 45 to 55 km/h for trucks. Although the tire-pavement noise is generated through a variety of mechanisms at the tire-pavement contact patch, it is recognized that a proper design of Portland cement concrete (PCC) pavement surface may assist in reducing noise levels and thus has prompted the evaluation of new macrotextures. However, an optimization process must be carried out to achieve adequate friction while reducing noise generation through macrotexture because large macrotexture can increase friction and generate excessive noise due to an inadequate tire-pavement interaction.

Next Generation Concrete Surface (NGCS) is the first new concrete pavement texture introduced in the United States in the last 20 to 30 years. NGCS also has the quietest texture developed for conventional concrete pavements, mainly through macrotexture modification. The construction process uses conventional diamond grinding equipment, but the blades have a different configuration in the drum. Currently, after the evaluations of long term pavement performance and noise characteristics of the NGCS, concerns have been reported regarding durability and increased noise level over time.

In this research, a laboratory investigation examined how friction, noise absorption, and surface durability can be improved by modifying the concrete microtexture. The innovative approach of this

research involved investigating those properties of concrete pavement through microtexture modification using nanotechnology. Nanotechnology involves manipulating materials at scales below 100 nm. Two different products were investigated: nanosilica applied in the cement paste, and a nano lotus leaf solution applied as a coating to mimic the lotus leaf effect.

Several concrete mixes were prepared and tested in the laboratory. Results reveal that microtexture modification through the addition of nanosilica can change the properties of fresh concrete, hardened concrete, and concrete durability. In fresh concrete, the main findings indicate that nanosilica reduces the concrete slump and also reduces the air content for a given water cement ratio; however, the slump and air content can be adjusted using High Range Water Reduced and Air Entraining Admixtures. In hardened concrete, results reveal that a small amount of nanosilica can accelerate the hydration process and enhance the compressive strength and the friction response. Results also reveal that nanosilica cannot significantly modify the sound absorption coefficient. Scanning Electron Microscope (SEM) images in hardened concrete provide insight into the impact that the nanosilica has on the Interfacial Transition Zone (ITZ). Nanosilica can reduce ettringite crystal formation in voids and can also produce a denser and a more compact cement paste. Regarding durability, several abrasion tests using the rotating cutter method indicate that nanosilica can enhance the concrete's abrasion response, resulting in better wear resistance and durability of PCC road surfaces. Freezing and thawing, and scaling resistance results show that nanoconcrete is able to reduce the external damage on the PCC surface.

Regarding the coating mimicking the lotus leaf effect, several concrete mixes were prepared and tested in the laboratory. Visual inspections demonstrate that it is possible to create the lotus leaf effect on concrete surfaces. Laboratory results reveal that the coating is able to maintain the friction response of concrete surfaces; however, results also reveal that the sound absorption coefficient is not significantly affected by the coating. Further research must be done to determine the coating impact on the hydroplaning effect when a heavy rainfall is present.

Acknowledgements

I would like to express my sincere acknowledgements to the many people who have supported me during the successful completion of my PhD. First, my deepest gratitude is given to my advisor Dr. Susan Tighe. It was a complete privilege and honor to work with her. Many thanks for her advice, guidelines, patience, generosity, and contributions as she made my PhD program very enriching and productive. Second, I give many thanks to my lovely family (Gloria and Matias) for their emotional support and for believing in my decisions. As well, my heart goes out to my parents (Fernando and Maria) for their continuous emotional and economic support. I am grateful to my brothers (Eduardo y Fernando), Lela, Camila, Rodrigo and Paz, for their continuous concern and support. To my mother-in-law Gloria for her endless help and generosity. To Jazmina, Renato, Gabriel and Angela for their support too.

Special thanks to Dr. Jeffrey West, Dr. Mahesh Pandey and Dr. Boxin Zhao for their kind disposition and for providing advice. Also, I want to acknowledge Dr. Jeffery Roesler for his interest in my research and his role as the external examiner. Special thanks to Dr. John Medley for his assistance in providing me with valuable insight on tribology.

The contributions of the Chilean National Scholarship Program from CONICYT for sponsoring my PhD is much appreciated.

Special gratitudes goes to my friend Cleyton Viera de Vargas for his friendship, generosity and good sense of humor. Thanks goes to Cibele Oliveira as well for her kind friendship.

Special thanks to Dr. Guillermo Thenoux who mentored me during my first steps as researcher and Dr. Alondra Chamorro for encouraging me to pursue my PhD in Canada.

Special gratitude to Dr. Li Ningyuan and his family for their kind friendship with me and my family.

Thanks to Dr. Md. Safiuddin for his help and advice on the experimental design during the initial phases of my research. Thanks to Jodi Norris from the Center of Pavement Transportation Technology (CPATT) for her help as I was beginning my research. Also I would like to acknowledge the contribution and continuous collaboration of Mr. Alain Francq (Managing Director of Waterloo Institute of Nanotechnology (WIN)). I am also thankful to Dr. Boxin Zhao, and his PhD student Hamed Shahsavan for their assistance with the tribology test and Nina Heinig for her assistance in the SEM tests.

I want to acknowledge the support and contribution of the Cement Association of Canada (CAC), particularly Rico Fung, Director of CAC's Markets and Technical Affairs in Ontario. As well, the Natural Science and Engineering Research Council of Canada is appreciated through their Collaborative Research Development Program. In addition, the author is grateful to Mr. Cam Monroe from BASF Canada for the supply of chemical admixtures used in the present study. Also, my gratitude to St Mary's and Holcim Cement for the supply of cement used in the present study.

Special thanks to my friends Gonzalo Sandoval, Carlos Montes and Erick Saavedra for their continuous support and motivation.

My special acknowledgements goes to the University of Waterloo's staff Richard Morrison, Douglas Hirst, Rob Sluban, Terry Ridgway, Anne Allen, Mark Merlau, Mark Sobon, Laura Wilson and Victoria Tolton. They provided unlimited technical help during my research. Also, thanks to Mary McPherson of UW´s grad writing services.

Finally, my heartfelt thanks to my colleagues and friends from the Center for Pavement Transportation Technology (CPATT) as they provided much joy during my research: Doubra Ambaiowei, Zaid Alyami, Janki Bhavsar, Laura Bland, Amin Hamdi, Hanaa Alwan, Karolina Konarski, Andrew Northmore, Aleli Osorio, Dan Pickel, Alain Duclos, Xiomara Sanchez, Sonia Rahman, Cheng Zhang and Gulfam Jannat. To Pino, Kathy and Adam, co-op students from CPATT, many thanks for their continuous help and great work in the lab. To Federico Irali and Mattia Longhi, visiting students from Italy for their friendship and for their support in the experimental work. To Maria Jose, Jesus, Olivier, Jean Charles and Alex, for their friendship and also for their continuous support. Special gratitude to Dan, Kathy and Andrew, for their assistance in my writing process.

Dedication

This thesis is dedicated to my wife Gloria and my son Matias, who are my inspiration and provide me with never-ending patience and support. I want also to dedicate this thesis to my aunt Luisa, my grandmother Maria and my cousin Gonzalo, whom I lost during my permanence in Canada.

Table of Contents

List of Figures

List of Tables

Chapter 1
Introduction

1.1 Introduction

Portland cement concrete (PCC) pavement can create two primary functional "failures" related to surface texture: inadequate skid resistance and excessive tire-pavement noise generation (Byrum et al., 2010). According to the United States Federal Highway Administration (FHWA), wet pavement, often associated with reduced skid resistance, is the more important factor contributing to departure crashes on roads (FHWA, 2012). Highway crashes cost Canada $67 billion Canadian Dollars annually (Vodden et al., 2007). In the United States (U.S.) this annual cost exceeds $230 billion American Dollars (FHWA, 2012). Due to the importance of road safety the U.S. FHWA introduced a highway safety improvement program that indicated 70% of wet pavement crashes can be minimized or prevented by pavement friction improvements; therefore, an optimum level of friction must be maintained in order to reduce accidents (FHWA, 2012).

The friction of a concrete pavement is affected by the microtexture as related to the sand and cement contents in the mortar phase of the concrete mixture, and its macrotexture which is defined as the measurable grooves formed in the plastic concrete during the finishing operation (Hall et al., 2009-1). This macrotexture can also be achieved in the hardened pavement surface with cutting heads consisting of uniformly spaced circular diamond saw blades.

In addition to friction, traffic noise is another concern for the public health and economy of a country (Ahammed, 2009). Tire-pavement noise predominates over other sources of roadway noise in many circumstances; under accelerating conditions, the tire-pavement noise is dominant at speeds greater than 35 to 45 km/h for cars, and 45 to 55 km/h for trucks (Bernhard et al., 2005). Although the tire-pavement noise is generated through a variety of complex mechanisms at the tire-pavement contact patch, proper design of concrete pavement surfaces may assist in reducing noise levels and thus has prompted the evaluation of new macrotextures. Moreover, an optimization process must be carried out to achieve adequate friction while reducing noise generation through macrotexture because a large macrotexture can increase friction but also generate excessive noise due to an inadequate tire-pavement interaction (Byrum et al., 2010).

According to Scofield (Scofield, 2011), the Next Generation Concrete Surface (NGCS) is the most recent concrete pavement texture introduced in the United States. The NGCS also has the quietest

texture developed for conventional concrete pavements, mainly through macrotexture modification. The construction process uses conventional diamond grinding equipment, but the blades have a different configuration in the drum and can be applied to both new and older in-service concrete pavements. Previous attempts to increase friction and reduce the noise intensity at the contact patch have focused on creating different surface textures through macrotexture improvements (Scofield, 2011). The Washington State Department of Transportation (WSDoT) in the United States evaluated long-term pavement performance and noise characteristics of NGCS. The WSDoT concluded that using NGCS textures was not a viable noise-reduction strategy because their noise level increases more rapidly than those of traditional surfaces (Anderson et al., 2014). The increase in noise level was attributed to the lack of durability in the surface characteristics (loss of aggregate and general roughening of the PCC pavement surface). Therefore, there is a strong motivation to maintain the surface characteristics or durability over time, since NGCS is the quietest texture developed for conventional PCC pavements. Moreover, in a Canadian context, exposure to the weather may cause deterioration in concrete.

This research investigates how friction, sound absorption, and durability can potentially be improved by modifying the PCC microtexture. In order to evaluate those properties, a laboratory research program has been developed at the Centre for Pavement and Transportation Technology (CPATT) at the University of Waterloo (UW) in partnership with the Cement Association of Canada (CAC) and The Natural Sciences and Engineering Research Council of Canada (NSERC). The innovative approach of this research involves investigating the friction, sound absorption, and durability of concrete pavement through microtexture modification using nanotechnology. Nanotechnology involves manipulating matter and materials at scales below 100 nm. The combination of the new microtexture and the possibility to modify PCC macrotexture through diamond grinding techniques is providing insight that can be used to establish the next generation of concrete pavement surfaces in Canada.

1.2 Nanotechnology

The applicability of nanotechnology to a variety of fields has received increased attention (Gopalakrishnan et al., 2011). Internationally, countries have realized the potential of nanotechnology for future growth and development, and have established initiatives for the development of research and products related to nanotechnology. These initiatives include organizations in Canada, China,

Japan, USA and the European Union. The changes brought about by nanotechnology will be observed in terms of their environmental, social and economic impacts.

According to Persons (Persons et al., 2014) nanomanufacturing with nanotechnology can be described as a future megatrend that may potentially match or go beyond the digital revolution's influence on society and the economy. Since concrete is the most used construction material in the world (Kosmatka et al., 2011) and because it has been recognized that nanomaterials can enhance concrete's properties and durability, nanotechnology could be a promising and revolutionary tool to improve the behavior and performance of this material (Grove et al., 2010).

1.3 Research Hypotheses, Objectives and Methodology

This section defines the research hypotheses, objectives, scope and methodology.

1.3.1 Research Hypotheses

The hypotheses for this research are as follows:

- Microtexture modification through nanotechnology can enhance the surface friction and noise absorption in concrete materials.
- Microtexture modification through nanotechnology can improve microstructure and durability in concrete materials.
- Macrotexture modifications using diamond grinding techniques can be applied to nanoconcrete to design new surface textures.

1.3.2 Research Objectives and Scope

The overall objective of this research is to advance the state of the art of next generation concrete pavement surfaces, suitable for Canadian conditions, with increased friction and reduced noise generation. The focus is to modify concrete microtexture through nanotechnology.

The specific objectives of this research are to:

- Identify and understand the fundamentals of friction and noise generation in concrete pavements.
- Identify and understand the fundamentals of nanotechnology and their effects on concrete materials and pavement surfaces.

- Identify and evaluate at least two nanomaterials and quantify their impact on the friction and noise absorption of concrete materials.
- Propose a new concrete microstructure with increased durability in terms of abrasion resistance, freeze-thaw resistance and scaling resistance.

Many of today´s concrete mixtures for PCC pavements contain supplementary cementitious materials (SCMs) such as silica fume or slag, generally in large amounts (up to 10% by weight of cement) (Kosmatka et al., 2011). In contrast, much smaller amounts of nanomaterials such as nanosilica can be used to positively alter the concrete microstructure and the microtexture of the concrete surface (Gopalakrishnan et al., 2011). Thus, the latter represents a significant departure from state-of-the-practice and thus it is the sole focus of this thesis. Nanosilica and the lotus leaf coating were chosen to be studied in this thesis for the following reasons. First, when this research began, nanosilica was the most studied nanomaterial in concrete and was readily available. Carbon nanofibres and nanotubes were also considered, however difficulties achieving good dispersion in the PCC matrix were reported in the literature. This was the main reason why these alternatives were not included in the experiments and only nanosilica was used inside of the concrete mix. Finally, the lotus leaf coating was chosen because according to Ashby (Ashby et al., 2009), coatings are widely used because they provide a direct and cost-efficient way of imparting particular surface qualities to a material without the need to modify the entire material.

1.3.3 Research Methodology

The laboratory research methodology is presented in Figure 1-1. The first step involved defining the problem and identifying gaps in the current state of PCC pavement friction and noise absorption/emission. The main challenge with changing the pavement's macrotexture to increase the friction of concrete pavements is the associated noise generation from tire-pavement interactions. Thus, the goal is to increase friction but at the same time reduce the overall noise generation. This thesis aims to do that through the application of a new type of concrete that incorporates nanomaterials. Using nanomaterials to modify microtextures may potentially provide benefits to Portland cement concrete (PCC).

The next stage of the research involved a laboratory experimental design plan. This design included an experimental matrix, a feasibility analysis of applying nanomaterials in concrete, and the definition of the specific nanomaterials to be investigated. Several tests were selected to address the thesis

objectives and to be conducted selectively in three different water/cement (w/c) ratios. A material characterization and mix design based on Canadian standards was also developed. Two types of procedures were carried out; the first involved incorporating nanosilica with both the concrete and the mortar mixes, and the second involved applying a coating on the concrete surface to obtain a lotus leaf effect selected to provide high water repellence. Since the nanosilica was used in powder form, a batching procedure was designed to avoid fume generation and the dispersion of particles into the air while still achieving proper dispersion in the concrete or mortar matrix.

Several concrete and mortar mixes were then prepared with different proportions of nanomaterials. Specific tests, including compressive strength, friction response and noise absorption response are described in Figure 1-1. The friction response was evaluated using two different tests: the British Pendulum Tester and a novel experiment designed using a tribometer. For noise absorption an Impedance Tube was used. A surface profiler was used in the mortars to determine the impact of nanomaterials in the surface morphology. Scanning Electron Microscope (SEM) images were taken to examine changes in the concrete microstructure and surface characteristics at both the microscale and nanoscale. For the concrete mixes with nanosilica, additional durability testing was performed under simulated extreme climate conditions to observe how nanomaterials impact concrete performance. The durability tests included abrasion resistance, freeze-thaw resistance and scaling resistance. For concrete mixes with a lotus leaf coating, the tests included concrete compressive strength, friction response (using the British Pendulum Tester) and noise absorption response (using an Impedance Tube).

Statistical analyses and test hypotheses were developed to draw conclusions and to determine the significance in the modifications. Finally, the results and conclusions were summarized and incorporated into this thesis.

1.4 Thesis Structure

This thesis is composed of six chapters as follows:

Chapter 1 introduces a general background of the topic and describes the problem, objectives, methodology and the thesis structure. The chapter also introduces the concept of nanotechnology.

Chapter 2 presents an extensive review of the relevant literature related to concrete pavements, materials, concrete microstructure, and pavements' surface characteristics. It also describes the mechanisms of friction and noise emission. The nanotechnology and nanomaterials used in this research are also discussed in detail.

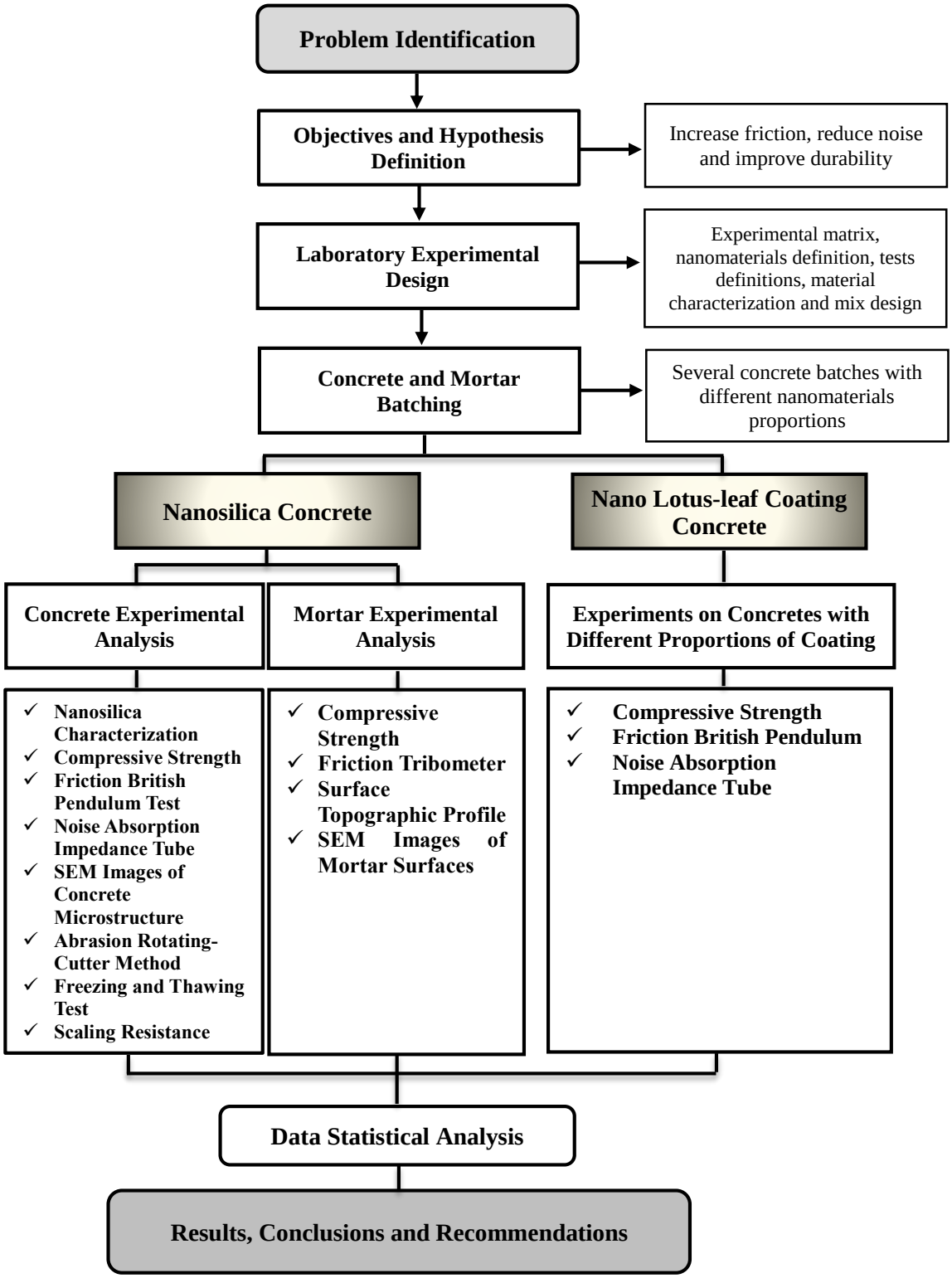

Figure 1-1: Research Methodology

Chapter 3 describes the materials and methods as well as the experimental design and the experimental matrix, with a summary of the tests that were conducted.

Chapter 4 presents an analysis and discussion of the main results obtained.

Chapter 5 presents a summary of the statistical analysis and describes the test hypothesis used to determine the significance in the modifications.

Chapter 6 concludes the main body of the thesis and provides recommendations drawn from this research.

The thesis also includes seven **Appendices** with the following information:

- Appendix A: Concrete Mix Design
- Appendix B: GU Cement Characterization
- Appendix C: Results From Freezing and Thawing Test
- Appendix D: Pictures of Scaling Resistance Evaluation
- Appendix E: Statistical Analysis Tables
- Appendix F: ANOVA Calculation Details
- Appendix G: t-Student Analysis

Chapter 2
Literature Review

This chapter presents a literature review focused on concrete pavements, materials and specifications, concrete microstructure, fundamentals of friction, fundamentals of noise absorption/production and main distresses in Portland cement concrete (PCC) pavement surfaces. Background information about nanotechnology and its interaction with concrete materials are also presented.

2.1 Concrete Pavements, Material Specifications and Mix Design

2.1.1 Concrete Pavements

Concrete pavements are referred to as rigid pavements because the pavement structure deflects minimally under traffic load. A concrete pavement structure typically has a PCC layer on the surface, a middle layer termed the subbase, and the whole structure is placed over the subgrade. Figure 2-1 presents a typical cross section of PCC pavement (Papagiannakis and Masad, 2008).

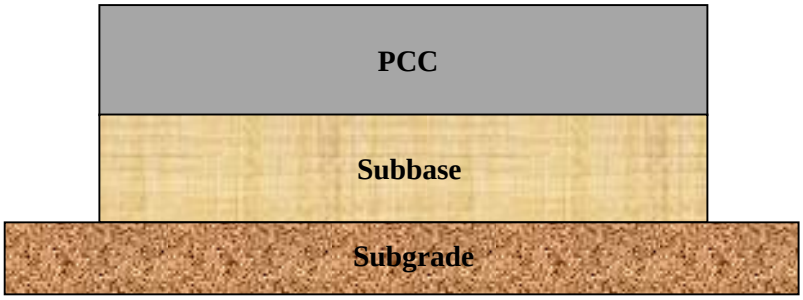

Figure 2-1: Typical PCC pavement structure

The surface layer is in direct contact with traffic loading. It is designed to provide a smooth, low-noise, high friction surface, while providing adequate surface drainage. The properties of the concrete material control the functional integrity of the concrete pavement (Papagiannakis and Masad, 2008).

The three primary types of conventional concrete pavements are defined as follows (Tighe, 2013):

- **Jointed Plain Concrete Pavements (JPCP):** JPCP is the most common type of concrete pavement in Canada and consists of slabs defined by closely spaced contraction joints. The load transfer in joints is achieved through the aggregate/paste interlock or dowels.
- **Jointed Reinforced Concrete Pavements (JRCP):** JRCP contain steel reinforcement (typically

wire mesh) in order to allow longer joint spacing. Due to the longer spacing, dowel bars are required to achieve adequate load transfer.

- **Continuously Reinforced Concrete Pavements (CRCP):** This type of pavement contains continuous reinforcement with the objective of eliminating joints. Also, CRCP allows a reduction in the slab thickness of around 70% to 80% (obtained empirically). The formation of transverse cracks is a typical characteristic of CRCP.

2.1.2 Materials Specifications

The Ontario Provincial Standards and Specifications (OPSS) for Roads and Public Works Organization provide standards for pavement construction (OPSS, 2013). The specification provide the minimum standard to produce high quality pavements. The applicable specifications for this research are outlined herein.

2.1.2.1 Fine Aggregates for Concrete

Fine aggregates represent approximately 24% to 28% of the absolute volume in air-entrained concrete (Kosmatka et al., 2011). Fine aggregates are usually comprised of natural sand or crushed stone with most particles smaller than 5 mm. The gradation requirements for fine aggregates according to the OPSS are presented in Table 2-1.

Table 2-1: Gradation requirements for fine aggregate (OPSS 1002) (OPSS, 2013)

MTO Sieve Designation	Percent Passing
9.5 mm	100
4.75 mm	95 - 100
2.36 mm	80 - 100
1.18 mm	50 - 85
600 mm	25 - 60
300 mm	30-oct
150 mm	0 - 10
75 mm	0 - 3 Natural Sand 0 - 6 Manufactured Sand

The OPSS also establishes the requirements presented in Table 2-2 for fine aggregates.

Table 2-2: Physical requirements for fine aggregate (OPSS 1002) (OPSS, 2013)

Laboratory Test Name	MTO or CSA Lab. Test Number	Acceptance Limit
Organic Impurities Test, Maximum organic plate number	LS-610	3
Micro-Deval Abrasion Test, % maximum lost at 14 days	LS-619 or CSA A23.2-23A	20
Accelerated Mortar Bar Test, % maximum at 14 days	LS-620 or CSA A23.2-25A	0.15
Concrete Prism Expansion Test, % maximum at 1 year	CSA A23.2-14A	0.04

2.1.2.2 Coarse Aggregates for Concrete

Coarse aggregates represent approximately 31% to 51% by absolute volume in air-entrained concrete. Both types of aggregates (fine and coarse) represent about 60% to 75% of the concrete (Kosmatka et al., 2011). The gradation requirements for coarse aggregates according to the OPSS (OPSS, 2013) are presented in Table 2-3. Table 2-4 presents the physical requirements of coarse aggregate for concrete pavements.

Table 2-3: Gradation requirements (LS-602) - coarse aggregate for concrete pavement or concrete base

Nominal Maximun Size	37.5 mm	19.0 mm	Combined
MTO Sieve Designation	**Percent Passing**		
53 mm	100	-	100
37.5 mm	90-100	-	95-100
26.5 mm	20-55	100	-
19.0 mm	0-15	85-100	35-70
9.5 mm	0-5	20-55	oct-30
4.75 mm	-	0-10	0-5

2.1.2.3 Cement, Hydration and Hardened Concrete Microstructure

In Canada, the Canadian Standards Association standard CSA 3001 defines six types of Portland cements which are identified as follows (CSA, 2009):

- Type GU: General-Use Portland cement
- Type MS: Moderate Sulphate-resistant Portland cement
- Type MH: Moderate-Heat of hydration Portland cement
- Type HE: High Early-strength Portland cement
- Type LH: Low-Heat of hydration Portland cement
- Type HS: High Sulphate-resistant Portland cement

Table 2-4: Physical requirements – coarse aggregates for concrete

Laboratory Test Name	MTO or CSA Lab. Test Number	Acceptance Requeriments for Pavement
Material Finer than 75 µm Sieve, by washing. % maximun	LS-601	
For gravel		1.0
For crushed rock		2.0
Absorption, % maximun	LS-604 or CSA A23.2-12A	2.0
Unconfined Freeze-Thaw Loss, % maximun	LS-614 or CSA A23.2.24	6
Flat and Elongated Particles, % maximun	LS-608	20
Petrographic Number, Concrete, maximun	LS-609	125
Micro-Deval Abrasion Loss, % maximun	LS-618 or CSA A23.2-29A	14
Acceletarted Mortar Bar Expansion, % maximun at 14 days	LS-620 or CSA A23.2-25A	0.150
Potential Alkali-Carbonate Reactivity of Quarried Carbonate Rock	CSA A23.2-25A	Chemical Composition Must Plot in the Non-Expansive Field of Fig.1 of Test Method
Concrete Prism Expansion Test, % maximun at 1 year	CSA A23.2-14A	0.040
Alternative Requirement to Unconfined Freeze-Thaw Loss (LS-614)		
Magnesium Sulphate Soundness, 5 Cycles, % maximun loss	LS-606	12

Portland cement chemically reacts with water resulting in hydration. Hydration is initiated when water makes contact with cement particles; this process produces cement hydrates on the surface of each cement particle, creating the cement paste (cement, water, and air). In conventional concrete, cement paste in combination with aggregates (sand and gravel) creates the concrete material where the paste acts as an adhesive resulting in a monolithic mass.

The constituent breakdown of Portland cement is presented in Table 2-5. According to Taylor (Taylor, 1997) tricalcium silicate (also known as alite) reacts relatively quickly with water and is the most important phase because it is responsible for the strength development in concrete up to 28 days; alite constitutes between 50 to 70 % of unhydrated cement. Dicalcium silicate (also known as belite) reacts slowly with water, therefore it is important in the long term strength development after 28 days; belite constitutes between 15 to 30 % of unhydrated cement. Tricalcium aluminate (which constitutes 5 to 10 % of unhydrated cement) reacts rapidly with water and may cause undesirable rapid setting. Gypsum is often added as a set-controlling agent to counteract the effects of tricalcium aluminate. Ferrite constitutes 5 to 15% of unhydrated cement and its rate of reaction with water is variable, although in general this rate is initially high and becomes low or very low at later ages.

Table 2-5: Major constituents of Portland cement (adapted from Taylor (1997))

Mineral	Chemical formula	Abbreviation	Amount (%)
Tricalcium silicate (alite)	Ca_3SiO_5	C3S	50 to 70
Dicalcium silicate (belite)	Ca_2SiO_4	C2S	15 to 30
Tricalcium aluminate	$Ca_3Al_2O_4$	C3A	5 to 10
Tetracalcium aluminoferrite	$Ca_4Al_nFe_{2-n}O_7$	C4AF	5 to 15

Hardened concrete has the composition presented in Table 2-6. Calcium Silicate Hydrate (C-S-H) is the main component of hardened concrete (around 50% for water/cement (w/c) ratio of 0.5) and is responsible for enhancing the strength and durability of the cement paste. According to Taylor (Taylor, 1997), C-S-H can be described as a nearly amorphous material and presents properties of a rigid gel. In addition to the solid phase, C-S-H gel develops tiny internal pores (gel pores) which have dimensions on the order of nanometers and are considerably smaller in comparison with capillary pores. According to Selvam (Selvam, 2009), the concrete microstructure has two types of C-S-H gel: low density and high density. Each has different mechanical behaviors; high density C-S-H has higher stiffness and hardness values than low density C-S-H (Selvam, 2009).

Table 2-6: Major constituents of hydrated Portland cement (w/c = 0.5) (adapted from Barnes & Bensted (2002) and Selvam R. et al (2009))

Component	**Approximate Volume (%)**	**Comments**
Calcium Silicate Hydrate (C-S-H)	50	Includes gel pores. Poorly crystalline/ amorphous structure
Calcium Hydroxide (CH)	12	Crystalline structure
Ettringite and monosulphate phases (AFt and AFm phases)	13	Crystalline structure
Unreacted Cement particles	5	Depends on hydration. Mainly affected by temperature, water amount, and curing moisture
Capillary Pores	20	Dependant on w/c ratio

Calcium hydroxide (CH) occupies about 12% of the volume of a normal Portland cement paste. A large portion of the CH is responsible for forming the low-density C-S-H. CH only provides very minor contributions to the strength and impermeability of the paste in comparison to C-S-H.

The most common AFt (Al_2O_3-Fe_2O_3-tri) phase in hydrated cement is ettringite. Ettringite is composed of rod-like crystals in the early stages of the hydration reaction. The formation of ettringite in the cement system depends on the ratio of calcium and calcium sulfate to tri-calcium aluminate (C3A). AFt formation is commonly followed by a significant increase in the volume. Shrinkage-compensating cements can be used to adjust for the controlled formation of ettringite. AFm (Al_2O_3-FeO_3-mono) phase or Calcium monosulphoaluminate hydrate appear in the later stages of hydration, approximately one or two days after batching.

Porosity represents the volume of voids as a proportion of the total concrete volume (Kosmatka et al., 2011). In the concrete pore structure, it is possible to identify capillary and gel pores. Capillary pores are the product of the water-filled space between the hydrated cement grains. Depending on the w/c ratio and the degree of hydration these pores may produce a low density C-S-H gel (i.e. high porosity). According to Table 2-6, for a w/c of 0.5, capillary pores represent around 20% of the total gel volume. Gel pores are an intrinsic part of the C-S-H and are much smaller in size than capillary pores. Gel pores form approximately 28% of the total volume of gel, but they have only a small impact on strength and permeability. Permeability, can be defined as the ability of concrete to allow penetration by water or other substances (liquid, gas, ions, etc.) (Kosmatka et al., 2011) and is influenced by the porosity of the concrete. It can be classified as the most important property affecting concrete durability (He X. & Shi X., 2008).

2.1.3 Concrete Strength

Strength is the most common concrete property measured because it indicates how well the concrete can resist external loads and is relatively easy to measure (Lamond & Pielert, 2006). Compressive strength is measured to provide an overall representation of the concrete quality, since strength is directly related to the structure of the hydrated cement paste (Neville, 1996).

Concrete can be considered as a two-phase composite, consisting of aggregates and cement paste (Lamond & Pielert, 2006). Thus, under loading, the response of concrete depends on the interactions between both phases and the interfacial region between them. The interfacial zone, called interfacial transition zone (ITZ) is a weak area of concrete because it is an area of high porosity. The variation of porosity within the ITZ depends on the distance from the aggregate; at 10 μm from the aggregate the porosity is approximately 22%, while at 30 μm it drops to approximately 10% (Neville, 1996). Under loading, microcracks are initiated in the ITZ. Silica fume particles, which are much finer than cement

particles, are an effective addition to increase the strength in the ITZ (Neville, 1996). The mechanisms by which silica fume acts are explained in Section 2.1.3.2.

Before external loads are applied to concrete materials, small cracks exist in concrete at the paste-aggregate interface (Neville, 2006). These cracks are generated from differences between the hydrated paste and the coarse aggregates in the mechanical properties, shrinkage rates, and thermal effects. When an external load is applied to the concrete, these small cracks are stable until approximately 30% of the concrete's ultimate strength, and begin to grow as the load exceeds this level. When the load reaches 70 to 90% of the ultimate strength the cracks penetrate the bulk paste (composed of cement paste and fine aggregates) and grow until a point where the concrete cannot support additional load. Figure 2-2 represents the internal microcracking development in loaded concrete (Lamond & Pielert, 2006).

Based on the above explanation, it is clear that the strength of the cement paste plays a key role in the ultimate strength of concrete and also the bonding quality between the cement paste and aggregates. Several factors influence paste quality, however the paste density is the single most important factor affecting paste strength (Lamond & Pielert, 2006).

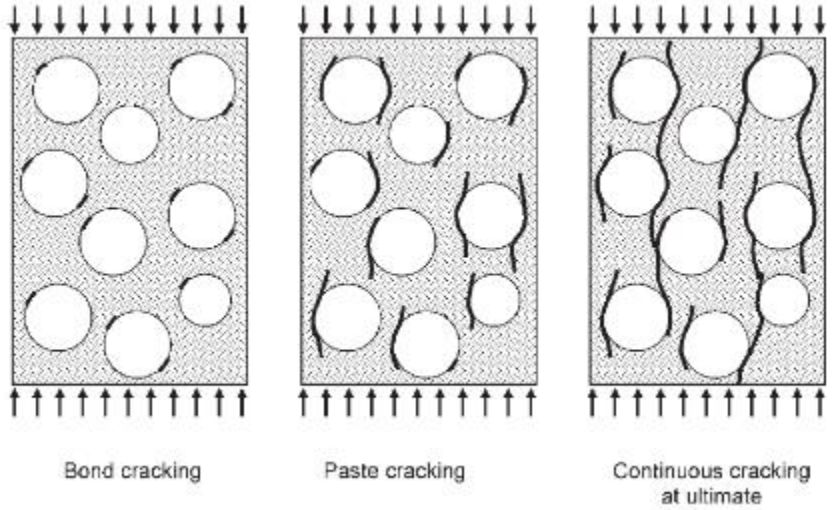

Figure 2-2: Microcracking development in concrete under load (Adapted from Lamond & Pielert, 2006).

2.1.3.1 Chemical Admixtures

Admixtures are chemicals that can be added to a concrete either before or during mixing. Different admixtures serve different purposes and include: air-entrainers, plasticizers, water-reducers,

accelerators, air detrainers, foaming agents, and more. Admixtures are useful because they make it much easier to achieve a certain desired effect.

According to Kosmatka (Kosmatka et al., 2011) the main reasons to use admixtures in concrete are:

- To minimize the cost of concrete construction
- To obtain better and more effective properties
- To maintain the concrete quality during: mixing, transporting, placing and curing in adverse weather conditions
- To control particular emergencies during concrete installations in the event that they occur

For the purposes of this research, only two types of admixtures were considered: Air-Entraining Admixtures (AEA) and High-Range Water Reducing Admixtures (HRWR). The purpose of using AEA is to enhance the concrete response under freezing and thawing. The use of HRWR is recommended to maintain the concrete slump within a desired range.

Air-Entraining Admixtures (AEA)

Air-entrainers are common additives that introduce discrete and stable tiny bubbles of air when mixed with concrete. These bubbles form "closely spaced, spherical pores" that are embedded permanently in the concrete paste once it hardens (Taylor, 1997). AEAs have been universally accepted for enhancing the ability of concrete to resist the potential destructive effects from exposure to freeze-thaw cycles. AEA should be mandatory for environments when chemical de-icers are being used, for instance, in pavements and bridge decks (Lamond & Pielert, 2006).

Air-entrainers are commonly composed of synthetic detergents, petroleum acids, proteinaceous material, fatty and resinous acids, organic salts of sulfonated hydrocarbons, salts of wood resin and sulphonated lignin (Lamond & Pielert, 2006).

AEAs are able to modify the properties of fresh and hardened concrete. In fresh concrete, these air bubbles act like ball bearings, which help increase the workability of the concrete. It is also recognized that AEAs can improve concrete's plasticity, and reduce segregation and bleeding (Lamond & Pielert, 2006). In hardened concrete, the main benefit of using AEA is to provide resistance to freezing and thawing, particularly when chemical de-icers are used. In order to achieve improvements in hardened concrete, the main factors are the total volume of air, spacing factor, and size and distribution of the air voids. Freezing water increases its volume by approximately 9%; thus, during winter as the water within

the concrete expands, it generates an internal hydraulic pressure, which is responsible for distressing PCC materials (Lamond & Pielert, 2006). The air voids act to relieve pressure caused by the expansion of freezing water, thus releasing tension from the concrete to prevent bursting.

AEAs add voids to the cement paste which reduce the strength of the concrete. It is estimated that in moderate to high-strength concrete, for every 1% of air introduced into the concrete, the strength will be reduced by 2-9% (Kosmatka at al., 2011).

High-Range Water Reducing Admixtures (HRWR)

HRWRs reduce the water demand, creating a concrete with a reduced w/c ratio and thus increasing the concrete's strength (Kosmatka et al., 2011). Alternatively, they can be used to produce self-consolidating concrete. In PCC water reduction results in less capillary pore formation in concrete. Therefore the transport properties are reduced and the durability of the concrete is enhanced. HRWRs can also help in the hydration process by allowing mixtures to obtain higher strength earlier and reducing void sizes.

HRWR admixtures are made from sulphonated melamine formaldehyde condensates, sulphonated naphthalene formaldehyde condensates, lignosulphonates, and polycarboxylates. These HRWR will reduce the water content by approximately 12-30% (versus regular water reducers that can reduce by 5-10%). They are much more efficient than regular water reducers and leads to higher compressive strengths (greater than 70 MPa). As well, they are able to provide more early strength gain, reduce chloride-ion penetration and provide the benefits of a lower water/cement ratio concrete.

Certain types of HRWR admixtures give cement particles a highly negative charge so that the particles repel each other. As a result, HRWRs provide dispersion of the cement particles, generating an increase in the concrete workability (Neville, 1996). The latest development in HRWR is the introduction of a class of polymer material called polycarboxylate. These polymers are highly efficient dispersants. They are generally 2 to 3 times more effective than naphthalene or melamine-based HRWR and result in excellent workability retention (Lamond & Pielert, 2006).

2.1.3.2 Mineral Admixtures

Mineral admixtures (silica fume, fly ash, natural pozzolans, calcined clays, and slags) are usually added to concrete in large amounts to improve the properties of hardened concrete (FHWA, 2014; Kosmatka

et al., 2011). This is because they may provide hydraulic activity, pozzolanic activity, or both to the concrete. These materials are usually referred to as supplementary cementing materials (SCMs). According to Kosmatka (Kosmatka et al., 2011) “a pozzolan is a siliceous or aluminosiliceous material, that in a finely divided form and in the presence of moisture, chemically reacts with the Calcium Hydroxide released by the hydration of Portland cement to form Calcium Silicate Hydrate and other cementing compounds”. Since the focus of this study is nanosilica, this section will only cover a description of silica fume. Other mineral admixtures present some similarities in their effects on PCC.

Silica fume (also known as microsilica or condensed silica fume) is a by-product of the reduction of high-quality quartz with coal in electric furnaces (FHWA, 2014; Kosmatka et al., 2011). Silica fume was discharged to the atmosphere before the mid 1970s but after environmental concerns were raised it became necessary to collect and dispose the microsilica in landfills. Thus the use of this material in various applications provides the additional benefit of reducing landfill waste.

According to Kosmatka (Kosmatka et al., 2011), silica fume has the following overall characteristics: average particle size around 0.1 μm, maximum sizes around 1 μm, chemical composition of more than 85% silicon dioxide and specific surface area around 20 m^2/g . In concrete materials, silica fume is commonly used in amounts between 5% and 10% by mass of the total cementing material (Kosmatka et al., 2011). The small particles of silica fume can enter the space between the particles of cement, and therefore is able to improve the packing (Neville, 1996).

According to the Federal Highway Administration, silica fume is used in concrete to improve its properties. It has been found that silica fume improves compressive strength, bond strength, and abrasion resistance. It also reduces permeability and therefore helps in protecting reinforcing steel from corrosion (FHWA, 2014). In concretes containing silica fume or fly ash, the abrasion resistance is enhanced by improved compressive strength (Lamond & Pielert, 2006). In addition, for this special type of concrete, the cement paste plays a key role in abrasion resistance and can be considered to be more important than the aggregate´s quality (Lamond & Pielert, 2006).

Silica fume particles are effective to increase the strength in the ITZ (Neville, 1996). The mechanism can be explained as follows: since the surface of the aggregate is covered with a thin layer of Calcium Hydroxide, followed by a thin layer of Calcium Silica Hydrate, and finally a thicker layer of the same materials but without any unhydrated cement. The strength of the ITZ can increase because silica fume can act in a pozzolanic reaction which forms Calcium Silicate Hydrate and other cementing compounds, instead of Calcium Hydroxide.

2.2 Microtexture and Macrotexture in Concrete Pavements and their Relationship with Friction and Noise

Pavement surface texture, characterized by microtexture, macrotexture, and megatexture, is a property used to describe the functional condition of pavements. It can be defined as the deviations of the pavement surface from a planar surface. These deviations occur at three different levels defined by wavelength (λ) and the peak-to-peak amplitude (A) (Hall et al., 2009-1). The scales of microtexture, macrotexture and megatexture are defined below:

- Microtexture: $\lambda < 0.5$ mm and A = 1 to 500 μm
- Macrotexture: $\lambda = 0.5$ mm to 50 mm and A = 0.1 to 20 mm
- Megatexture: $\lambda = 50$ mm to 500 mm and A = 0.1 to 50 mm

Figure 2-3 illustrates the concept of microtexture and macrotexture. Figure 2-3 a) presents the concept of macrotexture constructed by longitudinal broom finishing on a tunnel pavement made of concrete. Figure 2-3 b) presents a photo taken on a microscope (bar scale 1 mm) where the microstructure of the surface of an in-service concrete pavement is formed by mortar (sand and cement paste). The concept presented in Figure 2-3 b) is consistent with the definition of "microtexture" given by the American Concrete Institute (Duncan et al., 1998) where the microtexture has been related to the mortar phase of concrete.

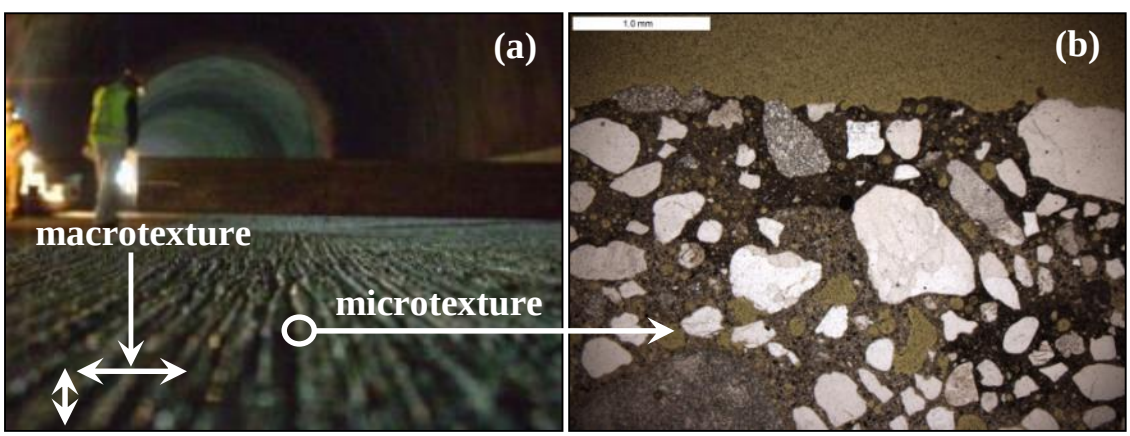

Figure 2-3: a) Concept of macrotexture and b) concept of microtexture

Figure 2-4 presents the influences on pavement-tire interactions due to texture wavelength. According to Hall et al (Hall et al., 2009-2) microtexture provides a significant contribution to on surface friction of dry pavements at all speeds and on wet pavements at slower speeds. Macrotexture

has a significant impact on the surface friction of wet pavements surfaces with vehicles traveling at higher speeds. Highway noise is affected mainly by the macrotexture of a roadway.

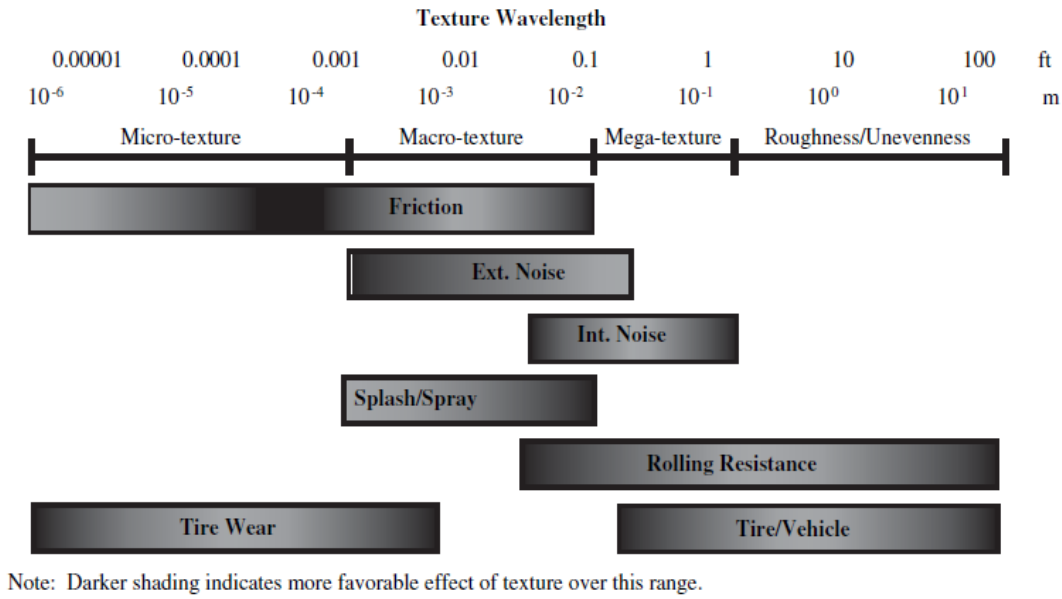

Figure 2-4: Influences on pavement-tire interactions due to texture wavelength (Adapted from Hall et al., 2009-2)

2.2.1 Friction in Concrete Pavements

Friction under wet conditions is a primary property affecting the safety of roads. The coefficient of friction between the tire and pavement is critical in providing the required Stopping Sight Distance (SSD) and the circular curve radius (R). These characteristics are both associated with the vertical and horizontal alignment of the road.

Friction can be defined as the resistance obtained by one body in moving over another (Hutchings, 1992). In a rolling movement as presented in Figure 2-5, the pavement frictional force F is the resistive force produced by the tire when it brakes over the pavement surface. According to Hutchings (Hutchings, 1992) the friction force F is proportional to the normal load W. Therefore, the mathematical expression is:

$$\mathbf{F = \mu W} \qquad \textbf{(Equation 1)}$$

Thus, the coefficient of friction, μ, can be determined by:

$$\mathbf{\mu = F / W} \qquad \textbf{(Equation 2)}$$

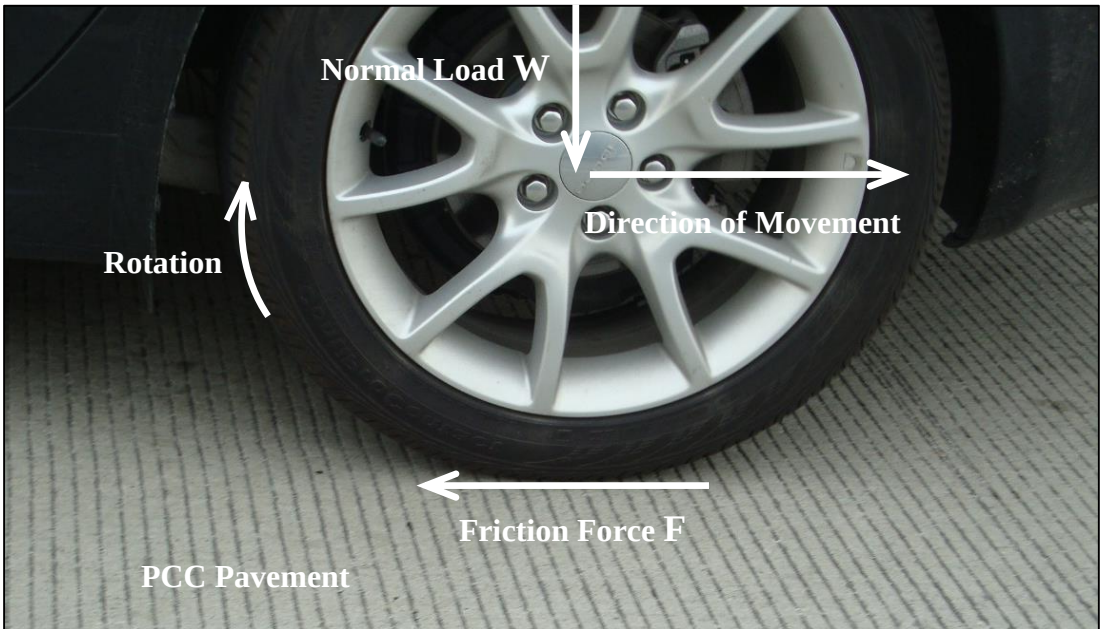

Figure 2-5 Concept of frictional force in a rolling movement (Adapted from (Hutchings, 1992) and (Hall et al., 2009-1))

According to Hall et al. (Hall et al., 2009-1), pavement friction is the result of two primary frictional force components: adhesion and hysteresis. Adhesion, established at the contact patch, is the friction resulting from the small-scale bonding/interlocking of the vehicle tire and the pavement surface; it is a function of the interface shear strength and contact area. Notice that in this definition the shear is parallel to the direction of tire movement. Cheng (Cheng & Robbins, 2010) notes that defining contact at the atomic level remains challenging. According to Gohar (Gohar & Rahnejat, 2008), adhesion occurs with the contact between asperities (contact junctions), which define the real contact area. Therefore, adhesion occurs on the atomic scale and is related to the number of atoms forming bonds (Cheng & Robbins, 2010).

The hysteresis components of frictional forces result from the energy lost due to bulk deformation of the vehicle tire. Figure 2-6 presents the friction mechanisms in the pavement–tire interaction. Other components of friction such as tire rubber shear are deemed to be insignificant (Hall et al., 2009-1). Friction can be expressed as the addition of the adhesion and hysteresis frictional forces. Both components depend mostly on the characteristics of the pavement surface, the contact between tire and pavement, and the properties of the tire. Also, because tire rubber is a visco-elastic material, the temperature and sliding speed affect both components.

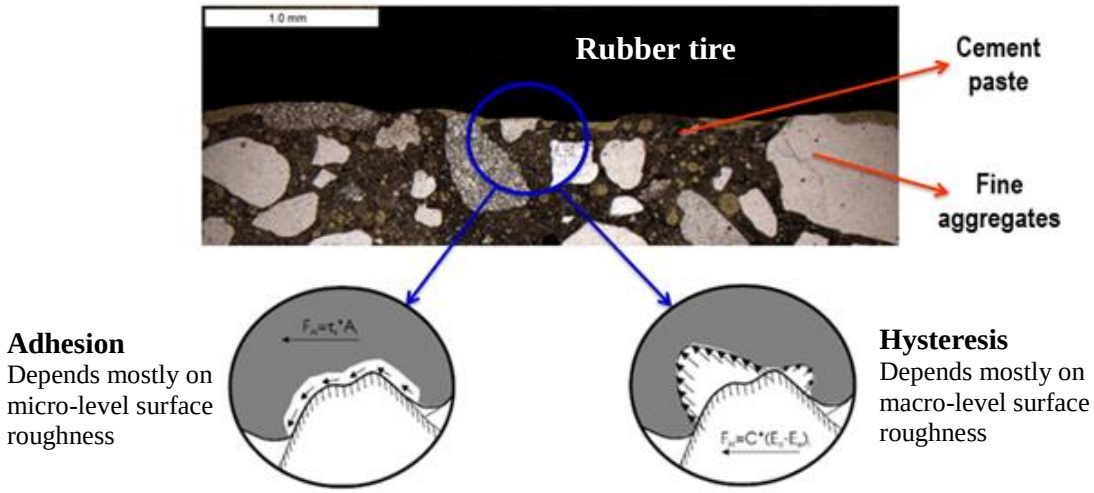

Figure 2-6: Adhesion and hysteresis in the pavement-tire interaction (Adapted from Hall et al., 2009-1).

At high speeds, the water film thickness is crucial for the friction response caused by the lubrication effect. According to Figure 2-7, the coefficient of friction, measured as a Skid Number at 40 mph (SN40) decreases exponentially as the water film thickness increases (Hall et al., 2009-1 and Henry, 2000). Also, the thicker water film causes a higher degree of hydroplaning, which is a complex phenomenon that depends on several parameters such as water depth, vehicle speed, pavement macrotexture, tire tread depth, tire inflation pressure, and contact area between the tire and pavement (Hall et al., 2009-1).

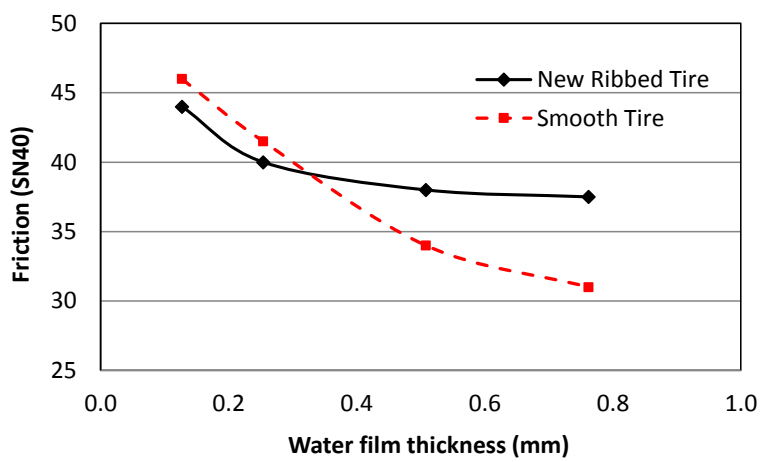

Figure 2-7: Water film thickness effect on friction measured as Skid Number (Adapted from Hall et al., 2009-1)

According to Hall (Hall et al., 2009-2) the durability of pavement's friction is governed by the polish and abrasion properties of the exposed aggregate and by the wear resistance of the mix. In concrete material, according to Kosmatka (Kosmatka et al., 2011), the paste in concrete constitutes about 25 to 40% of the total volume. Therefore, an important point to analyze in this research is whether the changes in the cement paste can affect friction, noise absorption capabilities, and friction durability on both the microtexture and macrotexture of the pavement.

2.2.1.2 Friction Response Assessment

The friction response in the laboratory and the field is often measured using the British Pendulum skid resistance tester as presented in Figure 2-8. The British Pendulum test provides a measure of the frictional properties and microtexture of surfaces (ASTM, 2008). The device contains a dynamic pendulum with a rubber friction patch. As the rubber on the pendulum slides over a surface, the device measures the energy loss. The test is performed on a wet surface and determines the British Pendulum Number (BPN) of a given sample.

Although the British Pendulum Number quantifies the overall friction response due to a microtexture response, according to Ahammed (Ahammed & Tighe, 2012) the BPN represents the response from both the microtexture and macrotexture of the surface. This research will test the friction response due to microtexture modification, therefore, to eliminate the macrotexture effects, smooth surfaces should be consider for evaluating microtextures.

Figure 2-8: British pendulum tester

The tribometer is a different and more sophisticated device than the British Pendulum Test, which can also be used to evaluate friction of a surface. The device measures the friction coefficient (μ_T) arising from nanotexture, microtexture and macrotexture properties. The experimental setup and the device description will be presented in Section 3.1.9. Figure 2-9 displays the theoretical shape of the friction coefficient versus displacement plot that is observed from the results of a tribometer. The maximum friction occurs after a short sliding distance from the origin. In Figure 2-9 it is possible to differentiate two regions (Davim, 2011): the static friction which is the force needed to overcome the potential energy between atoms in order to initiate the sliding, and the dynamic friction which is the mechanism for dissipating energy as atoms slide over each other.

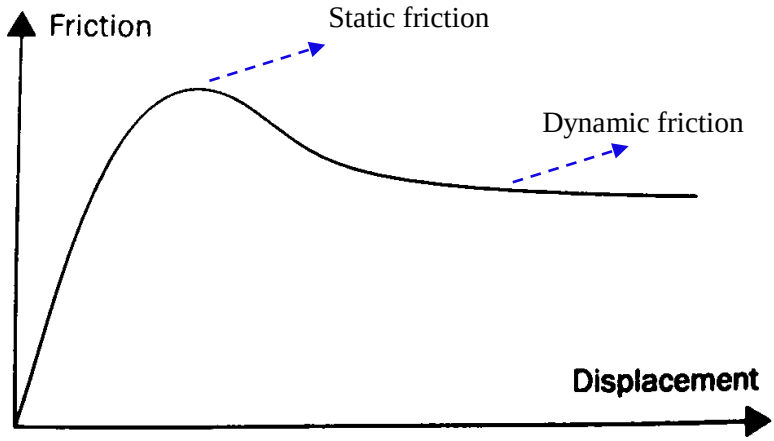

Figure 2-9: Variation of the friction coefficient with the sliding distance (Adapted from (Davim, 2011)

2.2.1.3 Surface Roughness and Surface Roughness Assessment

According to Davim (Davim, 2011), the surface interaction between two materials depends on the shape of the surface. Both the nature of the material as well as the production process will affect how smooth or rough the surface is. No matter how smooth a surface appears to be, once magnified to a fine scale, deviations in the surface smoothness exist. The surface roughness is characterized by asperities, which are the maximum peaks that occur with varying amplitudes and spacing (Davim, 2011). Therefore, the random deviation of peaks and valleys from a surface's three-dimensional topography create the surface texture of a material (Gohar & Rahnejat, 2008). Surfaces with a higher amount of asperities will

produce a higher friction response. Figure 2-10 below shows a close-up two dimensional representation of a surface texture, where the asperities can be observed.

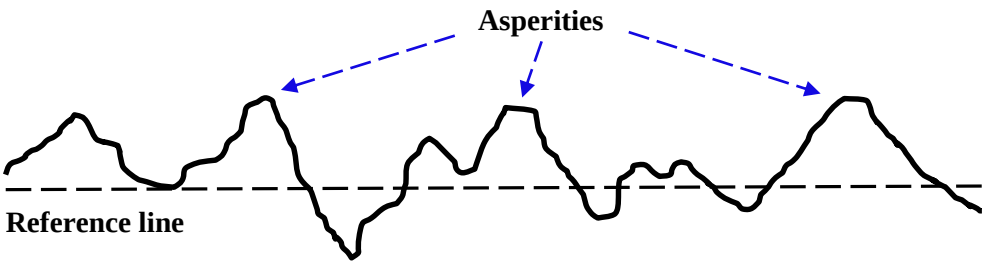

Figure 2-10: Representation of the surface roughness in 2D

A stylus profilometer is the most common technique used in assessing surface topography. The output of the profilometer can be seen in Figure 2-10. Asperities are measured from a reference line and the graph is in two dimensions. The device uses a fine stylus which is dragged over a surface; the displacement of the stylus is translated into an electric signal. This signal is calibrated to the displacement of the stylus, and amplified to a chart recorder (Figure 2-11). The chart recorder then provides the profile of the surface as shown in Figure 2-10 (Davim, 2011 and Hutching, 1992).

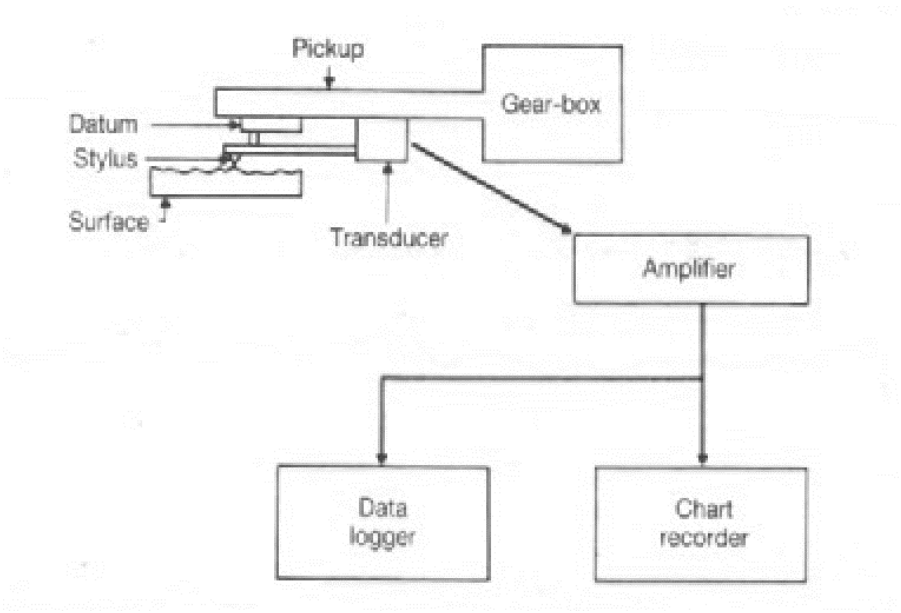

Figure 2-11: Components of a typical stylus surface-measuring instrument (Adapted from Hutching 1992)

2.3 Noise Generation in Concrete Pavements

Sound results from small pressure variations in the air and can be desirable or undesirable. Undesirable sound is typically referred to as noise and the sound produced by the interaction between the tire and pavement is an example of this (Bernhard, 2005).

Currently, traffic noise is an important concern for people's health and affects the economy of a country (Ahammed, 2009). This is because noise can produce negative health effects such as hearing loss, high blood pressure, hypertension, and sleep disturbance, to name a few. These effects produce an impact on the people's quality of life and therefore on their productivity. Under accelerating conditions, the tire-pavement noise dominates over other sources of roadway noise, such as engine and braking noise.

According to Bernhard (Bernhard, 2005) the main mechanisms behind noise generation in pavements are summarized in Figure 2-12 and as follows:

- **Tread impact:** This refers to the impact between the tread block and pavement surface when a wheel is in movement. This mechanism can be compared to a rubber hammer impacting the pavement material and causing vibrations on impact and therefore noise.
- **Air pumping:** This dynamic interaction occurs in the contact patch and is generated by air compression. It is similar to the sound generated by clapping hands.
- **Slip-stick:** Tractive forces between the tire and pavement will also produce noise when the horizontal forces exceed the limits of friction. The tire block then slips briefly and later re-attaches to the surface pavement. The mechanism is similar with the squeaking sound produced by athletic shoes on a gym floor.
- **Stick-snap:** Due to the adhesion between the tire rubber and the pavement surface, the adhesive forces clamp the tread block. When the tread block releases, it creates noise and vibrations. This mechanism can be compared to releasing a suction cup.

2.3.1 Tools to Measurement the Tire-Pavement Noise Generation and Noise Absorption

Several options are available to measure the noise production in pavements. Statistical Passby Method (SPB), Controlled Passby Method (CPB), Closed Proximity Method (CPX), and the On-Board Sound Intensity (OBSI) Method are examples of methodologies used to measure noise in the field. In terms

of noise absorption properties, the Impedance Tube Method is the most common laboratory test used and as such, it was used in this research. The OBSI, CPX and the Impedance Tube Method are described in the following sections.

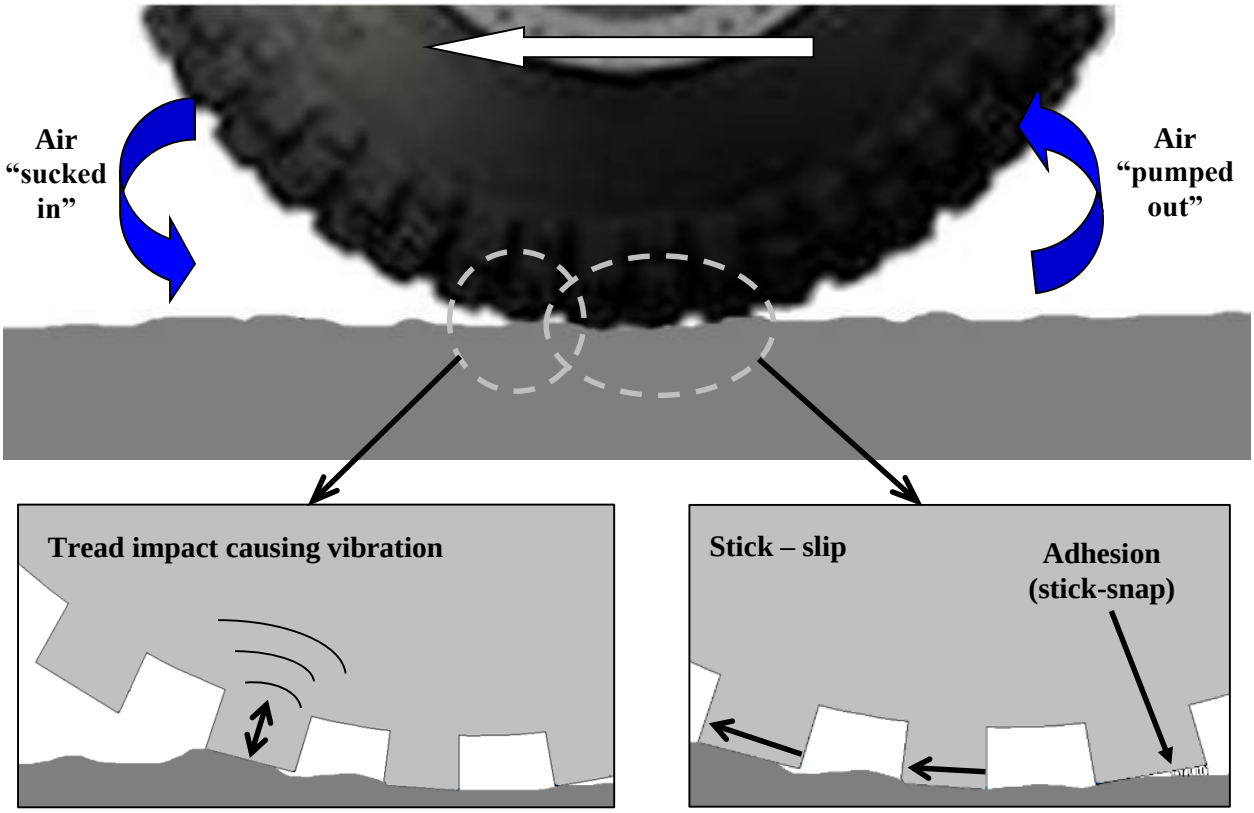

Figure 2-12: Source generation mechanism (Adapted from (Bernhard, 2005))

2.3.1.1 On-Board Sound Intensity (OBSI) Method and Closed Proximity Method (CPX)

Although several devices are available to determine the noise level in roads, Donavan (Donavan & Lodico, 2009) indicates that the primary tools to evaluate the sound production at the source are the Closed Proximity Method (CPX) and On-Board Sound Intensity (OBSI) method. The OBSI method can use either a single or double sound intensity probe. Figure 2-13 shows the OBSI and CPX setup which is owned by the Centre for Pavement and Transportation Technology (CPATT) at the University of Waterloo. Figure 2-13 a) shows the microphone's position with respect to the tire and Figure 2-13 b) illustrates the configuration used to perform field measurements. This configuration allows the measurement of noise at the tire-pavement interaction when a car drives across a pavement section.

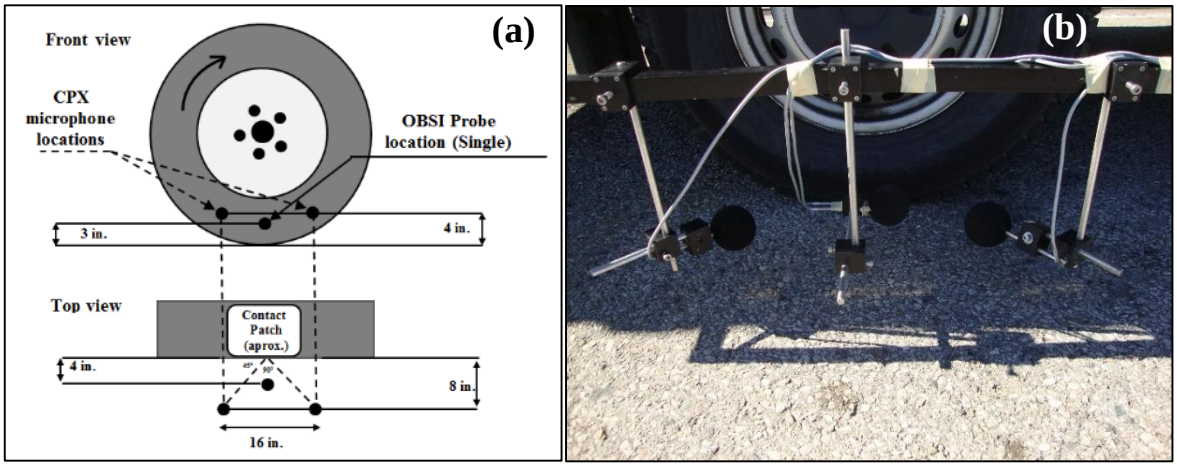

Figure 2-13: a) On-Board Sound Intensity (OBSI) and CPX microphones locations and b) picture from the configuration owned by CPATT (microphones with windscreens)

According to Otto (Otto et al., 2011) the OBSI method is able to measure the sound intensity as defined by the acoustic power per unit area (units Watts/m^2). The first standard was developed by AASHTO in 2008 as a provisional standard called "Standard Method of Test for Measurement of Tire/Pavement Noise Using the On-Board Sound Intensity (OBSI) Method" (AASHTO TP-76, 2013).

According to Otto (Otto et al., 2011), the main factors to be controlled during the testing include:

- **The test tire**: The OBSI standard specifies a Standard Reference Test Tire (SRTT) (P225/60R16) however, the NGCS research was performed with a Goodyear Aquatred 3 tire (Scofield, 2011). Differences in the tread pattern and rubber properties can affect noise measurements, and the SRTT is typically quieter as compared with the Goodyear Aquatred 3.
- **Vehicle speed**: The standard speed is 96 km/h or 60 mph. If noise cannot be measured at 96 km/h a correction factor may be applied for speed variations less than $\pm$ 3 mph. For speed variations greater than this, errors can be accounted for in the calculations.
- **Vehicles noises**: External noises such as squeaking caused by the vehicle braking must be avoided because these can contaminate the intensity level.

OBSI can be reported as a single overall sound intensity level (value in dBA) or if frequency is included, as a value on the sound intensity spectrum. CPX allows for measuring the sound pressure level and the CPATT's device meets the ISO/CD 11819-2 standard but does not include an acoustic enclosure (i.e., trailer).

2.3.1.2 Impedance Tube Method

The impedance tube method measures the sound absorption coefficient of a material. The absorption coefficient is an indicator of how well a material can absorb sound. When a sound wave reaches a pavement surface, a portion of the sound energy is reflected and the remaining portion is absorbed. The ratio between the absorbed energy and the total incident energy is the absorption coefficient. The ratio is between zero and one, where one means 100% absorption. Pavement material absorption coefficient is related to the noise production because the highest absorption coefficient will generate less noise overall. Figure 2-14 shows the Impedance Tube which is owned by the CPATT at the University of Waterloo.

Figure 2-14: Impedance Tube Equipment

The impedance tube test is performed in accordance with ASTM E1050-10 (ASTM, 2010). The arrangement includes the analyzer, the tube, the sample, two microphones and a power source. The tube has a speaker at one end while the sample is placed at the other end. The sound signal is generated by the speaker and it travels to the sample. Both microphones measure the sound energy lost and based on this result the absorption coefficient can be calculated.

2.4 Next Generation of Concrete Surface

According to Scofield (Scofield, 2011), the Next Generation Concrete Surface (NGCS) is the most recent concrete pavement texture in the United States. The NGCS has the quietest texture developed for conventional concrete pavements, mainly through macrotexture modification. The construction process uses conventional diamond grinding equipment and blades, but with a different configuration in the drum. The NGCS development was initiated using the Tire Pavement Test Apparatus (TPTA)

located at Purdue University as shown in Figure 2.15 a). Figure 2.15 b) shows the diamond grinding head being used at a laboratory scale to produce different texture configurations.

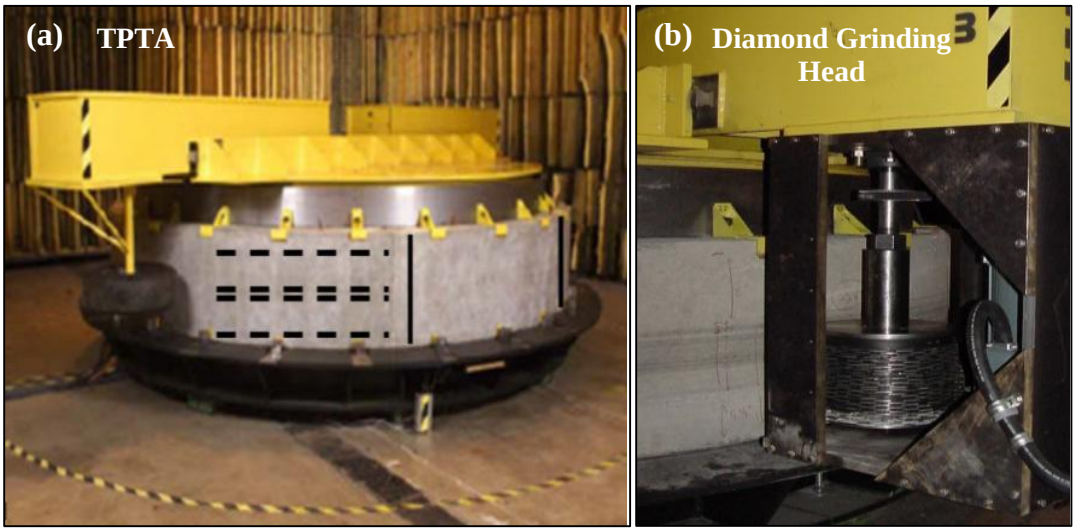

Figure 2-15: a) Purdue Tire Pavement Test Apparatus (TPTA) and b) diamond grinding head (Adapted from (Scofield, 2011))

The Minnesota Department of Transportation (MnDOT), Arizona DOT, Illinois DOT and ACPA developed field applications to verify the benefits of the NGCS. Currently at least 13 sections are in evaluation across the USA; Figure 2.16 shows a picture of one example of NGSC developed by MnDOT.

Figure 2-16: NGCS LITE test strip at MnROAD (Adapted from (Scofield, 2011))

Different studies have shown that the controlling factor in noise generation is the fin profile on the surface (Anderson et al., 2014). Positive textures (ridges) were shown to produce more noise compared

with negative textures (valleys). Thus, an appropriate way to reduce noise in PCC pavements is to have negative textures while grinding in a uniform transversal and longitudinal profile. This is the main principle behind the design of Next Generation Concrete Surface (NGCS).

Figure 2-17 presents the results of noise evaluation using the OBSI method in the states of Minnesota and Kansas, as well as in the province of Ontario. The tested concrete surface types included transverse tining, longitudinal tining, exposed aggregate and conventional diamond grinding. Transverse tining has been measured to be the loudest of the textures with the noise generated at intensities between 104 – 106 dB. Specifically, according to Figure 2-17, transverse tining in Ontario is one of the noisier surface textures. Longitudinal tining is second loudest with decibel levels of 102 dB. According to Figure 2-17 Next Generation Concrete Surface (NGCS) is the quietest (100 – 101 dB range) in comparison to the conventional pavement.

Potential improvements to the Ontario road network in terms of noise reduction may be further examined by local researchers. However, given snow and ice conditions in Ontario winters, the ability to change the texture to optimize noise and improve durability may be limited.

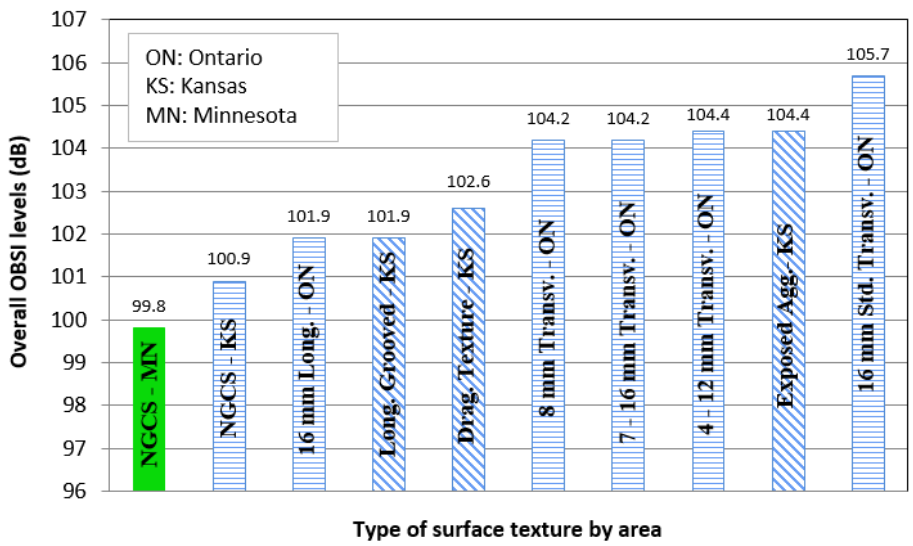

Figure 2-17 Sound Intensity Level with OBSI method in different states or provinces (Adapted from (Scofield, 2011) and (Byrum et al., 2010))

A report published in January 2014 by the Washington State Department of Transportation (WSDoT) summarized their experiments using NGCS (Anderson et al., 2014). Their objective was to investigate the long-term pavement performance of NGCS when compared to conventional diamond

grinding (CDG). In this study, NGCS was compared with CDG and installed in 2010 on Highway I-82 in Sunnyside, Washington.

For the field tests, the NGCS was constructed and installed using two methods, single pass and two pass. In the single-pass method, the pavement surface is ground smooth and cut all in one pass. The two-pass method involves grinding the surface in one pass and then cutting the grooves in a separate pass. It is common to use the two-pass method if the surface is particularly hard to cut. Figure 2-18 presents pictures showing the CDG and CDG plus grooving. The test section was two lanes wide and 1500 ft long. On each lane, the first portion in the direction of traffic is CDG and the second portion is NGCS. The cost of building the NGCS was $12.75/square yard compared with a statewide average of $8.26/square yard for CDG. Noise data was measured and observed for a period of 2.5 years, from November 2010 until April 2013 (Anderson et al., 2014).

Figure 2-18: Conventional diamond grinding (CDG) and grooving

The noise data from the study showed that at the beginning, in November 2010, there was about a 3 dB difference between the NGCS and CDG on both lanes. In Lane 1 the respective noise levels of the NGCS and CDG sections were 101 dB and 104 dB. In Lane 2, these levels were 99 dB and 103 dB, respectively. However, by April 2013, the NGCS was no longer quieter than the CDG. In fact, the NGCS and CDG had both increased to the same noise levels of approximately 105 dB and 103 dB in Lane 1 and Lane 2, respectively. Lane 2 was the passing lane, thus it is used less which explains the difference between the two lanes (Anderson et al., 2014).

The NGCS most likely performed worse over time due to the degradation of the surface from long-term interaction with the tires. It should be noted that studded tires were used in this specific project.

Images taken at the end of the two year period show a vast contrast from the surface at the beginning. From the images, one can clearly see pieces of aggregate missing from the road. It can also be seen that the flush surface is no longer smooth and resembles positive textures.

Thus the WSDOT concluded that the performance of NGCS cannot be maintained in the long-term, despite initial noise reduction. The NGCS surface was found to eventually wear down and perform similarly to CDG, and WSDOT decided that NGCS was not a viable option. The WSDOT report identified that the benefits of noise reduction from NGCS is not sustainable in the long-term unless a solution to reduce the wear of the pavement surface can be found.

2.5 Main Distresses on PCC Surfaces Affecting Surfaces Characteristics

Since friction and noise production are two properties dependent on the surface characteristics of a PCC pavement, this section will cover the main distresses that can affect rigid pavement surfaces, including stressors present in Canadian climates.

2.5.1 Freezing and Thawing and Scaling

Freezing and thawing is the terminology used to describe the action as well as destruction that occurs in concrete over time when water in exposed concrete freezes and thaws repeatedly, creating a cumulative effect. Overall, this destruction is caused by the 9% volume increase associated with water when it turns from a liquid to solid (ice). This expansion occurs in the paste, aggregates, or both (Kosmatka et al., 2011). When freezing and thawing occur in the presence of deicers, localized failures or mortar degradation of the exposed surface arise; this phenomena is called “scaling” (Lamond & Pielert, 2006). Aggregates susceptible to scaling can generate popouts and D-Cracking, which is damage in the form of a D-shape that is often observed near to joints.

Even though there is an extensive amount of published literature on this subject, the mechanisms behind freezing and thawing and salt scaling are complex and still not fully understood (Kosmatka et al., 2011). Their effects can be detrimental to pavement performance, ride quality, safety, and noise production.

There are a few theories that explain the distressing of PCC materials subject to freezing and thawing (Lamond & Pielert, 2006). The water freezes into layers of ice, and these layers grow bigger as water travels towards it. Later on, the hydraulic pressure theory indicates that water will move away from the frozen areas. Investigations show that when this water is displaced from the area of freezing, it creates

a pressure against the cement. When the water flow is longer than a critical length, the pressure becomes greater than the resistant strength of the cement paste, and thus, the cement is damaged. This happens when the water content is higher than the concrete's critical saturation point.

Another theory, termed the osmotic pressure hypothesis, reasons that water does not just flow away from areas of freezing (Lamond & Pielert, 2006). It has been shown that at a uniform temperature of concrete, the water in the pores will freeze at different stages dependent on the size of the pore. The smaller the pores, the lower the freezing temperature of the water in those pores. The frozen pores have a higher water concentration which causes water to move from unfrozen areas to the frozen areas to reduce the concentration gradient. Further studies show that the cement paste and aggregates in the concrete must be considered separately. This is because water will be excreted from the aggregates and the paste will take the pressure from this water.

Concretes that experience freezing and thawing will often be exposed to de-icing chemicals. Scaling occurs when these de-icing chemicals lead to localized failures of the exposed surfaces or "surface mortar deterioration" (Lamond & Pielert, 2006). Scaling occurs due to freeze and thawing, as the chemicals are not strong enough to deteriorate the surface without the cyclic freeze and thaw action. This is also due to concentration gradients. De-icers have a lower freezing temperature than water and increase the water concentration gradient, causing water to move from areas of low concentration to high concentration.

Special considerations also apply to individual particles of some coarse aggregates. Since porous aggregates can absorb water they often expand due to the effect of freezing. Low porosity aggregates or aggregates with capillary systems interrupted by a sufficient number of macropores are not vulnerable (Neville, 1996). If a vulnerable particle is close to the PCC pavement surface, it can cause a popout.

D-Cracking is another type of failure associated with vulnerable aggregates. This failure can occur in PCC roads, bridges, and airfield PCC pavements. D-Cracking consists of the development of fine cracks near the free edges of slabs. The initial failure starts lower in the slab where moisture accumulates and the coarse aggregates become saturated to the critical level. Therefore, the failure essentially starts in the aggregates, but the freezing and thawing cycles increase the degree of saturation and finally cause the damage in the surrounding mortar (Neville, 1996). Figure 2-19 presents pictures that show the scaling distress, the popouts, and the D-Craking distress in PCC Pavements.

Figure 2-19: a) Scaling b) popouts and c) D-Crakings distresses in PCC pavements

ASTM C666 (ASTM, 2008) is the standardized test for freeze and thaw durability of concrete. The test is a rapid test as it allows four to twelve cycles to take place in a 24-hr period. Increased concerns for scaling on highways and bridge deck pavements led to the standardization of ASTM C672 (ASTM, 2012). The methodology of ASTM C672 uses blocks of concrete or mortar and a dike placed around the surface so that ponding of the de-icers can occur (Lamond & Pielert, 2006). Both standard methods are covered in the next chapter.

2.5.2 Abrasion

According to Lamond (Lamond & Pielert, 2006) the factors affecting concrete´s abrasion resistance are: the quality of aggregates, compressive strength, water/cement (w/c) ratio, type of concrete finishing procedures, curing methods and surface treatments. The use of hardened coarse aggregates has a strong influence on abrasion resistance. For instance, high-quality quartz will increase wear resistance (ACI, 2008). Compressive strength is one of the most important factors affecting abrasion resistance; according to Lamond (Lamond & Pielert, 2006) for the same type of aggregates and finishing, abrasion resistance increases with an increase in the concrete's compressive strength. The w/c ratio is also responsible for the abrasion response, because for the same types of aggregates, abrasion response is improved when the w/c ratio is decreased.

Macrotexture in concrete pavement can be related to the pavement´s ability to drain surface water and also affects the hysteresis component of frictional force. According to Hall (Hall at al., 2009-2) macrotexture durability is dependent on cumulative traffic; however, no specific relation is reported based on concrete mix properties. Macrotexture durability is related to a reduction in texture depth (Hall at al., 2009-2). Because of this, abrasion response may affect the durability of a macrotexture, and

therefore a better abrasion response can be beneficial for the hysteresis component of frictional force in the long term.

2.6 Nanotechnology and Nanoconcrete

Nanotechnology involves manipulating matter and materials at scales below 100 nm. According to Grove, nanotechnology could be a revolutionary tool for engineering applications (Grove et al., 2010). Nanotechnology is revolutionary because it allows us to take advantage of different material properties that appear at the nano scale which is the boundary between atoms and molecules at the macro level (Ashby et al., 2009 and WIN, 2013). Also, it is revolutionary because the atomic scale is where the fundamental behaviors and material properties are dictated (Ashby et al., 2009). In addition, reductions in particle size can increase the specific surface area of materials which can have a significant impact. Figure 2-20 shows the range of specific surface areas for different materials used in concrete.

Regarding the constituent materials of concrete, the Strategic Development Council from USA states that there exists a variety of research needs to improve "energy efficiency, productivity, and the performance of concrete and concrete products" (Strategic Development Council, 2002). These research needs may be categorized into three groups: new materials, measurement and prediction, and reuse and recycling. Nanomaterials can be considered as new materials.

Nanoconcrete may be defined as a concrete made of Portland cement which uses particles with sizes smaller than 500 nm as a cementing agent (Sanchez & Sobolev, 2010 and Balaguru & Chong, 2006). The most important reasons to consider incorporating nanotechnology into concrete are to control material behaviour, achieve superior mechanical and durability performance, and provide novel properties in concrete such as low electrical resistivity, self-sensing capability, self-cleaning, self-healing abilities, high ductility, and self-control of cracks (Sanchez & Sobolev, 2010).

The application of nanotechnology in a variety of fields is receiving extended attention (Gopalakrishnan et al., 2011). In concrete materials, the applications have been reduced (compared with the applications of supplementary cementitious materials), but the results are promising because the innovations in experimental techniques and advances in computational modeling and simulations allow for better understanding of the fundamental behaviour of nanoconcrete.

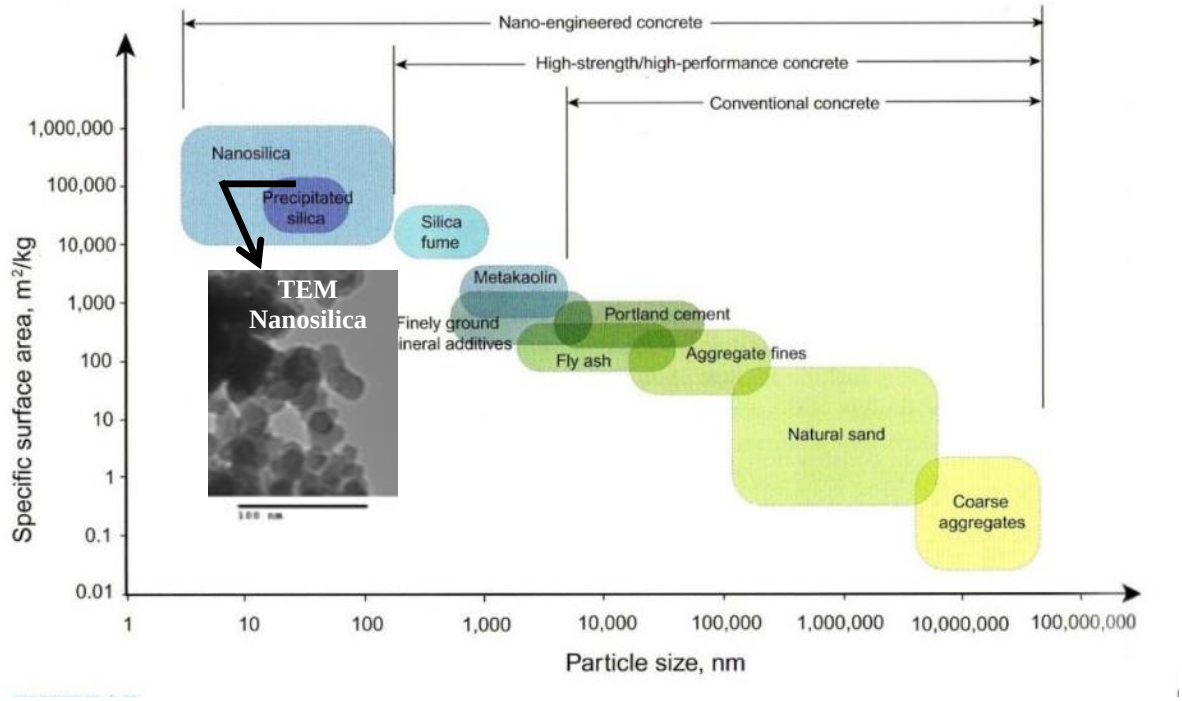

Figure 2-20: Specific surface areas of different concrete material components, Nano-engineered concrete definition and TEM image of nanosilica (Adapted from (Ashby et al., 2009))

Currently it is possible to identify a variety of nanomaterials available to enhance concrete properties, most of which can be applied to improve the upper layer of concrete pavements. The literature survey identified the following nanometarials that may be used in concrete materials and therefore in rigid pavements. They are nanosilica (Nano-SiO_2), carbon nanotubes (CNTs), nanofibers, nano titanium dioxide (Nano-TiO_2) and coatings to mimic the lotus leaf effect. Table 2-7 presents a summary of the effects of nanomaterials on concrete performance and the effects in concrete that can be potentially be investigated for PCC pavement applications.

The next sections present descriptions of the main nanomaterials used in concrete and their effects on the properties and durability of concrete.

2.6.1 Nanosilica (Nano SiO_2)

To date, nanosilica is the most thoroughly investigated nanomaterial for use in concrete. The main chemical component of nanosilica is silicon dioxide (SiO_2) which can be present in crystalline and amorphous forms. The amorphous nanosilica is most commonly used in nanoconcrete (Quercia et al., 2012). Nanosilica has spherical morphology and its particles' size is variable. According to Quercia

(Quercia et al., 2012), the particle size varied in the range of 5 to 658 nanometers in six different nanosilica products.

Table 2-7 Nanomaterials descriptions, main effects on hardened concrete and effects that can potentially be investigated

Type of nanomaterial	Description	Main effects investigated in concrete	Effects in concrete to be investigated
Nanosilica	SiO_2	Improve compressive strength, flexural strength and abrasion	Frictional and noise absorption response
Carbon nanotubes	Carbon (C) atoms interconnected together by C-C bonds	Improve compressive strength, flexural strength and fracture toughness	Frictional and noise absorption response. Abrasion
Carbon nanofibers	Nanofibers are fibers with a diameters of less than 100 nm	Improve compressive strength, flexural strength and fracture toughness	Frictional and noise absorption response. Abrasion
Nano titanium dioxide	TiO_2	Enhance compressive strength, flexural strength and abrasion	Frictional and noise absorption response
Nano lotus leaf	Generally used as coating	Response as self-cleaning surface	Frictional and noise absorption response

Nanosilica is available in powder and slurry forms. The slurry form is attractive in order to mitigate health problems caused by inhalation. Figure 2-21 presents a Transmission Electron Microscope (TEM) image of a commercially available nanosilica, where the sphericale morphology is very clear.

According to Chung (Chung, 2002 and 2004), silica fume in concrete can improve the sound absorption ability of the material by increasing vibration damping capacity. Nanosilica may show a similar effect. In materials, damping requires energy dissipation. In terms of acoustics, this means that certain materials can absorb noise or sound.

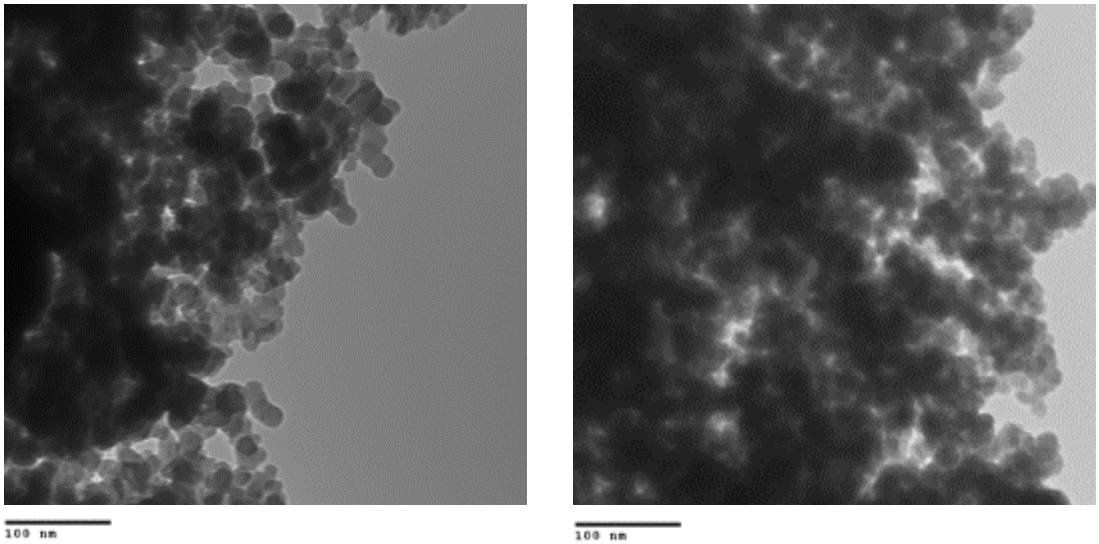

Figure 2-21: Transmission Electron Microscope (TEM) images of nanosilica

2.6.2 Carbon Nanotubes

Carbon nanotubes (CNTs) were discovered in Japan by Sumio Ijima during Transmission Electron Microscopy (TEM) observation in 1991 (Ashby et al., 2009). The discovery was accidental and was due to an electrical discharge between two carbon electrodes. CNTs can be defined as cylindrical molecules with a diameter of approximately 1 to 3 nm and a length typically lower than 3 μm. CNTs are made of carbon atoms interconnected together by carbon-carbon (C-C) bonds (Al-Rub, 2012). Based on the manufacturing conditions, CNTs can be generated as single-walled, double-walled or multi-walled structures. The hexagonal structure of the carbon lattice in the CNTs results in a very strong structure. Single-walled and multi-walled CNT's morphologies are presented in Figure 2-22. Multi-walled carbon nano-tubes (MWCNT) are less expensive and more readily available than single-walled carbon nano-tubes (SWCNT) (Makar, 2011).

Carbon nanotubes have several exceptional properties (Ashby et al., 2009): very high Young´s modulus of 1000 GPa, high tensile strength of 30 GPa, superior current densities of 10^9 A/cm^2, and high thermal conductivity of 6000 W/mK. CNTs possess better material properties than carbon nanofibers and according to the National Research Council of Canada (NRCC) they are ideal reinforcing materials for concrete (Makar, 2011).

It is recognized that MWCNT can act as sound dampers because the interfacial sliding between tubes creates frictional energy dissipation which leads to enhanced damping characteristics (Ashby et

al., 2009). Therefore, carbon nanotubes may potentially absorb noise in PCC pavements; however the application as a noise mitigation alternative has been unexplored. At the same time, the potential impact on surface friction has been also unexplored.

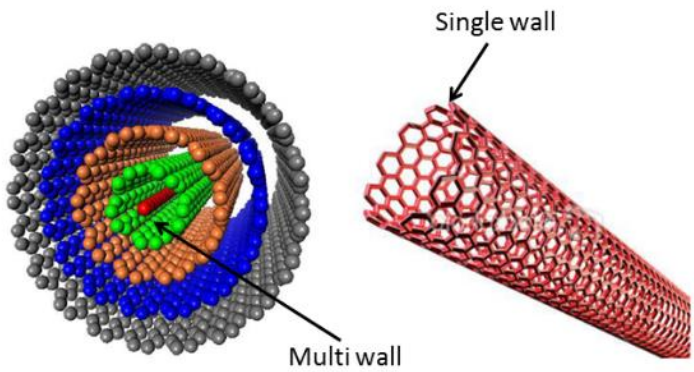

Figure 2-22: Single-walled and multi-walled CNTs (Adapted from Al-Rub, 2012)

2.6.3 Carbon Nanofibers

Carbon nanofibers (CNFs) play a very significant role in cement concrete because of their extraordinary and useful properties, such as exceptional tensile strength, high stiffness, low density, good chemical stability, and high electrical and thermal conductivity (Zhang et al., 2007). CNFs (Figure 2-23) have cylindrical nanostructures with diameters less than 100 nm. Also, Tyson (Tyson et al., 2011) reported that CNFs possess a Young´s modulus of 400 GPa and a tensile strength of 7 GPa.

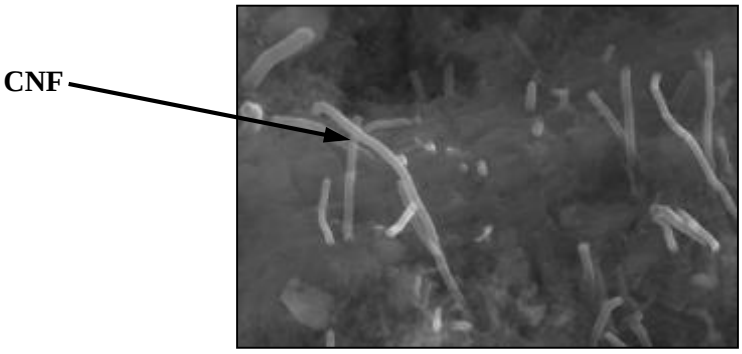

Figure 2-23: Scanning Electron Microscope (SEM) image of CNF-composite (Adapted from Gay & Sanchez, 2010)

In nanoconcrete, the exceptional properties of CNFs as well as CNTs are utilized through mixing process engineering which ensures the nanofilaments' dispersion in the paste matrix and the bond

strength between the matrix and surface of CNFs or CNTs. The proper dispersion of CNFs is shown in Figure 2-23. Relevant research is included and discussed in the following sections.

2.6.4 Nano Titanium Dioxide (Nano-TiO_2)

Titanium dioxide (TiO_2) is the naturally occurring oxide of titanium. In nature, it is present in the following minerals: rutile, anatase and brookite. TiO_2 has historically been used in a wide range of applications such as paints, cosmetics, and drugs because of its low toxicity, semi-conductivity, high chemical stability, availability, and low industrial cost (Hamdy et al., 2011). TiO_2 can also be supplied as nano titanium dioxide (Nano-TiO_2), which is most widely used as a photo-catalyst due to its extraordinary photo-catalytic activity (Chen & Poon, 2012). It has also been used in concrete (Chen & Poon, 2012, Jalal et al., 2012 and Diamanti et al., 2008) to increase strength, abrasion and chloride penetration.

2.6.5 Nano Lotus Leaf

The literature survey also reveals that some coatings can mimic the lotus leaf effect, which exhibits an exceptional ability to keep itself clean and dry due to the lotus effect (Sobolev & Gutierrez, 2005). In recent years, the use of lotus fundamentals and hydrophobic effects has received growing attention all over the world. Current research has indicated that the lotus leaf has some self-cleaning properties.

The self-cleaning properties are believed to be related to the special surface structure and low free surface energy (Mozumder et al., 2011, Kumar et al., 2011 and Su et al., 2010). The waxiness (greasiness) also provides a hydrophobic surface. The contact angle between the water droplet and surface usually remains at less than 30° for most of the hydrophilic surface (Forbes, 2008). However, for a hydrophobic surface, the contact angle can increase to greater than 90° (Forbes, 2008), thus decreasing the contact area between water droplet and surface. The minimization of the contact area between water droplet and leaf surface causes water droplets to easily roll off the leaf (Mozumder et al., 2011 and Forbes, 2008)). This phenomenon is well known as the 'lotus effect'. The concepts of hydrophobic and hydrophilic surfaces are presented in Figure 2-24, where γ_{lV} is liquid-to-vapor surface tension, γ_{lS} is liquid-to-solid surface tension, and γ_{SV} is solid-to-vapor surface tension. Also, the angle θ corresponds to the contact angle (Ashby et al., 2009). The lotus effect contributes to non-wetting, super water repellent, and super hydrophobic surfaces and thus enhances self-cleaning properties (Mozumder et al., 2011, Kumar et al., 2011 and Su et al., 2010).

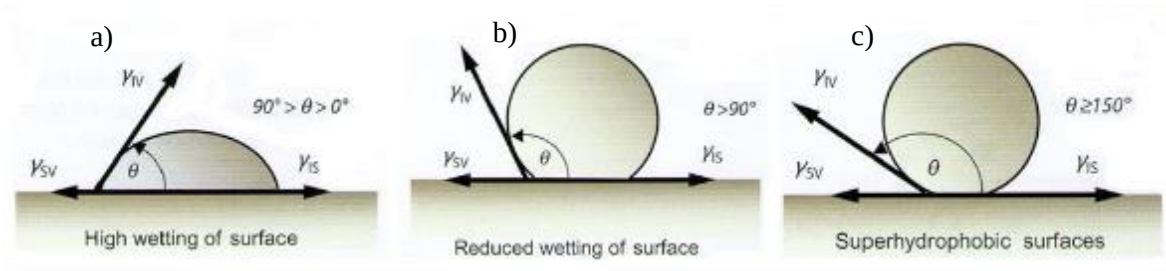

Figure 2-24: (a) Hydrophilic surface, (b) hydrophobic surface, and (c) super hydrophobic surface (adapted from (Ashby et al., 2009).

The super hydrophobicity of a lotus leaf surface does not only result from its waxiness, but also depends on the microstructure and nanostructure of the surface (Mozumder et al., 2011 and Forbes, 2008). The combination of microstructure and nanostructure causes the contact angle to exceed 150° and the sliding angle to be less than 10° (Mozumder et al., 2011 and Forbes, 2008).The double-scale structure contains micro-bumps that are 5 to 9 μm in diameter, nano-branches on the micro-bumps, and the area between every two bumps that are around 124 nm in diameter (Forbes, 2008). In this case, water forms spherical droplets on the leaf surface with very little contact area (Forbes, 2008). Indeed, the contact angle will continue to increase due to the air trapped between water droplet and leaf surface (Forbes, 2008). Figure 2-25 presents two pictures that illustrate the nano geometry of the lotus leaf surface.

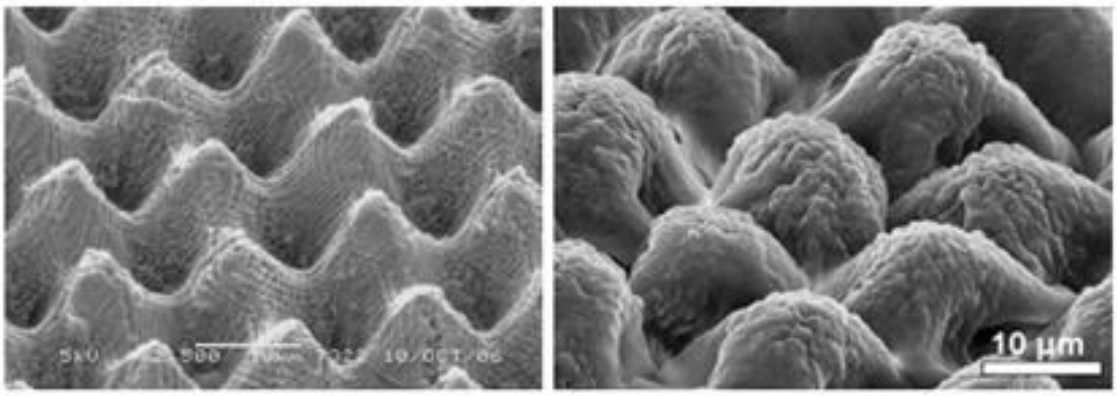

Figure 2-25: (a) Lotus leaf nano-geometry in polymer surface (phys.org, 2012) and (b) nanostructure in artificial petal surface (Park et al., 2011)

2.6.6 Effects of Nanomaterials on Different Characteristics of Concrete

Based on the literature review, nanomaterials influence both the fresh and hardened properties of concrete. The effects of nanomaterials on the fresh properties, cement hydration, microstructure, pore-structure, mechanical properties, and durability of concrete are summarized in the following sub-sections.

2.6.6.1 Effects on fresh concrete properties

The fresh properties of concrete are affected by the particle size distribution of constituent materials. Therefore, nanomaterials are expected to influence the fresh concrete properties due to their extremely small particle sizes. The research findings of Quercia (Quercia et al., 2012) showed that nanosilica significantly reduces the workability of concrete for a given water content due to high specific surface area. A similar effect was also observed in the case of nano-TiO_2 (Chen & Poon, 2012). This suggests that the water demand is strongly related with the specific surface area of nanomaterials. Quercia (Quercia et al., 2012) stated that a higher amount of water is needed for a constant workability when the surface area of nanosilica is increased. Nanosilica produces higher plasticity than traditional cementitious materials, it can improve the cohesiveness of the concrete and thus reduce the bleeding and segregation (Quercia et al., 2012).

Nanomaterials can significantly influence the rheology and stability of concrete. According to Jalal (Jalal et al., 2012), nano-TiO_2 is able to modify the rheological properties of self-compacting concrete. The rheological properties were studied through slump flow time and diameter, V-funnel flow time, and L-box tests. Nano-TiO_2 powder improved the consistency and homogeneity of the fresh concrete mixture which exhibited less bleeding and segregation. This is because nano-TiO_2 acts as filler in the mixture and improves the resistance to water movement in fresh concrete.

Certain nanomaterials might influence the setting of concrete. For example, the addition of nano-TiO_2 increases the overall fineness and decreases the setting time of concrete. This is related to the acceleration of the hydration process and associated heat release. Hydration heat peak increases when the nano-TiO_2 is added into the cement. The particle fineness and specific surface area play a dominant role in enhancing the dissolution rate of cement compounds at the early stage of cement hydration, thus increasing the rate of heat release (Chen & Poon, 2012).

CNFs and CNTs were reported by several authors (Al-Rub, 2012; Gay & Sanchez, 2010; Makar, 2011) to have dispersion problems, which negatively affect the fresh properties of concrete. According

to Nasibulina (Nasibulina et al., 2010) it is difficult to achieve homogeneous dispersion of CNTs and CNFs in concrete mixtures as they are prone to agglomerations. The attraction between particles of CNFs/CNTs due to Van der Waals forces might be responsible for these agglomerations however, the proper use of surfactants or ultrasonic mixers allows for adequate dispersion. Also, the use of high-range water-reducing admixture has also been successful in disaggregating the CNFs, thus improving the dispersion of nanofibers in the cement matrix (Gay & Sanchez, 2010).

2.6.6.2 Effects on cement hydration

The incorporation of nanomaterials such as nano-SiO_2, CNTs and nano-TiO_2 can positively influence the hydration reactions and the physical structure of C-S-H in cement (He & Shi, 2008; Makar, 2011; Chen & Poon, 2012). Using a Field Emission Scanning Electron Microscopy (FESEM), He and Shi (He & Shi, 2008) explained that nano-SiO_2 not only makes a more dense material but can also change the morphology of hydrated cement by producing more Type II C-S-H gel and less ettringite crystals. According to Ashby (Ashby et al., 2009), the drastic increase in surface area associated with nanosilica addition to concrete can affect the surface energy, morphology and the chemical reactions in concrete. The high specific surface area of nanosilica compared with other concrete materials is shown in Figure 2-20. Because of the low particle size and high surface fineness, nanosilica contributes to the creation of small-size crystals and clusters of calcium silicate hydrate (C-S-H) during pozzolanic reactions.

Like nanosilica, adequately dispersed SWCNT can also accelerate the hydration process compared with the control concrete (Makar, 2011). This is possibly due to SWCNTs acting as nucleating sites for C_3S hydration reactions, with the C-S-H forming directly on the SWCNT. Moreover, SWCNTs produce an increase in the maximum heat flow which may also enhance the hydration of cement in concrete. Furthermore, the incorporation of nano-TiO_2 in powder form can significantly accelerate the rate and degree of hydration at early stages by promoting the formation and precipitation of hydration products (Chen & Poon, 2012).

2.6.6.3 Effects on microstructure and pore-structure of concrete

Nanoparticles can potentially allow better void filling and positive filler effects due to the extremely low particle size in comparison with conventional materials of concrete (Ashby et al., 2009); the filler effects produce a concrete microstructure with improved density and reduced porosity (Sanchez & Sobolev, 2010). According to Ashby (Ashby et al., 2009), nanoparticles organize themselves in an efficient close-packing structure. In geometry, close-packing is a dense arrangement of congruent

spheres in an infinite and regular arrangement. He and Shi (He & Shi, 2008) explained that nanomaterial can act as filler creating a dense and less permeable mortar microstructure; also nanomaterial may act as nucleus to facilitate the creation of hydration products; thus nanomaterial may promote the formation of high-density C-S-H structures. Several authors (Hosseini et al., 2011, Said et al., 2012 and Ji, 2005) observed such effects in the case of nanosilica. Ji (Ji, 2005) showed the improvement of microstructure of concrete including nanosilica based on the FESEM test. It was concluded that the addition of nanosilica can make the microstructure of concrete more uniform and compact than normal cement. In 2010, Hosseini (Hosseini et al., 2010) carried out an experimental study to explain the modification of concrete microstructure when nanosilica is added. They summarized that nanosilica contributes to improve concrete microstructure in four ways: a) acting as a nucleus, b) generating better C-S-H, c) controlled crystallization, and d) filling of micro-voids.

The replacement of a certain amount of cement with nanosilica decreases the porosity of concrete (Shirgir et al., 2011, Said et al., 2012 and Mondal et al., 2010). The concrete mixtures with nanosilica have smaller threshold pore diameters than the control mixtures without nanosilica (Lin et al., 2008 and Said et al., 2012).

The porosity of concrete is also decreased when nano-TiO_2 is added to cement. Nano-TiO_2 can modify the pore size distribution and decrease the total pore volume by filling up the pore space gradually throughout the hydration process (Chen et al., 2012 and Nazari & Riahi, 2011). It was found that the pore structure of concrete containing nano-TiO_2 is finer than that with nano-SiO_2. Therefore, the concrete containing nano-TiO_2 can exhibit a higher resistance to the penetration of deleterious agents than the concrete containing nano-SiO_2.

2.6.6.4 Effects on mechanical properties of concrete

Nanomaterials improve the mechanical properties of concrete due to improved particle packing and better bonding between cement paste and aggregates. According to Quercia (Quercia et al., 2012), the properties of hardened concrete are governed by the overall grading of the solid materials. The increase in the particle size range including very small solid particles with dimensions below 300 nm improves particle packing. Based on the analysis of six commercial nanosilica products, Quercia (Quercia et al., 2012) reported that nanosilica is a suitable alternative to improve grading since its particle size ranges from 5 to 658 nanometers. In addition, nanomaterials produces a better interfacial bond between aggregate and cement paste (Gopalakrishnan et al., 2011).

Several studies indicated that the addition of nanosilica in cement paste can improve the compressive strength of concrete due to its high surface area and pozzolanic effect (Shih et al., 2006, Said et al., 2012, Ji, 2005 and Flores et al., 2010). It is already recognized from past research that silica fume (micro-silica) can result in a higher strength in concrete (Mondal et al., 2010). Due to a finer particle size and higher surface area, nanosilica is more effective than microsilica at increasing the compressive strength of concrete when compared at the same weight proportion. The addition of nano-TiO_2 up to 3wt% can also significantly increase the compressive strength of concrete by forming more hydrated products (Chen et al., 2012 and Nazari & Riahi, 2011).

Nanomaterials can also improve the flexural strength of concrete. Gopalakrishnan (Gopalakrishnan et al., 2011) reported that nanosilica increases both the compressive and flexural strengths of concrete. Similar results were also observed by (Hosseini et al., 2010) as shown in Figure 2-26 a) and b). The other nanomaterials such as nano-TiO_2 and CNFs also significantly improve the flexural strengths of concrete (Li et al., 2004, Li et al., 2007 and Metaxa et al., 2010).

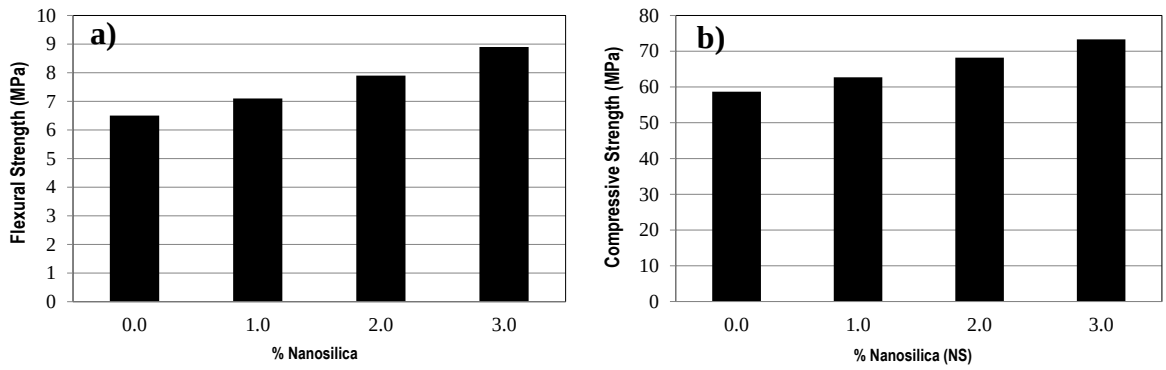

Figure 2-26: a) Flexural strength and b) compressive strength of nanosilica concrete (adapted from Hosseini et al., 2010)

The addition of nano-TiO_2 up to 3 wt% of cement can significantly increase the compressive strength of concrete by forming a larger amount of hydrated products (Chen & Poon, 2012 and Nazari & Riahi, 2011). Metaxa (Metaxa et al., 2010) tested the flexural strength of the concrete samples reinforced with 0.025%, 0.048%, 0.08% and 1% CNFs by weight of cement. They concluded that the optimal content of CNFs is 0.048wt%, which provides the strength increase up to 45%. Also, they mentioned that CNFs will ensure the full capacity of the fibers to transfer the load due to excellent bonding between the nano-fibers and the cement hydration products. According to the report of Li (Li et al., 2005), the addition of CNTs can also increase the flexural and compressive strengths of concrete.

This improvement is due to the modification of concrete microstructure from three aspects: a) CNTs interact with hydrates to produce a high bonding strength and increase the load transfer capacity, b) CNTs reduce the total pore volume in bulk cement paste, thus increasing the strength of concrete, c) CNTs treated with $H2SO_4$ and HNO_3 mixture solution act as the bridge connection between cracks and voids (Figure 2-27) to enhance the tension load transfer, thereby improving the flexural strength of concrete.

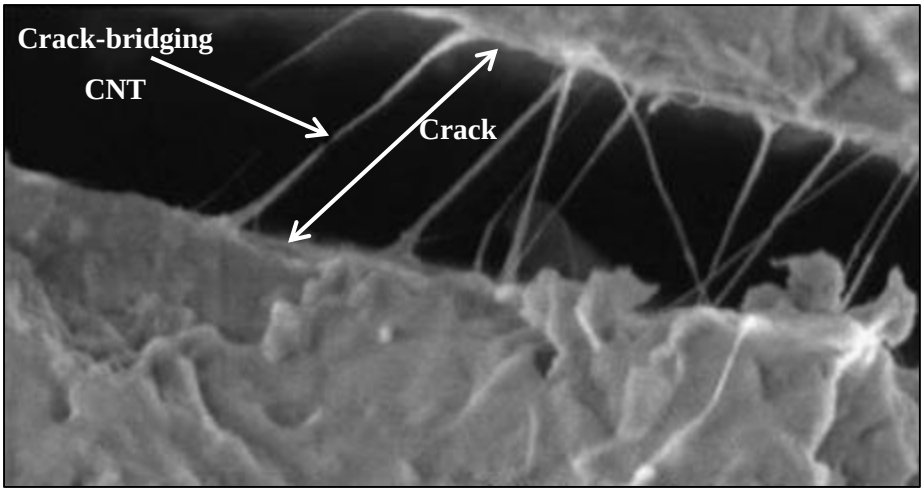

Figure 2-27: Scanning electron micrograph of cracked CNT-composite (Adapted from (Sanchez & Sobolev, 2010))

Some nanomaterials can significantly improve the toughness of concrete along with other properties. Al-Rub (Al-Rub, 2012) states that when a small amount of carbon nanotubes (0.1% CNTs) is incorporated into concrete the ultimate strain capacity increases by 142%, the flexural strength increases by 79%, and the fracture toughness increases by 242%. These results show that CNTs result in significant enhancement to the mechanical properties of concrete.

Nanomaterials can also improve some of the other properties of concrete. Li (Li et al., 2007) reported that nano-TiO_2 significantly enhances the flexural fatigue performance of concrete. In their study, the concrete with 1% nano-TiO_2 by weight of binder exhibited the best flexural fatigue performance.

2.6.6.5 Effects on transport properties and durability of concrete

Durability is the goal of any agency to ensure a sustainable development of concrete infrastructures. The incorporation of nano-materials such as nano-Fe_2O_3, nano-Al_2O_3, nano-TiO_2, nano-SiO_2 and nanoclays (montmorilonite) improves the chloride penetration resistance of the mortar phase of

concrete (He & Shi, 2008). Particularly, small amounts of nano-SiO_2 and nano-clays significantly enhanced the chloride penetration resistance of concrete. Said (Said et al., 2012) reported that the rapid chloride permeability significantly decreased when nanosilica was added into the concrete mixtures. They concluded that a small amount of nanosilica can provide a significant effect on reducing the penetration of chloride ions into concrete.

A recent study has also shown that the water absorption of concrete decreases when nanomaterials such as nanosilica are added (Jalal et al., 2012). The authors reported that the addition of 2% nanosilica for the binder contents of 400 and 500 kg/m^3 results in reductions of 58 and 54% of the capillary water absorption at the age of 3 days, respectively. It has been summarized that concrete containing nanosilica possesses a more densely packed microstructure, and thus exhibits less capillary absorption (Jalal et al., 2012). Nano-TiO_2 also greatly decreases the water absorption of concrete (Jalal et al., 2012).

Abrasion is a distress on concrete surfaces that may affect floors, pavements, and hydraulic structures (Kosmatka et al., 2011), therefore a concrete with high abrasion resistance is desirable. According to Gopalakrishnan (Gopalakrishnan et al., 2011), nanomaterials can enhance the abrasion resistance of concrete, because the incorporation of nanoparticles increases the homogeneity of the cement matrix and makes it more compact. Abrasion resistance is extraordinarily improved in concrete when nanomaterials are added to concrete, as is shown in Figure 2-8. This figure shows the abrasion resistance index that is defined by the quotient between the square root of the head revolutions and the depth of the abrasion grooves. The abrasion resistance of concrete can be increased by up to 157% when 1% nanosilica by weight of cement is used in a concrete mixture. The abrasion resistance of concrete can be increased by 181% when 1% nano-TiO_2 by weight of cement is used.

2.6.6.6 Health risks of using nanomaterials in concrete

Nanotechnology has remarkable potential in the construction industry. However, there are reasonable apprehensions that nanomaterials could cause severe health damages if not used cautiously (Ashby et al., 2009). Since nanomaterial consists of ultrafine particles with nano-scale dimensions ($\leq$ 100 nm), there are health risks due to the possible inhalation of nanoparticles. Napierska (Napierska et al,. 2010) reported that ultrafine particles (< 0.1 μm) have been revealed to cause considerably more dangerous inflammatory reactions and lung damages than fine particles of less than 2.5 μm size. Due to very small particle size, nanoparticles have the ability to penetrate cells, and thus they are more likely to cause biological problems.

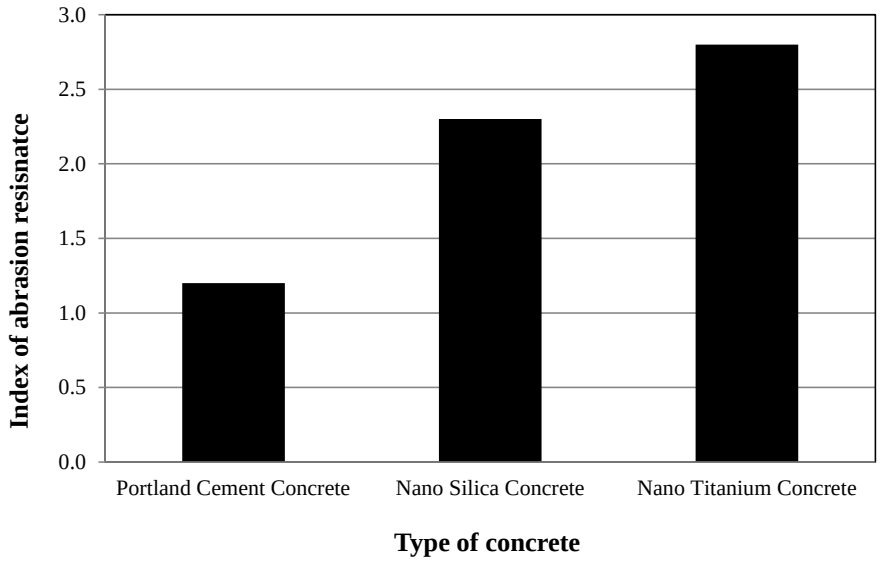

Figure 2-28: Abrasion resistance for different nano-concretes (Adapted from Gopalakrishnan et al., 2011)

Several adverse health effects, such as lung cancer, silicosis, chronic obstructive pulmonary disease are mainly related to crystalline silica (for example, quartz and cristobalite). Amorphous silica such as diatomaceous earth is considered less detrimental to health (Napierska et al., 2010). Nanosilica that has been used significantly in producing nanoconcrete contains an amorphous structure.

Nanomaterial is indeed a valuable technology that can be very useful for many kinds of applications. However, there still exist several implications that must be considered during the use of nanomaterials. These are related to the prospects of nanomaterials and the risks associated with their use in concrete (Ashby et al., 2009). In concrete material applications, construction procedures can adapt techniques to minimize or eliminate the labor risk of these materials (Birgisson, 2010).

2.7 Summary of Literature Review

The application of nanotechnology in concrete materials is still in its infancy and the potential to advance the state-of-the-art of this technology is promising. However, there is still a gap in the study of how nanomaterials can potentially enhance the behavior and performance of PCC pavements particularly in cold climates. At the nano scale, atomic and molecular interactions can occur, which can generate different responses which are observed on the macro scale.

According to Ashby (Ashby et al., 2009) nanomaterials can modify the surface morphology on materials, however its impact on friction response for highway applications has been practically

unexplored. Nanomaterials can increase concrete's compressive strength which has a strong correlation with abrasion resistance. Abrasion resistance in turn, may be related with macrotexture durability, and the application of nanomaterials may enhance the hysteresis component of the frictional force in the long term performance of a PCC pavement.

The discussions regarding how nanomaterials can influence acoustic properties have been limited because the noise waves, which have wavelength ranging from microns to kilometers, cannot be influenced by nano scale. However, since nanomaterials' properties vary from traditional materials, noise waves can be influenced by damping effects and this has been unexplored for highway applications.

Finally, nanomaterials may potentially improve the microstructure and transport properties of concrete. This can influence durability behavior under freezing and thawing when deicing agents are used because nanomaterials can improve the concrete packing and therefore produce a more dense and impermeable material. These effects are also largely unexplored.

Chapter 3
Materials and Methods

This chapter describes the methodology, the experimental matrix, as well as the materials and methods of the tests conducted. The tests were performed on two different nanomaterials: nanosilica and a solution designed to mimic the lotus leaf effect. Nanosilica was added to the concrete mixes and concrete mortars. The lotus leaf solution was applied on the surface of concrete samples.

3.1 Experimental Matrix and Methodology Applying Nanosilica

Table 3-1 presents the experimental matrix developed as part of this research. The matrix includes mixes and mortars with three different water/cement (w/c) ratios. The majority of the tests use a w/c ratio of 0.39.

Table 3-1: Research experimental matrix

Tests in concretes and mortars	Number of samples per age		water/cement (w/c) ratio (Kg of cement/m^3)*		
			0.31	0.39	0.45
	7 Days	28 Days	(496 kg/m^3)	(400 kg/m^3)	(340 kg/m^3)
Compressive strength in concretes	3	3	✓	✓	✓
Noise absorption using impedance tube	3	3	✓	✓	-
Friction response - British Pendulum Number - Broom finishing**	3	3	✓	✓	-
Friction response - British Pendulum Number - Broom finishing	-	15	✓	✓	-
Friction response - British Pendulum Number - Smooth finishing	5	5	-	✓	-
Friction response - Tribometer - Smooth finishing in mortars	-	3	-	✓	-
Compressive strength in mortars	3	3	-	✓	✓
Abrasion response - Broom finishing	5	5	-	✓	-
Abrasion response - Smooth finishing	5	5	-	✓	-
Rapid freezing and thawing	-	3	-	✓	-
Scanning Electron Microscope (SEM) images of mortar surfaces	-	2		✓	-
SEM images of concrete microstructure	-	2		✓	✓
Scaling resistance	-	4	-	-	✓

**: Overall for each w/c ratio differents proportions of nanosilica were considered*

***: For w/c ratio 0.39, five samples were included in the analysis*

For w/c = 0.31 tests include: 0.0% nanosilica (NS), 0.5% NS, 1.0% NS and 1.5% NS

For w/c = 0.39 tests include: 0.0% nanosilica (NS), 0.5% NS, 1.0% NS, 1.5% NS and 2.0% NS

For w/c = 0.45 tests include: 0.0% nanosilica (NS), 0.5% NS, 1.0% NS, 1.5% NS and 2.0% NS

3.1.1 Materials

The materials used throughout this research include: General Use (GU) Portland cement, policarboxylate based High-Range Water Reducer (HRWR), Air Entraining Admixture (AEA), fine and coarse aggregates, and nanosilica in the form of a fine powder. Nanosilica was included by partially

replacing the cement by weight. The properties of the nanosilica used in this research were provided by the supplier and are shown below:

- Material: Silicon Dioxide nanopowder (Nano SiO_2)
- Purity: > 99%
- Average Particle Size: 15 nm
- Color: White Powder
- Specific Surface Area (SSA): 100 m^2/g
- Morphology: Spherical

The chemical composition, particle size, color and morphology were verified in the lab and these results are presented in the next chapter.

The aggregates' properties (fine and coarse) meet the Ontario Provincial Standards and Specifications (OPSS, 2013). The admixtures, HRWR and AEA, were used to achieve the required properties in the fresh concrete mixes (slump and air content respectively). Microscopy images and chemical analyses were performed in order to verify the quality of the nanosilica. A Transmission Electron Microscope (TEM) and Scanning Electron Microscope (SEM) were used to take pictures at different scales. The results are reported in the following chapter.

3.1.2 Mixture Design and Proportions

The procedure used for producing the mixtures corresponded with the CSA A23.1-09/A23.2-09 standard (CSA, 2009), which specifies design parameters for the fresh mix of a slump ranging from 75 mm to 100 mm, air content from 5% to 8%, minimum specified compressive strength at 28 days of 32.0 MPa, required average compressive strength 43.5 MPa, Class C-2 exposure and 20 mm nominal maximum aggregate size. **Appendix A** presents the mix design, and also the criteria used to modify the w/c ratio. All mix proportions were weighed based on the w/c ratio. Table 3-2 presents the materials' proportions in kg/m^3. The w/c ratio was kept constant for the mixes that have different proportions of nanosilica.

The AEA and HRWR doses were determined based on the range define by the supplier (BASF) and also using trial mixes that were fabricated in the beginning of this research.

Nanosilica was added in proportion to the cement weight. For instance for the w/c ratio 0.39, 0.5% represent 2 kg of nanosilica that were added into the mix, mixed in ¼ of the total mixing water.

Table 3-2: Proportions for concretes mixes depending on the w/c ratio

Type of material	w/c		
	0.31	**0.39**	**0.45**
GU cement (kg/m^3)	495	400	343
Water (kg/m^3)	154	154	154
Coarse aggregates (kg/m^3)*	1046	1046	1046
Fine aggregates (kg/m^3)*	623	703	751
AEA doses in PCC (L/m^3)	0.28 to 0.95	0.19 to 0.29	0.13 to 0.23
HRWR doses in PCC (L/m^3)	3.78 to 6.57	3.1 to 4.26	2.52 to 3.1

**: Aggregates in dry condition.*

For mortars, coarse aggregates and AEA were eliminated from the batching process. The concrete slump was correlated with the mortar consistency using the following equation (Domone, 2006):

Concrete Slump Flow (mm) = 4.8 x Mortar Spread (mm) - 800 **(Equation 3)**

Therefore, according to Equation 3 concrete with a slump between 75 to 100 mm had a mortar spread range of 182 mm to 188 mm. Five different mortar mixes were produced: 0.0%, 0.5%, 1.0%, 1.5% and 2.0% of nanosilica. In the w/c ratio of 0.45 the nanosilica content was increased until 3.0%. In these concretes and mortars, 0.0% of nanosilica represents the Control Concrete (CC) and Control Mortar (CM), respectively.

3.1.3 Fresh Concrete and Mortar Preparation

The fresh concrete mixes were prepared in a revolving pan-type concrete mixer and with a laboratory bench mixer for mortars according to the following procedures. Nanosilica was diluted in the water to avoid fumes and to achieve a suitable dispersion in the concrete and mortar matrix (Figure 3-1).

Figure 3-1: Nanosilica incorporates in water during mixing a) in concrete mixes and b) mortars

- **Steps for Concrete Preparation:** The following steps were followed for concrete mixtures preparation.

  1. Coarse aggregates, fine aggregate and ¼ of Water: Mix for 1 minute.
  2. ¼ of water, AEA: Mix for 1 minute.
  3. Cement, nanosilica in ¼ of water: Mix for 3 minutes.
  4. 3 minutes rest covered with wet burlap.
  5. HRWR in ¼ of water: Mix for 3 minutes.

It was not feasible to put more than 2.0% nanosilica in ¼ of the total mixing water, as any mixture with this content of nanosilica or higher has a consistency close to a gel. Material of this consistency was challenging to put into the mixer. To avoid this issue in mortars that contain 2.5% and 3.0% nanosilica, all of the mixing water was used to dilute the nanosilica, rather than just 1/4.

- **Steps for Mortar Preparation:** The following steps were applied for concrete mortars preparation.

  1. Fine aggregate and ¼ of Water: Mix for 1 minute.
  2. ¼ of water: Mix for 1 minute.
  3. Cement, nanosilica in ¼ of water: Mix for 3 minutes.
  4. 3 minutes rest covered with wet burlap.
  5. HRWR in ¼ of water: Mix for 3 minutes.

3.1.4 Testing of Fresh Concretes

Each fresh concrete mixture was tested for slump to determine its consistency, and subsequently tested for air content and wet density, all according to ASTM C143/C143M-10a (ASTM, 2010), ASTM C231/C231M-10 (ASTM, 2010), and ASTM C138/C138M-12 (ASTM, 2012), respectively. Figure 3-2 a) presents the slump test in concrete.

3.1.5 Testing of Fresh Mortars

Each mixture was further evaluated by flow consistency according to ASTM C230 / C230M - 13 (ASTM, 2013) and ASTM C109/C109M − 11b (ASTM, 2011). Figure 3-2 b) presents the flow test in mortars.

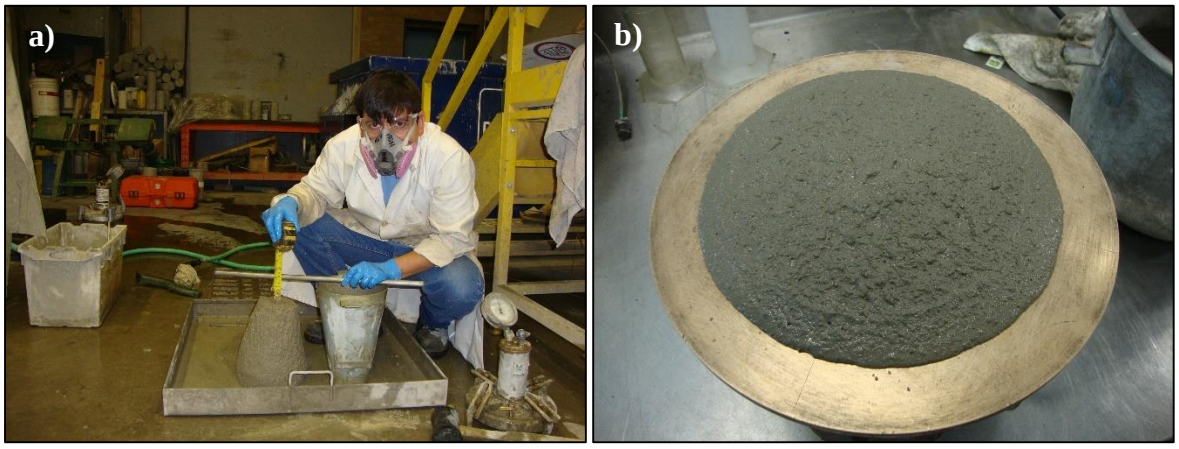

Figure 3-2: a) Slump test in concrete and b) flow consistency in mortars

3.1.6 Preparation of Hardened Concrete Test Specimens

When the concrete mixes achieved all required specifications, the samples as specified on Table 3-1 were cast. Standard cylinder specimens (100 mm diameter and 200 mm height) were cast for the compressive strength test and 152 mm diameter, 75 mm height specimens were cast for the noise absorption test (using the impedance tube), friction test (using the BPT) and abrasion test (using the rotating cutter method). For friction and abrasion responses, the specimens had broom and smooth finishing. To ensure consistency, visual inspection was made after casting and de-molding to ensure that the specimens have a similar surface finish. Broom finished samples were prepared by sliding a broom over the surface while the smooth finished samples were prepared using a square trowel. For freezing and thawing testing, prisms of 76.2 mm x 10.16 mm x 40.64 mm (depth, width, length) were prepared. For scaling resistance tests, slabs of 76 mm x 300 mm x 300 mm (depth, width, length) were used.

Twenty four hours after casting, all specimens were demolded and cured inside the curing room. Overall, samples were kept in the curing room until the start of each test. Figure 3-3 displays some fresh concrete specimens.

Figure 3-3: a) Casting of samples for compressive strength and noise absorption and b) casting of slabs for scaling resistance

3.1.7 Preparation of Hardened Mortar Test Specimens

Once the concrete mortars matched all specifications, the number of samples specified in Table 3-1 was cast. 50 mm x 50 mm x 50 mm cube specimens for compressive strength testing and 25 mm x 70 mm cylinder specimens (height x diameter) for friction tests using the tribometer were used. Similar to the other concrete tests, the cube specimens were demolded after twenty four hours and placed in the humidity room to cure. The cylinders for tribology were kept inside their plastic molds to prevent damage during curing/transportation. Figure 3-4 a) displays the preparation of mortar specimens and Figure 3-4 b) mortar specimens inside the curing room.

Figure 3-4: a) Casting of cube speciments and b) mortar samples inside the curing room

3.1.8 Testing of Hardened Concrete

Generally cast concrete specimens were tested at ages of 7 and 28 days, however certain specimens were tested at 28 days only (See Table 3-1). Specimens were tested for compressive strength according to ASTM C39/C39M-12 (ASTM, 2012), friction response using the British Pendulum Skid Resistance Tester according to E303-93 (Reapproved 2008) (ASTM, 2008) and abrasion response following ASTM C944 / C944M – 12 (ASTM, 2012).

Figure 3-5 a) shows cylinders in the process of being grinded, while Figure 3-5 b) displays the compressive machine used in this research; both are located in the structural lab of UW.

Figure 3-5: a) Grinding the cylinders before compressive strength testing and b) the compressive strength machine

Specimens for abrasion were tested according to ASTM C944 / C944M – 12 (ASTM, 2012). Abrasion occurs with long-term wear/use, but examination at 7 days were done to observe effect of nanoconcrete in PCC pavements when early openings to traffic may be required.

According to Lamond & Pielert (2006), abrasion testing using the rotating-cutter method is suitable and successfully determines the quality of concrete used in highways and bridges subject to traffic. This rapid method uses 152 mm diameter samples and is done with a very simple apparatus. The setup was built to obtain a vertical load of 197 N (double load) and a rotation speed of 200 rpm. The test reports the loss of weight on each sample after a period of 2 minutes. Figure 3-6 presents two pictures of the CPATT rotating-cutter drill press used in this research.

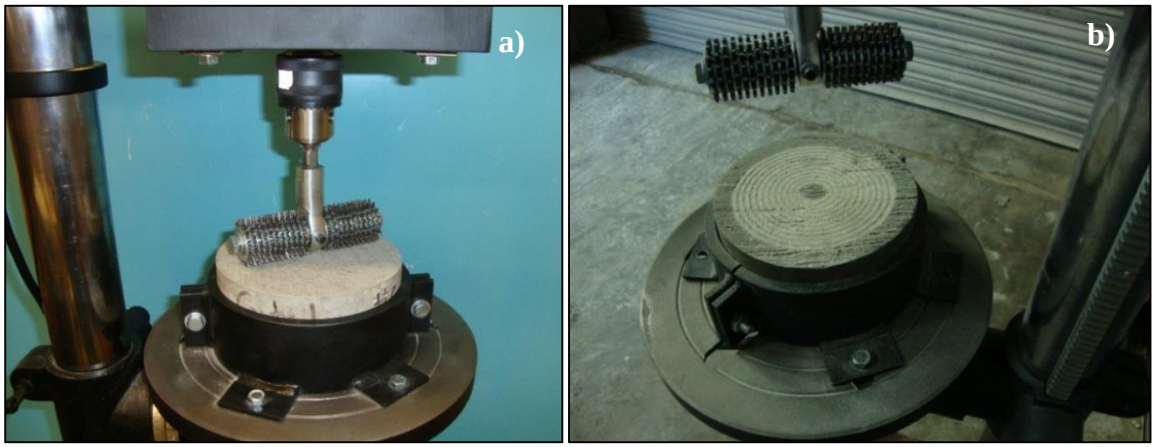

Figure 3-6: a) Rotating-cutter drill press owned by CPATT and b) tested sample

The test for measuring the resistance of concrete to rapid freezing and thawing was performed based on the standard procedure outlined in ASTM C666 (reapproved 2008) (ASTM, 2008). There are two procedures that can be taken, the first (Procedure A) is to conduct each freeze and thaw cycle in water, while the second (Procedure B) is to freeze the specimens in air, but thaw them in water. Since an automatic cabinet was used, procedure A was followed; the specimens were placed in a container submerged in water and the temperature of the water is automatically adjusted with a timer to achieve each freeze thaw cycle.

The freeze and thaw temperatures are dictated to be 0 deg F (-18° C) and 40 deg F (4° C) respectively, and each cycle must be conducted in two to five hours. In Procedure A, a minimum of 25% of the time is to be used for thawing.

The specimens were cast as prisms and were cured for 28 days. After that, the specimens were brought to thaw temperature and the transverse frequency and mass were measured. The specimens were subjected to at least 300 cycles. Fundamental transverse frequency and mass were measured at intervals of 36 cycles. The relative dynamic modulus of elasticity, durability factor, and mass percent change were calculated from the observations at the end of the test. In this thesis the percentage length change was not measured. Figure 3-7 presents pictures of the freezing and thawing samples.

Figure 3-7: a) Prism for freezing and thawing and b) sample being measured for the fundamental transverse frequency

The Relative Dynamic Modulus of Elasticity calculation involves the application of the following equation (ASTM, 2008):

$P_c = (n_1^2 / n^2) \times 100$ **(Equation 4)**

Where:

P_c = relative dynamic modulus of elasticity, after c cycles of freezing and thawing, percent.

n = fundamental transverse frequency at 0 cycles of freezing and thawing, and

n_1 = fundamental transverse frequency after c cycles of freezing and thawing

The Durability Factor calculation involves the application of the following equation (ASTM, 2008).

$DF = P \times N / M$ **(Equation 5)**

Where:

DF = Durability factor of the test specimen

P = relative dynamic modulus of elasticity, at N cycles, percent.

N = number cycles at which P reaches the specified minimum value for discontinuing the test or the specified number of cycles at which the exposure is to be terminated, whichever is less, and

M = specified number of cycles at which the exposure is to be terminated.

Scaling tests were performed in accordance with the Standard Test Method for Scaling Resistance of Concrete Surfaces Exposed to Deicing Chemicals according to ASTM C672 (ASTM, 2012). The procedure involves preparing the molds with oil and filling them with fresh concrete in one layer. The mold used was 300 mm x 300 mm, providing a total surface area of 0.09 m^2. The standard states that the concrete should be rodded once for every 2 in^{-2} of surface area.

The molds were leveled and surfaced with a flat steel trowel, and a light broom finishing was applied with a brush. After twenty four hours, samples were demolded and stored in the curing room for 28 days. Next, the samples were kept out in air at 23°C for 14 days. In order for the scaling test to occur, a 25 mm wide and 25 mm high dike was constructed around the perimeter of the sample, leaving an effective area of 0.0625 m^2 for the scaling test. The dike was made out of Plexiglas, which was adhered to the surface using silicone (See Figure 3-8). A brine of calcium chloride and water approximately 6 mm deep was then placed on the surface of each sample. The concentration of the solution should be such that there is 4 grams of anhydrous calcium chloride per 100 mL of solution. The specimens are frozen overnight for 16-18 hours, and then thawed for 6-8 hours. At the end of each cycle, water is added to maintain a depth of 6 mm of solution.

A visual inspection using the rating system outlined in Table 3-3 and brine replacement was conducted every five freeze-thaw cycles until the 25th cycle, after which a visual inspection was only conducted on the 50th cycle. Figure 3-8 a) illustrates the Plexiglas dike and Figure 3-8 b) shows all samples before the solution is added on the effective surface. Only one w/c ratio equal to 0.45 was used in the scaling resistance experiment since this ratio is recommended in the standard ASTM C672.

Table 3-3: Scale for scaling evaluation (ASTM, 2003)

Rating	Condition of Surface
0	No scaling
1	Very slight scaling (3 mm [1/8 in.] depth, max, no coarse aggregate visible)
2	Slight to moderate scaling
3	Moderate scaling (some coarse aggregate visible)
4	Moderate to severe scaling
5	Severe scaling (coarse aggregate visible over entire surface)

Figure 3-8: a) Sample with the dike of Plexiglass and b) samples before the first cycle began

3.1.9 Testing of Hardened Mortars

Compressive strength testing of the cast mortar specimens was performed at ages of 7 and 28 days according to ASTM C109/C109M − 11b (ASTM, 2011). Three 28-day old specimens were tested for friction response using the tribometer shown in Figure 3-9 a). In this experiment, smooth surfaces were used to eliminate the macrotexture effects. In the context of this research, a smooth surface can be defined as a horizontal surface with no visually observable grooves. The experiment was performed with the following configuration: Stroke length of 5 mm, sliding speed of 0.1 mm/s, two cycles, normal forces of 50 g and 100 g. Several trial configurations were performed before final testing.

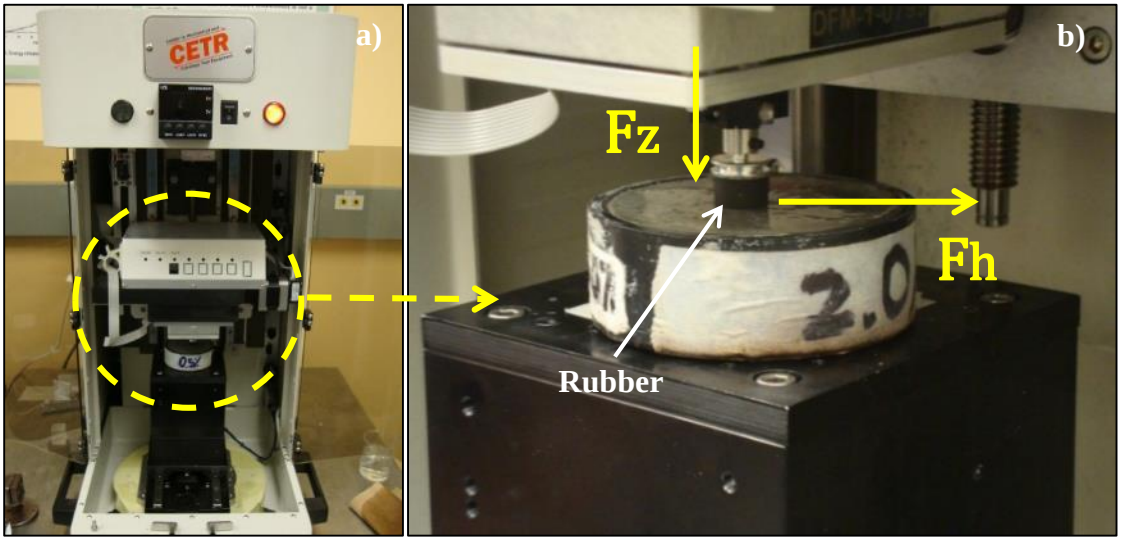

Figure 3-9: a) Tribometer and b) experiment setup and forces recorded during the test

Tribology testing records two different forces-vertical (Fz) and horizontal (Fh) when the tip slides on the material surface (Figure 3-9 b). The friction coefficient (μ_T) is defined by μ_T = Fh /Fz. Plotting the curve μ_T versus time differentiates the static and dynamic coefficients. Here, the dynamic coefficient was obtained as the average on the plateau section. The tribometer was modified using a tip with rubber from the BPT slider (Figure 3-9 b) to simulate a more realistic tire (rubber)-pavement interaction, since the original tip is made of steel. Figure 3-10 displays the rubber used from the British Pendulum slider to build the tribometer tip. During the test, a small amount of water was applied to the mortar surface to produce a wet surface.

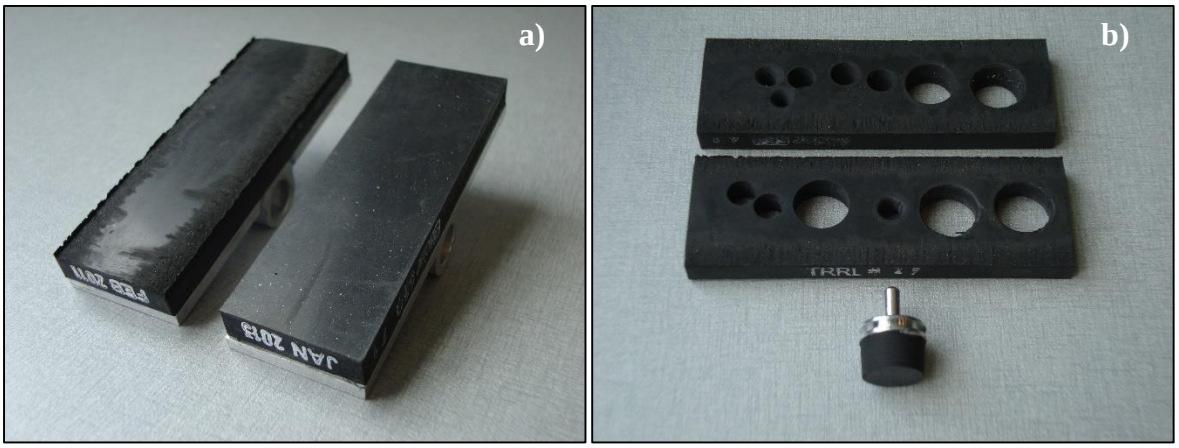

Figure 3-10: a) New and old rubber used in the BPT and b) tip constructed for the tribometer

The surface texture of the mortar was evaluated in two ways: firstly, by using a surface profilometer, and secondly, with a Scanning Electron Microscope (SEM). Surface profile assessments using a Tencor P-10 surface profilometer (Figure 3-11) evaluated the surface roughness of the mortar. The device has a 2 μm radius tungsten tip with a diamond embedded at its apex. Two scans were conducted for each specimen, with the scans perpendicular to each other. The following parameters were used in the scans:

- Length: 10,000 μm (1 cm)
- Speed: 400 μm/sec
- Stylus force: 3 mg
- Vertical Range: 327 μm
- Various roughness parameters, including Root Mean Square (RMS), roughness and Mean Peak Height was calculated from the scanned data using a Gaussian filter and long wave cut-off of 2500 μm.

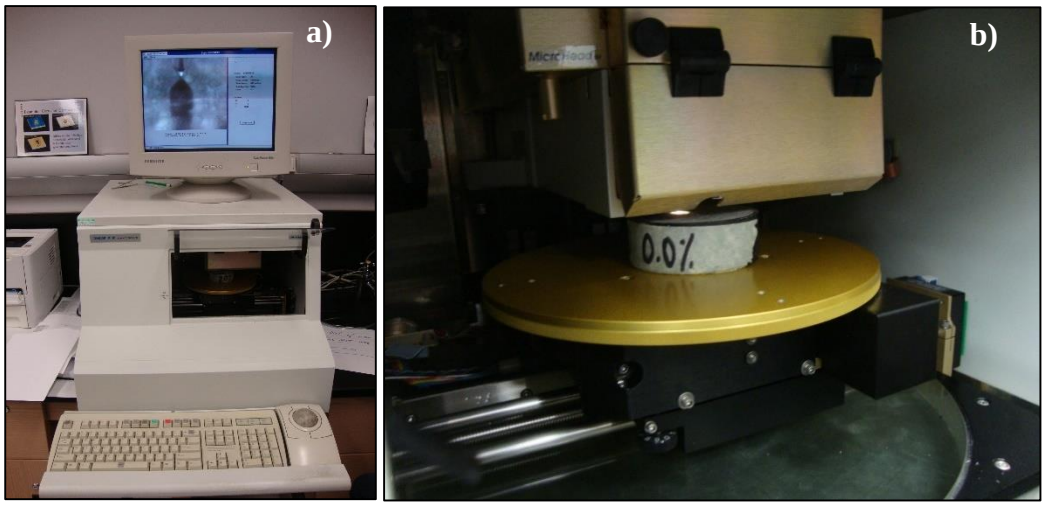

Figure 3-11: a) Tencor P-10 surface profilometer and b) sample being tested

3.1.10 Scanning Electron Microscope (SEM) and Transmission Electron Microscope (TEM) Images

In order to characterize nanosilica, cement, concrete microstructure and mortar surfaces a Scanning Electron Microscope (SEM) (Figure 3-12 a) and Transmission Electron Microscope (TEM) (Figure 3-12 b) were used.

SEM is mainly used to produce images of the surface of materials (Asby et al., 2009) when the sample size is less than 1 cm^3. SEM mortar samples were cut using a table saw with a blade. For the concrete samples; the sample surface was not disturbed. These concretes samples were obtained after compressive strength testing at 28 days and cut with the same table saw. Observations were made on fracture surfaces, which were not disturbed.

Sample preparation included placing a small piece of mortar/concrete over a conductive carbon tape attached to a circular metallic holder. To make the sample electrically conductive, a gold coating, 10 - 15 nm thick, was applied with a Denton sputter-coater. For nanosilica and cement, a small amount of material was placed over a conductive carbon tape attached to a circular metallic sample holder and finally the gold coating was applied.

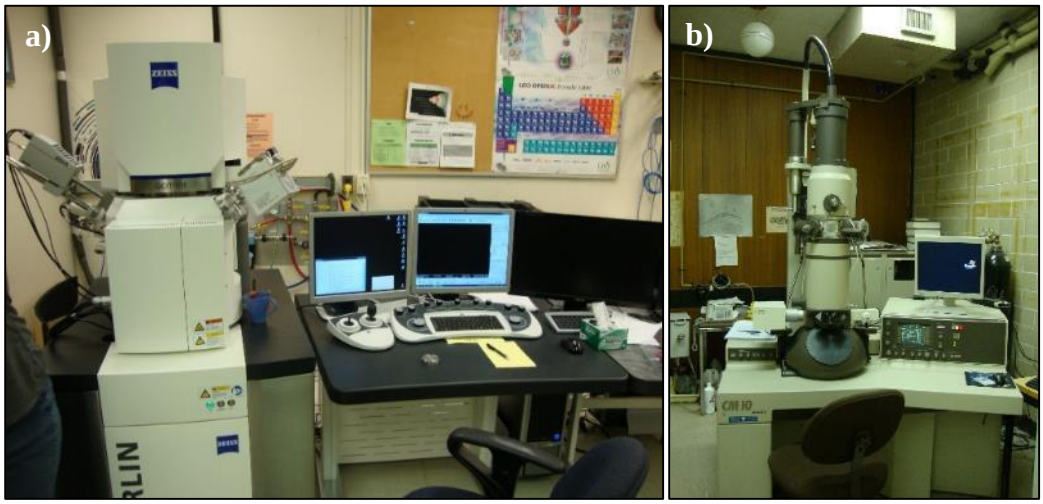

Figure 3-12: Pictures presenting a) Scanning Electron Microscope (SEM) and b) Transmission Electron Microscope (TEM) from UW

TEM images of nanosilica were captured using the Phillips CM10 equipment from UW's Biology Department (Figure 3-12 b). For TEM testing, 300 μm copper mesh grids were used and 0.05 g nanosilica was diluted in 4 g of water. One drop of solution was placed on the grid and dried for 24 hours before testing. SEM pictures of nanosilica were also taken; however, TEM presented better resolutions. Figure 3-13 a) presents the sample preparation for SEM using small pieces of mortars/concretes and Figure 3-13 b) displays the preparation of the TEM samples using nanosilica in the copper grids.

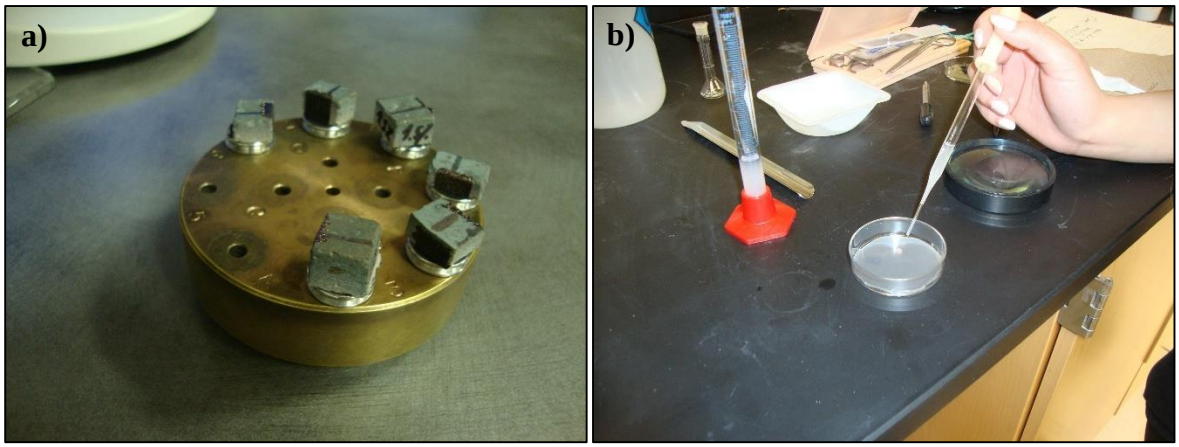

Figure 3-13: a) Mortars/Concretes samples preparation and b) TEM sample preparation

In order to obtain a different perspective of the mortar surfaces roughness, SEM images of mortars were captured with the sample surface set at 45° angle using a special metallic holder and with an angle of 0°. Figure 3-14 displays two pictures comparing both alternatives.

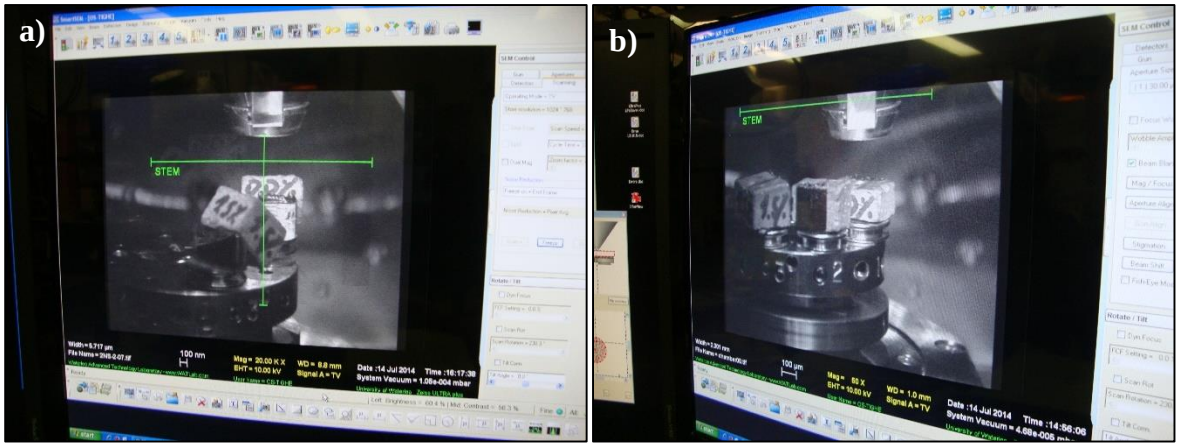

Figure 3-14: a) Mortars samples held at 45° and b) held at 0°

3.2 Methodology Using Lotus Leaf Coating

This section describes the methodology used to explore the feasibility of mimicking the lotus leaf effect on the concrete surface to determine the possible effects on friction and noise absorption.

3.2.1 Materials

The materials used in this part of the study were general-use (Type 10) Portland cement, fine and coarse aggregates, nano-lotus leaf solution products, polycarboxylate based high-range water reducer (HRWR), and air-entraining admixture (AEA). HRWR was used to achieve the target workability, and AEA was used to achieve the target air content.

Two different commercially available nano-lotus leaf products were used to obtain thin coatings on concrete surface. The first product was a solution formulated to create a waterproofing effect; it is a combination of acetic acid and zirconium acetate. The second product was particularly formulated for use on concrete and was applied as a spray; this product is fabricated using aliphatic petroleum distillates and additives created by the supplier. Both nano-lotus leaf coatings were examined to evaluate their effect on the friction and sound absorption properties of concrete pavement.

3.2.2 Mixture Design and Proportions

The mix design of concrete was based on the procedure depicted in CSA A23.1-09/A23.2-09 (CSA, 2009). The following parameters were defined in the mix design: slump from 75 mm to 100 mm, air content from 5% to 8% (tolerance: ±1.5%), 32.5 MPa specified compressive strength at 28 days, Class C-2 exposure, 43.5 MPa design strength, and 20 mm nominal maximum size of coarse aggregate.

The weight based proportions of the concrete were presented in Table 3-2. In this experiment, only one water to cement ratio (w/c = 0.31) was used. This was because in general the applied coating produces modifications at the surface level only (Ashby et al., 2009), therefore adjustments in the mass of the concrete material was considered not critical for this experiment.

3.2.3 Fresh Concrete Preparation

Concrete batches were produced in the laboratory using the mix proportions noted previously. The constituent materials were mixed in a revolving pan-type mixer to produce the concrete batches. The following mixing procedure was specifically used in this study:

1. Coarse aggregate + fine aggregate + ¼ water: mix for 1 min
2. ¼ water + AEA: mix for 1 min
3. Cement + ¼ water: mix for 3 min
4. Covering the concrete within mixer pan with wet burlap: resting for 3 min
5. ¼ water + HRWR: mix for 3 min

3.2.4 Testing of Fresh Concretes

After mixing, the fresh concrete batches were immediately tested for workability (slump), air content, and wet density following the procedures described in ASTM C143/C143M-10a (ASTM, 2010), ASTM C231/C231M-10 (ASTM, 2010), and ASTM C138/C138M-12 (ASTM, 2012), respectively.

3.2.5 Preparation of Hardened Concrete Test Specimens

Two sets of hardened test specimens were prepared from freshly mixed concrete batches. In each set, three 100 mm (diameter) × 200 mm (height) cylinders for the compression test and fifteen 150 mm (diameter) × 75 mm (height) cylinders for friction and sound absorption tests were cast. After molding, the top faces of the 150 mm × 75 mm cylinder specimens were given a broom finish to create macrotexture. All specimens were de-molded 24 hours after casting and immediately transferred to the

100% relative humidity room for wet curing. Visual inspection after casting and de-molding was performed to ensure that the specimens had similar macrotextures.

Nano lotus leaf coatings (NLLCs) were applied to the concrete surface two sets of samples using two commercially available solution products. Each coating was applied to twelve 150 mm × 75 mm cylinder specimens; three cylinders for each set were not coated and acted as the control specimens. Nano lotus leaf solution was used in both coatings in the following applications amount: 0.0 g/m^2 (CC), 30 g/m^2 (NLLCC1), 60 g/m^2 (NLLCC2), 90 g/m^2 (NLLCC3) and 110 g/m^2 (NLLCC4) where CC indicates the control concrete and NLLCC indicates the nano lotus leaf coated concrete. The amount of coating is defined in g/m^2, however originally the amount of coating was defined in order to achieve 0.0, 0.5, 1.0, 1.5 and 2.0 g of solution per sample. The two nano lotus leaf coatings were applied to 28 day old concrete surfaces. The first coating was applied by means of a brush and the second coating as spray. Figure 3-15 a) displays the application of the coating and Figure 3-15 b) shows the lotus effect on the coated surface of a concrete specimen.

Figure 3-15: a) Coating application and b) Lotus effect on the coated surface of a concrete specimen

3.2.6 Testing of Hardened Concrete

The hardened concrete specimens were tested for compressive strength, sound absorption, and friction at the age of 28 days. The compressive strength was determined using triplicate 100 mm (diameter) × 200 mm (height) cylinder specimens based on the procedure described in ASTM C39/C39M-12 (ASTM, 2012).

The sound absorption coefficient was determined using all fifteen 150 mm (diameter) × 75 mm (height) cylinders (12 coated and 3 uncoated specimens). The measurement for sound absorption was performed 24 hours after the coating application. The sound absorption measurement was carried out in accordance with the procedure given in ASTM 1050-10 (ASTM, 2010) using triplicate 150 mm (diameter) × 75 mm (height) cylinders. An impedance tube was used to evaluate sound absorption (Figure 3-16 a). The tube was isolated in a soundproof chamber to avoid any external noise perturbation.

After the sound absorption test, the same cylinder specimens were used to determine the surface friction value or skid resistance. The friction property of concrete surface was measured using the British pendulum tester (Figure 3-16 b) in accordance with ASTM E303-93 (ASTM, 2008). In the British pendulum test, the concrete specimens were first positioned in order to simulate transverse finishing and then the measurement was performed in dry and wet conditions. Tribology tests were not carried out in mortars with coating, since the results of British Pendulum Tester presented no significant differences.

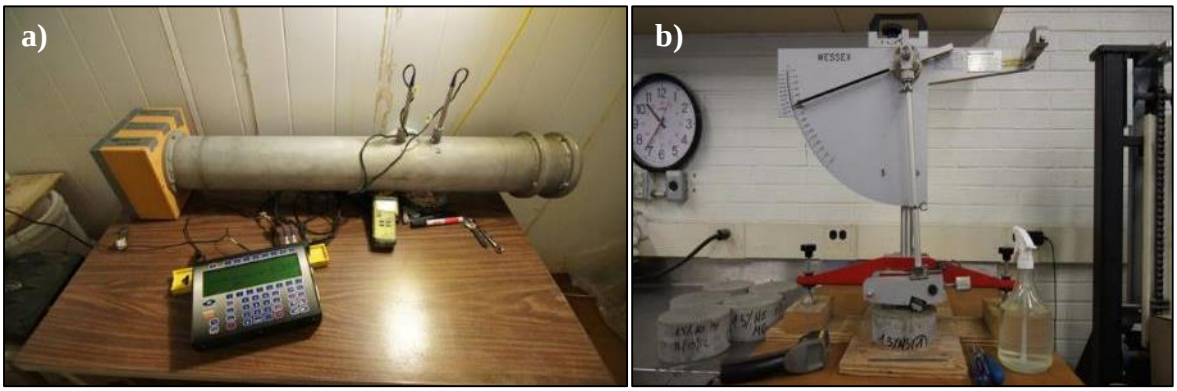

Figure 3-16: a) Impedance tube test for sound absorption and b) British Pendulum Tester

3.3 Summary of Materials and Methods

Several materials and methods were defined in this chapter to address the thesis objectives. Materials included the conventional constituents of concrete used in PCC pavements under Canadian conditions plus the addition of two nanomaterials. In the methodology several tests were integrated to characterize the PCC surfaces' characteristics, the noise absorption capabilities, the modification of the concrete microstructure and durability. In the specific case of surface friction response, a conventional British Pendulum Tester and a novel experiment using a tribometer were combined to measure the frictional response of PCC pavement using redundant tools. Sophisticated tools (a profilometer and a Scanning

Electron Microscope) were also used to characterize the modifications to the mortar and concrete's surface morphology. Specific durability tests to verify the response of concretes under severe weather conditions were also implemented.

Chapter 4
RESULTS AND DISCUSSION

This chapter presents the results and discussion for this research. The results are presented according to the same structure presented in the previous chapters.

4.1 Material Characterization

The material characterization results are presented in this section.

4.1.1 Fine and Coarse Aggregates Characterization

Table 4-1 presents the gradations of three samples of both fine and coarse aggregates, respectively. The physical properties of both aggregates are shown in Table 4-2. Both materials meet the gradation requirements (LS-602) for fine and coarse aggregates presented in the Ontario Provincial Standards and Specifications (OPSS) for Roads and Public Works (OPSS, 2013).

Table 4-1: Gradation of aggregates

Sieve size fine aggregates	Percent (%) Passing	Results gradation sample number		
		1 (% Passing)	2 (% Passing)	3 (% Passing)
9.5 mm	100	100	100	100
4.75 mm	95 - 100	99	99	99
2.36 mm	80 - 100	91	91	92
1.18 mm	50 - 85	75	75	78
600 mm	25 - 60	50	52	55
300 mm	10 - 30	17	20	21
150 mm	0 - 10	3	4	5
75 mm	0 - 6 (Manufactured Sand)	0	0	1

Sieve size coarse aggregates	Percent (%) Passing	Results gradation sample number		
		1 (% Passing)	2 (% Passing)	3 (% Passing)
26.5 mm	100	100	100	100
19 mm	85 - 100	91	91	86
9.5 mm	20 - 55	35	37	26
4.75 mm	0 - 10	7	9	6

Table 4-2: Physical properties of fine and coarse aggregates

Aggregate	Oven-dry based bulk density (kg/m^3)	Relative Density		Absorption (%)	Fineness modulus
		Oven-dry based	Saturated surface-dry based		
Fine	na	2.671	2.705	1.2	2.7
Coarse	1660	2.678	2.709	1.16	na

na = not applicable

Two Micro-Deval abrasion tests were performed for each of the fine and coarse aggregates (Figure 4-1). This test determines abrasion loss in the presence of water and an abrasive charge of steel balls. Both aggregate materials (coarse and fine) meet the OPSS for Roads and Public Works (10), with an abrasion loss in the fine aggregates of 12.9% and 10.7%, and in coarse aggregates of 11.6% and 11.2%.

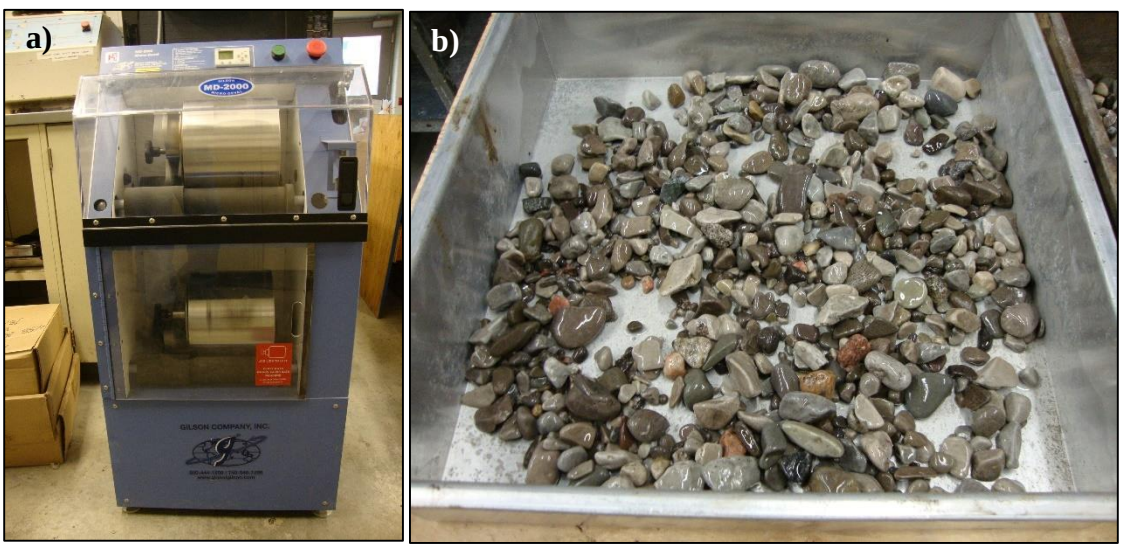

Figure 4-1: a) Micro-Deval apparatus and b) sample of coarse aggregates after the test

4.1.2 Nanosilica Characterization

The quality of the nanosilica was verified with TEM and chemical analysis. For TEM testing, three different samples were prepared. Figure 4-2 presents different TEM pictures captured using Phillips CM10 equipment from UW's Biology Department and shows the size of the nanosilica used and also its spherical morphology. The size of the particles was demonstrated to be approximately 20 nm.

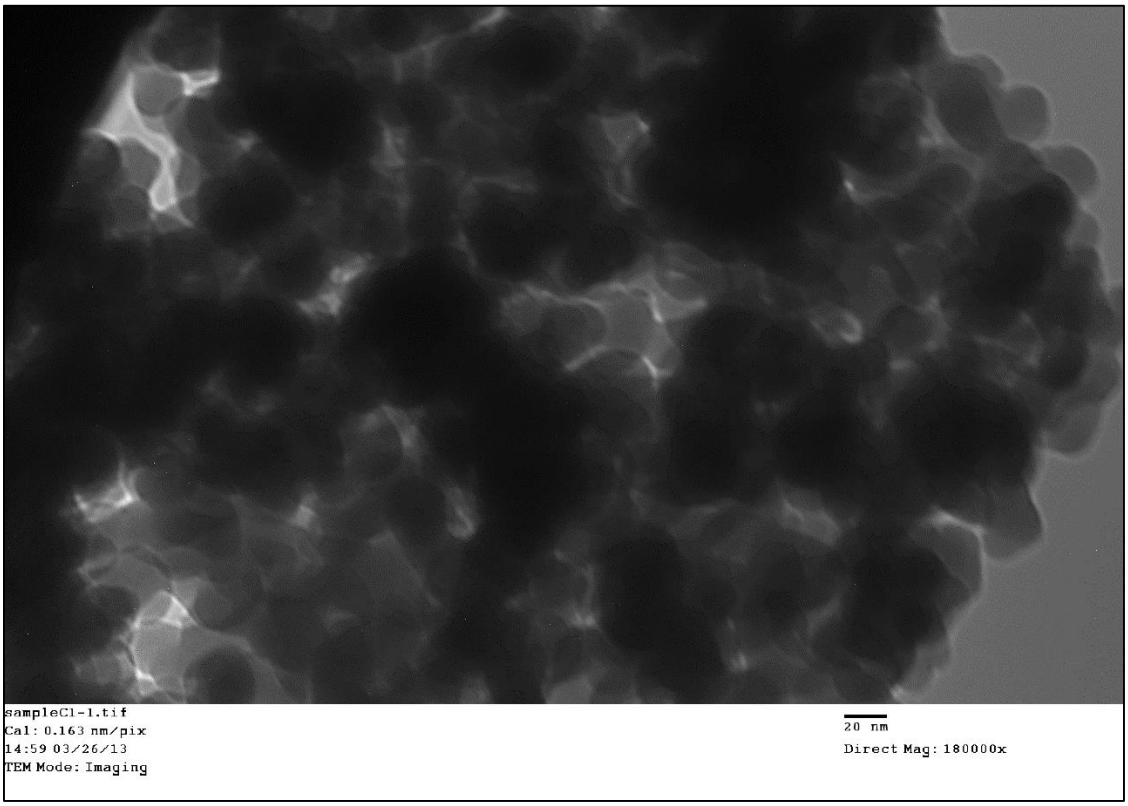

Figure 4-2: TEM image of nanosilica (bar scale 20 nm)

During this research, several questions regarding the differences between nanosilica and silica fume (or microsilica) were raised. The differences were discussed in Section 2 and even though silica fume was not used in this research, Figure 4-3 compared one image of silica fume (Figure 4-3 a) and one image of nanosilica (Figure 4-3 b). Based on this test, it is possible to conclude that silica fume is composed of larger particles since particle dimensions over 1000 nm (1 μm) were detected (Figure 4-3 b). SEM images of nanosilica present poor resolution but it is possible to differentiate the small particle size, which is consistent with TEM observations.

Chemical analysis was performed using EDAX software incorporated into a Scanning Electron Microscope (SEM) owned by UW´s Chemistry Department. Testing was performed in three areas of a nanosilica sample. Figure 4-4 a) shows Area 1, while Figure 4-4 b) presents both the predominant phases O and Si. Notice that in the context of Figure 4-4 b) K does not indicate potassium but instead indicates which energy level of the electron in the atom is excited.

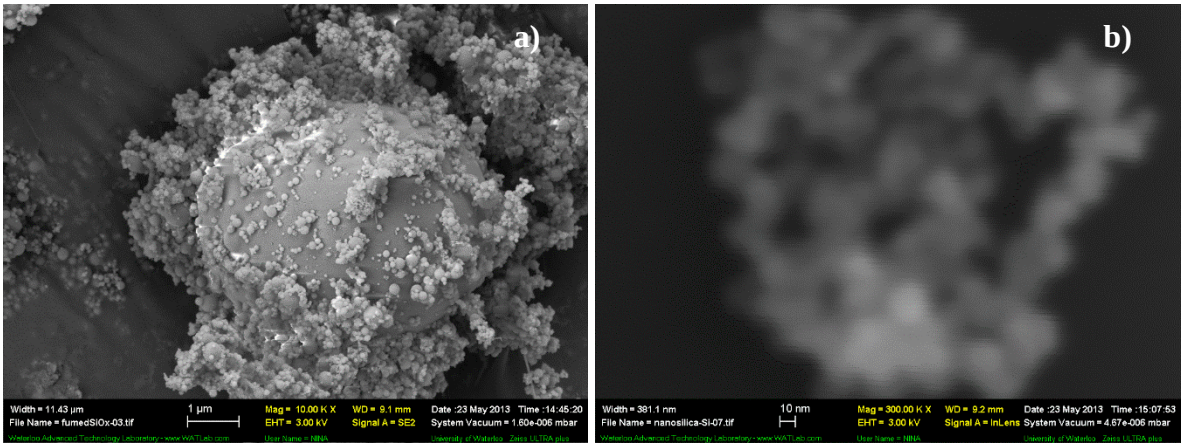

Figure 4-3: a) SEM image of silica fume (bar scale 1 µm) and b) SEM image of nanosilica (bar scale 10 nm)

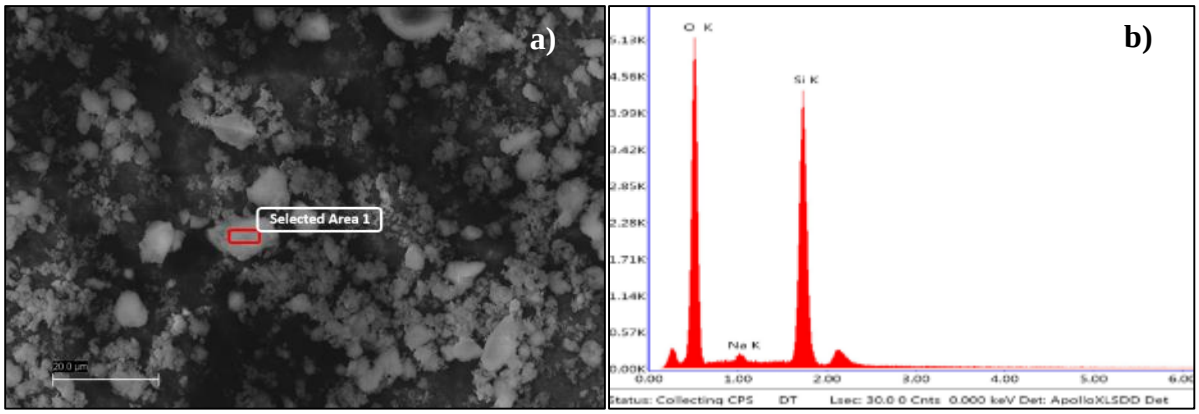

Figure 4-4: a) Area 1 of SEM analysis and b) predominant phases in the chemical analysis

Table 4-3 shows the measured SiO_2 content for nanosilica based on analysis results and compared to the purity listed in Section 3.1.1. In Table 4-3 the chemical analysis results reveal Oxygen (O) and Silicon (Si) as the predominant elements. Sodium (Na) is also present but only in insignificant quantities. Two smaller unnamed peaks also appear which indicate carbon, probably from the conductive carbon tape, and gold, from the conductive gold layer. Any carbon contamination in the nanosilica cannot be quantified because of the carbon tape used.

Table 4-3: Chemical analysis of nanosilica

Area Number	Atomic percentage (%) of each element		
	O	Si	Na
1	69.6	28.4	2.01
2	53.9	45.2	0.86
3	71.1	28.4	0.59

Based on SEM and TEM tests, it is possible to conclude that purity, particle size, and morphology of nanosilica matches the research specification.

4.1.3 Cement Characterization

Only General Use (GU) cement (or Type 10) was used in this research. St Marys Cement Inc. (Canada) was the supplier during the first two years of experimentation, whereas Holcim Canada was the cement supplier during the last year of research. The cement supplier changed because the first supplier is currently fabricating only General Use Limestone (GUL) cement instead of General Use (GU) cement. The second supplier was able to provide GU cement in order to maintain the same type of cement (GU) during the entire research study. The SEM images in Figure 4-5 reveal that the particles' sizes are in the normal range for GU cement.

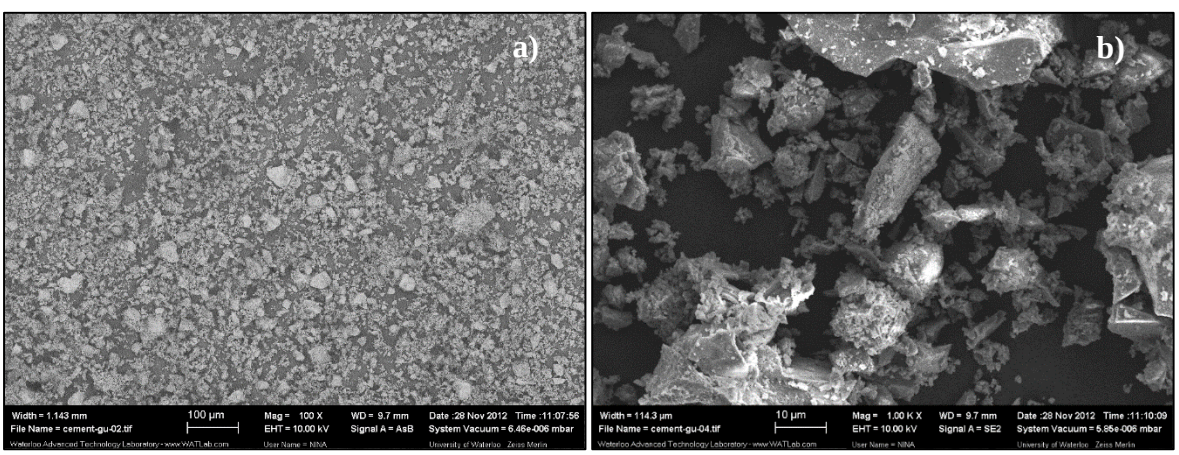

Figure 4-5: SEM pictures of GU cement a) 100 µm scale and b) 10 µm scale

Appendix B presents the physical and chemical composition of both GU cements used throughout the course of the research.

4.2 Results from Concretes and Mortars Applying Nanosilica

This section presents all results for concrete and mortar mixes produced with nanosilica, according to the procedures and proportions explained in the previous chapters.

4.2.1 Results of Fresh Concretes and Mortars

Tables 4-4, 4-5 and 4-6 present summaries of the fresh concrete properties for w/c 0.31, 0.39 and 0.45 respectively. The workability and air content of the concrete mixtures were found to be within the target range defined for this research. The demand for HRWR and AEA, respectively for the target slump and air content increased with higher amounts of nanosilica added to the mixtures. This can be explained by the fact that nanosilica adsorbs more water due to high specific surface area. Therefore, less free water was available to produce the lubrication effect in concrete and consequently, the demand for HRWR increased in order to achieve the target slump. Nanosilica increased the loss of air voids by reducing the effectiveness of the AEA. This was due to nanosilica's high fineness. Hence, the demand for AEA increased in order to achieve the target air content. Both behaviors are consistent when silica fume is used in concrete; silica fume added to concrete increases both the water demand (which can be compensated using HRWR) and the AEA demand (because the high surface area of silica fume reduces AEA's effectiveness) (FHWA, 2014).

Table 4-4: Fresh concrete properties and dosages of chemical admixtures w/c = 0.31

Mix	Nanosilica (%)	Slump (mm)	Air Content (%)	Wet Density (kg/m^3)	AEA (L/m^3)	HRWR (L/m^3)
1 (CC)	0.0	95	4	2436	0.28	3.78
2 (NSC 1)	0.5	95	5.5	2379	0.60	4.77
3 (NSC 2)	1.0	95	5.9	2379	0.72	5.17
4 (NSC 3)	1.5	90	5.4	2387	0.95	6.57

Note: CC: control concrete; NSC: nanosilica concrete.

Figure 4-6 summarizes the dosage demands for AEA admixture for different w/c ratios. The dosage demands for the HRWR admixture are summarized in Figure 4-7 for each of the w/c ratios. From both figures it is possible to conclude that for both admixtures the required dosages increase linearly with the amount of added nanosilica. The results also show a consistent trend for the w/c ratios, since in both cases when w/c decreased the admixture dosages increased; lower w/c means larger relative amounts

of cement and therefore, proportionately more nanosilica. More cement and nanosilica means higher specific surface area in the mix.

Table 4-5: Fresh concrete properties and dosages of chemical admixtures w/c = 0.39

Mix	Nanosilica (%)	Slump (mm)	Air Content (%)	Wet Density (kg/m^3)	AEA (L/m^3)	HRWR (L/m^3)
1 (CC)	0.0	82	7.0	2365	0.19	3.10
2 (NSC 1)	0.5	90	5.9	2379	0.19	3.29
3 (NSC 2)	1.0	85	5.2	2379	0.21	3.68
4 (NSC 3)	1.5	75	5.0	2401	0.24	4.26
5 (NSC 4)	2.0	90	6.5	2365	0.29	4.26

Note: CC: control concrete; NSC: nanosilica concrete.

Table 4-6: Fresh concrete properties and dosages of chemical admixtures w/c = 0.45

Mix	Nanosilica (%)	Slump (mm)	Air Content (%)	Wet Density (kg/m^3)	AEA (L/m^3)	HRWR (L/m^3)
1 (CC)	0.0	75	6.2	2358	0.13	2.52
2 (NSC 1)	1.0	65	5.3	2365	0.17	2.90
3 (NSC 2)	2.0	75	6.6	2337	0.23	3.10

Note: CC: control concrete; NSC: nanosilica concrete.

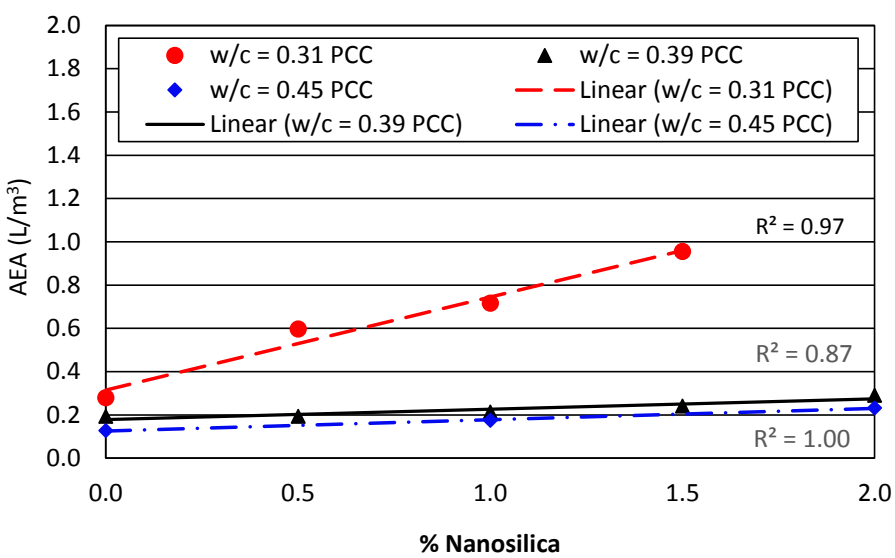

Figure 4-6: Summary of fresh concrete dosages of AEA admixture for different w/c ratios and different nanosilica proportions

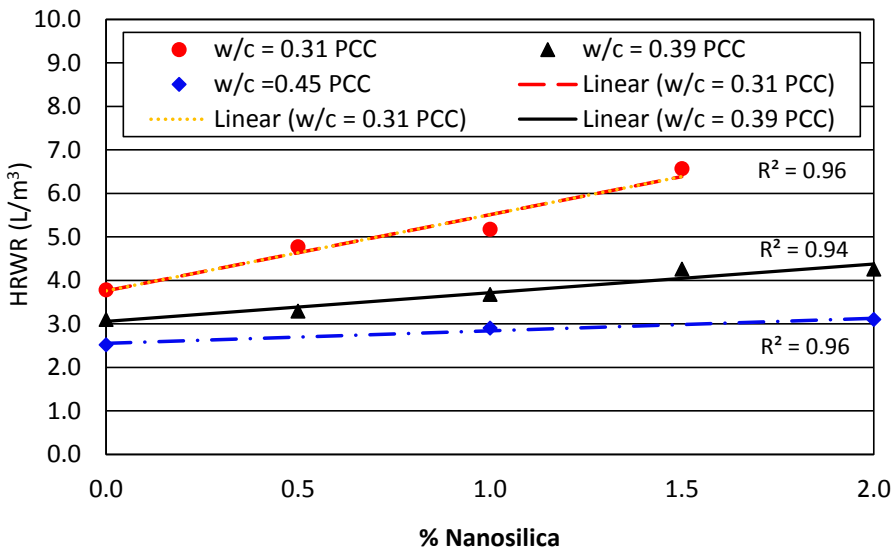

Figure 4-7: Summary of fresh concrete dosages of HRWR admixture for different w/c ratios and different nanosilica proportions

Tables 4-7 and 4-8 summarize the fresh mortar properties for the research for w/c ratios of 0.39 and 0.45, respectively. The flow consistency was found to be within the target range correlated with the slump flow of the concrete mix.

Table 4-7: Fresh mortar properties and dosages of chemical admixtures w/c = 0.39

Mortar	Nanosilica (%)	Flow Diameter (mm)	HRWR (L/m^3)
1 (CM)	0.0	182	1.28
2 (NSM 1)	0.5	188	1.60
3 (NSM 2)	1.0	182	1.96
4 (NSM 3)	1.5	185	2.17
5 (NSM 4)	2.0	183	2.45

Note: CM: control mortar; NSM: nanosilica mortar.

Table 4-8: Fresh mortar properties and dosages of chemical admixtures w/c = 0.45

Mortar	Nanosilica (%)	Flow Diameter (mm)	HRWR (L/m^3)
1 (CM)	0.0	183	1.06
2 (NSM 1)	0.5	188	1.38
3 (NSM 2)	1.0	185	1.38
4 (NSM 3)	1.5	182	1.70
5 (NSM 4)	2.0	182	2.02
6 (NSM 5)	2.5	183	2.34
7 (NSM 6)	3.0	182	2.34

Note: CM: control mortar; NSM: nanosilica mortar.

Figure 4-8 summarizes the demand for the HRWR admixture (AEA was not used in mortars). From Figure 4-8 it is possible to conclude that the mortar results are consistent with the behavior observed in concretes, since the HRWR doses increase linearly with the amount of nanosilica. Also, results show a consistent trend for the w/c ratios; when w/c decrease the dosages of HRWR increase.

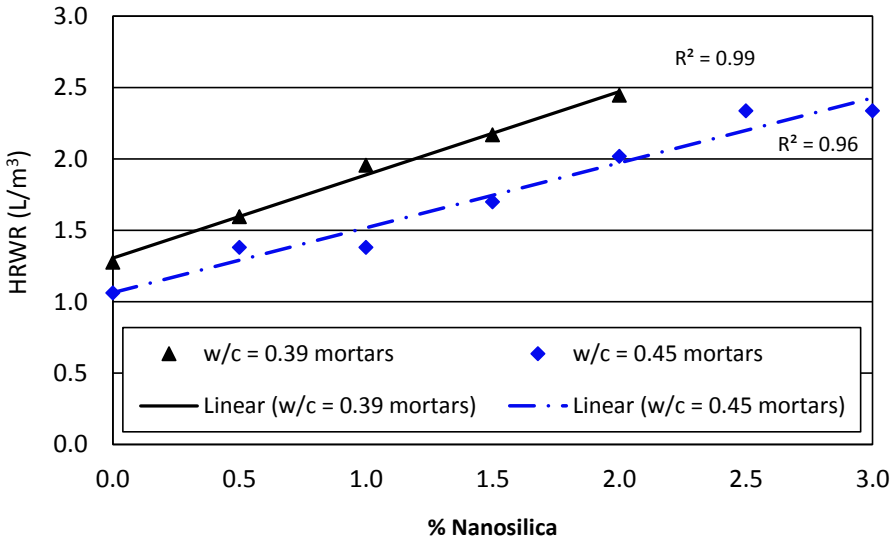

Figure 4-8: Summary of fresh mortar dosages of HRWR, for different w/c ratios and different nanosilica proportions

Results presented in Figure 4-8 present a similar trend to concrete mixes containing silica fume as reported by Chung (Chung, 2001). The summary of these results are presented in Figure 4-9. From

Figure 4-9 it is also possible to identify a linear relationship between the amount of HRWR needed and the amount of silica fume (Chung, 2001).

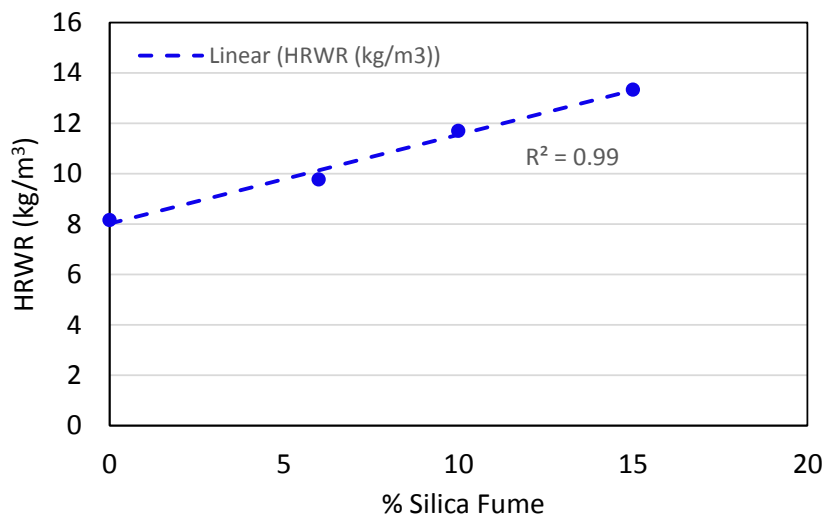

Figure 4-9: HRWR content versus percentage silica fume in fresh concrete (Adapted from Chung, 2001).

4.2.2 Results of Compressive Strength of Concretes and Mortars

The average results for compressive strength are presented in Figures 4-10, 4-11 and 4-12 for the w/c ratios 0.31, 0.39 and 0.45, respectively. Overall, the compressive strength increased when the amount of nanosilica increased. In general, the compressive strength increased when the w/c decreased and at 28 days is higher than those results at 7 days.

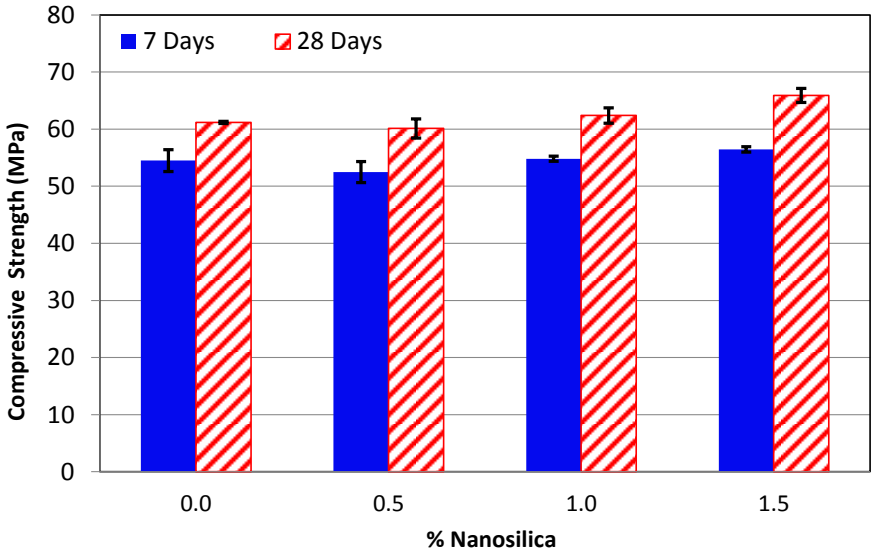

Figure 4-10: Compressive strength for different concretes at 7 and 28 days w/c = 0.31

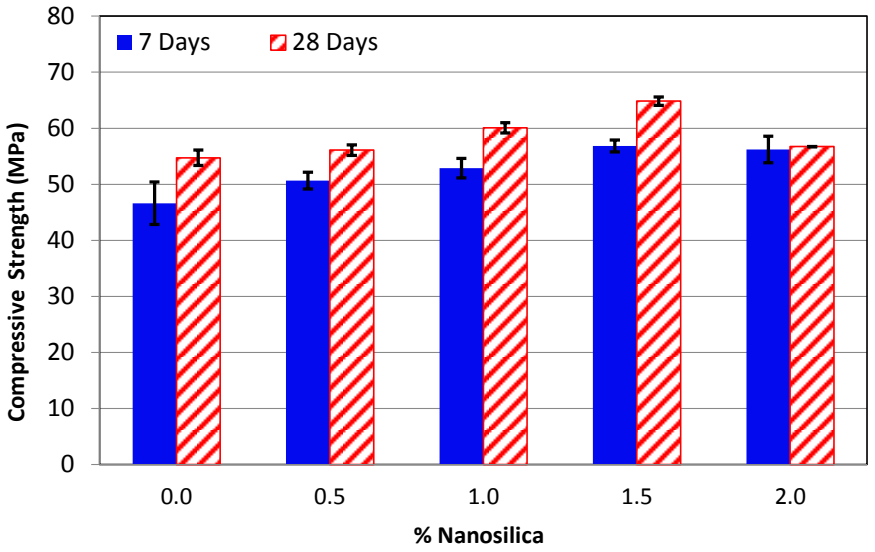

Figure 4-11: Compressive strength for different concretes at 7 and 28 days w/c = 0.39

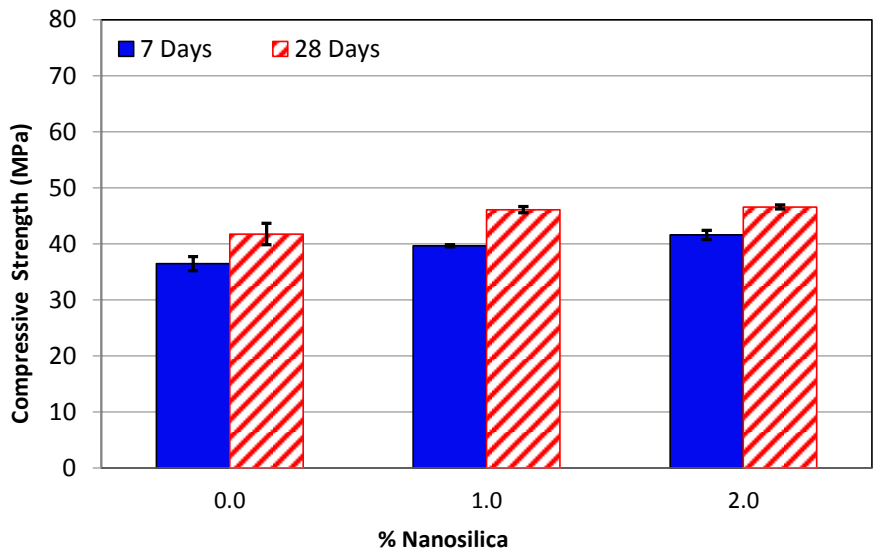

Figure 4-12: Compressive strength for different concretes at 7 and 28 days w/c = 0.45

Figures 4-13 and 4-14 present the results for compressive strength in mortar specimens. The overall trend is the same as compared to the concrete specimens where by the strength increased with an increase in the amount of nanosilica.

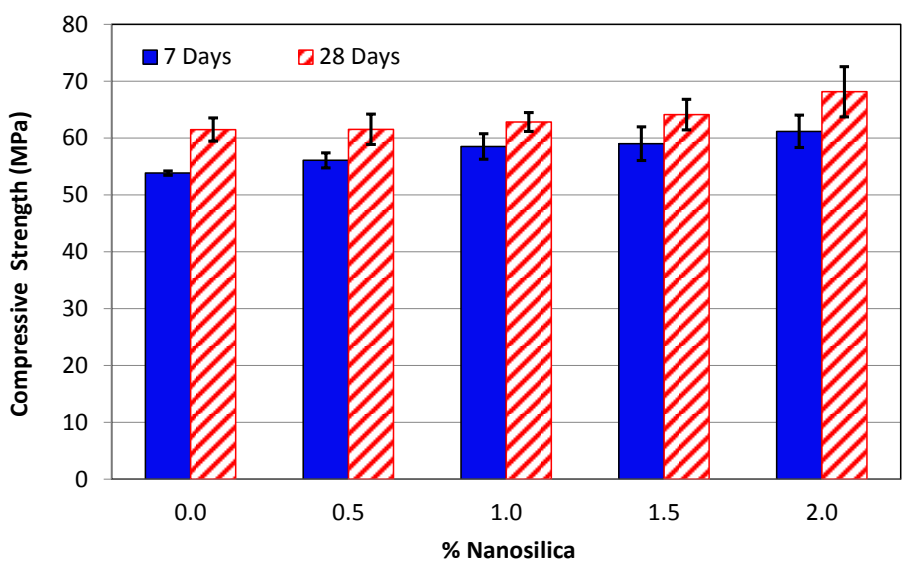

Figure 4-13: Compressive strength for different mortars at 7 and 28 days w/c = 0.39

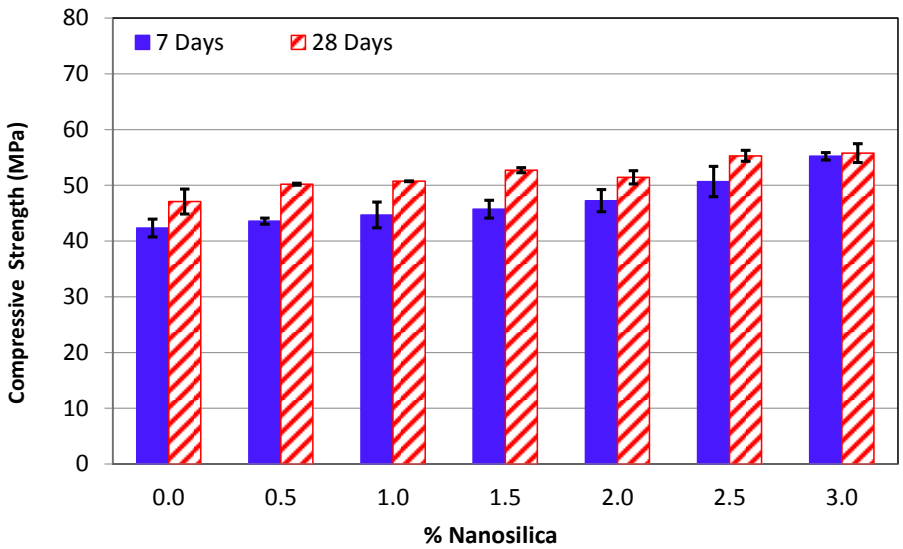

Figure 4-14: Compressive strength for different mortar at 7 and 28 days w/c = 0.45

Overall, compressive strength results are consistent, however for w/c = 0.39 the best results occurred with 1.5% of nanosilica instead of 2.0%. The difference between these two results may be explained by the air content observed in the 2.0% mixes (6.5% in 2.0% nanosilica versus 5.0% in 1.5% nanosilica).

Figure 4-15 presents a comparison of the concrete specimen and mortar specimen compressive strength results. According to Figure 4-15, mortar generally present higher strengths as compared to the concrete specimens at the same w/c ratio; this is expected behaviour since mortar mixes do not contain AEA and are not affected by coarse aggregate (Neville, 1996). Additional insights about why compressive strength increased are provided in the next section.

In Figure 4-15, all regression lines present an acceptable correlation except for w/c = 0.39 PCC (R^2 = 0.25). For this w/c ratio the best results occurred with 1.5% of nanosilica and not with 2.0% of nanosilica (See also Figure 4-11), which is not a behavior that follows the overall trend. The difference between these two results were discussed previously and may be related to the air content differences between the mix with 1.5% and 2.0% nanosilica (6.5% versus 5.0%).

For PCC, the best improvement in compressive strength occurred in concretes with a w/c = 0.39 at 1.5% nanosilica. It was able to improve the compressive strength by 18.5% compared with the control concrete. This value is consistent with the enhancement presented in Figure 2-26 (adapted from Hosseini et al., 2010) who reported improvements of 16.2% (2.0% nanosilica) and 24.9% (3.0%

nanosilica). Also Gopalakrishnan (2011), reported an enhancement of 12.31% when 1.0% nanosilica is added in a PCC of w/c = 0.42.

In PCCs with w/c ratios of 0.31 and 0.45, nanosilica was able to enhance the compressive strength by 7.7% and 12.0%, respectively compared with the control concrete. In mortars with w/c ratios of 0.39 and 0.45, nanosilica is able to enhance the compressive strength by 10.8% and 18.4%, respectively compared to the control concrete. The mortars containing 2.0% nanosilica (for w/c = 0.39) and 3.0% nanosilica (for w/c = 0.45) had the highest observed compressive strength. These results are slightly lower than those reported in the literature. For mortars, results may have been affected by the mixing energy provided by the smaller mixer. This may have affected the overall nanosilica dispersion in the mortar matrix. It is recognized in the literature that a uniform dispersion of nanoparticles is essential to obtain the best results (Gopalakrishnan et al., 2011).

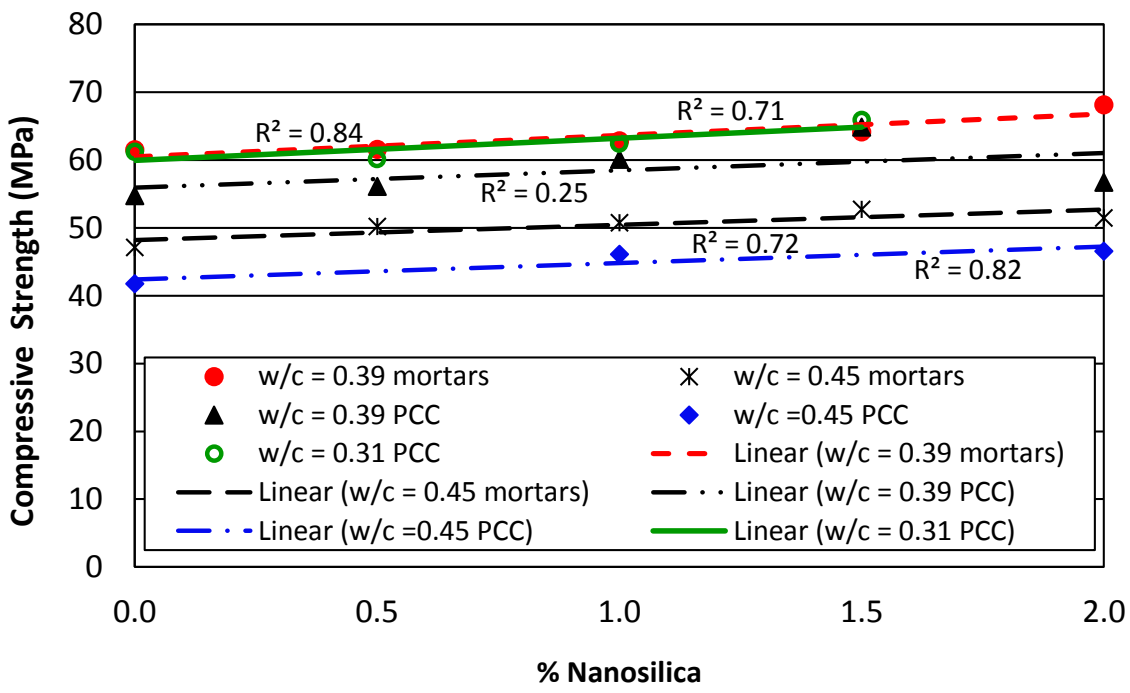

Figure 4-15: Summary of compressive strength results for different w/c ratios (Only 28 days results)

4.2.2.1 Scanning Electron Microscope (SEM) Images of Hardened Concrete

SEM testing was performed in hardened concrete at 28 days. Samples were obtained after compressive strength testing and observations were made on fracture surfaces. Figure 4-16 and Figure 4-17 present

SEM pictures which compare the concrete and nanoconcrete microstructures for w/c = 0.39 and w/c = 0.45, respectively. Figures 4-16 and 4-17 a) and b) compare both at a scale of 10 μm; Figures 4-16 and 4-17 c) and d) compare both at a scale of 1 μm and, Figures 4-16 and 4-17 e) and f) compare both at a scale of 100 nm.

In general the SEM pictures reveal modifications in the morphology of the cement paste, with the following findings:

- Adding nanosilica improved the bonding between the aggregates and the cement paste: compressive strength testing shows microcracking in the paste-aggregate interface (Figure 4-16 and 4-17 a). In Nanoconcrete with 2.0% nanosilica, fewer microcracks were observed in the paste-aggregate interface; for instance Figure 4-16 a) shows no microcracking in the interface, a finding explained by nanomaterial´s enhancement of the Interfacial Transition Zone (ITZ).
- Adding nanosilica reduces ettringite crystal formation in voids. Figures 4-16 and 4-17 c) display ettringite crystals in the form of needles filling the void. In contrast, Figures 4-16 and 4-17 d) show almost no crystals in voids of nanoconcrete. This result was not expected, however He and Shi (2008) reported that ettringite crystals were much less identifiable in concretes with nanomaterials. Also, according to Gopalakrishnan (2011), nanoparticles will prevent the crystal from growing as AFm. Ettringite formation can affect concrete durability; in concretes exposed to moisture for long periods, the ettringite crystals slowly dissolved. This resulted in less dense spots in the concrete matrix. Also a lower amount of ettringite crystals can be beneficial to protect concrete against sulfate attack, which can produce an expansive reaction (Kosmatka, 2011).
- The addition of nanosilica produces a more dense and compact cement paste, as can be seen in Figures 4-16 and 4-17 e) and f). According to He and Shi (He & Shi, 2008), nanomaterials promote the formation of high-density C-S-H structures, especially when nanosilica is added.

Supplementary cementing materials improve the microstructure and pore-structure of concrete through their filler effect (reducing microporosity), pozzolanic effect (replacing porous calcium hydroxide (CH) with C-S-H), wall effect (increasing density of ITZ) and pore blocking (by combination of the above factors). Nanosilica can also act like a supplementary cementing material due to the very small particle size and high silica content. SEM images provided evidence as to how the ITZ and the paste density were improved. From SEM images, only the filler effect can be observed directly.

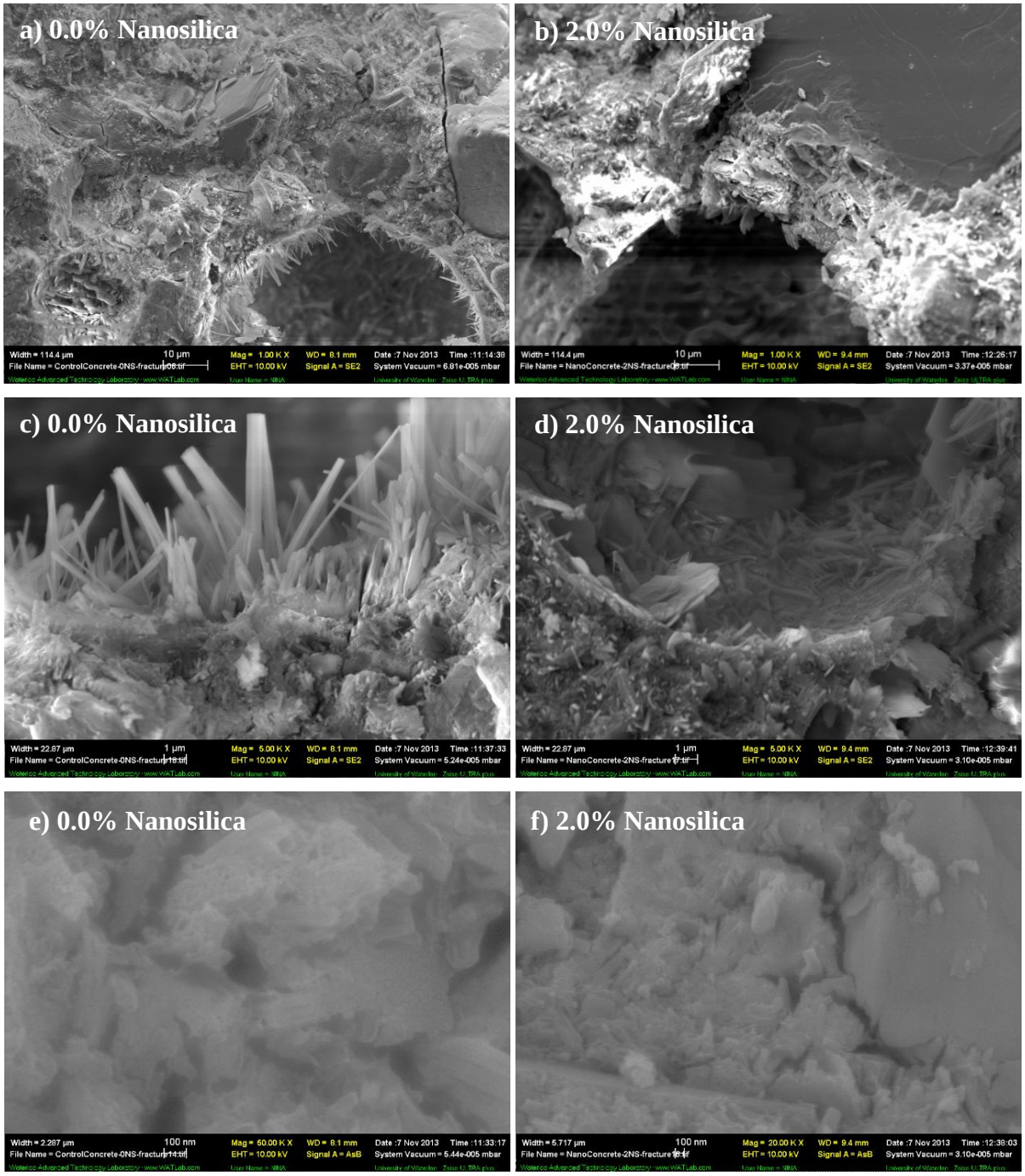

Figure 4-16: SEM pictures of hardened concrete, comparing concrete microstructures. Comparisons between control concrete and nanoconcrete (2.0% nanosilica) at different scales: a) and b) 10 μm scale; c) and d) 1 μm scale and, e) and f) 100 nm scale w/c = 0.39

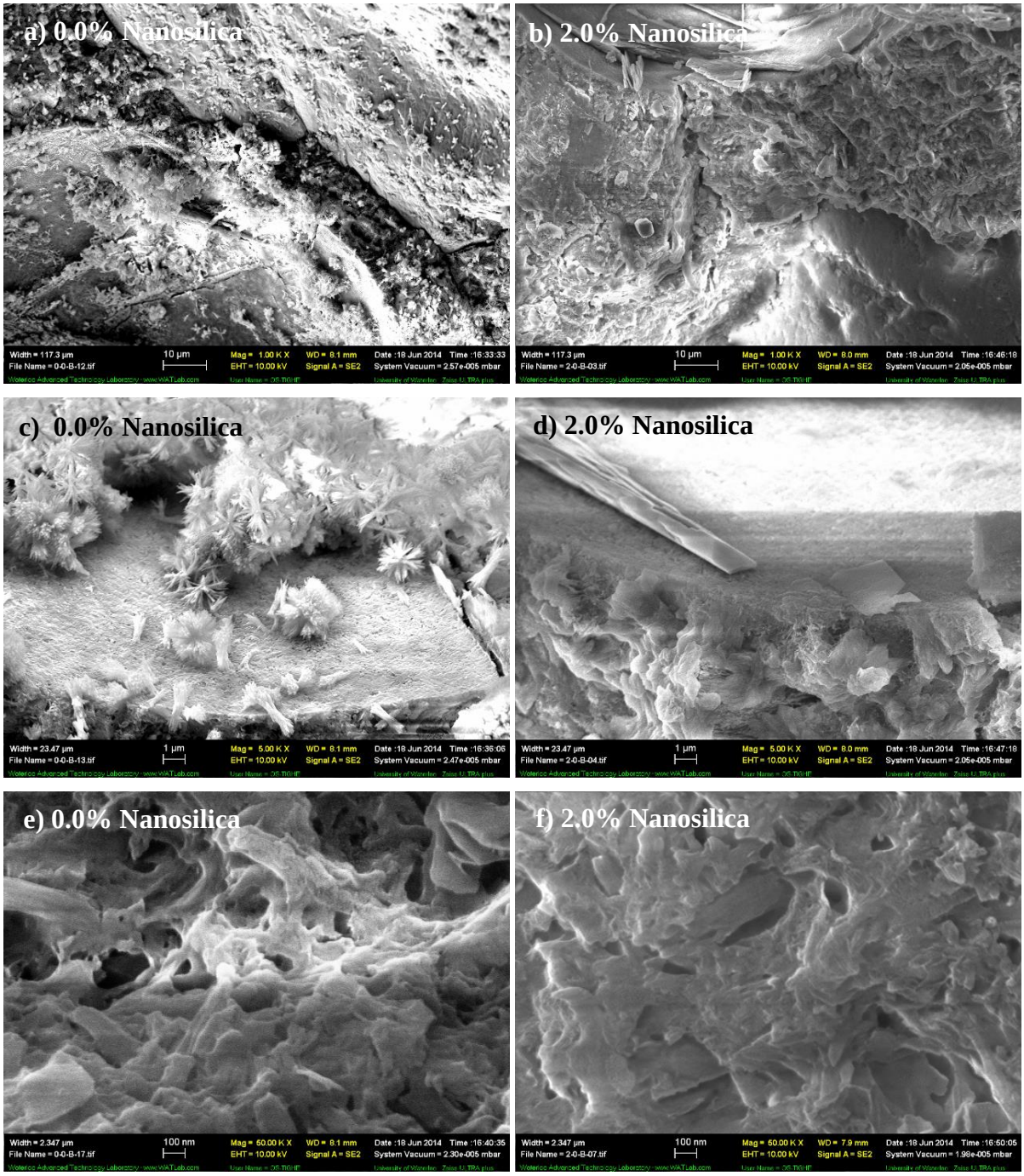

Figure 4-17: SEM pictures of hardened concrete, comparing concrete microstructures. Comparisons between control concrete and nanoconcrete (2.0% nanosilica) at different scales: a) and b) 10 μm scale; c) and d) 1 μm scale and, e) and f) 100 nm scale w/c = 0.45

As discussed in Chapter 2, the bonding quality between the cement paste and aggregates as well as the quality of the cement paste play a key role in the development of the strength of the concrete. Several factors influence paste quality, however the paste density is the most important single factor affecting paste strength (Lamond & Pielert, 2006). Figures 4-16 and 4-17 e) and f) which reveal the increased density of nanoconcrete, serve to reinforce this idea as the more dense concretes with nanosilica provide higher strengths than the control concrete.

4.2.3 Results of Friction Response of Concretes – Broom Finishing

The average results for the measured friction or skid resistance including three samples per sample age group as well as each nanosilica dosage amount are presented in Figures 4-18. In Figure 4-19 five samples are included. The friction property was measured with a British Pendulum Number (BPN). In general, the nanosilica concrete exhibited higher BPN values than the control concrete. Overall, friction at 7 days is lower than those at 28 days. The mechanism which results in increased friction will be discussed in the next section using the SEM pictures of mortar surfaces.

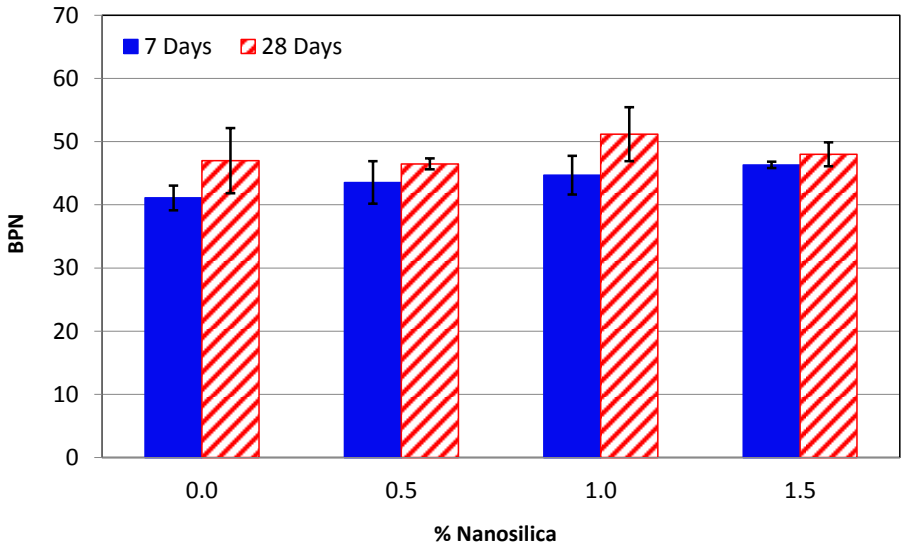

Figure 4-18: British Pendulum Number (BPN) for different concretes at 7 and 28 days, broom finishing (3 samples per % and age) w/c = 0.31

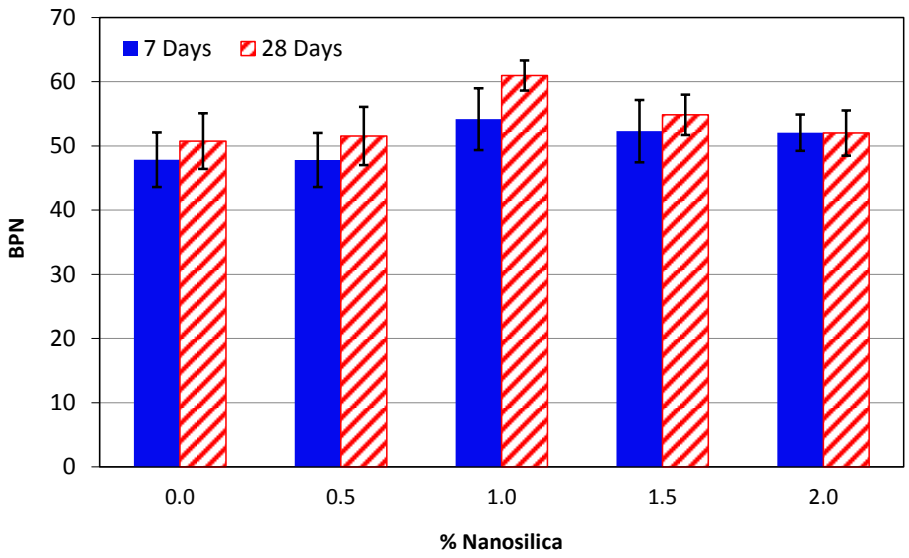

Figure 4-19: British Pendulum Number (BPN) for different concretes at 7 and 28 days, broom finishing (5 samples per % and age) w/c = 0.39

In order to have a higher number of samples per each nanosilica percentage, new mixes were developed and all samples were cured for 28 days. The average results for the measured friction are presented in Figures 4-20 and 4-21. In general, the nanosilica concretes present higher BPN values than the control concrete.

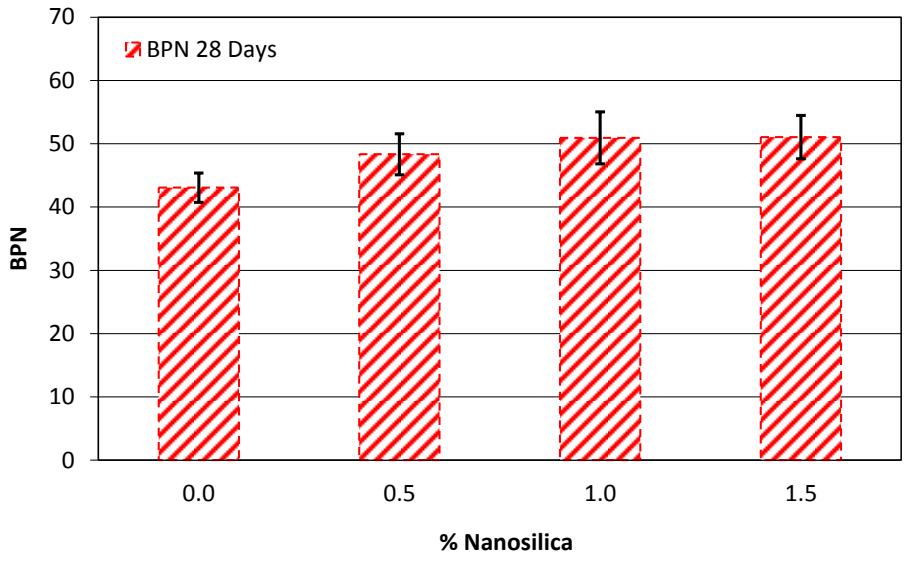

Figure 4-20: British Pendulum Number (BPN) for different concretes at 28 days, broom finishing (15 samples in each %) w/c = 0.31

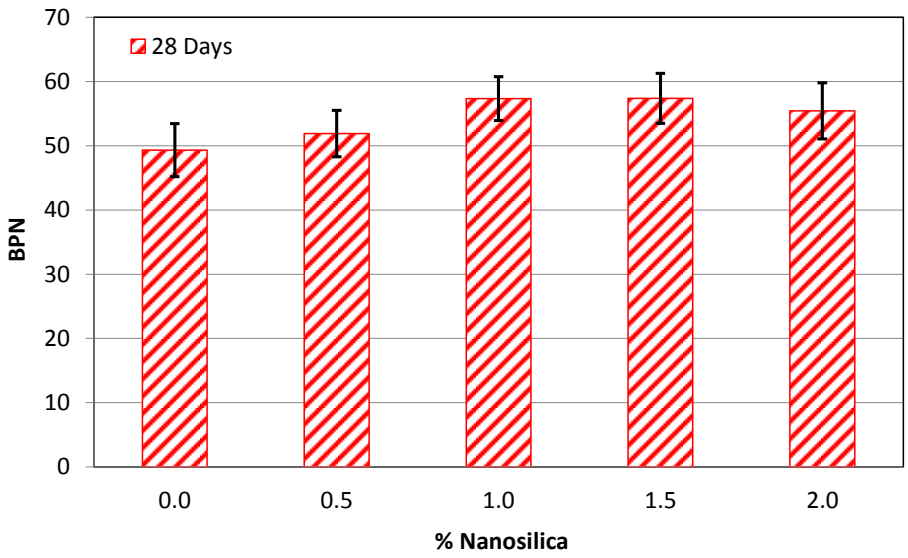

Figure 4-21: British Pendulum Number (BPN) for different concretes at 28 days, broom finishing (15 samples in each %) w/c = 0.39

In Figures 4-20 and 4-21, the enhancement in the mean of BPN between the control concrete and the 1.0% nanosilica concrete is 18.2% and 16.2%, respectively.

In the experiments with broom finish presented in Figure 4-20 and 4-21, the macrotexture can influence the variability of the results. Even though the macrotextures were visually inspected in this research, it was not feasible to measure and quantify the macrotexture in order to test only the samples with equivalent macrotexture. However, in practice pavement finishing also presents variability in the macrotexture, hence the criteria was to accept this variability of the samples since it is representative of what can be expected in the field.

From Figure 4-21 it is possible to see that the average results present a maximum BPN in 1.0% and 1.5% nanosilica concrete with a small decrease observed in the 2.0% nanosilica concrete. This behaviour will be explained in the next sections.

4.2.4 Results of Friction Response of Concretes and Mortars – Smooth Finishing

In order to eliminate the potential effect of macrotexture on the friction response, a new experiment was designed using concrete and mortar with smooth surfaces. This section presents the results for this experiment. The friction response increases with increased nanosilica content (Figure 4-22). Figure 4-23 presents the linear regression model for BPN at 28 days.

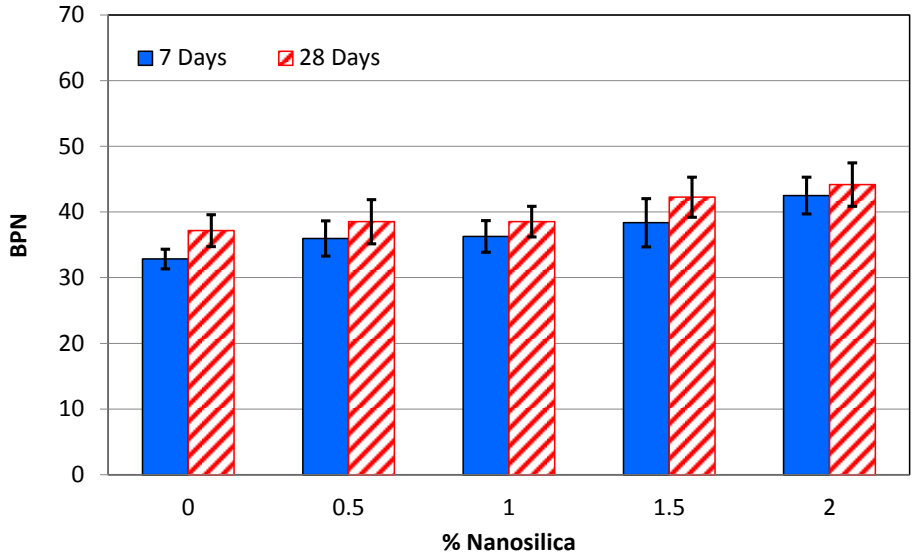

Figure 4-22: British Pendulum Number (BPN) for different concretes at 7 and 28 days, smooth finishing (5 samples per % and age) w/c = 0.39

In Figure 4-22, the enhancement in the mean BPN between the control mortar and the 1.5% and 2.0% nanosilica mortar is 13.7% and 18.8%, respectively.

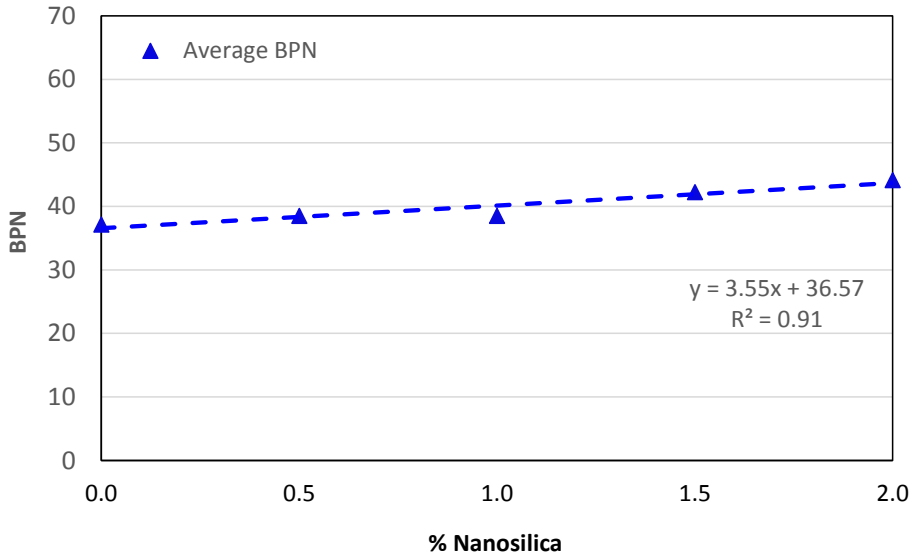

Figure 4-23: Linear regression model for BPN at 28 days w/c = 0.39

Figure 4-24 presents two outputs with the friction coefficient using the tribometer. In Figure 4-24 a) sample 2 with 0.0% nanosilica (Control mortar) is presented while Figure 4-24 b) shows the results

of sample 2 with 2.0% nanosilica. The comparison of both figures reveals that the friction coefficient in nanoconcrete is increased.

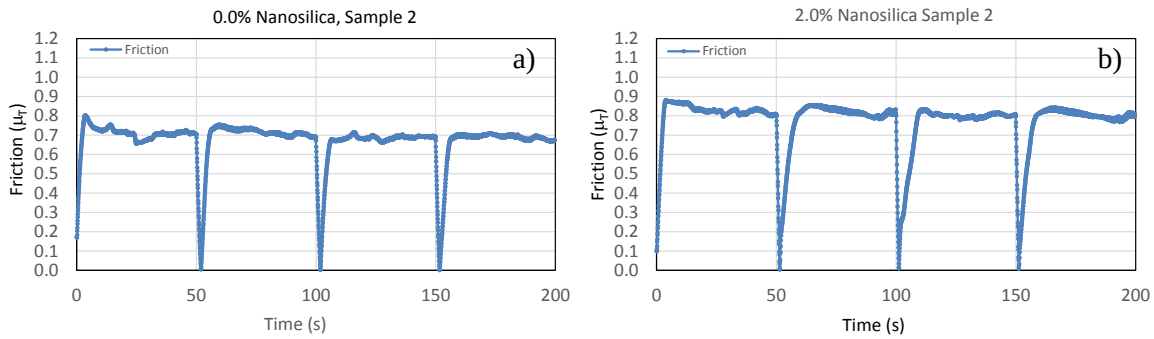

Figure 4-24: Examples of curves of friction using the tribometer: a) control concrete, sample 2 and b) 2.0 % nanosilica, 100 gr vertical force

In Chapter 3 it was indicated that plotting the friction curve versus time notable differences in the static and dynamic coefficients are observed. In the tribometer the dynamic coefficient was considered to be the average across the plateau section. Therefore for each sample, 4 different coefficients were calculated, and their average is the representative of each sample. This method was applied for each load. Figure 4-25 presents the friction coefficient results for different amounts of nanosilica and two different vertical forces. For these forces, the friction response increases with increased nanosilica, to a maximum value with 1.5% nanosilica; this behaviour will be explained in the next section using SEM images.

In Figure 4-25, the friction enhancement between the control mortar and the 1.5% nanosilica mortar is 25.4% and 19.5% for the 50 g and 100 g vertical forces, respectively. Since the results for each nanosilica proportion are very similar, Figure 4-26's linear regression model combines all these results to show this trend. With both devices, friction response rises when the amount of nanosilica is increased.

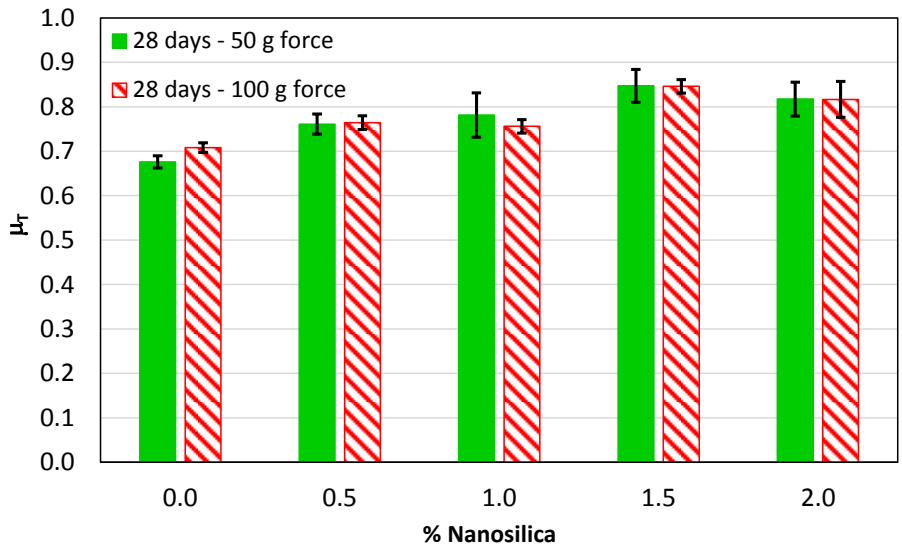

Figure 4-25: Friction coefficient μ_T using the tribometer, mortars 28 days old and w/c = 0.39

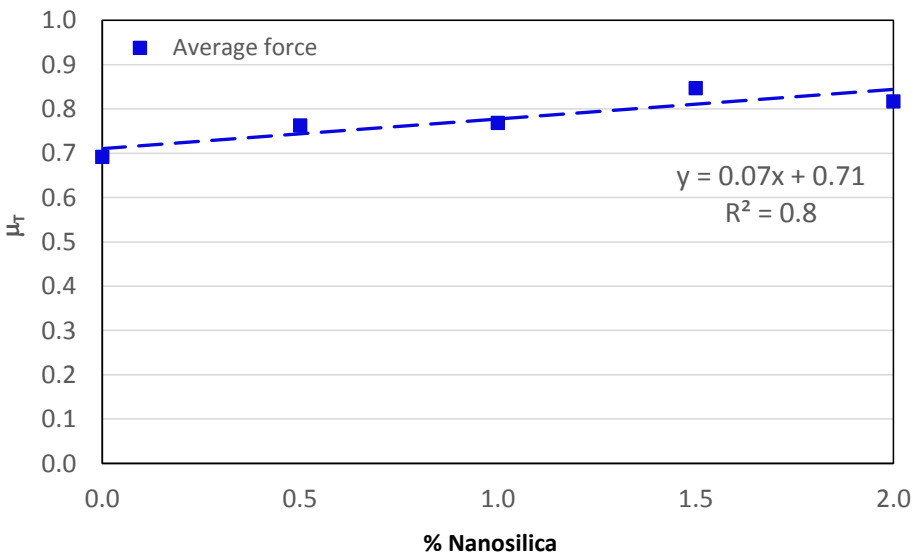

Figure 4-26: Linear regression model for friction response using the tribometer (w/c = 0.39)

4.2.4.1 Surface Profilometer Results

As shown in Figure 4-25 the highest friction coefficient in mortars occurred with 1.5% nanosilica. Thus, Figure 4-27 shows three control 0.0% nanosilica samples paired with three 1.5% nanosilica samples for comparison. The graphs were separated in pairs only for clarity. Small differences occur in the

surface morphology, which is related to the number of asperity peaks at macro-level; however, to determine whether this modification is significant, the RMS (Root Mean Square) indicator is analyzed.

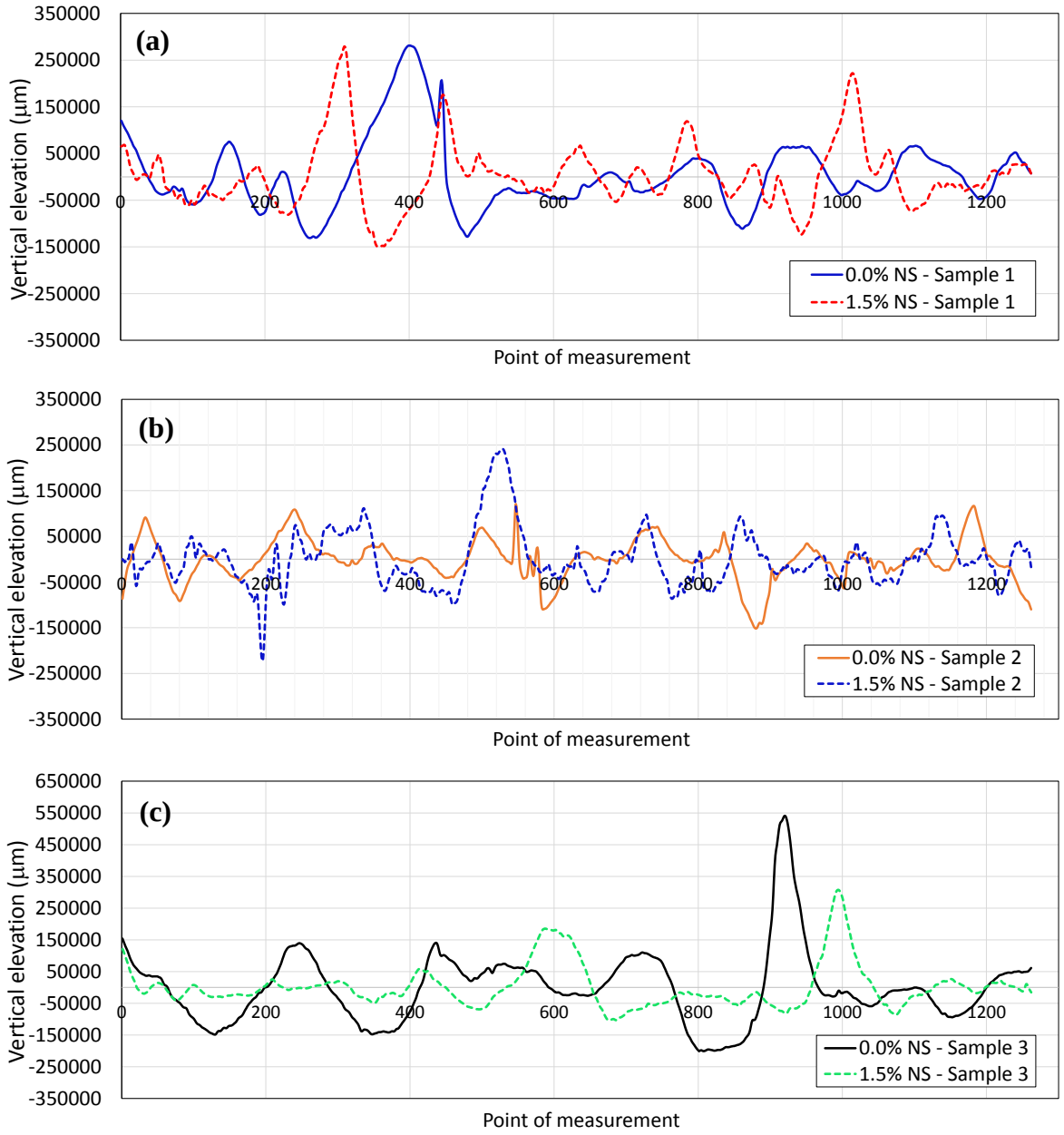

Figure 4-27: Surface roughness for mortars comparing samples with 0.0% nanosilica (minimum friction) and with 1.5% nanosilica (maximum friction): a) samples number 1 , b) samples number 2 c) samples number 3

- ***Root Mean Square (RMS) of Mortars***

According to Gohar (Gohar & Rahnejat, 2008), the RMS value represents the Standard Deviation of peak distribution in respect to the mean line. Therefore, the highest values represent more surface irregularities. The regression model of RMS results for each nanosilica proportion (Figure 4-28) presents a low coefficient of determination R^2, meaning that the friction improvement cannot be attributed to modifications at microscale, since the surface profilometer's tip radius is 2 μm. Therefore, a new approach for measurement of the surface modifications is presented in the next section.

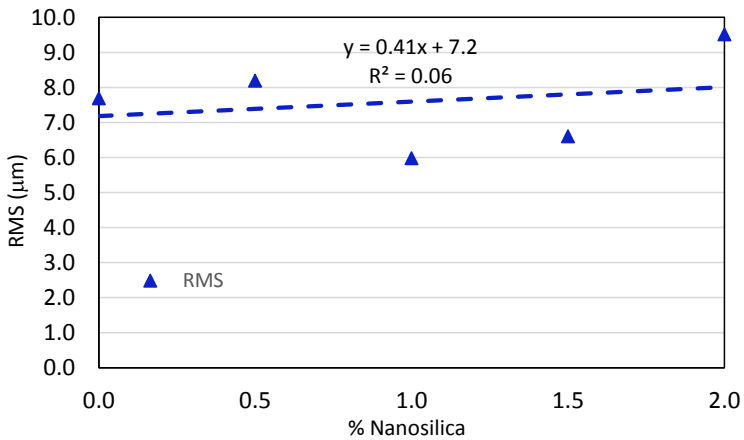

Figure 4-28: Regression model of RMS results

4.2.4.2 Scanning Electron Microscope (SEM) Images of Mortar Surfaces

Figure 4-29 presents SEM pictures which compare 28-day mortar surfaces with 0.0% and 1.5% nanosilica. Figures 4-29 a) and b) compare both at a scale of 10 μm; Figures 4-29 c) and d) compare both at a scale of 1 μm and Figures 4-29 e) and f) compare both at a scale of 200 nm. The SEM pictures reveal that adding nanosilica to the mortar mix roughens the surface morphology by creating a larger peak to valley heights with more asperities. The crystals' morphology on the surface also differs, because nanosilica particles modify the surface morphology of cement-based materials by acting as nucleation centers and allowing crystal growth on the surface of different shapes. These two effects result in an increased roughness and therefore, an increased friction response, since the asperities increase the real contact area between the rubber and pavement. According to Gopalakrishnan (2011) very fine materials such as nanomaterials promote nucleation in the cement paste, and thus the generation of C-S-H.

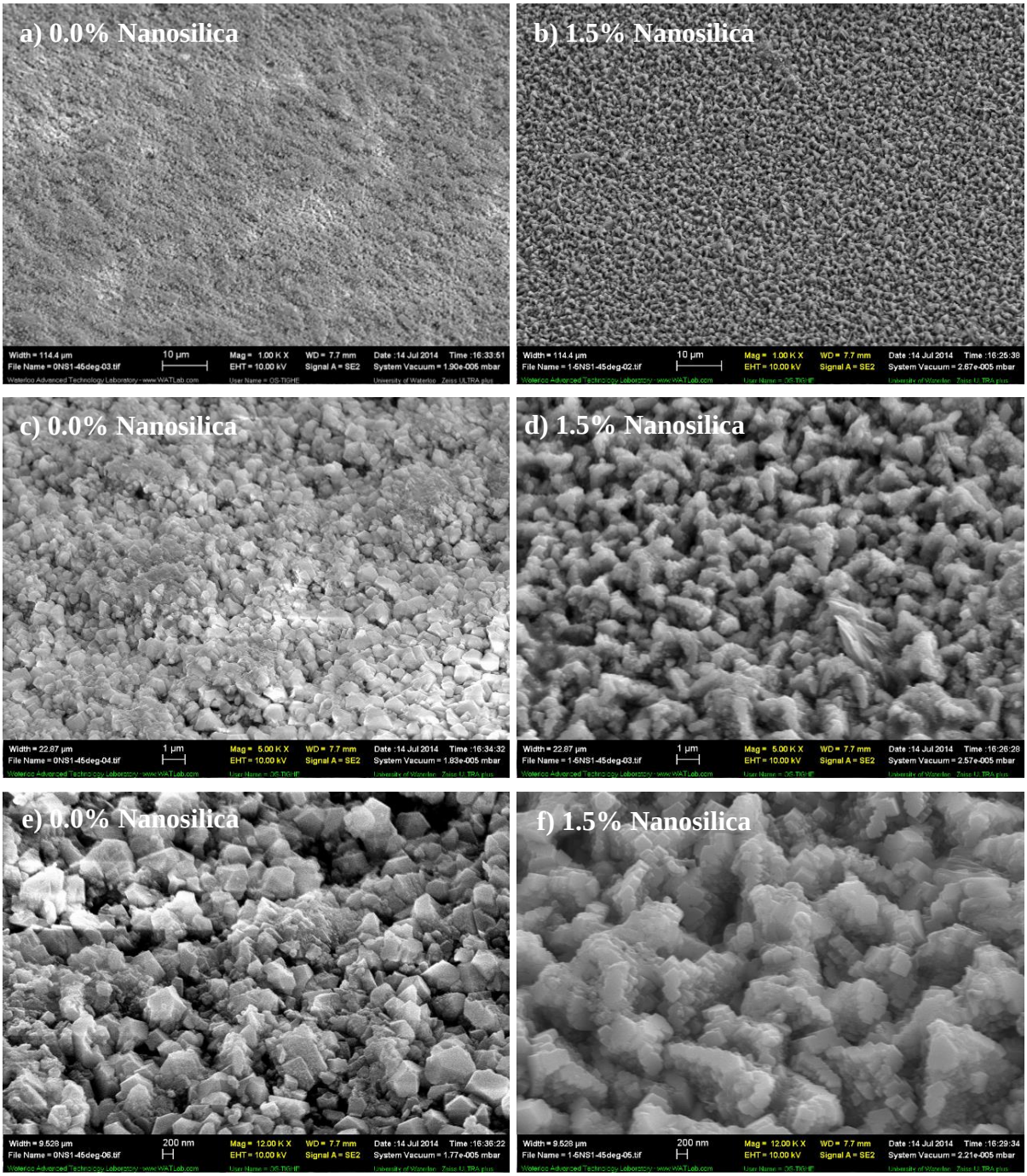

Figure 4-29: SEM images comparing mortars' surface texture. Comparison between control mortar (0.0% nanosilica) and nanomortar (1.5% nanosilica) at different scales: a) and b) 10 μm scale; c) and d) 1 μm scale and, e) and f) 200 nm scale

4.2.4.3 Scanning Electron Microscope (SEM) Images of Concrete Surfaces

Figure 4-30 presents SEM pictures of 28-day concrete surfaces with 0.0% and 1.5% nanosilica.

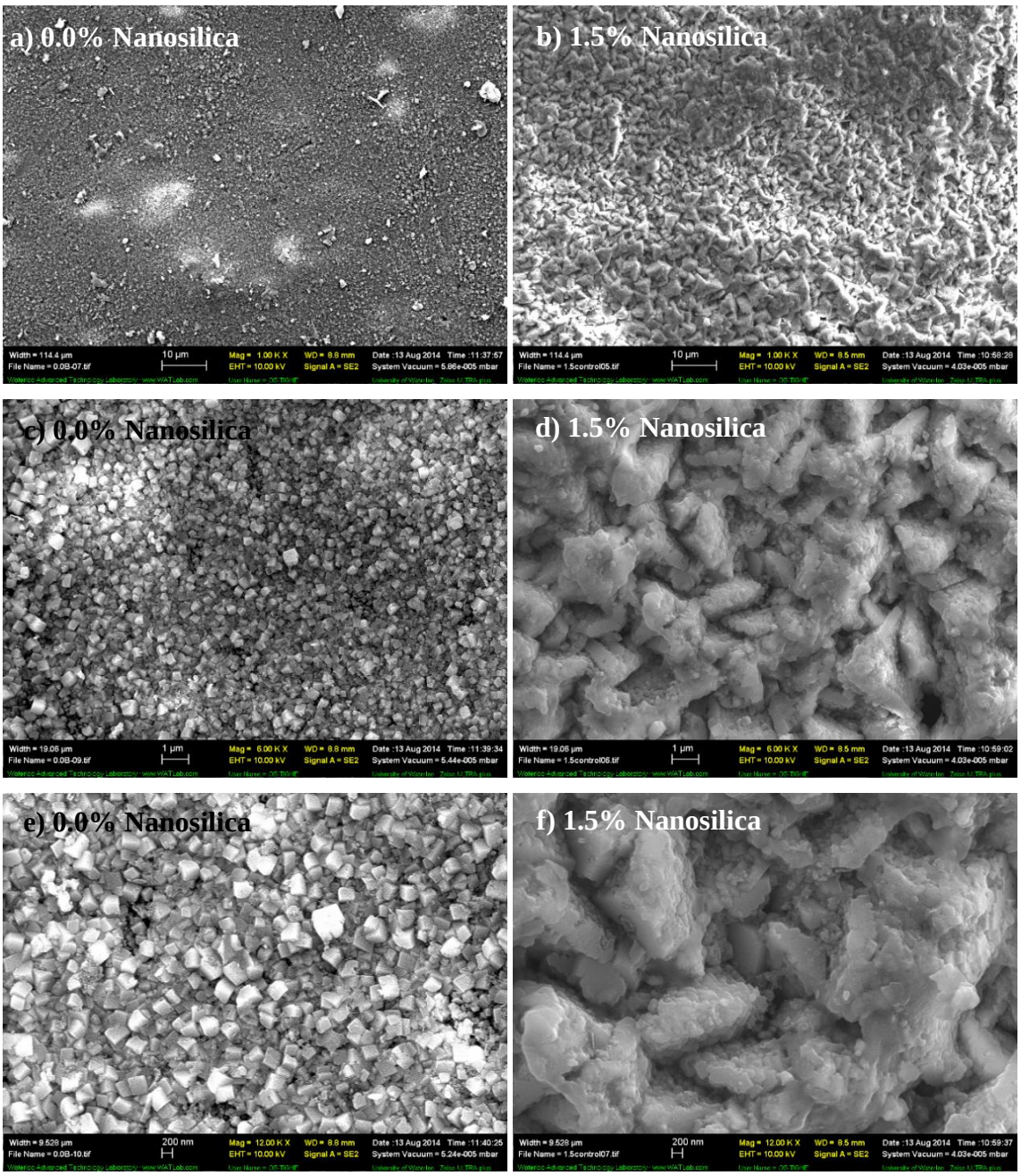

Figure 4-30: SEM images comparing concretes' surface texture. Comparison between control mortar (0.0% nanosilica) and nanomortar (1.5% nanosilica) at different scales: a) and b) 10 μm scale; c) and d) 1 μm scale and, e) and f) 200 nm scale

Figures 4-30 a) and b) compare both at a scale of 10 μm; Figures 4-30 c) and d) compare both at a scale of 1 μm and Figures 4-30 e) and f) compare both at a scale of 200 nm. The images reveal similar results as compared with SEM images from mortars (Figure 4-29) because adding nanosilica to the concrete mix roughens the surface morphology and creates a different crystal geometry.

Figure 4-21 and Figure 4-25 show a slight decrease in friction for the 2.0% nanosilica concretes. In order to explain this behaviour new SEM images were captured for mortars and concretes, which are presented in Figure 4-31. Figure 4-31 a) presents the nanomortar while Figure 4-31 b) presents the nanoconcrete, both at the scale of 1 μm. From these pictures it is possible to see that the surfaces are as rough as the images presented for 1.5% nanosilica (in mortars and concretes, Figures 4-29 and 4-30 respectivelly), however is also possible to see that some crystals that present a "smooth" peak. This characteristic may explain why the friction response slightly decreases.

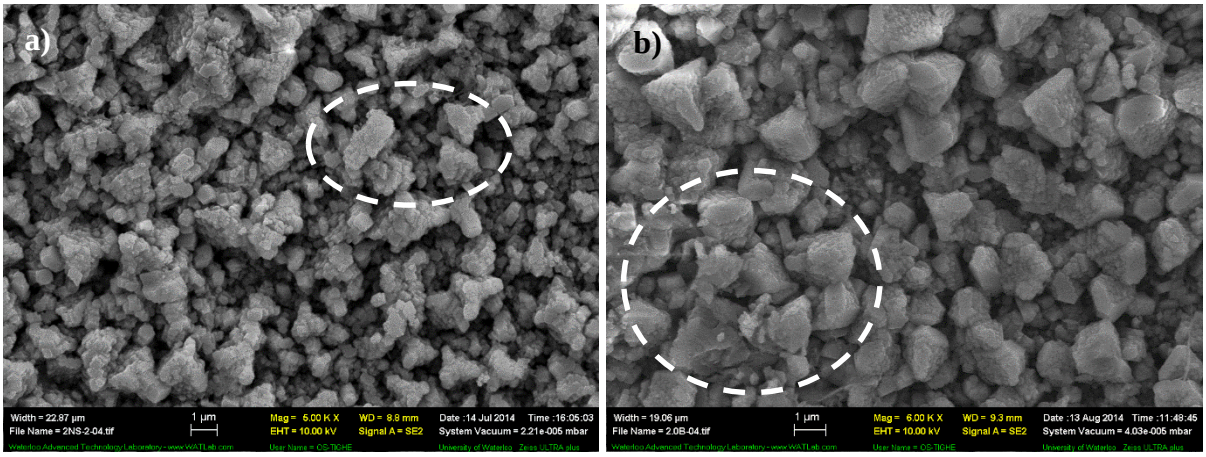

Figure 4-31: SEM images comparing 2.0% nanosilica mortar and 2.0% nanosilica concrete's surface texture (scale: 1 μm)

4.2.5 Noise Absorption of Concretes Samples

The acoustic sound absorption spectra for different concrete specimens with a w/c of 0.31 are presented in Figures 4-32 a) and b). Figure 4-33 presents the maximum sound absorption coefficients at 7 and 28 days for the w/c ratio of 0.31.

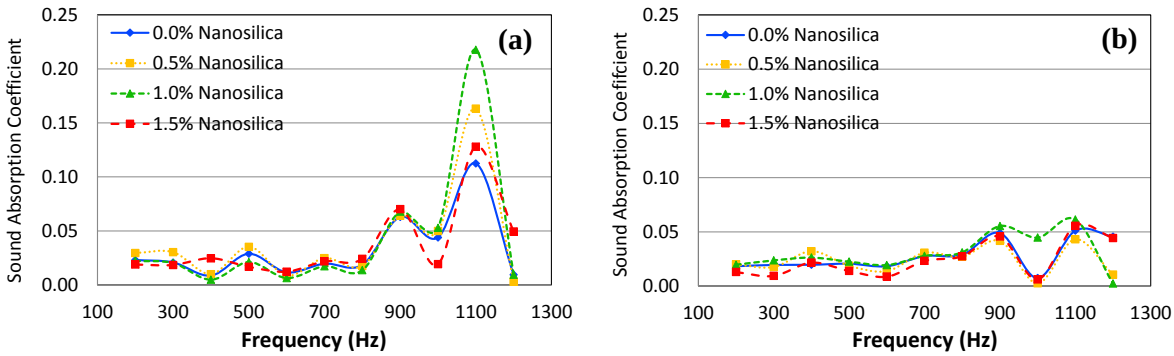

Figure 4-32: Acoustic absorption spectra for different a) 7 days and b) 28 days old concretes w/c = 0.31

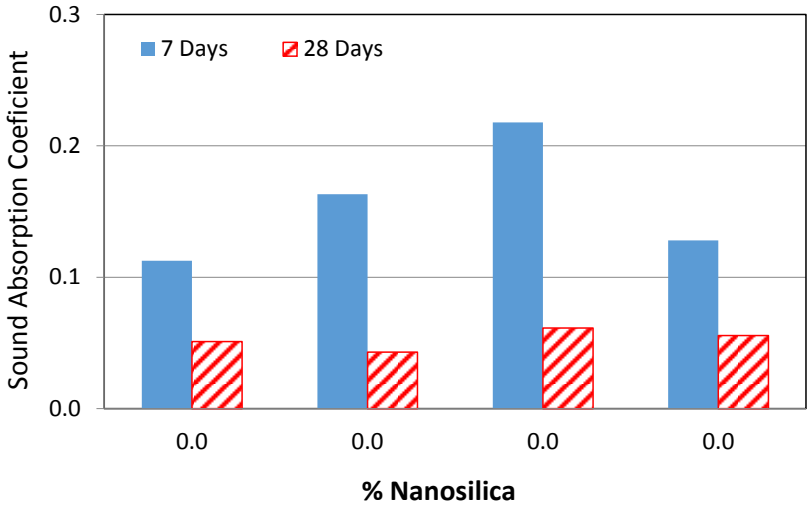

Figure 4-33: Maximum sound absorption coefficient for different concretes at 7 and 28 days w/c = 0.31

Figures 4-32 and 4-33 show that the absorption coefficient increased with the incremental amount of nanosilica. The increase occurred in the frequencies ranging from 800 to 1200 Hz. These results are consistent with the previous studies (Chung 2002 and 2004), which reported that certain supplementary cementing materials, such as silica fume, can improve the concrete sound absorption ability due to an enhancement in the damping capacity. Improved damping properties enhance energy dissipation and thus increase sound absorption (Ashby et al., 2009).

The effect of nanosilica for w/c = 0.39 on sound absorption of concrete is more obvious in Figure 4-33. This figure shows the maximum absorption coefficient of 7 and 28 day-old concrete specimens in the same range of frequencies (200 Hz to 1200 Hz). In all cases, the maximum sound absorption

occurred at 1100 Hz. The large differences were observed between the sound absorption coefficients of concrete at 7 days and 28 days. This could be explained by the relatively high porosity in the concrete microstructure at 7 days as compared to that in the concrete at 28 days. The young mortar possesses a higher porosity than the matured mortar at the nano scale (Taylor, 1997). In hardened concrete at 28 days, the highest levels of absorption coefficients occurred in concretes containing 1.0% and 1.5% nanosilica. According to Ahammed (Ahammed & Tighe, 2011), the conventional concrete pavement finish of broom finishing has a maximum sound absorption coefficient of 0.05. This is consistent with the absorption coefficient observed in the case of the control mix (0.0% nanosilica), presented in Figures 4-33 and 4-35. Also, as shown in Figures 4-33 and 4-35, at 28 days the sound absorption coefficients for the concretes with 1.0% and 1.5% nanosilica are higher than that of the control concrete. In the chapter discussing statistical analysis, the significance of this change will be analyzed.

The acoustic sound absorption spectra for different concrete specimen samples with a w/c of 0.39 are presented in Figures 4-34 a) and b). Figure 4-35 presents the maximum sound absorption coefficient at 7 and 28 days for the w/c ratio of 0.39.

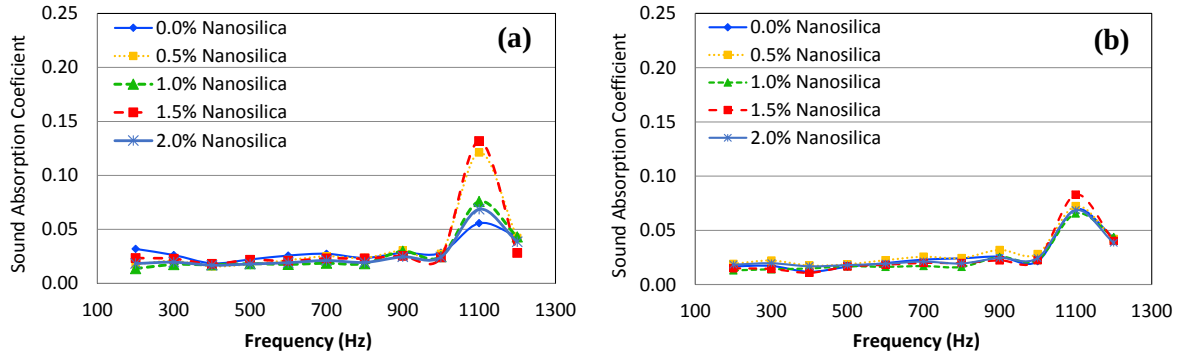

Figure 4-34: Acoustic absorption spectra for different a) 7 days and b) 28 days old concretes w/c = 0.39

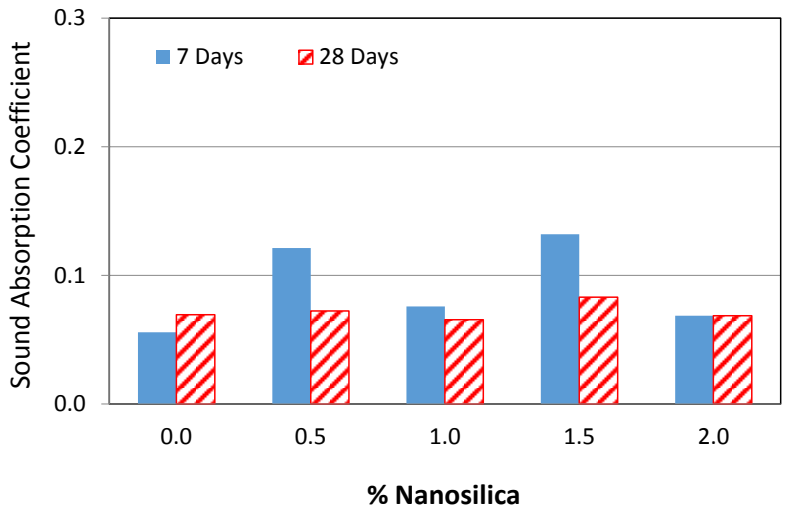

Figure 4-35: Maximum sound absorption coefficient for different concretes at 7 and 28 days w/c = 0.39

The general trend in the results with w/c = 0.39 is different than the results from the w/c = 0.31, since in Figure 4-35 is possible to see that the maximum absorption coefficient is observed in 0.5% and 1.5% nanosilica concretes, while 1.0% and 2.0% nanosilica concretes show no improvement over the control concrete (at 28 days).

4.2.6 Abrasion Response of Concretes – Smooth and Broom Finishing

The abrasion tests were conducted on both broom and smooth finished specimens (Figure 4-36). The results demonstrate a noticeable decreasing trend in the wear of the specimens with higher amounts of nanosilica, especially in those with smooth finishing. The surface finishing has a major impact on wear, as can be seen in the better relation between the results for the smooth finishing specimens compared to those with broom finishing. According to the Federal Highway Administration (FHWA, 2013), the abrasion resistance of a concrete material surface will vary depending on the finish of its surface. Broom-finished surfaces present significant variability in their abrasion response, as suggested in Figure 4-36. However, overall, the results support the fact that compressive strength enhances the abrasion resistance of concrete, because an increased compressive strength delivers better abrasion resistance results.

In Figure 4-36, 1.0% of nanosilica at 7 and 28 days for broom finishing shows higher mass loss than the other mixes, an inconsistency explainable by variability in the finishing process. Figure 4-37

compares a sample with 0.0% nanosilica (Figure 4-37 a) to one with 1.0% nanosilica (Figure 4-37 b), the latter showing surface irregularities easily removed by the cutters. The small scale of the measured weight loss (less than 10 g), makes the results very sensitive to error, which helps to explain the above inconsistency.

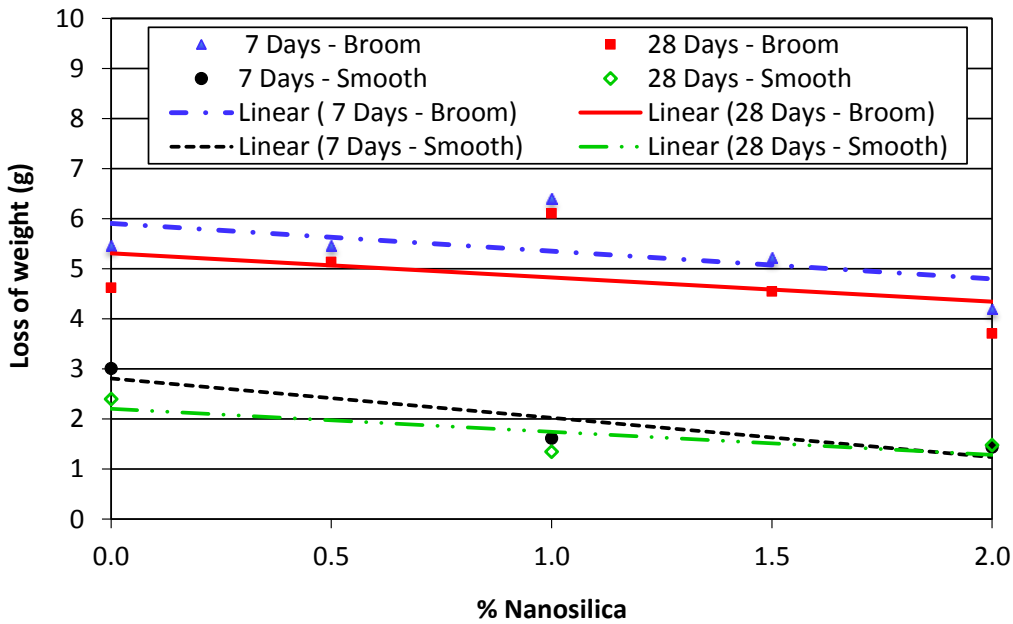

Figure 4-36: Abrasion resistance for different amount of nanosilica at 7 and 28 days old – broom and smooth finishing w/c = 0.39

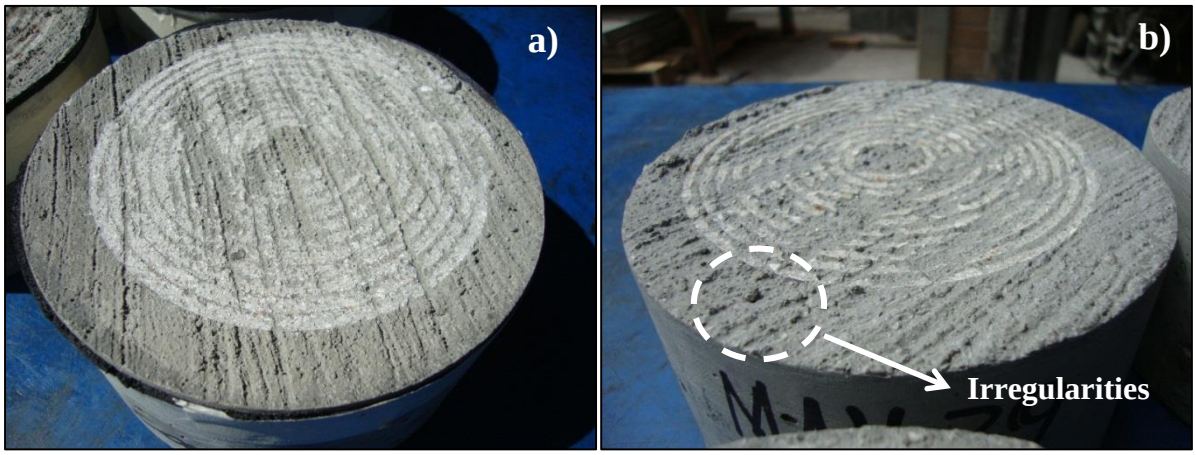

Figure 4-37: a) Control sample and b) 1.0% nanosilica sample - broom finishing w/c = 0.39

4.2.7 Rapid Freezing and Thawing

Mixture properties in fresh and hardened states for the concrete used to cast prisms are presented in Table 4-9 and Figure 4-38. The workability and air content of the concrete mixtures in the fresh condition were found to be within the target range defined in the present research. Compressive strength results show the same trend discussed previously. The compressive strength increases as the amount of nanosilica within the concrete increases (Figure 4-38).

Table 4-9: Fresh concrete properties and dosages of chemical admixtures w/c = 0.39

Mix	Nanosilica (%)	Slump (mm)	Air Content (%)	Wet Density (kg/m^3)	AEA (l/m^3)	HRWR (l/m^3)
1 (CC)	0.0	90	5.0	2379	0.21	3.10
2 (NSC 1)	1.0	75	5.0	2387	0.31	3.68
3 (NSC 2)	2.0	90	5.1	2379	0.70	6.00

Note: CC: Control concrete; NSC: nanosilica concrete

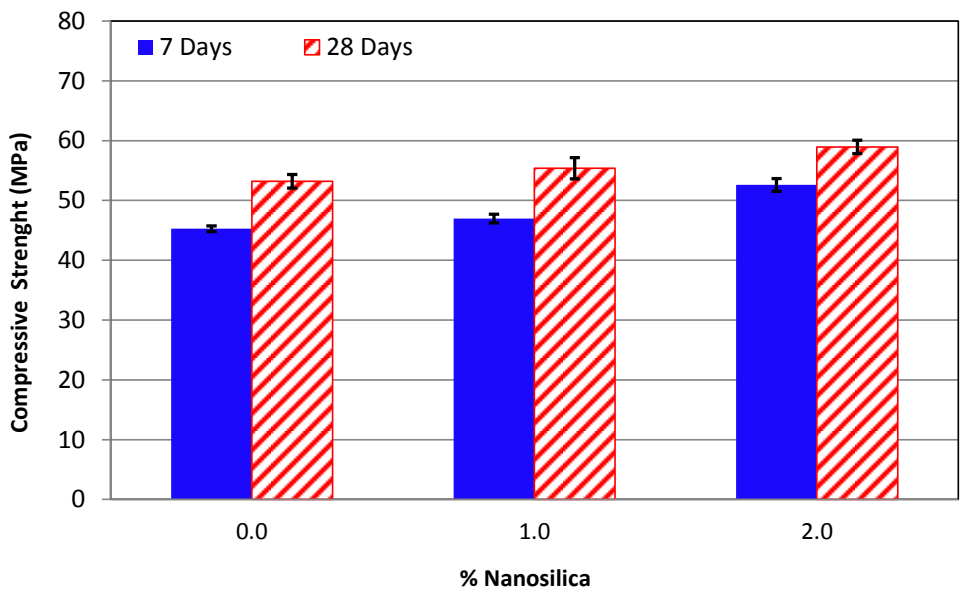

Figure 4-38: Compressive strength for different mixes freezing and thawing test, at 7 and 28 days w/c = 0.39

The results of the testing of concrete's resistance to rapid freezing and thawing are presented in Table 4-10 for the w/c ratio of 0.39. The table includes the results for the relative dynamic modulus of elasticity, the Durability Factor (DF) and the loss of mass after 324 cycles. In the test, results for the

fundamental transverse frequency and loss of mass were evaluated every 36 cycles. In **Appendix C** the all measurements supporting Table 4-10 are presented.

Freezing and thawing results show that all mixes perform similarly under the aggressive environment created by the cabinet. Figure 4-39 presents the variation of the relative dynamic modulus of elasticity over time, and illustrates that their variations are similar.

The Durability Factor (DF) is an indicator of the internal damage of the samples due to the thermal expansion and contraction effects of water (FHWA, 2013). The DF results are the same after 324 cycles (Table 4-10), but at the end of the test it was possible to identify different levels of external damage in the prisms, which can also be reflected in the weight loss results (Figure 4-40). The results reveal a noticeable decrease in weight loss of the specimens corresponding to higher amounts of nanosilica. Figures 4-41, 4-42 and 4-43 present the prisms after 324 cycles with 0.0% nanosilica, 1.0% nanosilica and 2.0% nanosilica, respectively. Pictures reveal the differences between them, where the concrete with 2.0% nanosilica present less external deterioration.

Table 4-10: Summary of rapid freezing and thawing results w/c = 0.39

Mix	Sample numer	Relative dynamic modulus of elasticity										Durability Factor (DF)	Loss of mass (%)
		Number of Freezing and Thawing Cycles											
		0	**36**	**72**	**108**	**144**	**180**	**216**	**252**	**288**	**324**		
0.0% NS	1	100	92	92	92	92	92	92	92	93	93	93	0.15
	2	100	91	91	84	92	92	92	92	93	93	93	0.14
	3	100	92	92	93	93	92	93	93	93	93	93	0.16
	Average	**100**	**92**	**92**	**90**	**93**	**92**	**93**	**93**	**93**	**93**	**93**	**0.15**
1.0% NS	1	100	93	92	93	92	93	93	93	93	93	93	0.11
	2	100	92	91	92	92	92	92	92	92	92	92	0.12
	3	100	92	92	92	91	92	92	92	92	93	93	0.12
	Average	**100**	**93**	**92**	**93**	**92**	**93**	**93**	**93**	**93**	**93**	**93**	**0.12**
2.0% NS	1	100	92	92	92	92	92	92	92	92	92	92	0.11
	2	100	91	91	92	91	92	92	91	93	94	94	0.08
	3	100	93	92	93	93	93	93	93	93	93	93	0.05
	Average	**100**	**92**	**92**	**93**	**92**	**93**	**93**	**92**	**93**	**93**	**93**	**0.08**

Note: NS = Nanosilica

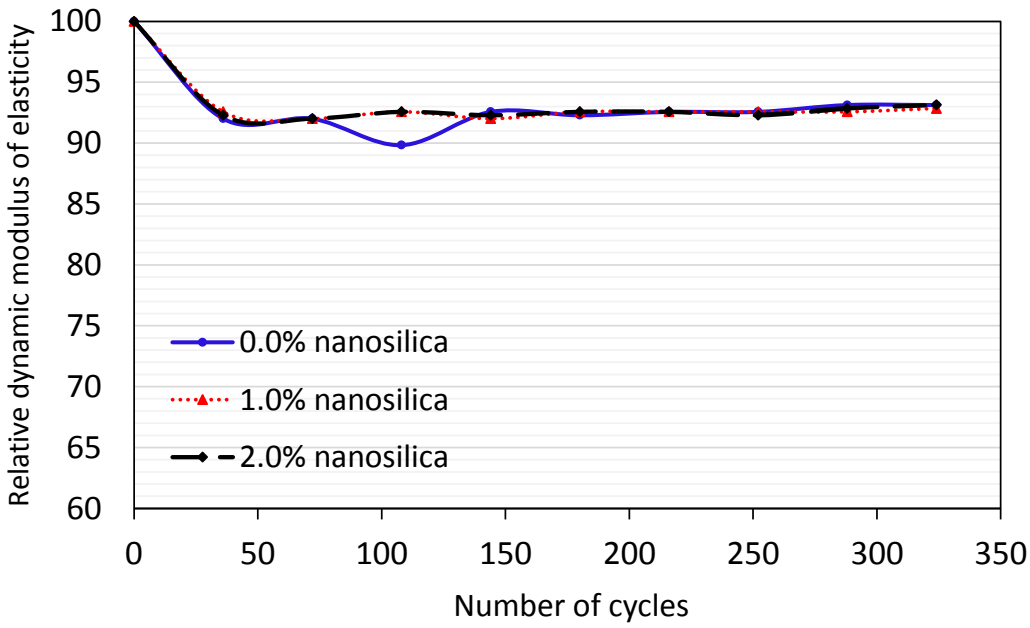

Figure 4-39: Average relative dynamic modulus of elasticity w/c = 0.39

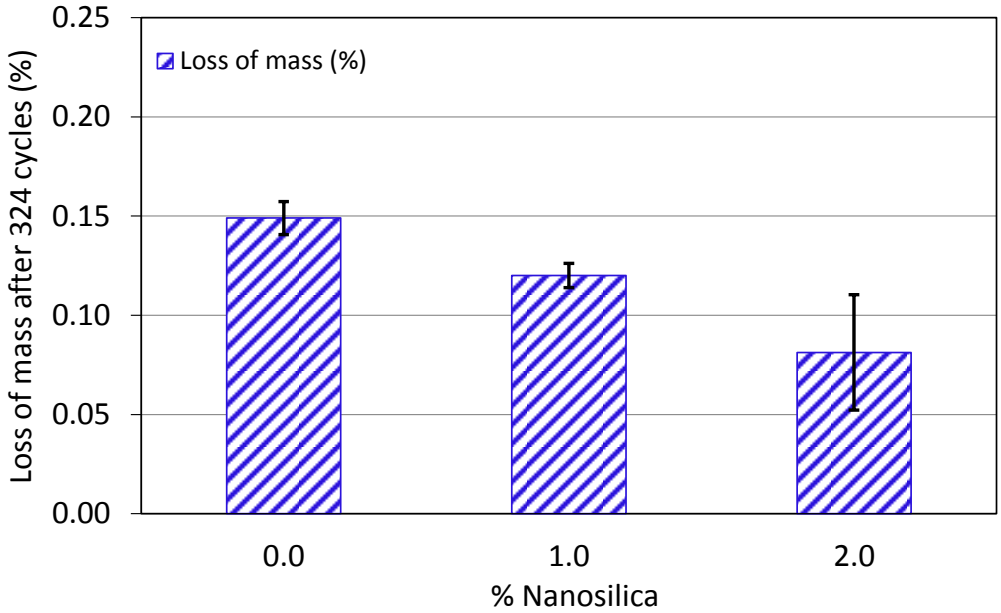

Figure 4-40: Average loss of mass after 324 cycles w/c = 0.39

Figure 4-41: Prisms with 0.0% nanosilica after 324 cycles of freezing and thawing w/c = 0.39

Figure 4-42: Prisms with 1.0% nanosilica after 324 cycles of freezing and thawing w/c = 0.39

Figure 4-43: Prisms with 2.0% nanosilica after 324 cycles of freezing and thawing w/c = 0.39

4.2.8 Scaling Resistance

Mixture properties for the concrete used to produce the slabs for the scaling resistance test are presented in Tables 4-11 and 4-12. Two different batches were prepared for each dosage level of nanosilica, in order to build more than 2 slabs for each nanosilica proportion. The standard procedure outlined in ASTM C672 recommends a minimum of two samples and the mixer capacity was not large enough to produce all of the required concrete in the same batch. The workability and air content of the concrete mixtures in fresh condition were found to be within the target range defined in the present research. Compressive strength results display the same trend as previously discussed (Figures 4-44 and 4-45). Batches with the same amount of nanosilica exhibited very similar strengths.

Table 4-11: Fresh concrete properties and dosages of chemical admixtures w/c = 0.45 – first batching

Mix	Nanosilica (%)	Slump (mm)	Air Content (%)	Wet Density (kg/m^3)	AEA (l/m^3)	HRWR (l/m^3)
1 (CC)	**0.0**	70	6.0	2365	0.14	2.13
2 (NSC 1)	**1.0**	83	6.2	2358	0.21	2.71
3 (NSC 2)	**2.0**	65	6.0	2351	0.29	3.29

Note: CC: Control concrete; NSC: nanosilica concrete

Table 4-12: Fresh concrete properties and dosages of chemical admixtures w/c = 0.45 – second batching

Mix	Nanosilica (%)	Slump (mm)	Air Content (%)	Wet Density (kg/m^3)	AEA (l/m^3)	HRWR (l/m^3)
1 (CC)	0.0	75	6.2	2358	0.13	2.52
2 (NSC 1)	1.0	65	5.3	2365	0.17	2.90
3 (NSC 2)	2.0	75	6.6	2337	0.23	3.10

Note: CC: Control concrete; NSC: nanosilica concrete

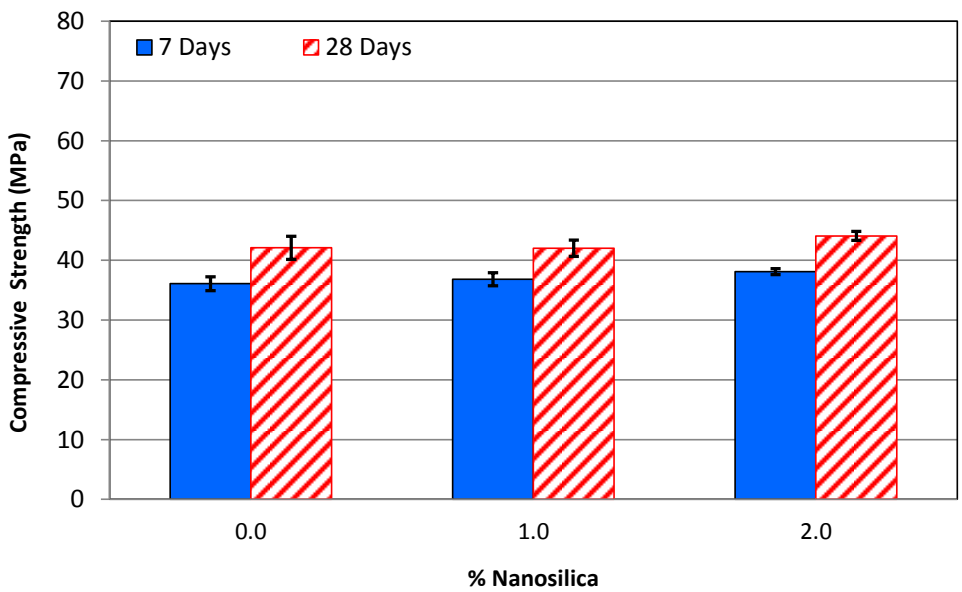

Figure 4-44: Compressive strength for different mixes for scaling resistance test, at 7 and 28 days w/c = 0.45, first batching

For the scaling resistance assessment of concrete at 25 and 50 cycles, all slabs were evaluated with rating 0 (zero means no scaling according to Table 3-3), even though it was possible to observe that overall nanoconcrete presented less surface deterioration. The surface deterioration was in the form of popouts and cement paste losses over coarse aggregates. Figure 4-46 presents two pictures illustrating the distresses of sample number 2 (0.0% nanosilica, second set of samples). Figure 4-47 presents two pictures illustrating the sample number 1 (2.0% nanosilica, second set of samples). Figure 4-48 presents two pictures illustrating the sample number 1 after 50 cycles (0.0% nanosilica, first set of samples). Figure 4-49 presents two pictures illustrating the sample number 1 after 50 cycles (2.0% nanosilica, first set of samples). After 25 and 50 cycles it was possible to observe that nanoconcrete performed

slightly better in terms of scaling surface deterioration even though the rating of the all samples 0 (zero). In **Appendix D** additional pictures are presented that include the all slabs that were tested.

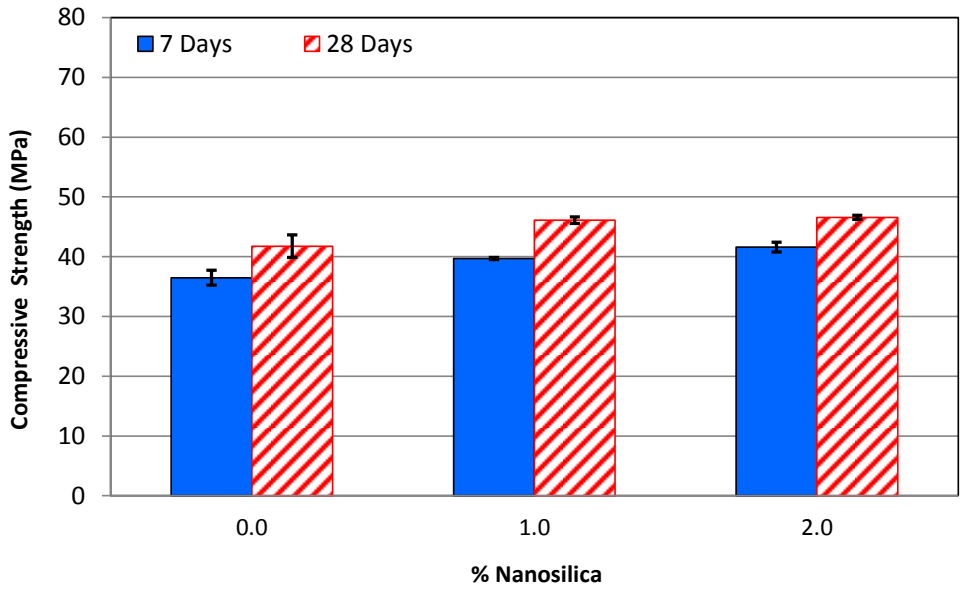

Figure 4-45: Compressive strength for different mixes for scaling resistance test, at 7 and 28 days w/c = 0.45, second batching

Weight measurements were taken, even though the weight assessment is not a key characteristic being studied in this test. One unexpected finding from this test was the fact that the sample's weight increased over the time. Since the initial weight of the samples was measured after 14 days in ambient environmental temperature (23° C), samples may have absorbed moisture and also salt from the solution.

4.3 Results Applying Nano Lotus Leaf Solution

Two different commercially available solution products of` nano lotus leaf were used to obtain thin coatings on concrete surface. Two batching were produce to test each coating with a w/c ratio of 0.31. The results for the first coating evaluation are presented herein.

4.3.1 Properties of Fresh Concrete (first coating)

The properties of the fresh concrete prepared are presented in Table 4-13, mix that was used to evaluate the first coating. The workability and air content of the concrete were found to be within the target ranges defined in the present study.

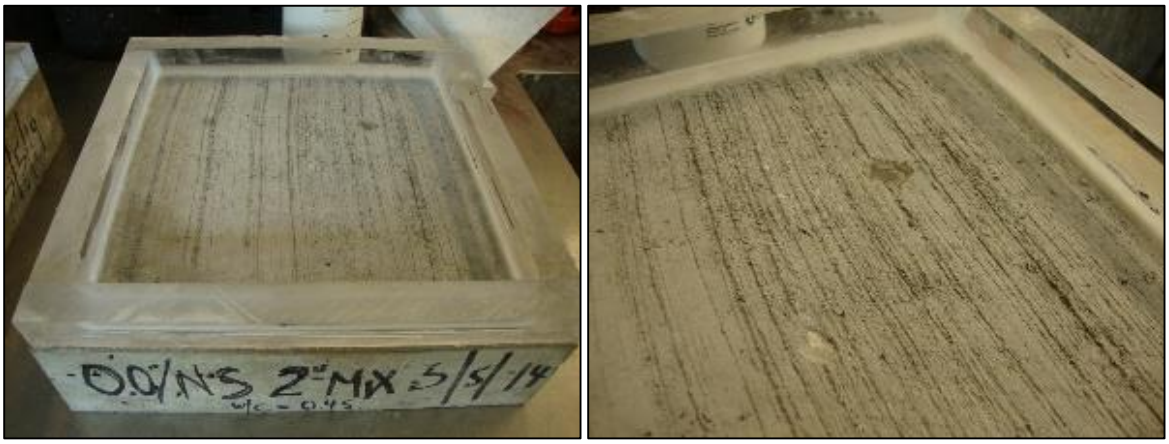

Figure 4-46: Scaling evaluation after 25 cycles, 0.0% nanosilica, sample number 2, second set of samples (second batch)

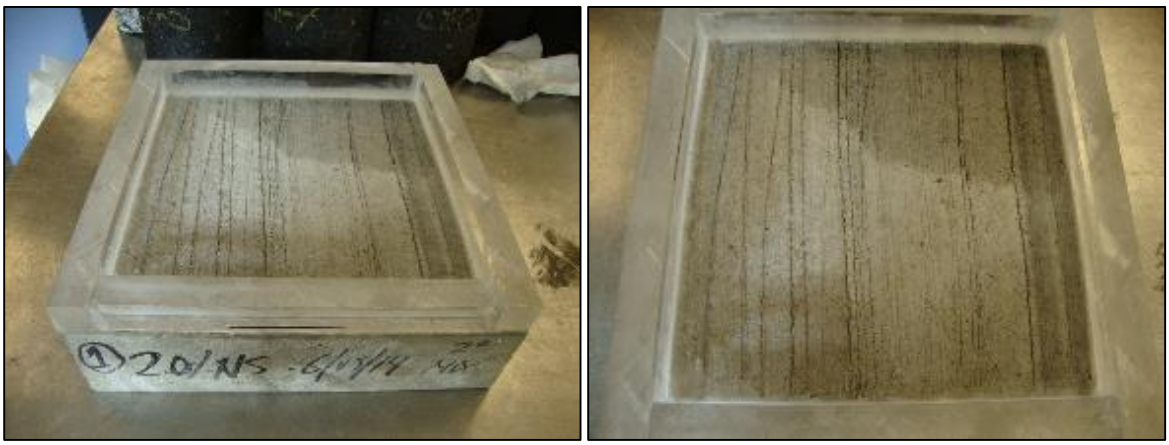

Figure 4-47: Scaling evaluation after 25 cycles, 0.0% nanosilica, sample number 2, second set of samples (second batch)

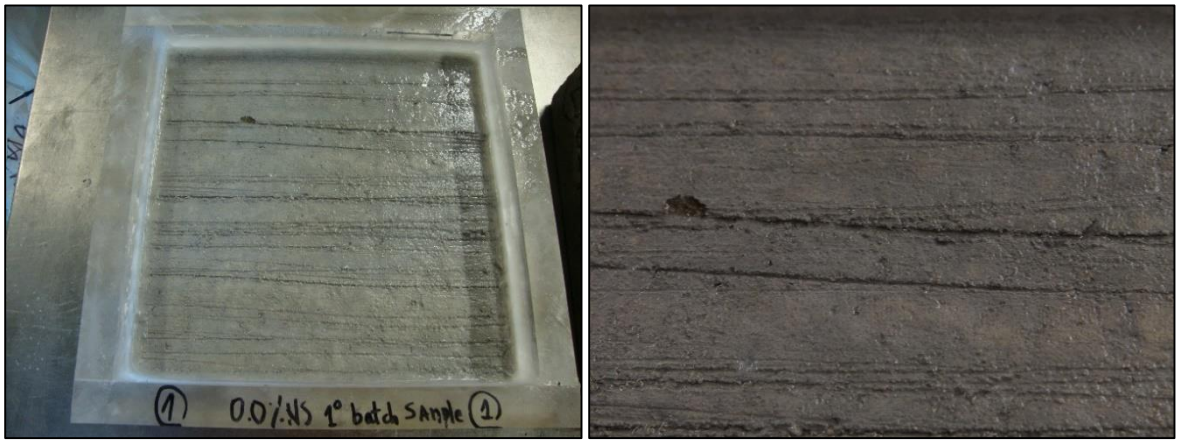

Figure 4-48: Scaling evaluation after 50 cycles, 0.0% nanosilica, sample number 1, first set of samples (first batch)

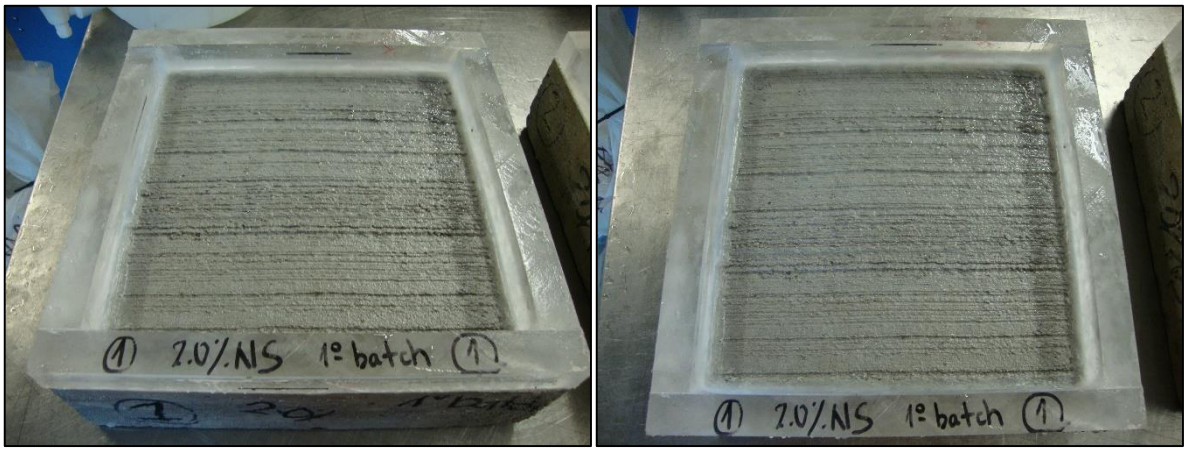

Figure 4-49: Scaling evaluation after 50 cycles, 2.0% nanosilica, sample number 1, first set of samples (first batch)

Table 4-13: Fresh properties of concrete used for the first coating

Slump (mm)	Air Content (%)	Wet Density (kg/m^3)	AEA (l/m^3)	HRWR (l/m^3)
95	5.1	2408	0.56	5.97

4.3.2 Compressive Strength (concrete for the first coating)

The average compressive strength of the concrete was 66 MPa, which can be considered normal for the w/c used in this part of this research (w/c = 0.31).

4.3.3 Friction Response First Coating

The average results for the corrected friction value, measured as British Pendulum Number (BPN), are presented in Figure 4-50. The measurement was performed in dry and wet conditions and 24 hours after applying the coating on 28 days old concrete specimens. Control concrete surface and the first amount of coating (30 g/m^2) exhibited practically the same friction value. The last two coatings (90 g/m^2 and 110 g/m^2) showed very close friction values. However, the general trend was a slight reduction in the friction property with an increased amount (increased thickness) of coating. This suggests that the first nano Lotus leaf coating was not effective in improving or retaining the friction property of concrete surface. Therefore, a second coating was proposed and evaluated, results are presented in the following section.

4.3.4 Properties of Fresh Concrete (concrete for the second coating)

For the evaluation of the second coating, the fresh concrete prepared had the properties presented in Table 4-14. The workability and air content of the concrete mixture were within the intended ranges.

Table 4-14: Fresh properties of concrete used for the second coating

Slump (mm)	Air Content (%)	Wet Density (kg/m^3)	AEA (l/m^3)	HRWR (l/m^3)
70	4.5	2422	0.60	4.38

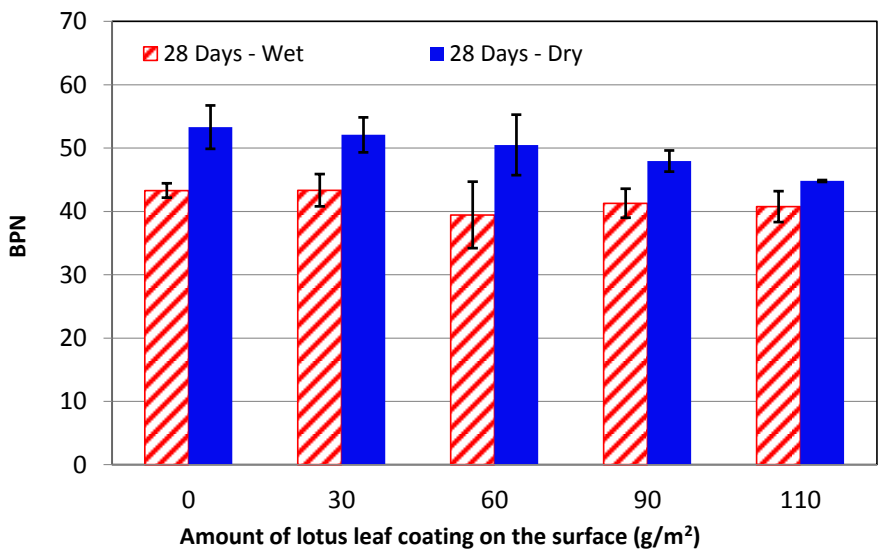

Figure 4-50: Corrected British pendulum number (BPN) for concrete with the first coating in dry and wet conditions

4.3.5 Compressive Strength (second coating)

The average compressive strength of the concrete was 68 MPa, which is close to that of the previous concrete batch. The strength achieved can be considered reasonable and consistent for the w/c ratio used in the concrete mixture (w/c = 0.31).

4.3.6 Friction Response First Coating (second coating)

The average results for the corrected friction value, measured as British Pendulum Number, are shown in Figure 4-51. The measurement was performed 24 hours after applying the coating on 28 days old concrete; the BPN was recorded in both dry and wet conditions. The main conclusion based on the test

results is that the second coating was able to retain the friction property of concrete surface in both dry and wet conditions.

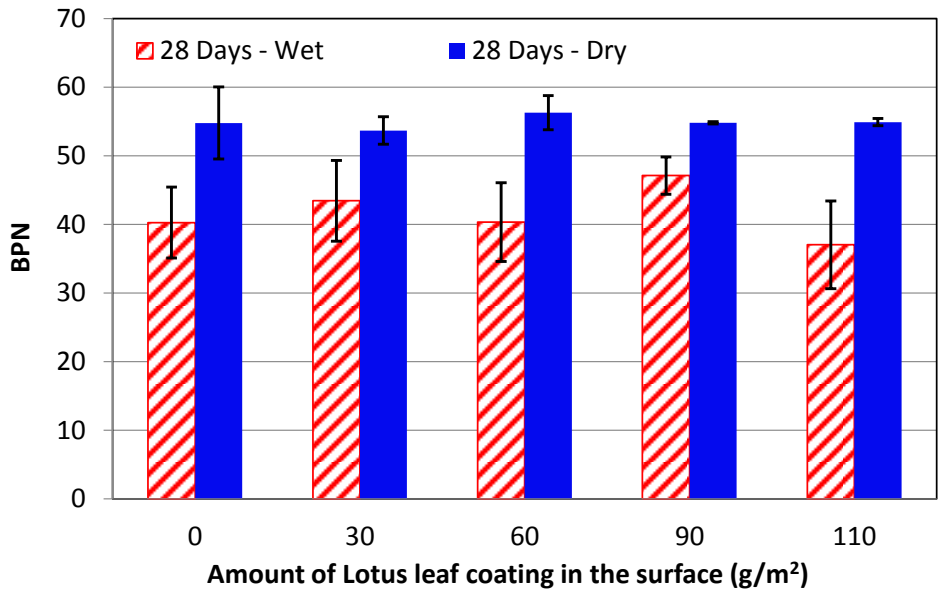

Figure 4-51: Corrected British pendulum number (BPN) for concrete with the second coating in dry and wet conditions

4.3.7 Sound Absorption

The average sound absorption spectra for the frequencies between 200 and 1200 Hz are presented in Figure 4-52. For each curve, the data presented summarizes the average from the three specimens that were tested. Figure 4-52 implies that the sound absorption coefficient in the frequencies of 900 to 1200 Hz did not have differences that were statistically significant. This finding suggests that the sound waves were not affected by the nano geometry of lotus leaf as shown in Figure 2-26. The wavelength of sound ranges from 3.4 m to 0.34 m at 100 to 1000 Hz frequency was evaluated (Bernhard, 2005). According to Santamarina (Santamarina & Fratta, 1998) low-frequency waves are not affected by small objects whereas large objects affect both low- and high-frequency waves.

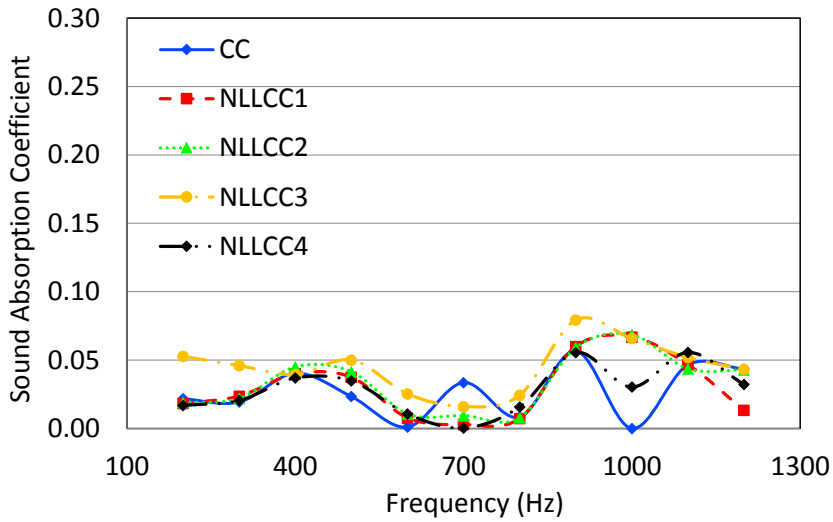

Figure 4-52: Average acoustic absorption spectra for 28 days old concrete coated with different amounts of second coating

The maximum sound absorption coefficients for the frequencies in the range of 200-1200 Hz were also obtained in Figure 4-52. These results are presented in Figure 4-53**.** Despite some variations in the maximum value, the impact of the second coating on sound absorption was insignificant. This suggests that the second coating did not significantly affect the sound absorption of concrete surface.

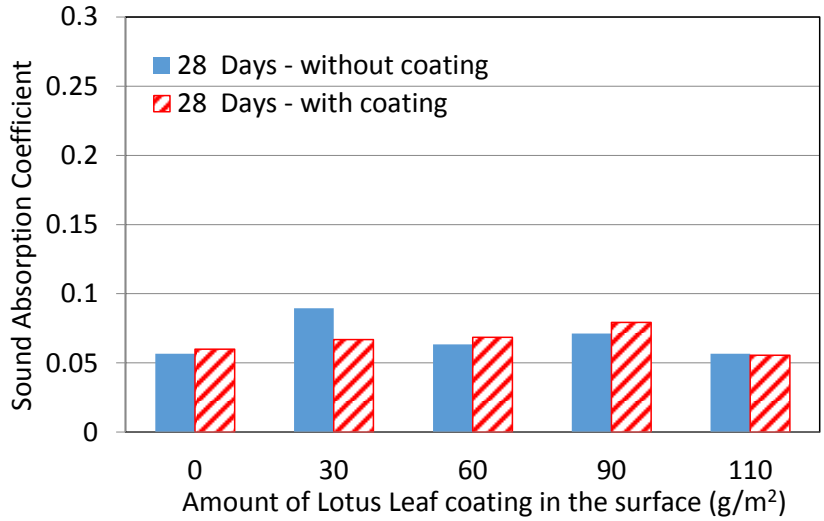

Figure 4-53: Maximum sound absorption coefficient for control (uncoated) and coated concrete specimens with different amounts of second coating

Chapter 5
STATISTIC ANALYSIS AND HYPOTESIS TESTS

This chapter presents a summary of the statistical analysis conducted on the results of this research. **Appendix E** presents all the results regarding the calculations of means, standard deviations and coefficients of variation. In general, the results show that the standard deviations and coefficients of variation obtained for the tests indicate that properties were consistent. Overall a coefficient of variation less than 10% was found in the calculations. However the results of sound absorption had a higher associated coefficient of variation. This can be explained because the mean values of sound absorption are relatively small numbers, thus, a small variation will produce a significant impact on the coefficient of variation. The abrasion response presented a coefficient of variation of less than 21%. According to ASTM C944 (2012), for a double load setup, a variation of less than 36% is acceptable for single operators; therefore results are also consistent.

An Analysis of Variance (ANOVA) was carried out to determine whether the impact produced by nanomaterials on the different measured properties are statistically significant, only for results at 28 days. In the analysis a one-way experimental layout was analyzed since in the experiments different mixes were contrasted using the same type of nanomaterial and always including a control mix as reference. The procedure that was followed is explained in this section, and the detailed calculations are presented in **Appendix F**.

The null hypothesis in this test assumed that there is no significant difference between the means (μ_i) of each group, which means that $\mu_1 = \mu_2 = \mu_3 = \mu_n$. The assumed level of significance was $\alpha = 5\%$. The sample size is defined by n which is divided into different r groups. For instance, if the compressive strength test at 28 days considers 3 samples per point and mixes with 0.0%, 0.5%, 1.0%, 1.5% and 2.0%, r is equal to 5 and n is equal to 15.

In the process the following procedure must be followed (Kreyszig, 1970):

$$\boldsymbol{x = \frac{1}{n}\sum_{i=1}^{r} n_i \mu_i} \qquad \textbf{Equation 6}$$

$$\boldsymbol{q_1 = \sum_{i=1}^{r} n_i\,(\mu_i - x)^2}$$ **Equation 7**

$$\boldsymbol{q_2 = \sum_{i=1}^{r} \sum_{k=1}^{n_i} (\mu_{ik} - x)^2}$$ **Equation 8**

After that, the following quotient is computed:

$$\boldsymbol{v_0 = \frac{q_1/(r-1)}{q_2/(n-r)}}$$ **Equation 9**

The solution of c in the following calculation must be determined:

$$\boldsymbol{P(V \leq c) = 1 - \alpha}$$ **Equation 10**

Where,

$n =$ size of the sample
$r =$ number of the groups
$x =$ mean of the entire sample
$q_1 =$ is the sum of squares between the group's means
$q_2 =$ sum of the squares within the groups
$v_o =$ quotient according to Equation 9
$c =$ is the solution for Equation 10 obtained from the table of F
$-$ Distrubution using $(r-1, n-r)$degrees of freedom.

Thus if $\boldsymbol{v_0 \leq c}$ the null hypothesis is not rejected and therefore $\mu_1 = \mu_2 = \mu_3 = \mu_n$, which indicates that the difference between the means is statistically insignificant.

If $\boldsymbol{v_0 > c}$ the hypothesis is rejected, then $\mu_1 \neq \mu_2 \neq \mu_3 \neq \mu_n$ and thus the means are significantly different.

Table 5-1 presents a summary of which properties are statistically significant. The ANOVA test is not applicable on tests that are based on observations (SEM and scaling resistance).

Table 5-1: Summary of ANOVA calculations

Tests in concretes and mortars	Number of samples per age		Statistical significance at 28 days water/cement (w/c) ratio		
	7 Days	28 Days	0.31	0.39	0.45
Compressive strength in concretes	-	3	YES	YES	YES
Noise absorption using impedance tube	-	3	NO	NO	-
Friction response - British Pendulum Number - Broom finishing*	-	3	NO	YES	-
Friction response - British Pendulum Number - Broom finishing	-	15	YES	YES	-
Friction response - British Pendulum Number - Smooth finishing	-	5	-	YES	-
Friction response - Tribometer - Smooth finishing in mortars	-	3	-	YES	-
Compressive strength in mortars	-	3	-	YES	YES
Abrasion response - Broom finishing	-	5	-	YES	-
Abrasion response - Smooth finishing	-	5	-	YES	-
Rapid freezing and thawing (Durability Factor)	-	3	-	NO	-
Rapid freezing and thawing (Loss of weight)	-	3	-	YES	
Scanning Electron Microscope (SEM) images of mortar surfaces	-	2	-	na	-
SEM images of concrete microstructure	-	2	-	na	na
Scaling resistance	-	4	-	-	na
*: For w/c ratio 0.39, five samples were included in the analysis					
na: not applicable					

Compressive strength was tested in three w/c ratios. As noted the results were statistically significant. This can be explained by the fact that nanosilica produces nano-crystals of C-S-H, which fills in the micro pores, thus increasing the paste density and improving the ITZ zone. This is also valid for results of compressive strength in mortars which are also statistically significant.

Noise absorption was tested using two w/c ratios. Even though the noise absorption tests show that the absorption coefficient increased, the ANOVA tests show that the improvements are not statistically significant. This may be due to a high variability present in the results. Although noise absorption improvements are not significant based on a microtexture modification, there is still a certain level of freedom to reduce the overall noise production from the construction of a different surface geometry.

Friction response was tested using two different methods (British pendulum and a tribometer) as well as two types of surfaces in each test. Using the British pendulum with broom finishing, two w/c ratios were explored. Results were statistically significant, except for w/c ratio of 0.31 as there were only three samples with this w/c ratio and the control concrete (0.0% nanosilica) presented a relatively higher variation; therefore for this case the null hypothesis was accepted. For the experiments using broom finishing but including 15 samples, the larger number of samples reduced the *c* value by a wide enough margin to make the results statistically different, leading to the rejection of the null hypothesis.

Experiments were developed on smooth surfaces using the British Pendulum and a tribometer for only one w/c ratio to increase redundancy. In both cases results were statistically significant. The increased friction in both broom and smooth finishing can be explained because nanosilica creates a rougher surface on concretes and mortars.

Based on the fact that friction is one the main focus areas of this research, Tables 5-2 and 5-4 present the BPN results used for the ANOVA calculations in the experiment using the British Pendulum Tester that included 15 samples and two different w/c ratios. Tables 5-3 and 5-5 present the ANOVA analysis from the BPN results. **Appendix F** presents the details for the ANOVA calculation of the other properties.

Table 5-2: BPN in broom finishing for w/c = 0.31 (15 samples)

Age	Mix	Nanosilica (%)	Sample number															Mean	SDV	COV (%)
			1	2	3	4	5	6	7	8	9	10	11	12	13	14	15			
28 days	1 (CC)	0.0	41	43	45	46	44	39	43	40	44	45	47	42	42	44	40	43	2.3	5.4
	2 (NSC 1)	0.5	52	49	43	49	44	48	52	52	44	52	53	46	46	47	47	48	3.2	6.7
	3 (NSC 2)	1.0	45	51	45	54	53	49	53	44	57	49	56	53	46	54	53	51	4.1	8.1
	4 (NSC 3)	1.5	49	50	55	50	46	55	52	56	55	50	55	50	49	46	49	51	3.4	6.7

Note: CC: control concrete; NSC: nanosilica concrete; SDV: Standard Deviation; COV: Coefficient of Variation.

Table 5-3: ANOVA calculations for BPN in broom finishing for w/c = 0.31 (15 samples)

r (number of groups)		4		
n (size of the sample)		60		
Mean of the entire sample		$\bar{y}$	48.3	
The sum of the squares between the means of the groups		$\mathbf{q_1}$	**167.1**	
The sum of the squares withing the groups		$\mathbf{q_2}$	**601.2**	
		ν_o	5.2	
Significance level α		α	0.05	
r -1 (m in Table D1)		2.8		
n - r (m in Table D1)		56		
For P (V ≤ c) = 0.95 ⇒	c =	2.8	≤	ν_o = 5.2
⇒ since $\nu_o \geq c$	the hypothesis is rejected and thus the means are statistically different			

Abrasion response of concretes with broom and smooth surfaces showed a significant reduction compared with control concrete, which means that nanoconcrete can improve the wear resistance on the surface independent of the type of finishing. Also, this improved behaviour may have an impact on the macrotexture durability, which can impact the friction and hydroplaning response over time. Finally, the rapid freezing and thawing tests showed that the Durability Factor cannot be influenced significantly with the addition of nanosilica. However, mass change results were statistically

significant. Samples with 0.0% nanosilica lost more mass than ones with nanosilica. This behaviour can be explained because nanosilica is able to improve the external deterioration of samples.

Table 5-4: BPN in broom finishing for w/c = 0.39 (15 samples)

Age	Mix	Nanosilica (%)	Sample number															Mean	SD	COV (%)
			1	2	3	4	5	6	7	8	9	10	11	12	13	14	15			
28 days	1 (CC)	0.0	50	57	49	45	53	46	51	43	49	43	48	46	51	55	53	49	4.1	8.4
	2 (NSC 1)	0.5	52	41	56	54	52	53	54	51	52	54	57	53	51	49	49	52	3.6	7.0
	3 (NSC 2)	1.0	60	58	61	62	64	57	54	55	54	55	55	61	55	53	56	57	3.4	6.0
	4 (NSC 3)	1.5	57	51	56	58	52	58	54	61	57	59	60	55	63	54	64	57	3.9	6.8
	5 (NSC 4)	2.0	50	51	50	58	51	53	49	55	59	56	59	60	58	60	62	55	4.4	7.9

Note: CC: control concrete; NSC: nanosilica concrete; SDV: Standard Deviation; COV: Coefficient of Variation.

Table 5-5: ANOVA calculations for BPN in broom finishing for w/c = 0.39 (15 samples)

r (number of groups)		5		
n (size of the sample)		75		
Mean of the entire sample		$\bar{y}$	54.3	
The sum of the squares between the means of the groups		q_1	**252.4**	
The sum of the squares withing the groups		q_2	**1023.2**	
		ν_o	4.3	
Significance level α		α	0.05	
r -1 (m in Table D1)		4		
n - r (n in Table D1)		70		
For P (V ≤ c) = 0.95 ⇒	c =	2.5	≤	ν_o = 4.3
⇒ since $\nu_o \geq c$	the hypothesis is rejected and thus the means are statistically different			

Table 5-6 presents a summary of the parameters ν_o and c calculated for the all properties tested.

Table 5-6: Summary of parameters of ANOVA analysis

Tests in concretes and mortars	Number of samples		water/cement (w/c) ratio					
	7 Days	28 Days	0.31		0.39		0.45	
			m_o	c	m_o	c	m_o	c
Compressive strength in concretes	-	3	16.5	4.1	96.7	3.5	15.7	5.1
Noise absorption using impedance tube	-	3	0.9	4.1	0.2	3.5	-	-
Friction response - British Pendulum Number - Broom finishing*	-	3	1.4	4.1	6.6	2.9	-	-
Friction response - British Pendulum Number - Broom finishing	-	15	5.2	2.8	4.3	2.5	-	-
Friction response - British Pendulum Number - Smooth finishing	-	5	-	-	5.0	2.9	-	-
Friction response - Tribometer - Smooth finishing in mortars (50 g load)	-	3	-	-	17.8	3.5	-	-
Friction response - Tribometer - Smooth finishing in mortars (100 g load)		3	-	-	30.0	3.5		
Compressive strength in mortars	-	3	-	-	4.6	3.5	15.1	3.5
Abrasion response - Broom finishing	-	5	-	-	7.0	2.9	-	-
Abrasion response - Smooth finishing	-	5	-	-	15.3	3.9	-	-
Rapid freezing and thawing (Durability Factor)	-	3	-	-	0.3	5.1	-	-
Rapid freezing and thawing (Loss of weigth)	-	3	-	-	10.9	5.1	-	-

*: For w/c ratio 0.39, five samples were included in the analysis

In **Appendix F** the details for the ANOVA calculations for the lotus leaf coatings are also included. According to these results both coatings result in statistically insignificant modifications in the friction and noise absorption properties.

5.1 t-Student Analysis

In order to confirm if the main properties obtained in this research are statistically modified, a second analysis using the t-Student test was performed. In this analysis the objective is to compare the control concrete/mortar with the nanoconcrete/mortar that presents the best enhancement. The following key properties were analyzed: compressive strength in concretes, friction response using the British Pendulum Tester, friction response using the tribometer and noise absorption.

The procedure used for the t-student calculations is the following:

a) A level of significance α = 5% was assumed for the calculations.

b) The degrees of freedom need to be calculated using the following equation: n1 + n2 – 2. Where n1 is the amount of samples of the control concrete and n2 represent the amount of samples for the group with nanosilica. In this research, the samples of the both groups to be compared have the same size and are represented only by n.

c) The means and the variances of both groups must be determined.

d) The value "c" must be determined using the Table G-1 presented in Appendix G for equation 11:

$$\boldsymbol{P(V \leq c) = 1 - \alpha} \qquad \textbf{Equation 11}$$

e) The critical value t_o is determined using the following equation:

$$\boldsymbol{t_0 = \sqrt{n}\frac{\mu_x - \mu_y}{\sqrt{S_x^2 + S_y^2}}} \qquad \textbf{Equation 12}$$

Where,

n = size of the sample
μ_x = mean of the control concrete
μ_y = mean of the nanosilica concrete
S_x^2 = variance of the control concrete
S_y^2 = variance of the nanosilica concrete
t_o = quotient according to Equation 12

Thus if $\boldsymbol{t_0 \leq c}$ the null hypothesis is not rejected and therefore $\mu_x = \mu_y$, which indicates that the difference between the means is statistically insignificant.

If $\boldsymbol{t_0} > \boldsymbol{c}$ the hypothesis is rejected, then $\mu_x \neq \mu_y$ and thus the means are significantly different.

All results are presented in **Appendix G**. According to the calculations is possible to determine that:

- ✓ Compressive strength in concretes, friction response using the British Pendulum Tester and friction response using the tribometer are statistically different, which reconfirm the impact of nanosilica in these properties.
- ✓ Noise absorption results are not statistically different.

Chapter 6
CONCLUSIONS AND RECOMMENDATIONS

This chapter presents the conclusions and recommendations that have been drawn from through this research.

6.1 Conclusions

The research conducted in this thesis supports the following conclusions:

✓ The introduction of nanosilica in concrete results in a slump loss in concrete mix due to the high specific surface area of the nanomaterial. However, the target slump of concrete can be maintained by using an appropriate dosage of high-range water reducer.

✓ The loss of air voids from fresh concrete is increased with a higher content of nanosilica. However, the required concrete air content can be achieved by increasing the dosage of air entraining admixture.

✓ Nanosilica increases the compressive strength of concrete. This is due to an improved microstructure/pore-structure of concrete. Nanosilica produces nano crystals of C-S-H, which fills in the micro pores. Also, the tiny particles of nanosilica that have filled in the micro-voids block the pore channels. As a result, the concrete microstructure is improved in the presence of nanosilica by creating a dense material. Results are supported by the SEM images.

✓ Nanosilica particles modify the surface morphology of mortars and concretes, creating a rough surface. Results are supported by the SEM images.

✓ Nanosilica enhances the friction response of concrete due to a microtexture modification. The rougher surface increases the number of asperities, and thus increases the real contact area, enhancing the adhesion component of concrete's frictional force.

✓ The impedance tube absorption test results show that nanosilica can slightly increase sound absorption of concrete material. However the results are not statistically significant.

✓ Nanosilica can enhance the abrasion response for both the broom and smooth finishing, resulting in better wear resistance of the concrete road surfaces. Better abrasion resistance can increase pavement macrotexture durability, providing long-term friction performance benefits. Abrasion resistance results indicate that nanosilica may provide better durability of the NGCS's macrotexture.

✓ Nanosilica enhances the interfacial transition zone in both the concrete and mortar samples. The observations are supported by the SEM images. This enhancement may create a better bond between the interface between paste and aggregates. In terms of pavement performance, the better bond may reduce the amount of missed aggregates from the surface (Figure 6-1 a) and therefore may potentially create a more durable NGCS (Figure 6-1 b).

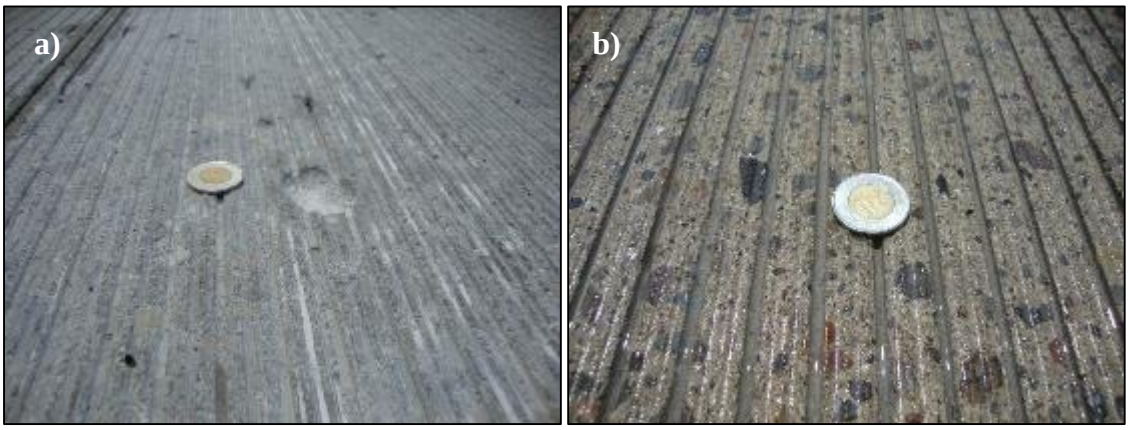

Figure 6-1: a) NGCS with a missed aggregate and b) NGCS without surface distress

✓ It is possible to create the lotus effect on concrete material. In wet conditions, the original friction property of concrete pavements (as measured by the British Pendulum Tester) can be retained by improving their water repellence through using a coating of nano lotus leaf. Also, it was demonstrated that the coating did not significantly affect the sound absorption in concrete.

✓ Results of freezing and thawing tests reveal that there were no significant differences in Durability Factor (DF), an indicator of the internal damage of concrete, between the conventional concrete and the nanoconcrete for the w/c = 0.39. However, from the same test it was possible to determine that prisms with nanosilica presented less external deterioration; results were statistically different, which implies that nanomaterials may help to mitigate external damage.

✓ Observations made in the samples subjected to the scaling resistance test, which simulates freezing and thawing in the presence of deicers, reveal that the slabs with nanosilica in general presented less surface damage.

6.2 Key findings

The innovative approach of applying nanomaterials in concrete in rigid pavements shows insights that PCC properties can be enhanced due to microstructure modifications. Two nanomaterials were evaluated from a technical point of view nanosilica has the potential to advance the state of the art practice in the design, construction and performance of concrete pavements.

Nanosilica can provide a better friction response to the adhesion of the component force, because it is able to modify the surface morphology of mortar and concrete. At the same time, nanosilica-enhanced concrete can provide better abrasion response as it gives the macrotexture a higher durability; therefore in the long term performance, nanosilica can influence the hysteresis component of the frictional force. Both enhancements may potentially improve safety of concrete pavements in wet conditions.

It was found that nanosilica cannot improve the sound absorption capabilities of the PCC significantly. It is feasible to consider creating the next generation Canadian concrete by combining grinding and grooving techniques with nanoconcrete. This could potentially provide a stronger durable concrete with altered micro and macrotexture properties from nanosilica and grinding/grooving respectively. However, this behaviour must be proved using a road trial section to replicate real operation conditions.

6.3 Preliminary Recommended Surface

The first proposed NGSC to be evaluated in the field had smooth surfaces and negative texture grooves as presented in Figure 6-2 a). Therefore, the technical suggestion is to adapt the NGSC to Canadian conditions by building a smooth PCC pavement with nanoconcrete and then apply grooving on the surface using a machine similar to Figure 6-2 b). The grooving machine is able to create the macrotexture without any disturbance to the nanoconcrete top. This implies that tires will be in contact directly with the nanoconcrete which has an improved microtexture.

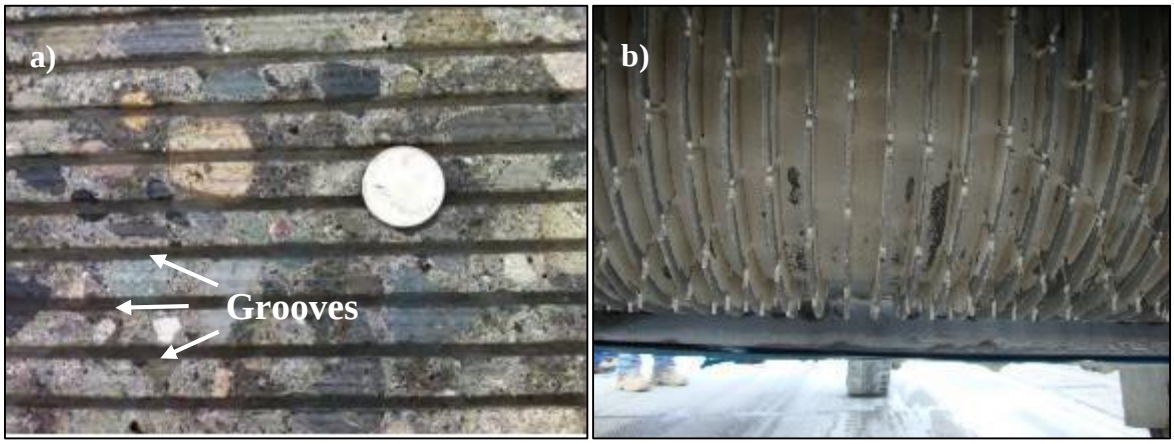

Figure 6-2: a) NGCS with smooth surfaces and grooves with negative texture (adapted from Anderson et al., 2014) and b) conventional grooving machine

6.3.1 Construction Recommendations

From this research is possible to give the following recommendations that must be applied during a construction process:

✓ It is recommended that the nanomaterials must be properly dispersed in the concrete mix in order for the nanosilica to fully react during the hydration process. Uneven distribution may produce clusters of nanosilica that remain inert during mixing. To achieve a good dispersion of the nanomaterials in the concrete, mixing should be through to avoid clusters of nanosilica that may clump and then consequently not react during the hydration process. During this research, concrete mixes showed an adequate nanosilica dispersion based on visual inspection and also from analyzing the concrete microstructure with SEM. However, in mortars one sample showed a nanosilica cluster (Figure 6-3).

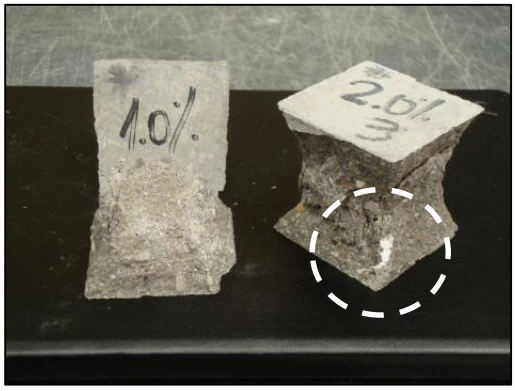

Figure 6-3: Example of cluster of nanosilica in mortars that must be avoided

✓ It is required that the exposure to nanomaterials be reduced during the construction process to avoid direct contact with them and also to reduce the risk of inhalation. Construction operations are labor intensive, therefore several precautions must be taken, such as the usage of special masks, gloves, clothing or other apparel to prevent dermal exposure.

✓ Since nanomaterials are expensive, a two lift pavement system may be explored which would incorporate nanoconcrete on the top layer and conventional concrete at the bottom of the PCC section.

6.4 Future Work

Based on this research, the following future research is suggested:

✓ Another nanomaterial such as nano titanium dioxide and carbon nanotubes may be analyzed to determine whether they can enhance the surface characteristics of PCC Canadian pavements. Nano titanium dioxide can create a self-cleaning and antipollutant concrete (Ashby et al. 2009), however the effect on friction is unexplored. Carbon nano tubes (CNTs) are also good candidates for highways applications since the multi wall CNTs are suitable to absorb noise, however the application to increase friction and reduce overall noise production in highways has been practically unexplored.

✓ Several options exist in the market to produce new surface geometries in the field. Therefore, it is recommended to study other geometries to create a NGCS which is appropriated for usage in Canada.

✓ The application of nanotechnology in concrete is still in its infancy. Therefore, there are many other potential applications for using nanoconcrete for civil infrastructure which should be explored.

✓ The ongoing research with nanomaterials has been based mainly on laboratory research. It would be beneficial to document the current applications with nanomaterials in engineering practice and to study potential applications.

✓ In the circumstances that nanomaterials can be made available in larger quantities for infrastructure applications, it is necessary to develop technical specifications and establish quality control procedures.

✓ In this research two nanomaterials were tested; nanosilica was added inside of the concrete mix and the lotus leaf coatings were applied to the surface. The decision to test both was based on the fact

that nanomaterials are currently expensive. Since nanosilica is mixed into concrete which can make up the full pavement thickness, the direct cost can be higher when compared with the lotus leaf coating. However, a coating may present a less durable technology and more applications may be necessary for the same pavement life. Therefore, the economic benefits of both alternatives must be evaluated with a Life Cycle Analysis Method; however, such analysis is beyond this research´s scope and is recommended as future work.

✓ Surface texture is characterized by the microtexture, macrotexture and megatexture. If the application of nanotechnology to enhance friction response in PCC pavements is successfully verified in the field, future work may be necessary to incorporate and study the concept of nanotexture.

Bibliography

Ahammed, M. A., & Tighe, S. L. (2011). Asphalt pavements surface texture and skid resistance - exploring the reality. Canadian Journal of Civil Engineering, 39(1), 1-9.

Ahammed, M. A. (2009). *Safe, quiet and durable pavement surfaces*. PhD Thesis, University of Waterloo, Waterloo, Ontario, Canada.

Al-Rub, R. K. A. (2012). *Nanotechnology-based system for damage-resistant concrete pavements*. No. SWUTC/12/476660-00017-1.Texas Transportation Institute, Zachry Department of Civil Engineering Texas A&M University, USA.

American Association of State Highway and Transportation Officials (AASHTO) (2013). *Standard method of test for measurement of Tire/Pavement noise using the on-board sound intensity (OBSI) method*. AASHTO TP 76. USA.

American Concrete Institute (ACI) (2008). *Guide to durable concrete*. No. ACI 201.2R-08. MI, U.S.A. American Concrete Institute.

Anderson, K., Uhlmeyer, J., Sexton, T., Russell, M., & Weston, J. (2014). *Evaluation of long-term pavement performance and noise characteristics of the next generation concrete surface: Final report*. No. WA-RD 767.2. USA. Washington State Department of Transportation.

Ashby, M. F., Schodek, D. L., & Ferreira, P. (2009). *Nanomaterials, nanotechnologies and design: An introduction for engineers and architects.* Butterworth-Heinemann.

AASHTO TP 76. *Standard Method of Test for Measurement of Tire/Pavement Noise Using the On-Board Sound Intensity (OBSI) Method*. 2013-01-01, 2013.

ASTM (American Society for Testing and Materials) (1993 (Reapproved 2008)). *Standard test method for measuring surface frictional properties using the British Pendulum Tester*. ASTM E303-93. ASTM International, Philadelphia, USA.

ASTM (American Society for Testing and Materials) (2003 (Reapproved 2008)). *Standard test method for resistance of concrete to rapid freezing and thawing*. ASTM C666/C666M–03. ASTM International, Philadelphia, USA.

ASTM (American Society for Testing and Materials) (2010). *Standard test method for air content of freshly mixed concrete by the pressure method*. ASTM C231/C231M-10. ASTM International, Philadelphia, USA.

ASTM (American Society for Testing and Materials) (2010). *Standard test method for impedance and absorption of acoustical materials using a tube, two microphones and a digital frequency analysis system*. ASTM E1050-10. ASTM International, Philadelphia, USA.

ASTM (American Society for Testing and Materials) (2010). *Standard test method for slump of hydraulic-cement concrete*. ASTM C143/C143M-10a. ASTM International, Philadelphia, USA.

ASTM (American Society for Testing and Materials) (2011). *Standard test method for compressive strength of hydraulic cement mortars (using 2-in. or [50-mm] cube specimens)*. ASTM C109/C109M − 11b. ASTM International, Philadelphia, USA.

ASTM (American Society for Testing and Materials) (2012). *Standard test method for abrasion resistance of concrete or mortar surfaces by the rotating-cutter method*. ASTM C944/C944M - 12. ASTM International, Philadelphia, USA.

ASTM (American Society for Testing and Materials) (2012). *Standard test method for compressive strength of cylindrical concrete specimens*. ASTM C39/C39M-12. ASTM International, Philadelphia, USA.

ASTM (American Society for Testing and Materials) (2012). *Standard test method for density (unit weight), yield, and air content (gravimetric) of concrete*. ASTM C138/C138M-12. ASTM International, Philadelphia, USA.

ASTM (American Society for Testing and Materials) (2012). *Standard test method for scaling resistance of concrete surfaces exposed to deicing chemicals*. ASTM C672/C672M – 12. ASTM International, Philadelphia, USA.

ASTM (American Society for Testing and Materials) (2013). *Standard specification for flow table for use in tests of hydraulic cement*. ASTM C230 / C230M - 13. ASTM International, Philadelphia, USA.

Balaguru, P., & Chong, K. (2006). *Nanotechnology and concrete research opportunities*. Proceedings of ACI Session on “Nanotechnology of Concrete: Recent Developments and Future Perspectives”. Denver, USA.

Barnes, P., & Bensted, J. (2002). *Structure and performance of cements*. CRC Press.

Bernhard, R. J., & McDaniel, R. S. (2005). *Basics of noise generation for pavement engineers*. Transportation Research Record: Journal of the Transportation Research Board, 1941(1), 161-166.

Bernhard, R., Wayson, R. L., Haddock, J., Neithalath, N., El-Aassar, A., Olek, J., Weiss, W. J. (2005). *An introduction to tire/pavement noise of asphalt pavement*. Institute of Safe, Quiet and Durable Highways, Purdue University,

Birgisson, B., Taylor, P., Armaghani, J., & Shah, S. P. (2010). *American road map for research for nanotechnology-based concrete materials*. Transportation Research Record: Journal of the Transportation Research Board, 2142(1), 130-137.

Byrum, C. R., Raymond, C., Swanlund, M., & Kazmierowski, T. (2010). *Experimental short-wavelength surface textures in portland cement concrete pavements*. Transportation Research Record: Journal of the Transportation Research Board, 2155(1), 170-178.

Canadian Standard Association (CSA). (2009). *Concrete materials and methods of concrete construction/test methods and standard practices for concrete*. A23.1-09/A23.2-09. Toronto, Ontario, Canada.

Chen, J., Kou, S., & Poon, C. (2012). *Hydration and properties of nano-TiO_2 blended cement composites*. Cement and Concrete Composites, 34(5), 642-649.

Cheng, S., & Robbins, M. O. (2010). *Defining contact at the atomic scale*. Tribology Letters, 39(3), 329-348.

Chung, D. (2001). *Applied Material Science: Applications of Engineering, Material in Structural, Electronics, Thermal and Other Industries*. ©2001 CRC Press LLC.

Chung, D. (2002). *Review: Improving cement-based materials by using silica fume*. Journal of Materials Science, 37(4), 673-682.

Chung, D. (2004). *Cement-matrix structural nanocomposites*. Metals and Materials International, 10(1), 55-67.

Davim, J. P. (2011). *Tribology for engineers: A practical guide*. Elsevier.

Diamanti, M. V., Ormellese, M., & Pedeferri, M. (2008). *Characterization of photocatalytic and superhydrophilic properties of mortars containing titanium dioxide*. Cement and Concrete Research, 38(11), 1349-1353.

Donavan, P. R., & Lodico, D. M. (2009). *Measuring tire-pavement noise at the source*. Transportation Research Board.

Domone, Peter. Mortar Tests for Self-Consolidating Concrete. Concrete International, CONINT 39, April 2006.

Duncan, R. L., Albright, R. O., Abu-Onk, W., Bollin, G., Fluhr, R. J., Greer Jr, W. C., Colucci, B. (1988). *Texturing concrete pavements*. ACI Materials Journal, 85(3), 202-211.

Federal Highway Administration (FHWA). *Material Property Characterization of Ultra-High Performance Concrete*. Publication Number: FHWA-HRT-06-103.: 04/23/2012 http://www.fhwa.dot.gov/publications/research/infrastructure/structures/06103/chapt3c.cfm, Accessed March 15, 2013.

Federal Highway Administration (FHWA). *Pavement friction*. Retrieved December/01, 2012, from http://safety.fhwa.dot.gov/roadway_dept/pavement/pavement_friction/

Federal Highway Administration (FHWA). *Admixtures*. Retrieved October/29, 2014, from http://www.fhwa.dot.gov/infrastructure/materialsgrp/admixture.html

Flores, I., Sobolev, K., Torres-Martinez, L., Cuellar, E., Valdez, P., & Zarazua, E. (2010). *Performance of cement systems with nano-SiO_2 particles produced by using the sol-gel method*. Transportation Research Record: Journal of the Transportation Research Board, 2141(1), 10-14.

Forbes, P. (2008). *Scientific american: Self-cleaning materials: Lotus leaf-inspired nanotechnology*. Scientific American Magazine, 1-5.

Gaitero, J. J., Campillo, I., & Guerrero, A. (2008). *Reduction of the calcium leaching rate of cement paste by addition of silica nanoparticles*. Cement and Concrete Research, 38(8), 1112-1118.

Gay, C., & Sanchez, F. (2010). *Performance of carbon nanofiber-cement composites with a high-range water reducer*. Transportation Research Record: Journal of the Transportation Research Board, 2142(1), 109-113.

Gohar, R., & Rahnejat, H. (2008). *Fundamentals of tribology*. World Scientific.

Gopalakrishnan, K., Birgisson, B., & Taylor, P. (2011). *Nanotechnology in civil infrastructure: A paradigm shift*. Springer.

Grove, J., Vanikar, S., & Crawford, G. (2010). *Nanotechnology: New Tools to Address Old Problems*. Transportation Research Record: Journal of the Transportation Research Board, 2141(1), 47-51.

Hamdy A., and Ion T. (2011). *Nanocoatings and Ultra-thin Films: Technologies and Applications.* Published by Woodhead Publishing Limited, ISBN 978-0-85709-490-2.

Hall, J. W., Smith, K. L., Titus-Glover, L., Wambold, J. C., Yager, T. J., & Rado, Z. (2009-1). *Guide for pavement friction*. National Cooperative Highway Research Program, Transportation Research Board of the National Academies.

Hall, J. W., Smith, K. L., & Littleton, P. C. (2009-2). *Texturing of concrete pavements*. No. National Cooperative Highway Research Program of the National Academies, Report 634. Washington, D.C. U.S.A.: Transportation Research Board.

He, X., & Shi, X. (2008). *Chloride permeability and microstructure of portland cement mortars incorporating nanomaterials*. Transportation Research Record: Journal of the Transportation Research Board, 2070(-1), 13-21.

Henry, J. J. (2000). *Evaluation of pavement friction characteristics*. Transportation Research Board.

Hosseini, P., Booshehrian, A., & Farshchi, S. (2010). *Influence of nano-SiO_2 addition on microstructure and mechanical properties of cement mortars for ferrocement*. Transportation Research Record: Journal of the Transportation Research Board, 2141(1), 15-20.

Hosseini, P., Booshehrian, A., & Madari, A. (2011). *Developing concrete recycling strategies by utilization of nano-SiO_2 particles*. Waste and Biomass Valorization, 2(3), 347-355.

Hutchings, I. M. (1992). *Tribology: Friction and wear of engineering materials*. Butterworth-Heinemann Ltd.

Jalal, M. (2012). *Durability enhancement of concrete by incorporating titanium dioxide nanopowder into binder.* Journal of American Science, 8(4), 289-294.

Jalal, M., & Noorzad, A. (2012). *Effect of binder content, pozzolanic admixtures and SiO_2 nanoparticles on thermal properties and capillary water absorption of high performance concrete*. Journal of American Science, 8(7), 395-399.

Jalal, M., Ramezanianpour, A. A., & Pool, M. K. (2012). *Effects of titanium dioxide nanopowder on rheological properties of self compacting concrete*. Journal of American Science, 8(4), 285-288.

Ji, T., 2005. *Preliminary study on the water permeability and microstructure of concrete incorporating nano-SiO_2*. Cement and Concrete Research, 35, 1943-1947.

Kosmatka, S., Kerkhoff, B., Hooton, R. D., & McGrath, R. J. (2011). *Design and control of concrete mixtures*. Ottawa, ON, Canada: Cement Association of Canada.

Kreyszig, E. (1970). *Introductory mathematical statistics: Principles and methods*. Wiley New York.

Kumar, V. R., Bhuvaneshwari, B., Maheswaran, S., Palani, G., Ravisankar, K., & Iyer, N. R. (2011). *An overview of techniques based on biomimetics for sustainable development of concrete*. Current Science (Bangalore),101(6), 741-747.

Lamond, J. F., & Pielert, J. H. (2006). *Significance of tests and properties of concrete and concrete-making materials*. (STP 169D) ASTM International.

Lin K. L., Chang W. C., Lin D. F., Luo H. L., and Tsai M. C. (2008). *Effects of nano-SiO_2 and different ash particle sizes on sludge ash–cement mortar*. Journal of Environmental Management 88, 708–714.

Li, G. Y., Wang, P. M., & Zhao, X. (2005). *Mechanical behavior and microstructure of cement composites incorporating surface-treated multi-walled carbon nanotubes*. Carbon, 43(6), 1239-1245.

Li, H., Xiao, H., & Ou, J. (2004). *A study on mechanical and pressure-sensitive properties of cement mortar with nanophase materials*. Cement and Concrete Research, 34(3), 435-438.

Li, H., Zhang, M., & Ou, J. (2007). *Flexural fatigue performance of concrete containing nano-particles for pavement. International Journal of Fatigue*. 29(7), 1292-1301.

Makar, J. (2011). *The effect of SWCNT and other nanomaterials on cement hydration*. No. NRCC-53569.National Research Council Canada – NRCC.

Metaxa, Z. S., Konsta-Gdoutos, M. S., & Shah, S. P. (2010). *Carbon nanofiber-reinforced cement-based materials*. Transportation Research Record: Journal of the Transportation Research Board, 2142(1), 114-118.

Mondal, P., Shah, S. P., Marks, L. D., & Gaitero, J. J. (2010). *Comparative study of the effects of microsilica and nanosilica in concrete*. Transportation Research Record: Journal of the Transportation Research Board, 2141(1), 6-9.

Mozumder, M. S., Zhang, H., & Zhu, J. (2011). *Mimicking lotus leaf: Development of Micro-Nanostructured biomimetic superhydrophobic polymeric surfaces by ultrafine powder coating technology*. Macromolecular Materials and Engineering, 296(10), 929-936.

Napierska, D., Thomassen, L., Lison, D., Martens, J. A., & Hoet, P. H. (2010). *The nanosilica hazard: Another variable entity*. Part Fibre Toxicol, 7(1), 39.

Nasibulina, L. I., Anoshkin, I. V., Shandakov, S. D., Nasibulin, A. G., Cwirzen, A., Mudimela, P. R., Tian, Y. (2010). *Direct synthesis of carbon nanofibers on cement particles*. Transportation Research Record: Journal of the Transportation Research Board, 2142(1), 96-101.

Nazari, A., & Riahi, S. (2011). *TiO_2 nanoparticles' effects on properties of concrete using ground granulated blast furnace slag as binder*. Science China Technological Sciences, 54(11), 3109-3118.

Neville, A. M. (1996). *Properties of concrete*. New York, U.S.A. New York. Pearson.

Ontario Ministry of Transportation (MTO). *Ontario provincial standards for roads and public works (OPSS)*. Retrieved February/05, 2013, from http://www.raqsb.mto.gov.on.ca/techpubs/OPS.nsf/OPSHomepage.

Otto, R., Sohane, R., & Wiegand, P. (2011). *Measuring and reporting tire-pavement noise using on-board sound intensity (OBSI).* Tech Brief, National Concrete Pavement Technology Center, Iowa State University, Institute for Transportation.

Papagiannakis, A., & Masad, E. A. (2008). *Pavement design and materials*. John Wiley & Sons.

Park, Y. M., Gang, M., Seo, Y. H., & Kim, B. H. (2011). *Artificial petal surface based on hierarchical micro-and nanostructures*. Thin Solid Films, 520(1), 362-367.

Persons, T. M., Droitcour, J. A., Larson, E. M., Armes, M. W., Ettaro, L. R., Farah, P. G., Ryen, T. S. (2014). *Nanomanufacturing: Emergence and implications for US competitiveness, the environment, and human health.*

Phys.org. *Self cleaning lotus leaf imitated in plastic by using a femtosecond laser*. Retrieved November, 24, 2012, from http://phys.org/news88088727.html

Quercia, G., Hüsken, G., & Brouwers, H. (2012). *Water demand of amorphous nano silica and its impact on the workability of cement paste*. Cement and Concrete Research, 42(2), 344-357.

Said, A., Zeidan, M. S., Bassuoni, M., & Tian, Y. (2012). *Properties of concrete incorporating nano-silica*. Construction and Building Materials, 36, 838-844.

Sanchez, F., & Sobolev, K. (2010). *Nanotechnology in concrete–a review*. Construction and Building Materials, 24(11), 2060-2071.

Santamarina, J. C., & Fratta, D. (1998). *Introduction to discrete signals and inverse problems in civil engineering*. ASCE.

Scofield, L. (2011). *Development and implementation of the next generation concrete surface*. American Concrete Pavement Association (ACPA). Final report.

Selvam, R. P., Subramani, V. J., Murray, S., & Hall, K. D. (2009). *Potential application of nanotechnology on cement based materials*. No. MBTC DOT 2095/3004.

Shekari, A., & Razzaghi, M. (2011). *Influence of nano particles on durability and mechanical properties of high performance concrete*. Procedia Engineering, 14, 3036-3041.

Shih, J., Chang, T., & Hsiao, T. (2006). *Effect of nanosilica on characterization of portland cement composite*. Materials Science and Engineering: A, 424(1), 266-274.

Shirgir, B., Hassani, A., & Khodadadi, A. (2011). *Experimental study on permeability and mechanical properties of nanomodified porous concrete*. Transportation Research Record: Journal of the Transportation Research Board, 2240(1), 30-35.

Sobolev, K., & Gutiérrez, M. F. (2005). *How nanotechnology can change the concrete world*. American Ceramic Society Bulletin, 84(10), 14.

Strategic Development Council – USA. (December, 2002.). *The U.S concrete industry roadmap.* Version 1.0

Su, C. (2010). *Facile fabrication of a lotus-effect composite coating via wrapping silica with polyurethane*. Applied Surface Science, 256(7), 2122-2127.

Taylor, H. F. (1997). *Cement chemistry*. Thomas Telford.

Tighe, S. (2013). *Pavement asset design and management guide*. Transportation Association of Canada (TAC).

Tyson, B. M., Abu Al-Rub, R. K., Yazdanbakhsh, A., & Grasley, Z. (2011). *Carbon nanotubes and carbon nanofibers for enhancing the mechanical properties of nanocomposite cementitious materials*. Journal of Materials in Civil Engineering, 23(7), 1028-1035.

Vodden, K., Smith, D., Eaton, F., & Mayhew, D. (2007). *Analysis and estimation of the social cost of motor vehicle collisions in Ontario*. No. Final Report, TP 14800F. Ottawa, Canada: Transport Canada.

Waterloo Institute for Nanotechnology (WIN). Retrieved January, 02, 2013, from http://uwaterloo.ca/institute-nanotechnology

Zhang, X., Li, Q., Holesinger, T. G., Arendt, P. N., Huang, J., Kirven, P. D., Zhao, Y. (2007). *Ultrastrong, stiff, and lightweight Carbon-Nanotube fibers*. Advanced Materials, 19(23), 4198-4201.

Zhou, Z., Lai, C., Zhang, L., Qian, Y., Hou, H., Reneker, D. H., & Fong, H. (2009). *Development of carbon nanofibers from aligned electrospun polyacrylonitrile nanofiber bundles and characterization of their microstructural, electrical, and mechanical properties*. Polymer, 50(13), 2999-3006.

Appendix A

Concrete Mix Design

The procedure used for producing the mixtures corresponded with the CSA A23.1-09/A23.2-09 standard (CSA, 2009), which specifies design parameters:

- **Type of cement:** General Use (GU)
- **Class of exposure:** C-2 (For details see Table 1 from CSA A23.1-09/A23.2-09).

Table 1
Definitions of C, F, N, A, and S classes of exposure
(See Clauses 3, 4.1.1.1.1, 4.1.1.5, 4.4.4.1.1.1, 4.4.4.1.1.2, 6.6.7.5.1, and 8.13.3, Tables 2 and 17, and Annex L.)

C-XL	Structurally reinforced concrete exposed to chlorides or other severe environments with or without freezing and thawing conditions, with higher durability performance expectations than the C-1, A-1, or S-1 classes.
C-1	Structurally reinforced concrete exposed to chlorides with or without freezing and thawing conditions. Examples: bridge decks, parking decks and ramps, portions of marine structures located within the tidal and splash zones, concrete exposed to seawater spray, and salt water pools.
C-2	Non-structurally reinforced (i.e., plain) concrete exposed to chlorides and freezing and thawing. Examples: garage floors, porches, steps, pavements, sidewalks, curbs, and gutters.

- **Minimum specified compressive strength at 28 days:** 32 MPa at 28 days (For details see Table 2 from CSA A23.1-09/A23.2-09). For the mix design a specified compressive strength of 35 MPa was assumed by the author. The required average compressive strength was 43.5 MPa (See Table 12-11 (Adapted from Kosmatka et al., 2011)). Several Tables used in the calculations are adapted from (Kosmatka et al., 2011).

Table 2
Requirements for C, F, N, A, and S classes of exposure
(See Clauses 4.1.1.1.1, 4.1.1.3, 4.1.1.4, 4.1.1.5, 4.1.1.6.2, 4.1.1.10.1, 4.1.1.10.3, 4.1.2.1, 4.3.1, 7.4.2.1, 8.7.3, 8.7.6.1, 8.13.3, and 8.13.5, Tables 1 and 2, and Annex L.)

Class of exposure*	Maximum water-to-cementing materials ratio†	Minimum specified compressive strength (MPa) and age (d) at test†	Air content category as per Table 4	Curing type (see Table 20)			Chloride ion penetrability requirements and age at test‡
				Normal concrete	HVSCM 1	HVSCM 2	
C-XL	0.40	50 within 56 d	1 or 2§	3	3	3	< 1000 coulombs within 56 d
C-1 or A-1	0.40	35 at 28 d	1 or 2§	2	3	2	< 1500 coulombs within 56 d
C-2 or A-2	0.45	32 at 28 d	1	2	2	2	—
C-3 or A-3	0.50	30 at 28 d	2	1	2	2	—

- **Air Content:** 5% to 8% (For details see Table 4 from CSA A23.1-09/A23.2-09).

Table 4
Requirements for air content categories
(See Clauses 4.1.1.1.1, 4.1.1.3, 4.1.1.4, 4.1.1.5, 4.3.1, 4.3.3.1, 4.3.3.2, and 4.4.4.1.1.1 and Table 2.)

	Range in air content* for concretes with indicated nominal maximum sizes of coarse aggregate, %		
Air content category	10 mm	14–20 mm	28–40 mm
1†	6–9	5–8	4–7
2	5–8	4–7	3–6

*At the point of discharge from the delivery equipment, unless otherwise specified.
†For hardened concrete, see Clause 4.3.3.2.
Notes:
(1) *The above difference in air contents has been established based upon the difference in mortar fraction volume required for specific coarse aggregate sizes.*
(2) *Air contents measured after pumping or slip forming may be significantly lower than those measured at the end of the chute.*

Table 10
Grading limits for fine aggregate (FA)
(See Clauses 4.2.3.2.2, 4.2.3.3.2.1, 4.2.3.3.2.2, 4.2.3.6, and 4.2.3.9.1.)

	Total passing sieve, percentage by mass	
Sieve size	FA1*	FA2*
10 mm	100	100
5 mm	95–100	80–90
2.5 mm	80–100	60–75
1.25 mm	50–90	35–50
630 µm	25–65	15–30
315 µm	10–35	5–15
160 µm	2–10	0–8
80 µm	0–3†	0–3†

Note: Tables partially reproduced from CSA A23.1-09/A23.2-09.

- **Slump range:** According to Table 12-5.

Table 12-11 Required Average Compressive Strength When Data Are Not Available to Establish a Standard Deviation

Specified compressive strength, f'_c, MPa	Required average compressive strength, f'_{cr}, MPa
Less than 21	f'_c + 7.0
21 to 35	f'_c + 8.5
Over 35	f'_c + 10.0

Adapted from ACI 318.

Adapted from (Kosmatka et al., 2011).

Table 12-3 Relationship Between Water to Cementing Materials Ratio and Compressive Strength of Concrete

Compressive strength at 28 days, MPa	Water-cementing materials ratio by mass	
	Non-air-entrained concrete	Air-entrained concrete
45	0.38	0.30
40	0.42	0.34
35	0.47	0.39
30	0.54	0.45
25	0.61	0.52
20	0.69	0.60
15	0.79	0.70

Strength is based on cylinders moist-cured 28 days in accordance with CSA A23.2-3C (ASTM C 31). Relationship assumes nominal maximum size aggregate of about 20 to 28 mm.
Adapted from ACI 211.1 and ACI 211.3.

Adapted from (Kosmatka et al., 2011).

Table 12-4 Bulk Volume of Coarse Aggregate Per Unit Volume of Concrete

Nominal maximum size of aggregate, mm	Bulk volume of dry-rodded coarse aggregate per unit volume of concrete for different fineness moduli of fine aggregate*			
	2.40	2.60	2.80	3.00
10	0.50	0.48	0.46	0.44
14	0.59	0.57	0.55	0.53
20	0.66	0.64	0.62	0.60
28	0.71	0.69	0.67	0.65
40	0.75	0.73	0.71	0.69
56	0.78	0.76	0.74	0.72
80	0.82	0.80	0.78	0.76
150	0.87	0.85	0.83	0.81

*Bulk volumes are based on aggregates in dry-rodded condition as described in CSA A23.2-10A (ASTM C 29). Adapted from ACI 211.1.

Adapted from (Kosmatka et al., 2011).

Table 12-5 Approximate Mixing Water and Air Content Requirements for Different Slumps and Nominal Maximum Sizes of Aggregate

Slump, mm	Water, kilograms per cubic metre of concrete, for indicated sizes of aggregate*							
	10 mm	14 mm	20 mm	28 mm	40 mm	56 mm**	80 mm**	150 mm**
	Non-air-entrained concrete							
25 to 50	207	199	190	179	166	154	130	113
75 to 100	228	216	205	193	181	169	145	124
150 to 175	243	228	216	202	190	178	160	—
Approximate amount of entrapped air in non-air-entrained concrete, percent	3	2.5	2	1.5	1	0.5	0.3	0.2
	Air-entrained concrete							
25 to 50	181	175	168	160	150	142	122	107
75 to 100	202	193	184	175	165	157	133	119
150 to 175	216	205	197	184	174	166	154	—
CSA A23.1 Recommended total air content percent†								
Category 1	6 to 9	5 to 8		4 to 7		—	—	—
Category 2	5 to 8	4 to 7		3 to 6		—	—	—

* These quantities of mixing water are for use in computing cementing material contents for trial batches. They are maximums for reasonably well-shaped angular coarse aggregates graded within limits of accepted specifications.

** The slump values for concrete containing aggregates larger than 40 mm are based on slump tests made after removal of particles larger than 40 mm by wet screening.

† See Tables 12-1 and 12-2 for class of exposure and corresponding air content category.

Adapted from CSA Standard A23.1, ACI 211.1, and ACI 318. Hover (1995) presents this information in graphical form.

Adapted from (Kosmatka et al., 2011).

Table A-1: Mix proportioning for w/c = 0.31

#	Property	Value	Unit	Comments
1	Specified Compressive Strength at 28 days	35	MPa	f´c
2	Air entrainment is required (Micro Air)	Yes	-	-
3	Slump	75 - 100	mm	-
4	Nominal Maximum Size	20	mm	-
5	No statistical data on previous mixes			
6	Type of cement (3.15 cement density)	Type 10 or type GU		
7	**Coarse aggregates**	Dufferin aggregates - Breslau Plant		
	Nominal Maximum Size	20	mm	
	Oven-dry Relative Density	2678	kg/m^3	
	Relative Density - SSD	2709	kg/m^3	
	Absorption	1.16	%	
	Oven-dry Bulk Density	1660	kg/m^3	
	Moisture content of lab. Samples	0.25	%	
8	**Fine aggregates**	Dufferin aggregates - Breslau Plant		
	Oven-dry relative density (Specific Gravity)	2671	kg/m^3	
	Relative density (Specific Gravity) - SSD	2705	kg/m^3	
	Absorption	1.2	%	
	Sample moisture content	0.11	%	
	Fineness modulus (2,72+2,68)/2	2.7		
9	Water reducer	Yes		
10	Required average compressive strength (f´c + 8.5 from Table 9-11)	43.5	MPa	f´cr
11	Maximum Water/Cementing Material Ratio (from Table 2)	0.45	-	w/c
12	Recommended w/c (Interpolated from Table 9.3)	0.31		
13	Air content - Category 1 (From Table 4)	5% - 8%	%	
14	Water content (from Table 9.5) with air content	184	kg/m^3	
15	Water content - reduce 12,5 Kg/m^3 by the gravel	172	(Crushed in 60%)	
16	Real water content (less 10% by the additive effect)	154	kg	
17	Cement content (Density of cement 3120 kg/m3)	495	kg	Ok > 340 kg
18	Coarse aggregates	1046	kg	
19	Bulk volume (Interpolated from Table 9-4)	0.63	volume/m^3 concrete	
20	Fine-aggregate content	0.233	m^3	
21	Fine-aggregate content	623	kg	

Mix proportions (w/c = 0.31)		
Water	154	Kg
Cement	495	Kg
Coarse aggregate (Dry)	1046	Kg
Fine aggregate (Dry)	623	Kg

For the two others w/c ratios (0.39 and 0.45), based on the same procedure presented in Table A-1, the water cement ratio was adjusted keeping constant the amount of water and therefore it was possible to calculate the amount of cement and the materials proportions presented in Table 3-2 in chapter 3 of this thesis.

Appendix B

GU Cement Characterization

St. Marys Cement

Great Lakes Region
St Marys Plant
P.O. Box 1000
585 Water Street South
St. Marys, ON
N4X 1B6
(519) 284-1020
(519) 284-4104

Mill Test Report - CSA A3001-13 Type GU

June 01, 2014 to June 30, 2014

Chemical Data

Loss on Ignition	2.6	%
SiO2	19.4	%
Fe2O3	2.95	%
Al2O3	4.7	%
CaO	62.4	%
Free CaO	1.7	%
MgO	2.6	%
SO3	3.43	%
K2O	0.59	%
Na2O	0.21	%
TiO2	0.48	%
Insoluble Residue	0.22	%
Total Alkali as Na2O	0.60	%

Physical Data

Fineness	Blaine SA	413	m2/kg
	Retained 325	3.3	%
Normal Consistency		27.0	%
Autoclave Expansion		0.09	%
Air Content		7	%
Sulphate Expansion		0.007	%
Vicat	Initial	112	Min.
	Final	245	Min.

Calculated Compounds

C2S	13	%
C3S	56	%
C3A	8	%
C4AF	9	%

Compressive Strengths

Age	MPa	PSI
1-Day	16.2	2350
3-Day	26.7	3873
7-Day	32.8	4757
28-Day	45.1	6541

Previous Month's 28 Day Avg

Testing methods and equipment comply with the requirements of the A3000-13 Compendium Specifications A3003-13, A3004-13 and A3005-13.
This Mill Test certifies this product to meet all the Standard Chemical and Physical requirements of CSA A3001-13 for Type GU Cement.

July 16, 2014
St. Marys Cement

April Innes
QC Supervisor

Holcim

Mississauga Plant
2391 Lakeshore Road West
Mississauga, Ontario
L5J 1K1

Phone (905) 822- 1653
Fax (905) 822- 7445
www.holcim.ca

06-02-2014

CEMENT TEST REPORT

Mississauga Plant

CEMENT TYPE : GU

SAMPLE PERIOD : 01-01-2014 - 01-02-2014

Chemical Analysis (%) :		Physical Analysis :	
LOI	2.21	Residue 45um (%)	3.22
SiO2	19.59	Blaine (m2/kg)	393
Al2O3	5.58	Air Content (%)	6.54
Fe2O3	2.35	Initial Set (mins.)	105
CaO	62.46	Auto. Exp. (%)	0.14
MgO	2.34	Sulf. Exp. (%) (prev month)	0.013
SO3	4.04		
Total Alkali	1.01	Compressive Strength (MPa)	
Free Lime	1.32	1 Day	20.06
Insol. (prev. month)	0.41	3 Days	28.80
		7 Days	34.92
		28 Days (prev month)	38.22
C3S	53.02		
C2S	16.18		
C3A	10.81		
C4AF	7.15		

This certifies compliance with C.S.A A3001-08 General use hydraulic cement (Type 10 Normal Portland cement)

Alain Peeters
Quality Manager

Strength. Performance. Passion.

Holcim (Canada) Inc.

Appendix C

Results From Freezing and Thawing Test

Table C-1: Results freezing and thawing prisms with 0.0% nanosilica – w/c = 0.39

Sample	Date (2014)	27-May	03-Jun	10-Jun	17-Jun	24-Jun	30-Jun	07-Jul	14-Jul	21-Jul	28-Jul
1	Weight (g)	7712.2	7707.4	7697	7706.7	7703.3	7702.6	7709.8	7702	7701.1	7701
	n	2290	2200	2200	2200	2200	2200	2200	2200	2210	2210
2	Weight (g)	7679.2	7674.7	7663.3	7670.9	7668.5	7666.3	7672.4	7666.4	7668.8	7668.2
	n	2290	2190	2190	2100	2200	2200	2200	2200	2210	2210
3	Weight (g)	7695.5	7690.3	7681.7	7689.3	7686	7685.9	7690.5	7683.9	7685.4	7683.3
	n	2280	2190	2190	2200	2200	2190	2200	2200	2200	2200

Table C-2: Results freezing and thawing prisms with 1.0% nanosilica – w/c = 0.39

Sample	Date (2014)	27-May	03-Jun	10-Jun	17-Jun	24-Jun	30-Jun	07-Jul	14-Jul	21-Jul	28-Jul
1	Weight (g)	7698.7	7697.5	7687.6	7694.2	7692.3	7689.9	7695	7688.4	7688	7690
	n	2280	2200	2190	2200	2190	2200	2200	2200	2200	2200
2	Weight (g)	7656.2	7653	7641.7	7651.3	7651.9	7647.4	7652	7645.3	7644.8	7646.7
	n	2290	2200	2190	2200	2200	2200	2200	2200	2200	2200
3	Weight (g)	7718.9	7716.3	7705.8	7714.3	7714.7	7710.9	7714.3	7709.2	7708.6	7709.4
	n	2290	2200	2200	2200	2190	2200	2200	2200	2200	2210

Table C-3: Results freezing and thawing prisms with 2.0% nanosilica – w/c = 0.39

Sample	Date (2014)	27-May	03-Jun	10-Jun	17-Jun	24-Jun	30-Jun	07-Jul	14-Jul	21-Jul	28-Jul
1	Weight (g)	7619.9	7618.2	7607.9	7617.6	7616.3	7613.3	7619.1	7611.5	7612.1	7611.4
	n	2290	2200	2200	2200	2200	2200	2200	2200	2200	2200
2	Weight (g)	7727.5	7725.9	7714.8	7723.6	7716.2	7720	7726	7718.8	7719.9	7721.4
	n	2300	2200	2200	2210	2200	2210	2210	2200	2220	2230
3	Weight (g)	7673.5	7670.2	7660.6	7668.9	7666.5	7666.6	7673.1	7665.5	7665	7669.4
	n	2280	2200	2190	2200	2200	2200	2200	2200	2200	2200

Note: n is the fundamental transverse frequency.

Appendix D

Pictures of Scaling Resistance Evaluation

Surface deteriorations are indicated within red circles on photographs.

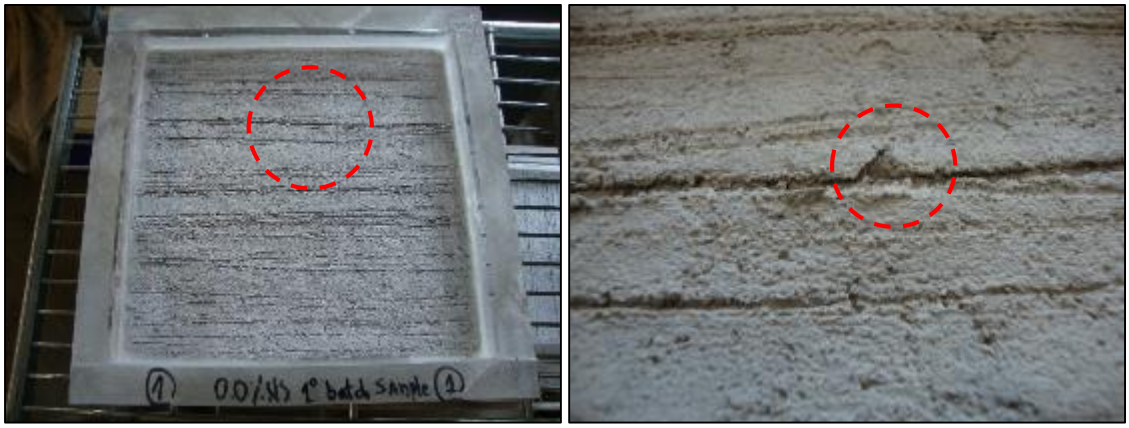

Figure D1: Pictures after 25 cycles – 0.0% nanosilica, sample 1, first batch

Figure D2: Pictures after 25 cycles – 0.0% nanosilica, sample 2, first batch

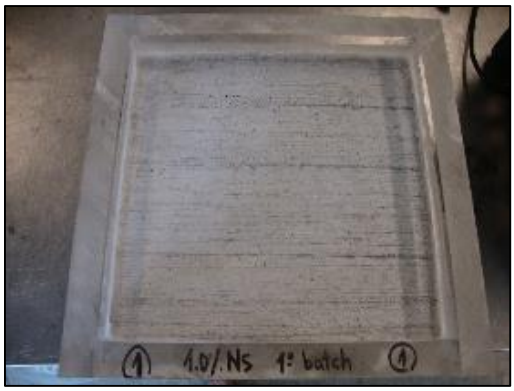

Figure D3: Picture after 25 cycles – 1.0% nanosilica, sample 1, first batch

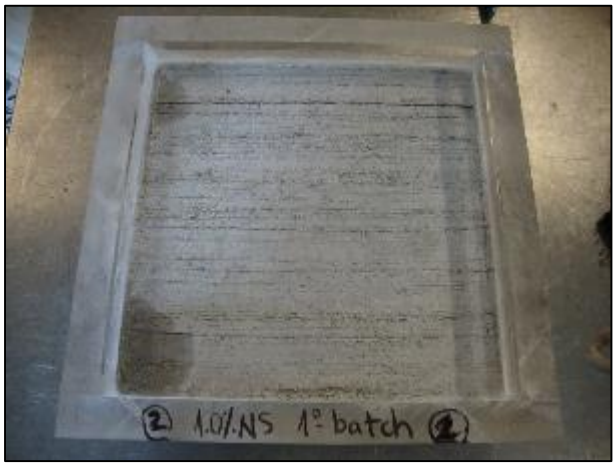

Figure D4: Picture after 25 cycles – 1.0% nanosilica, sample 2, first batch

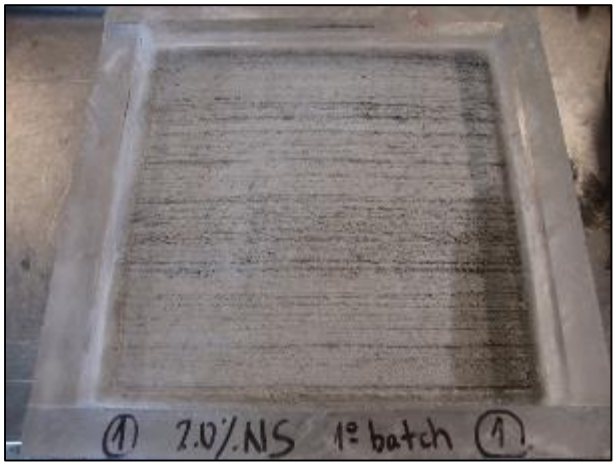

Figure D5: Picture after 25 cycles – 2.0% nanosilica, sample 1, first batch

Figure D6: Pictures after 25 cycles – 2.0% nanosilica, sample 2, first batch

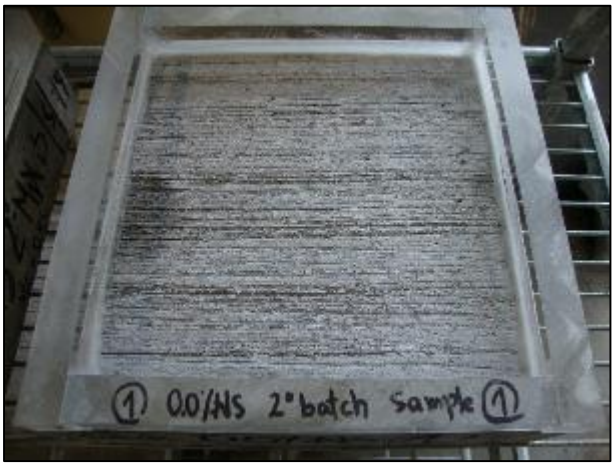

Figure D7: Picture after 25 cycles – 0.0% nanosilica, sample 1, second batch

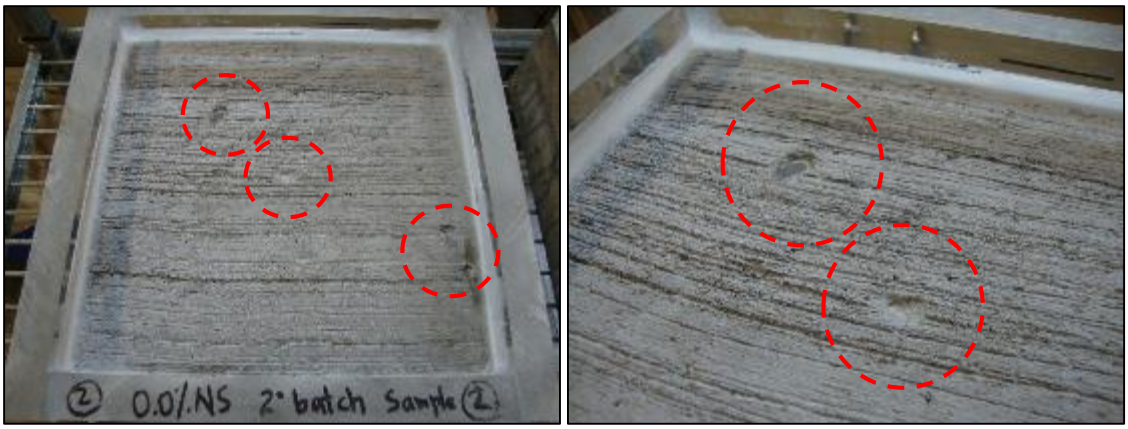

Figure D8: Pictures after 25 cycles – 0.0% nanosilica, sample 2, second batch

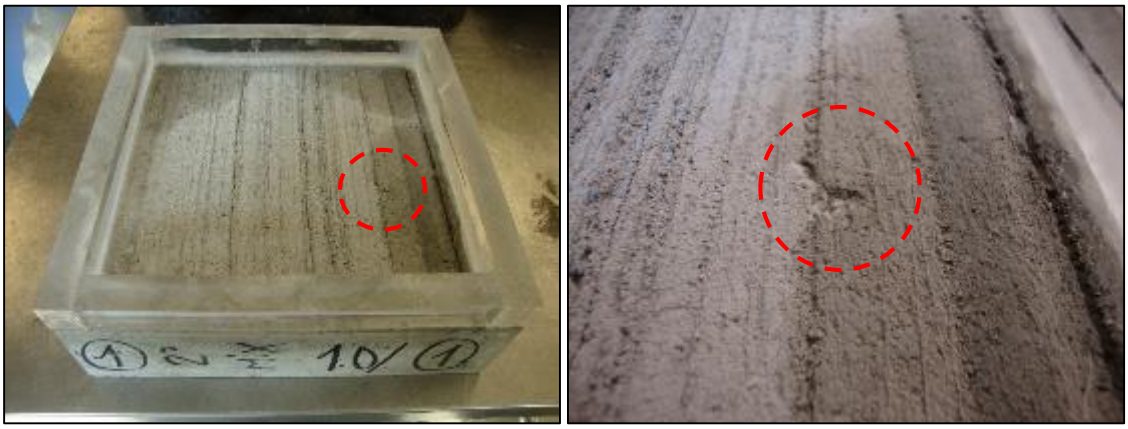

Figure D9: Pictures after 25 cycles – 1.0% nanosilica, sample 1, second batch

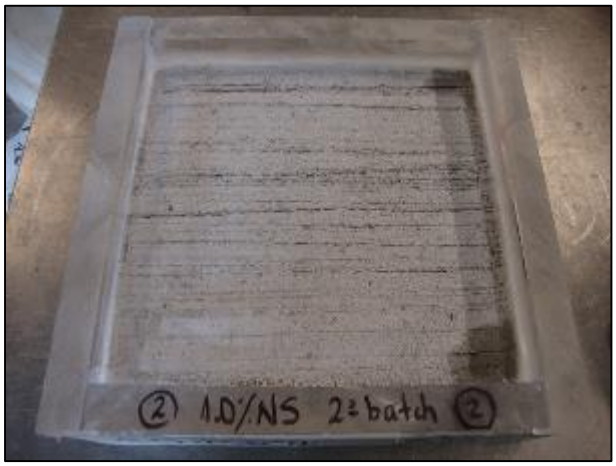

Figure D10: Picture after 25 cycles – 1.0% nanosilica, sample 2, second batch

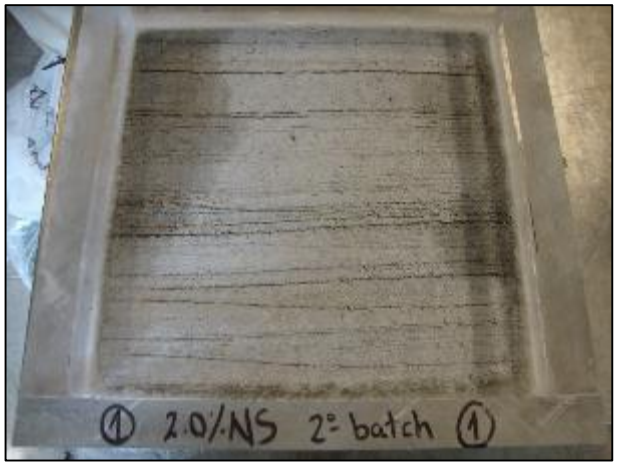

Figure D11: Picture after 25 cycles – 2.0% nanosilica, sample 1, second batch

Figure D12: Picture after 25 cycles – 2.0% nanosilica, sample 2, second batch

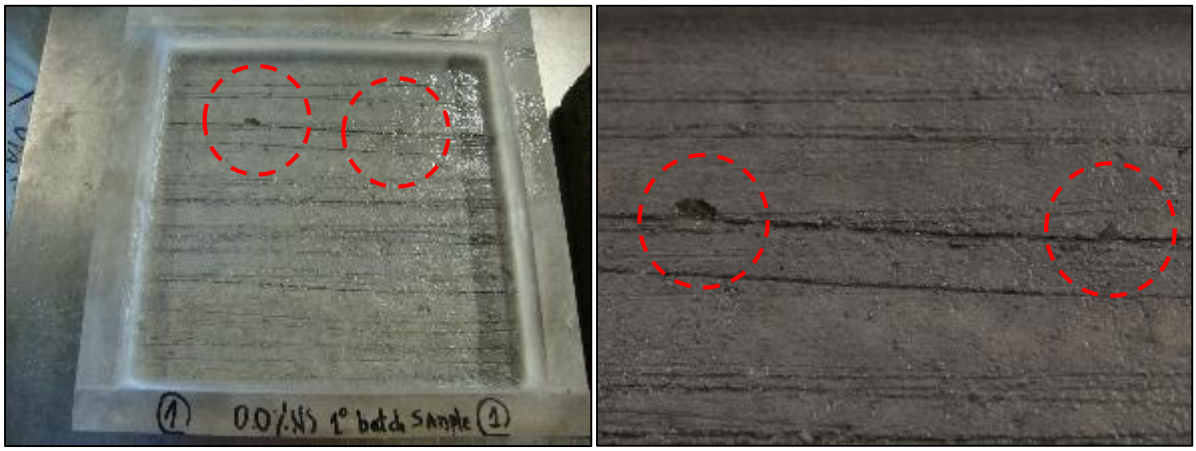

Figure D13: Pictures after 50 cycles – 0.0% nanosilica, sample 1, first batch

Figure D14: Pictures after 50 cycles – 0.0% nanosilica, sample 2, first batch

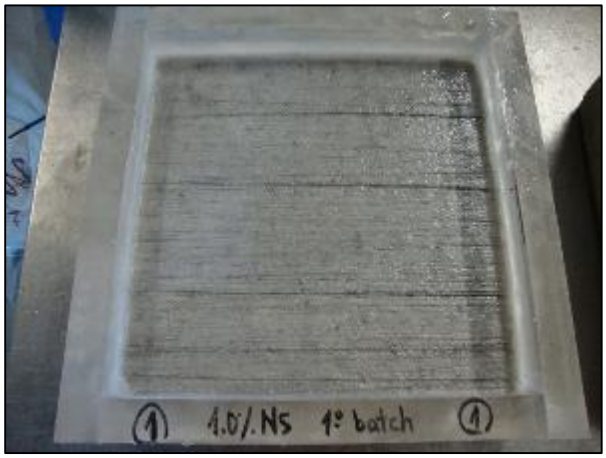

Figure D15: Picture after 50 cycles – 1.0% nanosilica, sample 1, first batch

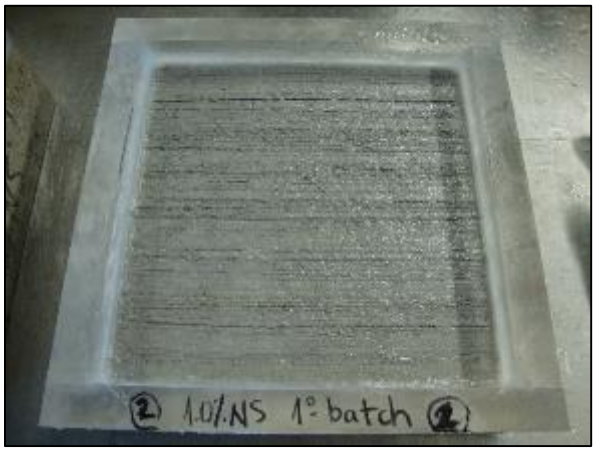

Figure D16: Picture after 50 cycles – 1.0% nanosilica, sample 2, first batch

Figure D17: Picture after 50 cycles – 2.0% nanosilica, sample 1, first batch

Figure D18: Pictures after 50 cycles – 2.0% nanosilica, sample 2, first batch

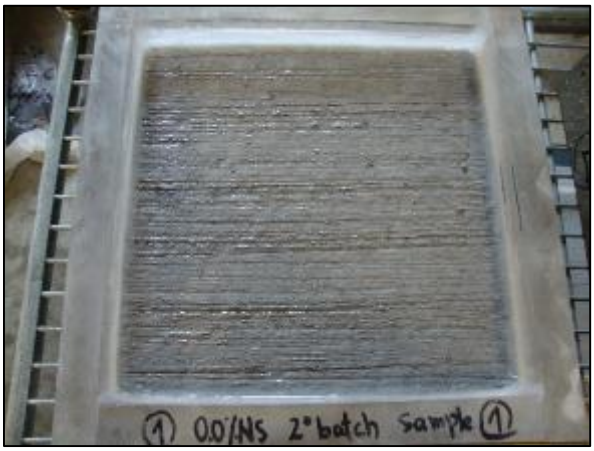

Figure D19: Picture after 50 cycles – 0.0% nanosilica, sample 1, second batch

Figure D20: Pictures after 50 cycles – 0.0% nanosilica, sample 2, second batch

Figure D21: Pictures after 50 cycles – 1.0% nanosilica, sample 1, second batch

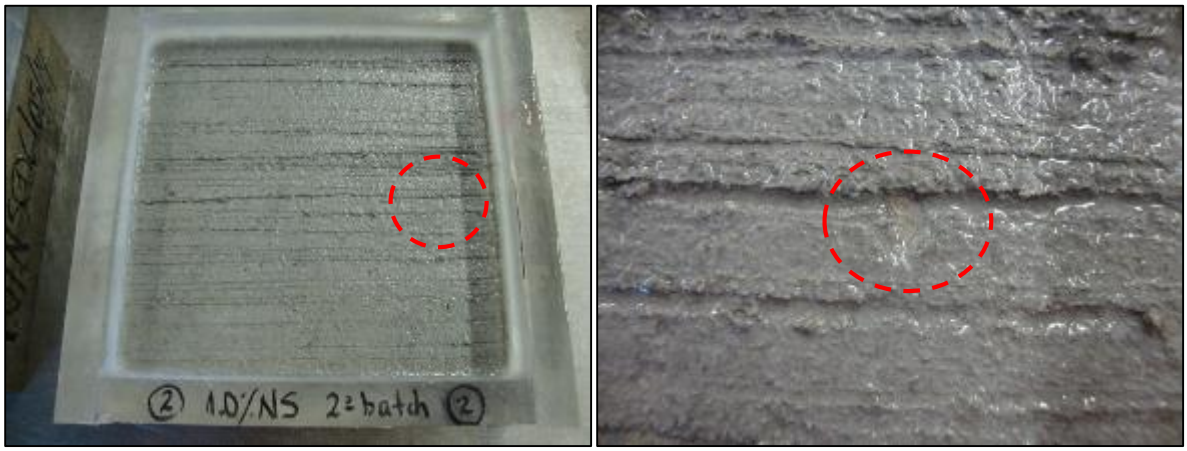

Figure D22: Pictures after 50 cycles – 1.0% nanosilica, sample 2, second batch

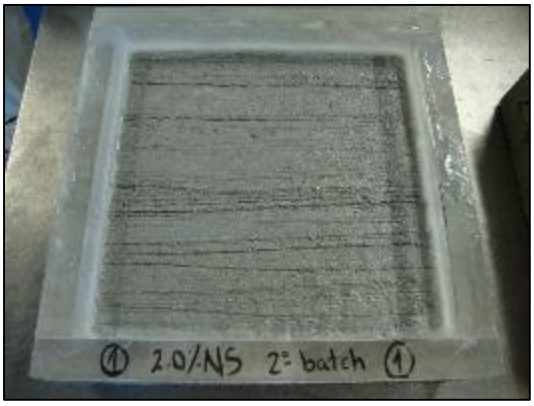

Figure D23: Picture after 50 cycles – 2.0% nanosilica, sample 1, second batch

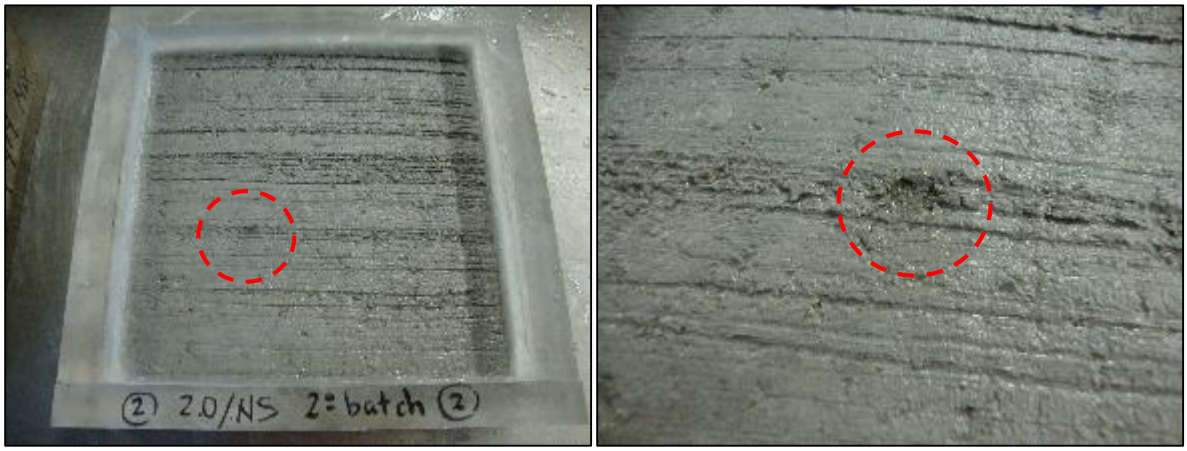

Figure D24: Pictures after 50 cycles – 2.0% nanosilica, sample 2, second batch

Appendix E

Tables with Statistical Analysis

Table E-1: Statistical analysis of hardened concrete properties w/c = 0.31

Age	Mix	Nanosilica (%)	Mean (MPa)	Standard Deviation	Coefficient of Variation (%)
7 days	1 (CC)	0.0	55	1.9	3.5
	2 (NSC 1)	0.5	52	1.8	3.5
	3 (NSC 2)	1.0	55	0.5	0.9
	4 (NSC 3)	1.5	56	0.5	0.8
28 days	1 (CC)	0.0	61	0.2	0.3
	2 (NSC 1)	0.5	60	1.7	2.8
	3 (NSC 2)	1.0	62	1.4	2.2
	4 (NSC 3)	1.5	66	1.2	1.9
Note: CC: control concrete; NSC: nanosilica concrete.					

Table E-2: Statistical analysis of hardened concrete properties w/c = 0.39

Age	Mix	Nanosilica (%)	Mean (MPa)	Standard Deviation	Coefficient of Variation (%)
7 days	1 (CC)	0.0	47	3.8	8.1
	2 (NSC 1)	0.5	51	1.5	2.9
	3 (NSC 2)	1.0	53	1.4	2.6
	4 (NSC 3)	1.5	57	1.1	1.9
	5 (NSC 4)	2.0	56	2.4	4.2
28 days	1 (CC)	0.0	55	1.4	2.5
	2 (NSC 1)	0.5	56	0.9	1.7
	3 (NSC 2)	1.0	60	0.9	1.5
	4 (NSC 3)	1.5	65	0.8	1.2
	5 (NSC 4)	2.0	57	0.0	0.1
Note: CC: control concrete; NSC: nanosilica concrete.					

Table E-3: Statistical analysis of hardened concrete properties w/c = 0.45

Age	Mix	Nanosilica (%)	Mean (MPa)	Standard Deviation	Coefficient of Variation (%)
7 days	1 (CC)	0.0	36	1.3	3.4
	2 (NSC 1)	1.0	40	0.6	1.4
	3 (NSC 2)	2.0	42	0.8	2.0
28 days	1 (CC)	0.0	42	1.9	4.6
	2 (NSC 1)	1.0	46	0.5	1.2
	3 (NSC 2)	2.0	47	0.4	0.8
Note: CC: control concrete; NSC: nanosilica concrete.					

Table E-4: Statistical analysis of hardened mortar properties w/c = 0.39

Age	Mix	Nanosilica (%)	Mean (MPa)	Standard Deviation	Coefficient of Variation (%)
7 days	1 (CM)	0.0	54	0.4	0.7
	2 (NSM 1)	0.5	56	1.3	2.4
	3 (NSM 2)	1.0	59	2.2	3.7
	4 (NSM 3)	1.5	59	3.0	5.0
	5 (NSM 4)	2.0	61	2.9	4.7
28 days	1 (CM)	0.0	62	2.0	3.3
	2 (NSM 1)	0.5	62	2.7	4.4
	3 (NSM 2)	1.0	63	1.7	2.6
	4 (NSM 3)	1.5	64	2.7	4.2
	5 (NSM 4)	2.0	68	4.4	6.5
Note: CM: control mortar; NSM: nanosilica mortar.					

Table E-5: Statistical analysis of hardened mortar properties w/c = 0.45

Age	Mix	Nanosilica (%)	Mean (MPa)	Standard Deviation	Coefficient of Variation (%)
7 days	1 (CM)	0.0	42	1.6	3.8
	2 (NSM 1)	0.5	44	0.5	1.2
	3 (NSM 2)	1.0	45	2.2	5.0
	4 (NSM 3)	1.5	46	1.6	3.5
	5 (NSM 4)	2.0	47	2.0	4.2
	6 (NSM 5)	2.5	51	2.7	5.4
	7 (NSM 6)	3.0	55	0.6	1.2
28 days	1 (CM)	0.0	47	2.2	4.8
	2 (NSM 1)	0.5	50	0.2	0.4
	3 (NSM 2)	1.0	51	0.7	1.5
	4 (NSM 3)	1.5	53	0.5	0.9
	5 (NSM 4)	2.0	51	1.2	2.3
	6 (NSM 5)	2.5	55	1.0	1.8
	7 (NSM 6)	3.0	56	1.7	3.0

Note: CM: control mortar; NSM: nanosilica mortar.

Table E-6: Statistical analysis of BPN broom finishing (3 samples per % and age) w/c = 0.31

Age	Mix	Nanosilica (%)	Mean	Standard Deviation	Coefficient of Variation (%)
7 days	1 (CC)	0.0	41	2.0	4.8
	2 (NSC 1)	0.5	44	4.4	10.2
	3 (NSC 2)	1.0	45	2.2	5.0
	4 (NSC 3)	1.5	46	0.5	1.1
28 days	1 (CC)	0.0	47	5.2	10.97
	2 (NSC 1)	0.5	46	0.9	1.9
	3 (NSC 2)	1.0	51	4.3	8.3
	4 (NSC 3)	1.5	48	1.9	4.0

Note: CC: control concrete; NSC: nanosilica concrete.

Table E-7: Statistical analysis of BPN broom finishing (5 samples per % and age) w/c = 0.39

Age	Mix	Nanosilica (%)	Mean	Standard Deviation	Coefficient of Variation (%)
7 days	1 (CC)	0.0	48	4.3	8.9
	2 (NSC 1)	0.5	48	4.2	8.8
	3 (NSC 2)	1.0	55	4.7	8.5
	4 (NSC 3)	1.5	52	4.3	8.2
	5 (NSC 4)	2.0	52	2.4	4.7
28 days	1 (CC)	0.0	51	4.3	8.5
	2 (NSC 1)	0.5	52	4.5	8.8
	3 (NSC 2)	1.0	61	2.4	3.9
	4 (NSC 3)	1.5	55	3.1	5.7
	5 (NSC 4)	2.0	52	3.5	6.7
Note: CC: control concrete; NSC: nanosilica concrete.					

Table E-8: Statistical analysis of BPN broom finishing (15 samples in each %) w/c = 0.31

Age	Mix	Nanosilica (%)	Mean	Standard Deviation	Coefficient of Variation (%)
28 days	1 (CC)	0.0	43	2.3	5.4
	2 (NSC 1)	0.5	48	3.2	6.7
	3 (NSC 2)	1.0	51	4.1	8.1
	4 (NSC 3)	1.5	51	3.4	6.7
Note: CC: control concrete; NSC: nanosilica concrete.					

Table E-9: Statistical analysis of BPN broom finishing (15 samples in each %) w/c = 0.39

Age	Mix	Nanosilica (%)	Mean	Standard Deviation	Coefficient of Variation (%)
28 days	1 (CC)	0.0	49	4.1	8.4
	2 (NSC 1)	0.5	52	3.6	7.0
	3 (NSC 2)	1.0	57	3.4	6.0
	4 (NSC 3)	1.5	57	3.9	6.8
	5 (NSC 4)	2.0	55	4.4	7.9
Note: CC: control concrete; NSC: nanosilica concrete.					

Table E-10: Statistical Analysis of BPN smooth finishing (5 samples per % and age) w/c = 0.39

Age	Mix	Nanosilica (%)	Mean	Standard Deviation	Coefficient of Variation (%)
7 days	1 (CC)	0.0	33	1.5	4.6
	2 (NSC 1)	0.5	36	2.7	7.5
	3 (NSC 2)	1.0	36	2.4	6.7
	4 (NSC 3)	1.5	38	3.2	8.3
	5 (NSC 4)	2.0	42	2.8	6.6
28 days	1 (CC)	0.0	37	2.4	6.6
	2 (NSC 1)	0.5	39	3.4	8.8
	3 (NSC 2)	1.0	39	2.3	6.1
	4 (NSC 3)	1.5	42	3.0	7.2
	5 (NSC 4)	2.0	44	3.3	7.5

Note: CC: control concrete; NSC: nanosilica concrete.

Table E-11: Statistical Analysis of μ_T smooth finishing two vertical forces, mortars 28 days old and w/c = 0.39

Age	Mix	Nanosilica (%)	Mean	Standard Deviation	Coefficient of Variation (%)
28 days - 50 gr load	1 (CM)	0.0	0.68	0.01	2.0
	2 (NSM 1)	0.5	0.76	0.02	3.0
	3 (NSM 2)	1.0	0.78	0.05	6.4
	4 (NSM 3)	1.5	0.85	0.04	4.4
	5 (NSM 4)	2.0	0.82	0.04	4.6
28 days - 100 gr load	1 (CM)	0.0	0.71	0.01	1.6
	2 (NSM 1)	0.5	0.76	0.02	2.0
	3 (NSM 2)	1.0	0.76	0.02	2.0
	4 (NSM 3)	1.5	0.85	0.02	1.8
	5 (NSM 4)	2.0	0.82	0.04	4.9

Table E-12: Statistical analysis of sound absorption coefficint (3 samples per % and age) w/c = 0.31

Age	Mix	Nanosilica (%)	Mean	Standard Deviation	Coefficient of Variation (%)
7 days	1 (CC)	0.0	0.11	0.02	19.0
	2 (NSC 1)	0.5	0.16	0.04	26.3
	3 (NSC 2)	1.0	0.22	0.03	14.4
	4 (NSC 3)	1.5	0.13	0.13	100.3
28 days	1 (CC)	0.0	0.05	0.01	19.0
	2 (NSC 1)	0.5	0.04	0.00	9.2
	3 (NSC 2)	1.0	0.06	0.03	50.2
	4 (NSC 3)	1.5	0.06	0.00	7.9
Note: CC: control concrete; NSC: nanosilica concrete.					

Table E-13: Statistical analysis of sound absorption coefficient (3 samples per % and age) w/c = 0.39

Age	Mix	Nanosilica (%)	Mean	Standard Deviation	Coefficient of Variation (%)
7 days	1 (CC)	0.0	0.06	0.02	36.8
	2 (NSC 1)	0.5	0.12	0.07	55.5
	3 (NSC 2)	1.0	0.08	0.01	18.8
	4 (NSC 3)	1.5	0.13	0.06	47.0
	5 (NSC 4)	2.0	0.07	0.02	24.6
28 days	1 (CC)	0.0	0.07	0.03	44.2
	2 (NSC 1)	0.5	0.07	0.03	46.3
	3 (NSC 2)	1.0	0.07	0.02	31.3
	4 (NSC 3)	1.5	0.08	0.06	73.4
	5 (NSC 4)	2.0	0.07	0.02	24.6
Note: CC: control concrete; NSC: nanosilica concrete.					

Table E-14: Statistical analysis of abrasion response broom finishing w/c = 0.39

Age	Mix	Nanosilica (%)	Mean (g)	Standard Deviation	Coefficient of Variation (%)
7 days - broom finishing	1 (CC)	0.0	5.5	0.7	12.9
	2 (NSC 1)	0.5	5.5	0.2	4.2
	3 (NSC 2)	1.0	6.4	0.4	5.9
	4 (NSC 3)	1.5	5.6	0.9	16.9
	5 (NSC 4)	2.0	4.4	0.6	13.4
28 days - broom finishing	1 (CC)	0.0	4.6	1.0	21.0
	2 (NSC 1)	0.5	5.1	0.5	10.5
	3 (NSC 2)	1.0	6.1	1.1	17.4
	4 (NSC 3)	1.5	4.5	0.6	13.1
	5 (NSC 4)	2.0	3.7	0.2	5.8

Note: CC: control concrete; NSC: nanosilica concrete.

Table E-15: Statistical analysis of abrasion response smooth finishing w/c = 0.39

Age	Mix	Nanosilica (%)	Mean (g)	Standard Deviation	Coefficient of Variation (%)
7 days - broom finishing	1 (CC)	0.0	3.0	0.6	20.9
	2 (NSC 2)	1.0	1.6	0.1	6.7
	3 (NSC 4)	2.0	1.4	0.2	16.5
28 days - broom finishing	1 (CC)	0.0	2.4	0.4	17.5
	2 (NSC 2)	1.0	1.4	0.1	5.3
	3 (NSC 4)	2.0	1.5	0.1	4.1

Note: CC: control concrete; NSC: nanosilica concrete.

Table E-16: Statistical analysis of compressive strength for freezing and thawing samples w/c = 0.39

Age	Mix	Nanosilica (%)	Mean (MPa)	Standard Deviation	Coefficient of Variation (%)
7 days	1 (CC)	0.0	45.3	0.5	1.1
	2 (NSC 1)	1.0	47.0	0.5	1.1
	3 (NSC 2)	2.0	52.6	1.1	2.0
28 days	1 (CC)	0.0	53.2	1.1	2.1
	2 (NSC 1)	1.0	55.4	1.8	3.2
	3 (NSC 2)	2.0	59.0	1.1	1.9

Note: CC: control concrete; NSC: nanosilica concrete.

Table E-17: Statistical analysis of Durability Factor (DF) freezing and thawing test w/c = 0.39

Mix	Nanosilica (%)	Mean	Standard Deviation	Coefficient of Variation (%)
1 (CC)	0.0	93	0.0	0.02
2 (NSC 1)	1.0	93	0.5	0.51
3 (NSC 2)	2.0	93	0.9	0.92
Note: CC: control concrete; NSC: nanosilica concrete.				

Table E-18: Statistical analysis of loss of weight during the freezing and thawing test w/c = 0.39

Mix	Nanosilica (%)	Mean (g)	Standard Deviation	Coefficient of Variation (%)
1 (CC)	0.0	0.15	0.0	5.6
2 (NSC 1)	1.0	0.12	0.0	5.1
3 (NSC 2)	2.0	0.08	0.0	35.8
Note: CC: control concrete; NSC: nanosilica concrete.				

Table E-19: Statistical analysis of compressive strength for freezing and thawing samples, first batch, w/c = 0.45

Age	Mix	Nanosilica (%)	Mean (MPa)	Standard Deviation	Coefficient of Variation (%)
7 days	1 (CC)	0.0	36	1.2	3.2
	2 (NSC 1)	1.0	37	2.0	5.3
	3 (NSC 2)	2.0	38	0.5	1.3
28 days	1 (CC)	0.0	42	1.9	4.6
	2 (NSC 1)	1.0	42	1.4	3.3
	3 (NSC 2)	2.0	44	0.8	1.7
Note: CC: control concrete; NSC: nanosilica concrete.					

Table E-20: Statistical analysis of compressive strength for freezing and thawing samples, second bath, w/c = 0.45

Age	Mix	Nanosilica (%)	Mean (MPa)	Standard Deviation	Coefficient of Variation (%)
7 days	1 (CC)	0.0	36	1.3	3.4
	2 (NSC 1)	1.0	40	0.6	1.4
	3 (NSC 2)	2.0	42	0.8	2.0
28 days	1 (CC)	0.0	42	1.9	4.6
	2 (NSC 1)	1.0	46	0.5	1.2
	3 (NSC 2)	2.0	47	0.4	0.8
Note: CC: control concrete; NSC: nanosilica concrete.					

Table E-21: Statistical analysis of BPN using the first coating wet condition

Type of mix	Mean	Standard Deviation	Coefficient of Variation (%)
CC (0.0 g/m^2)	44	1.1	2.6
NLLCC1 (30 g/m^2)	43	2.5	5.9
NLLCC2 (60 g/m^2)	39	5.3	13.3
NLLCC3 (90 g/m^2)	41	2.3	5.6
NLLCC4 (110 g/m^2)	41	2.4	6.0

Note: NLLCC = Nano-lotus leaf coated concrete.

Table E-22: Statistical analysis of BPN using the second coating wet condition

Type of mix	Mean	Standard Deviation	Coefficient of Variation (%)
CC (0.0 g/m^2)	40	5.2	12.8
NLLCC1 (30 g/m^2)	43	5.9	13.6
NLLCC2 (60 g/m^2)	40	5.7	14.2
NLLCC3 (90 g/m^2)	47	2.7	5.8
NLLCC4 (110 g/m^2)	37	6.4	17.2

Note: NLLCC = Nano-lotus leaf coated concrete.

Table E-23: Statistical analysis of sound absorption coefficient second coating

Mix	Mean	Standard Deviation	Coefficient of Variation (%)
CC (0.0 g/m^2)	0.06	0.01	9.7
NLLCC1 (30 g/m^2)	0.07	0.01	16.7
NLLCC2 (60 g/m^2)	0.07	0.01	12.2
NLLCC3 (90 g/m^2)	0.08	0.01	10.9
NLLCC4 (110 g/m^2)	0.06	0.01	19.1

Note: NLLCC = Nano-lotus leaf coated concrete.

Appendix F

Details of ANOVA Calculations

Table F-1: Values for x for which the Distribution Function of the F-Distribution with (m, n) Degrees of Freedom

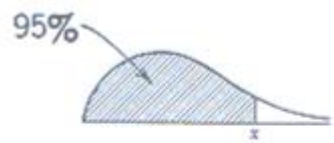

Example. For (7, 4) degrees of freedom, $F = 0.95$ when $x = 6.09$.

The value of x for which $F = 0.05$ in the case (n, m) degrees of freedom equals the reciprocal of that x for which $F = 0.95$ in the case of (m, n) degrees of freedom.

Example. For (7, 4) degrees of freedom, $F = 0.05$ when $x = 1/4.12 = 0.24$.

n	$m = 1$	$m = 2$	$m = 3$	$m = 4$	$m = 5$	$m = 6$	$m = 7$	$m = 8$	$m = 9$
1	161	200	216	225	230	234	237	239	241
2	18.5	19.0	19.2	19.2	19.3	19.3	19.4	19.4	19.4
3	10.1	9.55	9.28	9.12	9.01	8.94	8.89	8.85	8.81
4	7.71	6.94	6.59	6.39	6.26	6.16	6.09	6.04	6.00
5	6.61	5.79	5.41	5.19	5.05	4.95	4.88	4.82	4.77
6	5.99	5.14	4.76	4.53	4.39	4.28	4.21	4.15	4.10
7	5.59	4.74	4.35	4.12	3.97	3.87	3.79	3.73	3.68
8	5.32	4.46	4.07	3.84	3.69	3.58	3.50	3.44	3.39
9	5.12	4.26	3.86	3.63	3.48	3.37	3.29	3.23	3.18
10	4.96	4.10	3.71	3.48	3.33	3.22	3.14	3.07	3.02
11	4.84	3.98	3.59	3.36	3.20	3.09	3.01	2.95	2.90
12	4.75	3.89	3.49	3.26	3.11	3.00	2.91	2.85	2.80
13	4.67	3.81	3.41	3.18	3.03	2.92	2.83	2.77	2.71
14	4.60	3.74	3.34	3.11	2.96	2.85	2.76	2.70	2.65
15	4.54	3.68	3.29	3.06	2.90	2.79	2.71	2.64	2.59
16	4.49	3.63	3.24	3.01	2.85	2.74	2.66	2.59	2.54
17	4.45	3.59	3.20	2.96	2.81	2.70	2.61	2.55	2.49
18	4.41	3.55	3.16	2.93	2.77	2.66	2.58	2.51	2.46
19	4.38	3.52	3.13	2.90	2.74	2.63	2.54	2.48	2.42
20	4.35	3.49	3.10	2.87	2.71	2.60	2.51	2.45	2.39
22	4.30	3.44	3.05	2.82	2.66	2.55	2.46	2.40	2.34
24	4.26	3.40	3.01	2.78	2.62	2.51	2.42	2.36	2.30
26	4.23	3.37	2.98	2.74	2.59	2.47	2.39	2.32	2.27
28	4.20	3.34	2.95	2.71	2.56	2.45	2.36	2.29	2.24
30	4.17	3.32	2.92	2.69	2.53	2.42	2.33	2.27	2.21
32	4.15	3.30	2.90	2.67	2.51	2.40	2.31	2.24	2.19
34	4.13	3.28	2.88	2.65	2.49	2.38	2.29	2.23	2.17
36	4.11	3.26	2.87	2.63	2.48	2.36	2.28	2.21	2.15
38	4.10	3.24	2.85	2.62	2.46	2.35	2.26	2.19	2.14
40	4.08	3.23	2.84	2.61	2.45	2.34	2.25	2.18	2.12
50	4.03	3.18	2.79	2.56	2.40	2.29	2.20	2.13	2.07
60	4.00	3.15	2.76	2.53	2.37	2.25	2.17	2.10	2.04
70	3.98	3.13	2.74	2.50	2.35	2.23	2.14	2.07	2.02
80	3.96	3.11	2.72	2.49	2.33	2.21	2.13	2.06	2.00
90	3.95	3.10	2.71	2.47	2.32	2.20	2.11	2.04	1.99
100	3.94	3.09	2.70	2.46	2.31	2.19	2.10	2.03	1.97
150	3.90	3.06	2.66	2.43	2.27	2.16	2.07	2.00	1.94
200	3.89	3.04	2.65	2.42	2.26	2.14	2.06	1.98	1.93
1000	3.85	3.00	2.61	2.38	2.22	2.11	2.02	1.95	1.89
∞	3.84	3.00	2.60	2.37	2.21	2.10	2.01	1.94	1.88

- **Compressive strength in concretes - w/c = 0.31 (3 samples)**

Age	Mix	Nanosilica (%)	Sample 1	Sample 2	Sample 3	Mean (MPa)	Standard Deviation	Coefficient of Variation (%)
28 days	1 (CC)	0.0	61	61	61	61	0.2	0.3
	2 (NSC 1)	0.5	59	60	62	60	1.7	2.8
	3 (NSC 2)	1.0	62	64	61	62	1.4	2.2
	4 (NSC 3)	1.5	65	67	66	66	1.2	1.9

Note: CC: control concrete; NSC: nanosilica concrete.

r (number of groups)		4		
n (size of the sample)		12		
Mean of the entire sample		$\bar{y}$	62.4	
The sum of the squares between the means of the groups		q_1	**76.9**	
The sum of the squares within the groups		q_2	**12.45**	
		ν_o	16.5	
Significance level α		α	0.05	
r -1 (m in Table F-1)		3		
n - r (n in Table F-1)		8		
For P (V ≤ c) = 0.95 ⇒	c =	4.07	≤	ν_o = 16.5
⇒ since $\nu_o \geq c$	the hypothesis is rejected and thus the means are statistically different			

- **Compressive strength in concretes - w/c = 0.39 (3 samples)**

Age	Mix	Nanosilica (%)	Sample 1	Sample 2	Sample 3	Mean (MPa)	Standard Deviation	Coefficient of Variation (%)
28 days	1 (CC)	0.0	54	56	54	55	1.4	2.5
	2 (NSC 1)	0.5	56	55	57	56	0.9	1.7
	3 (NSC 2)	1.0	59	61	59	60	0.9	1.5
	4 (NSC 3)	1.5	64	65	65	65	0.8	1.2
	5 (NSC 4)	2.0	57	57	57	57	0.0	0.1

Note: CC: control concrete; NSC: nanosilica concrete.

r (number of groups)		5		
n (size of the sample)		15		
Mean of the entire sample		$\bar{y}$	58.4	
The sum of the squares between the means of the groups		$\mathbf{q_1}$	**323.1**	
The sum of the squares within the groups		$\mathbf{q_2}$	**8.35**	
		ν_o	96.7	
Significance level α		α	0.05	
r -1 (m in Table F-1)		4		
n - r (n in Table F-1)		10		
For P (V ≤ c) = 0.95 ⇒	c =	3.48	≤	ν_o = 96.7
⇒ since $\nu_o \geq c$	the hypothesis is rejected and thus the means are statistically different			

- **Compressive strength in concretes - w/c = 0.45 (3 samples)**

Age	Mix	Nanosilica (%)	Sample 1	Sample 2	Sample 3	Mean (MPa)	Standard Deviation	Coefficient of Variation (%)
28 days	1 (CC)	0.0	40	43	43	42	1.9	4.6
	2 (NSC 1)	1.0	46	47	46	46	0.5	1.2
	3 (NSC 2)	2.0	47	47	46	47	0.4	0.8

Note: CC: control concrete; NSC: nanosilica concrete.

r (number of groups)		3		
n (size of the sample)		9		
Mean of the entire sample		$\bar{y}$	44.8	
The sum of the squares between the means of the groups		**q_1**	**42.3**	
The sum of the squares within the groups		**q_2**	**8.08**	
		ν_o	15.7	
Significance level α		α	0.05	
r -1 (m in Table F-1)		2		
n - r (n in Table F-1)		6		
For P (V ≤ c) = 0.95 ⇒	c =	5.14	≤	νo = 15.7
⇒ since $\nu o \geq c$	the hypothesis is rejected and thus the means are statistically different			

- **Noise absorption - w/c = 0.31 (3 samples)**

Age	Mix	Nanosilica (%)	Sample 1	Sample 2	Sample 3	Mean	Standard Deviation	Coefficient of Variation (%)
28 days	1 (CC)	0.0	0.06	0.04	0.05	0.05	0.01	19.0
	2 (NSC 1)	0.5	0.04	0.04	0.05	0.04	0.00	9.2
	3 (NSC 2)	1.0	0.10	0.05	0.04	0.06	0.03	50.2
	4 (NSC 3)	1.5	0.06	0.06	0.05	0.06	0.00	7.9

Note: CC: control concrete; NSC: nanosilica concrete.

r (number of groups)		4		
n (size of the sample)		12		
Mean of the entire sample		$\bar{y}$	0.053	
The sum of the squares between the means of the groups		$\mathbf{q_1}$	**0.001**	
The sum of the squares within the groups		$\mathbf{q_2}$	**0.002**	
		ν_o	0.9	
Significance level α		α	0.05	
r -1 (m in Table F-1)		3		
n - r (n in Table F-1)		8		
For P (V ≤ c) = 0.95 ⇒	c =	4.07	≥	$\nu_o = 0.9$
⇒ since $\nu_o \leq c$	the hypothesis is accepted and thus the means are statistically equal			

- **Noise absorption - w/c = 0.39 (3 samples)**

Age	Mix	Nanosilica (%)	Sample 1	Sample 2	Sample 3	Mean	Standard Deviation	Coefficient of Variation (%)
28 days	1 (CC)	0.0	0.10	0.06	0.04	0.07	0.03	44.2
	2 (NSC 1)	0.5	0.11	0.06	0.05	0.07	0.03	46.3
	3 (NSC 2)	1.0	0.09	0.05	0.06	0.07	0.02	31.3
	4 (NSC 3)	1.5	0.06	0.03	0.15	0.08	0.06	73.4
	5 (NSC 4)	2.0	0.05	0.07	0.09	0.07	0.02	24.6

Note: CC: control concrete; NSC: nanosilica concrete.

r (number of groups)		5		
n (size of the sample)		15		
Mean of the entire sample		$\bar{y}$	0.1	
The sum of the squares between the means of the groups		$\mathbf{q_1}$	**0.001**	
The sum of the squares withing the groups		$\mathbf{q_2}$	**0.01**	
		ν_o	0.2	
Significance level α		α	0.05	
r -1 (m in Table F-1)		4		
n - r (n in Table F-1)		10		
For P (V ≤ c) = 0.95 ⇒	c =	3.48	≥	$\nu_o = 0.2$
⇒ since $\nu_o \leq c$	the hypothesis is accepted and thus the means are statistically equal			

- **Friction response – BPN – broom finishing - w/c = 0.31 (3 samples)**

Age	Mix	Nanosilica (%)	Sample 1	Sample 2	Sample 3	Mean	Standard Deviation	Coefficient of Variation (%)
28 days	1 (CC)	0.0	43	45	53	47	5.2	10.97
	2 (NSC 1)	0.5	46	46	47	46	0.9	1.9
	3 (NSC 2)	1.0	46	54	53	51	4.3	8.3
	4 (NSC 3)	1.5	49	46	49	48	1.9	4.0

Note: CC: control concrete; NSC: nanosilica concrete.

r (number of groups)		4		
n (size of the sample)		12		
Mean of the entire sample		$\bar{y}$	48.2	
The sum of the squares between the means of the groups		$\mathbf{q_1}$	**53.2**	
The sum of the squares withing the groups		$\mathbf{q_2}$	**98.3**	
		ν_o	1.4	
Significance level α		α	0.05	
r -1 (m in Table F-1)		3		
n - r (n in Table F-1)		8		
For P (V ≤ c) = 0.95 ⇒	c =	4.07	≥	ν_o = 1.4
⇒ since $\nu_o \leq c$	the hypothesis is accepted and thus the means are statistically equal			

- **Friction response – BPN – broom finishing - w/c = 0.39 (5 samples)**

Age	Mix	Nanosilica (%)	Sample number						Standard Deviation	Coefficient of Variation (%)
			1	2	3	4	5	Mean		
28 days	1 (CC)	0.0	50	57	49	45	53	51	4.3	8.5
	2 (NSC 1)	0.5	52	44	56	54	52	52	4.5	8.8
	3 (NSC 2)	1.0	60	58	61	62	64	61	2.4	3.9
	4 (NSC 3)	1.5	57	51	56	58	52	55	3.1	5.7
	5 (NSC 4)	2.0	50	51	50	58	51	52	3.5	6.7

Note: CC: control concrete; NSC: nanosilica concrete.

r (number of groups)	5			
n (size of the sample)	25			
Mean of the entire sample	$\bar{y}$	54.0		
The sum of the squares between the means of the groups	q_1	**350.0**		
The sum of the squares within the groups	q_2	**267.2**		
	ν_o	6.6		
Significance level α	α	0.05		
r -1 (m in Table F-1)	4			
n - r (n in Table F-1)	20			
	2.8			
For P (V ≤ c) = 0.95 ⇒	c =	7	≤	ν_o = 6.6
⇒ since $\nu_o \geq c$	the hypothesis is rejected and thus the means are statistically different			

- **Friction response – BPN – broom finishing - w/c = 0.31 (15 samples)**

Age	Mix	Nanosilica (%)	Sample number															Mean	SD	COV (%)
			1	2	3	4	5	6	7	8	9	10	11	12	13	14	15			
28 days	1 (CC)	0.0	41	43	45	46	44	39	43	40	44	45	47	42	42	44	40	43	2.3	5.4
	2 (NSC 1)	0.5	52	49	43	49	44	48	52	52	44	52	53	46	46	47	47	48	3.2	6.7
	3 (NSC 2)	1.0	45	51	45	54	53	49	53	44	57	49	56	53	46	54	53	51	4.1	8.1
	4 (NSC 3)	1.5	49	50	55	50	46	55	52	56	55	50	55	50	49	46	49	51	3.4	6.7

Note: CC: control concrete; NSC: nanosilica concrete; SDV: Standard Deviation; COV: Coefficient of Variation.

r (number of groups)		4		
n (size of the sample)		60		
Mean of the entire sample		$\bar{y}$	48.3	
The sum of the squares between the means of the groups		$\mathbf{q_1}$	**167.1**	
The sum of the squares within the groups		$\mathbf{q_2}$	**601.2**	
		ν_o	5.2	
Significance level α		α	0.05	
r -1 (m in Table F-1)		2.8		
n - r (m in Table F-1)		56		
For P (V ≤ c) = 0.95 ⇒	c =	2.8	≤	$\nu_o = 5.2$
⇒ since $\nu_o \geq c$	the hypothesis is rejected and thus the means are statistically different			

- **Friction response – BPN – broom finishing - w/c = 0.39 (15 samples)**

Age	Mix	Nanosilica (%)	Sample number															Mean	SD	COV (%)
			1	2	3	4	5	6	7	8	9	10	11	12	13	14	15			
28 days	1 (CC)	0.0	50	57	49	45	53	46	51	43	49	43	48	46	51	55	53	49	4.1	8.4
	2 (NSC 1)	0.5	52	41	56	54	52	53	54	51	52	54	57	53	51	49	49	52	3.6	7.0
	3 (NSC 2)	1.0	60	58	61	62	64	57	54	55	54	55	55	61	55	53	56	57	3.4	6.0
	4 (NSC 3)	1.5	57	51	56	58	52	58	54	61	57	59	60	55	63	54	64	57	3.9	6.8
	5 (NSC 4)	2.0	50	51	50	58	51	53	49	55	59	56	59	60	58	60	62	55	4.4	7.9

Note: CC: control concrete; NSC: nanosilica concrete; SDV: Standard Deviation; COV: Coefficient of Variation.

r (number of groups)		5		
n (size of the sample)		75		
Mean of the entire sample		$\bar{y}$	54.3	
The sum of the squares between the means of the groups		$\mathbf{q_1}$	**252.4**	
The sum of the squares within the groups		$\mathbf{q_2}$	**1023.2**	
		ν_o	4.3	
Significance level α		α	0.05	
r -1 (m in Table F-1)		4		
n - r (m in Table F-1)		70		
For P (V ≤ c) = 0.95 ⇒	c =	2.5	≤	ν_o = 4.3
⇒ since $\nu_o \geq c$	the hypothesis is rejected and thus the means are statistically different			

- **Friction response – BPN – smooth finishing - w/c = 0.39 (5 samples)**

Age	Mix	Nanosilica (%)	Sample number					Mean	Standard Deviation	Coefficient of Variation (%)
			1	2	3	4	5			
28 days	1 (CC)	0.0	36	40	40	35	36	37	2.4	6.6
	2 (NSC 1)	0.5	39	35	35	44	39	39	3.4	8.8
	3 (NSC 2)	1.0	39	38	35	40	41	39	2.3	6.1
	4 (NSC 3)	1.5	40	41	44	47	39	42	3.0	7.2
	5 (NSC 4)	2.0	43	44	49	40	45	44	3.3	7.5

Note: CC: control concrete; NSC: nanosilica concrete.

r (number of groups)		5		
n (size of the sample)		25		
Mean of the entire sample		$\bar{y}$	40.1	
The sum of the squares between the means of the groups		$\mathbf{q_1}$	**173.7**	
The sum of the squares within the groups		$\mathbf{q_2}$	**172.1**	
		ν_o	5.0	
Significance level α		α	0.05	
r -1 (m in Table F-1)		4		
n - r (n in Table F-1)		20		
For P (V ≤ c) = 0.95 ⇒	c =	2.9	≤	$\nu_o = 5.0$
⇒ since $\nu_o \geq c$	the hypothesis is rejected and thus the means are statistically different			

- **Friction response – using a tribometer – w/c = 0.39 – 50 g force (3 samples)**

Age	Mix	Nanosilica (%)	Sample 1	Sample 2	Sample 3	Mean	Standard Deviation	Coefficient of Variation (%)
28 days - 50 gr force	1 (CM)	0.0	0.69	0.67	0.67	0.68	0.01	2.0
	2 (NSM 1)	0.5	0.79	0.75	0.75	0.76	0.02	3.0
	3 (NSM 2)	1.0	0.77	0.74	0.83	0.78	0.05	6.4
	4 (NSM 3)	1.5	0.89	0.83	0.82	0.85	0.04	4.4
	5 (NSM 4)	2.0	0.86	0.79	0.80	0.82	0.04	4.6

Note: CM: control mortar; NSM: nanosilica mortar.

r (number of groups)		5		
n (size of the sample)		15		
Mean of the entire sample		$\bar{y}$	0.8	
The sum of the squares between the means of the groups		$\mathbf{q_1}$	**0.1**	
The sum of the squares within the groups		$\mathbf{q_2}$	**0.01**	
		ν_o	17.8	
Significance level α		α	0.05	
r -1 (m in Table F-1)		4		
n - r (n in Table F-1)		10		
For P (V ≤ c) = 0.95 ⇒	c =	3.5	≤	ν_o = 17.8
⇒ since $\nu_o \geq c$	the hypothesis is rejected and thus the means are statistically different			

- **Friction response – using a tribometer – w/c = 0.39 – 100 g force (3 samples)**

Age	Mix	Nanosilica (%)	Sample 1	Sample 2	Sample 3	Mean	Standard Deviation	Coefficient of Variation (%)
28 days - 100 gr force	1 (CM)	0.0	0.72	0.70	0.70	0.71	0.01	1.6
	2 (NSM 1)	0.5	0.78	0.76	0.75	0.76	0.02	2.0
	3 (NSM 2)	1.0	0.77	0.74	0.75	0.76	0.02	2.0
	4 (NSM 3)	1.5	0.86	0.84	0.83	0.85	0.02	1.8
	5 (NSM 4)	2.0	0.86	0.82	0.78	0.82	0.04	4.9

Note: CM: control mortar; NSM: nanosilica mortar.

r (number of groups)		5		
n (size of the sample)		15		
Mean of the entire sample		$\bar{y}$	0.8	
The sum of the squares between the means of the groups		$\mathbf{q_1}$	**0.1**	
The sum of the squares within the groups		$\mathbf{q_2}$	**0.005**	
		ν_o	30.0	
Significance level α		α	0.05	
r -1 (m in Table F-1)		4		
n - r (n in Table F-1)		10		
For P (V ≤ c) = 0.95 ⇒	c =	3.5	≤	$\nu_o = 30.0$
⇒ since $\nu_o \geq c$	the hypothesis is rejected and thus the means are statistically different			

- **Compressive strength in mortars - w/c = 0.39 (3 samples)**

Age	Mix	Nanosilica (%)	Sample 1	Sample 2	Sample 3	Mean (MPa)	Standard Deviation	Coefficient of Variation (%)
28 days	1 (CM)	0.0	59	63	62	62	2.0	3.3
	2 (NSM 1)	0.5	65	60	61	62	2.7	4.4
	3 (NSM 2)	1.0	65	62	62	63	1.7	2.6
	4 (NSM 3)	1.5	67	62	63	64	2.7	4.2
	5 (NSM 4)	2.0	73	66	65	68	4.4	6.5

Note: CM: control mortar; NSM: nanosilica mortar.

r (number of groups)		5		
n (size of the sample)		15		
Mean of the entire sample		$\bar{y}$	63.6	
The sum of the squares between the means of the groups		$\mathbf{q_1}$	**150.8**	
The sum of the squares within the groups		$\mathbf{q_2}$	**81.4**	
		ν_o	4.6	
Significance level α		α	0.05	
r -1 (m in Table F-1)		4		
n - r (n in Table F-1)		10		
For P (V ≤ c) = 0.95 ⇒	c =	3.48	≤	ν_o = 4.6
⇒ since $\nu_o \geq c$	the hypothesis is rejected and thus the means are statistically different			

- **Compressive strength in mortars - w/c = 0.45 (3 samples)**

Age	Mix	Nanosilica (%)	Sample 1	Sample 2	Sample 3	Mean (MPa)	Standard Deviation	Coefficient of Variation (%)
28 days	1 (CM)	0.0	45	47	49	47	2.2	4.8
	2 (NSM 1)	0.5	50	50	50	50	0.2	0.4
	3 (NSM 2)	1.0	50	50	52	51	0.7	1.5
	4 (NSM 3)	1.5	53	53	52	53	0.5	0.9
	5 (NSM 4)	2.0	51	53	51	51	1.2	2.3
	6 (NSM 5)	2.5	56	56	54	55	1.0	1.8
	7 (NSM 6)	3.0	56	54	57	56	1.7	3.0

Note: CM: control mortar; NSM: nanosilica mortar.

r (number of groups)		7		
n (size of the sample)		21		
Mean of the entire sample		$\bar{y}$	51.9	
The sum of the squares between the means of the groups		**q_1**	**143.6**	
The sum of the squares within the groups		**q_2**	**22.14**	
		ν_o	15.1	
Significance level α		α	0.05	
r -1 (m in Table F-1)		6		
n - r (n in Table F-1)		14		
For P (V ≤ c) = 0.95 ⇒	c =	3.48	≤	ν_o = 15.1
⇒ since $\nu_o \geq c$	the hypothesis is rejected and thus the means are statistically different			

- **Abrasion response - w/c = 0.39 – broom finishing (5 samples)**

Age	Mix	Nanosilica (%)	Sample number					Mean (g)	Standard Deviation	Coefficient of Variation (%)
			1	2	3	4	5			
28 days - broom finishing	1 (CC)	0.0	4.2	3.4	4.4	5.5	5.7	4.6	1.0	21.0
	2 (NSC 1)	0.5	4.9	4.4	5.4	5.1	5.9	5.1	0.5	10.5
	3 (NSC 2)	1.0	4.3	6.8	6.8	6.0	6.6	6.1	1.1	17.4
	4 (NSC 3)	1.5	4.1	3.7	4.9	5.0	4.9	4.5	0.6	13.1
	5 (NSC 4)	2.0	4.0	3.5	3.8	3.7	3.5	3.7	0.2	5.8

Note: CC: control concrete; NSC: nanosilica concrete.

r (number of groups)		5		
n (size of the sample)		25		
Mean of the entire sample		$\bar{y}$	4.8	
The sum of the squares between the means of the groups		$\mathbf{q_1}$	**15.5**	
The sum of the squares within the groups		$\mathbf{q_2}$	**11.06**	
		ν_o	7.0	
Significance level α		α	0.05	
r -1 (m in Table F-1)		4		
n - r (n in Table F-1)		20		
For P (V ≤ c) = 0.95 ⇒	c =	2.87	≤	ν_o = 7.0
⇒ since $\nu_o \geq c$	the hypothesis is rejected and thus the means are statistically different			

- **Abrasion response - w/c = 0.39 – smooth finishing (5 samples)**

Age	Mix	Nanosilica (%)	Sample number					Mean (g)	Standard Deviation	Coefficient of Variation (%)
			1	2	3	4	5			
28 days - broom finishing	1 (CC)	0.0	2.1	3.0	2.2	2.7	2.1	2.4	0.4	17.5
	2 (NSC 2)	1.0	1.5	1.4	1.5	1.4	1.3	1.4	0.1	5.3
	3 (NSC 4)	2.0	1.5	1.4	1.6	1.4	1.5	1.5	0.1	4.1

Note: CC: control concrete; NSC: nanosilica concrete.

r (number of groups)		3		
n (size of the sample)		15		
Mean of the entire sample		$\bar{y}$	1.8	
The sum of the squares between the means of the groups		$\mathbf{q_1}$	**1.9**	
The sum of the squares within the groups		$\mathbf{q_2}$	**0.75**	
		ν_o	15.3	
Significance level α		α	0.05	
r -1 (m in Table F-1)		2		
n - r (n in Table F-1)		12		
For P (V ≤ c) = 0.95 ⇒	c =	3.89	≤	$\nu o = 15.3$
⇒ since $\nu o \geq c$	the hypothesis is rejected and thus the means are statistically different			

- **Rapid freezing and thawing (Durability factor) - w/c = 0.39 (3 samples)**

Mix	Nanosilica (%)	Sample 1	Sample 2	Sample 3	Mean	Standard Deviation	Coefficient of Variation (%)
1 (CC)	0.0	93	93	93	93	0.0	0.02
2 (NSC 1)	1.0	93	92	93	93	0.5	0.51
3 (NSC 2)	2.0	92	94	93	93	0.9	0.92

Note: CC: control concrete; NSC: nanosilica concrete.

r (number of groups)		3	
n (size of the sample)		9	
Mean of the entire sample		$\bar{y}$	93.0
The sum of the squares between the means of the groups		$\mathbf{q_1}$	**0.2**
The sum of the squares within the groups		$\mathbf{q_2}$	**1.92**
		ν_o	0.3
Significance level α		α	0.05
r -1 (m in Table F-1)		2	
n - r (n in Table F-1)		6	
For P (V ≤ c) = 0.95 ⇒	c =	5.14	≥ $\nu o = 0.3$
⇒ since $\nu o \leq c$	the hypothesis is accepted and thus the means are statistically equal		

- **Rapid freezing and thawing (Loss of weight) - w/c = 0.39 (3 samples)**

Mix	Nanosilica (%)	Sample 1	Sample 2	Sample 3	Mean (g)	Standard Deviation	Coefficient of Variation (%)
1 (CC)	0.0	0.15	0.14	0.16	0.15	0.0	5.6
2 (NSC 1)	1.0	0.11	0.12	0.12	0.12	0.0	5.1
3 (NSC 2)	2.0	0.11	0.08	0.05	0.08	0.0	35.8

Note: CC: control concrete; NSC: nanosilica concrete.

r (number of groups)		3	
n (size of the sample)		9	
Mean of the entire sample		$\bar{y}$	0.1
The sum of the squares between the means of the groups		$\mathbf{q_1}$	**0.007**
The sum of the squares within the groups		$\mathbf{q_2}$	**0.002**
		ν_o	10.9
Significance level α		α	0.05
r -1 (m in Table F-1)		2	
n - r (n in Table F-1)		6	
For P (V ≤ c) = 0.95 ⇒	c =	5.14	≤ ν_o = 10.9
⇒ since $\nu o \geq c$	the hypothesis is rejected and thus the means are statistically different		

- **Friction response – BPN – first coating - w/c = 0.31 (3 samples)**

Type of mix	Sample 1	Sample 2	Sample 3	Mean	Standard Deviation	Coefficient of Variation (%)
CC (0.0 g/m^2)	43	43	45	44	1.1	2.6
NLLCC1 (30 g/m^2)	46	42	42	43	2.5	5.9
NLLCC2 (60 g/m^2)	45	37	36	39	5.3	13.3
NLLCC3 (90 g/m^2)	40	40	44	41	2.3	5.6
NLLCC4 (110 g/m^2)	39	42	-	41	2.4	6.0
Note: NLLCC = Nano-lotus leaf coated concrete.						

r (number of groups)			5	
n (size of the sample)			14	
Mean of the entire sample			$\bar{y}$	41.7
The sum of the squares between the means of the groups			**q_1**	**65.2**
The sum of the squares within the groups			**q_2**	**87.2**
			ν_o	1.7
Significance level α			α	0.05
r -1 (m in Table 9.a)			4	
n - r (n in Table 9a)			9	
For P (V ≤ c) = 0.95 ⇒	c =	3.48	≥	ν_o = 1.7
⇒ since $\nu_o \leq c$	the hypothesis is accepted and thus the means are statistically equal			

- **Friction response – BPN – second coating - w/c = 0.31 (3 samples)**

Type of mix	Sample 1	Sample 2	Sample 3	Mean	Standard Deviation	Coefficient of Variation (%)
CC (0.0 g/m^2)	40	46	35	40	5.2	12.8
NLLCC1 (30 g/m^2)	40	40	50	43	5.9	13.6
NLLCC2 (60 g/m^2)	35	40	46	40	5.7	14.2
NLLCC3 (90 g/m^2)	47	45	50	47	2.7	5.8
NLLCC4 (110 g/m^2)	38	43	30	37	6.4	17.2

Note: NLLCC = Nano-lotus leaf coated concrete.

r (number of groups)			5	
n (size of the sample)			15	
Mean of the entire sample			$\bar{y}$	41.6
The sum of the squares between the means of the groups			$\mathbf{q_1}$	**290.4**
The sum of the squares within the groups			$\mathbf{q_2}$	**285.3**
			ν_o	2.5
Significance level α			α	0.05
r -1 (m in Table 9.a)			4	
n - r (n in Table 9a)			10	
For P (V ≤ c) = 0.95 ⇒	c =	3.48	≥	ν_o = 3.0
⇒ since $\nu_o \leq c$	the hypothesis is accepted and thus the means are statistically equal			

Appendix G

t Student Analysis

Table G-1: Student's t-Distribution (Adapted from (Kreyszig, 1970)).

$F(z)$	Number of Degrees of Freedom									
	1	2	3	4	5	6	7	8	9	10
0.5	0.00	0.00	0.00	0.00	0.00	0.00	0.00	0.00	0.00	0.00
0.6	0.33	0.29	0.28	0.27	0.27	0.27	0.26	0.26	0.26	0.26
0.7	0.73	0.62	0.58	0.57	0.56	0.55	0.55	0.55	0.54	0.54
0.8	1.38	1.06	0.98	0.94	0.92	0.91	0.90	0.89	0.88	0.88
0.9	3.08	1.89	1.64	1.53	1.48	1.44	1.42	1.40	1.38	1.37
0.95	6.31	2.92	2.35	2.13	2.02	1.94	1.90	1.86	1.83	1.81
0.975	12.7	4.30	3.18	2.78	2.57	2.45	2.37	2.31	2.26	2.23
0.99	31.8	6.97	4.54	3.75	3.37	3.14	3.00	2.90	2.82	2.76
0.995	63.7	9.93	5.84	4.60	4.03	3.71	3.50	3.36	3.25	3.17
0.999	318.3	22.3	10.2	7.17	5.89	5.21	4.79	4.50	4.30	4.14

$F(z)$	Number of Degrees of Freedom									
	11	12	13	14	15	16	17	18	19	20
0.5	0.00	0.00	0.00	0.00	0.00	0.00	0.00	0.00	0.00	0.00
0.6	0.26	0.26	0.26	0.26	0.26	0.26	0.26	0.26	0.26	0.26
0.7	0.54	0.54	0.54	0.54	0.54	0.54	0.53	0.53	0.53	0.53
0.8	0.88	0.87	0.87	0.87	0.87	0.87	0.86	0.86	0.86	0.86
0.9	1.36	1.36	1.35	1.35	1.34	1.34	1.33	1.33	1.33	1.33
0.95	1.80	1.78	1.77	1.76	1.75	1.75	1.74	1.73	1.73	1.73
0.975	2.20	2.18	2.16	2.15	2.13	2.12	2.11	2.10	2.09	2.09
0.99	2.72	2.68	2.65	2.62	2.60	2.58	2.57	2.55	2.54	2.53
0.995	3.11	3.06	3.01	2.98	2.95	2.92	2.90	2.88	2.86	2.85
0.999	4.03	3.93	3.85	3.79	3.73	3.69	3.65	3.61	3.58	3.55

$F(z)$	Number of Degrees of Freedom									
	22	24	26	28	30	40	50	100	200	∞
0.5	0.00	0.00	0.00	0.00	0.00	0.00	0.00	0.00	0.00	0.00
0.6	0.26	0.26	0.26	0.26	0.26	0.26	0.26	0.25	0.25	0.25
0.7	0.53	0.53	0.53	0.53	0.53	0.53	0.53	0.53	0.53	0.52
0.8	0.86	0.86	0.86	0.86	0.85	0.85	0.85	0.85	0.84	0.84
0.9	1.32	1.32	1.32	1.31	1.31	1.30	1.30	1.29	1.29	1.28
0.95	1.72	1.71	1.71	1.70	1.70	1.68	1.68	1.66	1.65	1.65
0.975	2.07	2.06	2.06	2.05	2.04	2.02	2.01	1.98	1.97	1.96
0.99	2.51	2.49	2.48	2.47	2.46	2.42	2.40	2.37	2.35	2.33
0.995	2.82	2.80	2.78	2.76	2.75	2.70	2.68	2.63	2.60	2.58
0.999	3.51	3.47	3.44	3.41	3.39	3.31	3.26	3.17	3.13	3.09

- **Compressive strength in concretes - w/c = 0.31 (3 samples)**

Age	Mix	Nanosilica (%)	Sample 1	Sample 2	Sample 3	Mean (MPa)	Variance	Standard Deviation	Coefficient of Variation (%)
28 days	1 (CC)	0.0	61	61	61	61	0.03	0.2	0.3
	4 (NSC 3)	1.5	65	67	66	66	1.53	1.2	1.9

Note: CC: control concrete; NSC: nanosilica concrete.

n1	3	amount of samples in the first group
n2	3	amount of samples in the second group
n1 + n2 - 2	4	degrees of freedom

to = 6.65 > c = 2.78 Hypothesis is rejected, the means are statistically different

c is obtained from Table G-1 (Student's t-Distribution) using (n1 + n2 - 2) degrees of freedom

- **Compressive strength in concretes - w/c = 0.39 (3 samples)**

Age	Mix	Nanosilica (%)	Sample 1	Sample 2	Sample 3	Mean (MPa)	Variance	Standard Deviation	Coefficient of Variation (%)
28 days	1 (CC)	0.0	54	56	54	55	1.9	1.4	2.5
	4 (NSC 3)	1.5	64	65	65	65	0.6	0.8	1.2

Note: CC: control concrete; NSC: nanosilica concrete.

n1	3	amount of samples in the first group
n2	3	amount of samples in the second group
n1 + n2 - 2	4	degrees of freedom

to = 11.06 > c = 2.78 Hypothesis is rejected, the means are statistically different

c is obtained from Table G-1 (Student's t-Distribution) using (n1 + n2 - 2) degrees of freedom

- **Compressive strength in concretes - w/c = 0.45 (3 samples)**

Age	Mix	Nanosilica (%)	Sample 1	Sample 2	Sample 3	Mean (MPa)	Variance	Standard Deviation	Coefficient of Variation (%)
28 days	1 (CC)	0.0	40	43	43	42	3.6	1.9	4.6
	3 (NSC 2)	2.0	47	47	46	47	0.1	0.4	0.8

Note: CC: control concrete; NSC: nanosilica concrete.

n1	3	amount of samples in the first group
n2	3	amount of samples in the second group
n1 + n2 - 2	4	degrees of freedom

to = 4.31 > c = 2.78 Hypothesis is rejected, the means are statistically different

c is obtained from Table G-1 (Student's t-Distribution) using (n1 + n2 - 2) degrees of freedom

- **Noise absorption - w/c = 0.31 (3 samples)**

Age	Mix	Nanosilica (%)	Sample 1	Sample 2	Sample 3	Mean	Variance	Standard Deviation	Coefficient of Variation (%)
28 days	1 (CC)	0.0	0.06	0.04	0.05	0.05	0.0001	0.01	19.0
	4 (NSC 3)	1.5	0.06	0.06	0.05	0.06	0.0000	0.00	7.9

Note: CC: control concrete; NSC: nanosilica concrete.

n1	3	amount of samples in the first group
n2	3	amount of samples in the second group
n1 + n2 - 2	4	degrees of freedom

to 0.74 ≤ c = 2.78 Hypothesis is not rejected, the means are statistically equal

c is obtained from Table G-1 (Student's t-Distribution) using (n1 + n2 - 2) degrees of freedom

- **Noise absorption - w/c = 0.39 (3 samples)**

Age	Mix	Nanosilica (%)	Sample 1	Sample 2	Sample 3	Mean	Variance	Standard Deviation	Coefficient of Variation (%)
28 days	1 (CC)	0.0	0.10	0.06	0.04	0.07	0.0009	0.03	44.2
	4 (NSC 3)	1.5	0.06	0.03	0.15	0.08	0.0037	0.06	73.4

Note: CC: control concrete; NSC: nanosilica concrete.

n1	3	amount of samples in the first group
n2	3	amount of samples in the second group
n1 + n2 - 2	4	degrees of freedom

to 0.35 ≤ c = 2.78 Hypothesis is not rejected, the means are statistically equal

c is obtained from Table G-1 (Student's t-Distribution) using (n1 + n2 - 2) degrees of freedom

- **Friction response – BPN – broom finishing - w/c = 0.31 (15 samples)**

Age	Mix	Nanosilica (%)	Sample number															Mean	Variance	SDV	COV (%)
			1	2	3	4	5	6	7	8	9	10	11	12	13	14	15				
28 days	1 (CC)	0.0	41	43	45	46	44	39	43	40	44	45	47	42	42	44	40	43	5.4	2.3	5.4
	3 (NSC 2)	1.0	45	51	45	54	53	49	53	44	57	49	56	53	46	54	53	51	17.0	4.1	8.1

Note: CC: control concrete; NSC: nanosilica concrete; SDV: Standard Deviation; COV: Coefficient of Variation.

n1	15	amount of samples in the first group
n2	15	amount of samples in the second group
n1 + n2 - 2	28	degrees of freedom

to 6.44 > c = 2.06 Hypothesis is rejected, the means are statistically different

c is obtained from Table G-1 (Student's t-Distribution) using (n1 + n2 - 2) degrees of freedom

- **Friction response – BPN – broom finishing - w/c = 0.39 (15 samples)**

Age	Mix	Nanosilica (%)	Sample number															Mean	Variance	SDV	COV (%)
			1	2	3	4	5	6	7	8	9	10	11	12	13	14	15				
28 days	1 (CC)	0.0	50	57	49	45	53	46	51	43	49	43	48	46	51	55	53	49	17	4.1	8.4
	3 (NSC 2)	1.0	60	58	61	62	64	57	54	55	54	55	55	61	55	53	56	57	12	3.4	6.0

Note: CC: control concrete; NSC: nanosilica concrete; SDV: Standard Deviation; COV: Coefficient of Variation.

n1	15	amount of samples in the first group
n2	15	amount of samples in the second group
n1 + n2 - 2	28	degrees of freedom

to 5.78 > c = 2.06 Hypothesis is rejected, the means are statistically different

c is obtained from Table G-1 (Student's t-Distribution) using (n1 + n2 - 2) degrees of freedom

- **Friction response – BPN – smooth finishing - w/c = 0.39 (5 samples)**

Age	Mix	Nanosilica (%)	Sample number					Mean	Variance	Standard Deviation	Coefficient of Variation (%)
			1	2	3	4	5				
28 days	1 (CC)	0.0	36	40	40	35	36	37	5.9	2.4	6.6
	5 (NSC 4)	2.0	43	44	49	40	45	44	10.9	3.3	7.5

Note: CC: control concrete; NSC: nanosilica concrete.

n1	5	amount of samples in the first group
n2	5	amount of samples in the second group
n1 + n2 - 2	8	degrees of freedom

to 3.81 > c = 2.31 Hypothesis is rejected, the means are statistically different

c is obtained from Table G-1 (Student's t-Distribution) using (n1 + n2 - 2) degrees of freedom

- **Friction response – using a tribometer – w/c = 0.39 – 50 g force (3 samples)**

Age	Mix	Nanosilica (%)	Sample 1	Sample 2	Sample 3	Mean	Variance	Standard Deviation	Coefficient of Variation (%)
28 days -	1 (CM)	0.0	0.69	0.67	0.67	0.68	0.0002	0.01	2.0
50 gr	4 (NSM 3)	1.5	0.89	0.83	0.82	0.85	0.0014	0.04	4.4

Note: CM: control mortar; NSM: nanosilica mortar.

n1	3	amount of samples in the first group
n2	3	amount of samples in the second group
n1 + n2 - 2	4	degrees of freedom

to 7.55 > c = 2.78 Hypothesis is rejected, the means are statistically different

c is obtained from Table G-1 (Student's t-Distribution) using (n1 + n2 - 2) degrees of freedom

- **Friction response – using a tribometer – w/c = 0.39 – 100 g force (3 samples)**

Age	Mix	Nanosilica (%)	Sample 1	Sample 2	Sample 3	Mean	Variance	Standard Deviation	Coefficient of Variation (%)
28 days -	1 (CM)	0.0	0.72	0.70	0.70	0.71	0.0001	0.01	1.6
100 gr	4 (NSM 3)	1.5	0.86	0.84	0.83	0.85	0.0002	0.02	1.8

Note: CM: control mortar; NSM: nanosilica mortar.

n1	3	amount of samples in the first group
n2	3	amount of samples in the second group
n1 + n2 - 2	4	degrees of freedom

to 12.79 > c = 2.78 Hypothesis is rejected, the means are statistically different

c is obtained from Table G-1 (Student's t-Distribution) using (n1 + n2 - 2) degrees of freedom